Untersuchung der Substratspezifitäten von Adenylierungsdomänen aus Ascomyceten und Basidiomyceten

---

Dissertation

zur Erlangung des akademischen Grades

„doctor rerum naturalium“ (Dr. rer. nat.)

vorgelegt dem Rat der Biologisch-Pharmazeutischen Fakultät der Friedrich-Schiller- Universität Jena

von Eileen Brandenburger,
Master of Science

geboren am 18.10.1987
in Beeskow

Tag der Einreichung: 03.02.2017

Gutachter: Prof. Dr. Dirk Hoffmeister
Friedrich-Schiller-Universität, Jena

Dr. Pierre Stallforth
Friedrich-Schiller-Universität, Jena

Prof. Dr. Elke Dittmann
Universität Potsdam

Tag der Disputation: 08.06.2017

Meinen Liebsten

Inhaltsverzeichnis

Inhaltsverzeichnis I

1. Einleitung 7

1.1 Sekundärmetabolite – Ihre Produzenten und ihr breites Anwendungsspektrum 7

1.2 Die Biosynthese sekundärer Naturstoffe 9

1.2.1 Biosynthese nichtribosomaler Peptide 11

1.3 Strukturelle Vielfalt der nichtribosomalen Peptidsynthetasen 13

1.3.1 Monomodulare NRPSs mit C-terminaler Reduktasedomäne 14

1.3.2 NRPS-ähnliche Enzyme vom Typ A-T-R-X 16

1.3.3 NRPS mit unvollständigen Modulen 16

2. Zielsetzung dieser Arbeit 19

2.1 Untersuchung adenylierender Reduktasen aus Heterobasidion annosum (Russuales) und Serpula lacrymans (Boletales) 19

2.2 Charakterisierung der Siderophorsynthetase CsNPS2 aus Ceriporiopsis subvermispora 19

2.3 Charakterisierung der A-Domäne von FsqF aus Aspergillus fumigatus 20

3. Publikationen 21

3.1 Publikation 1, Brandenburger et al. (2016), Fungal Genetics and Biology 21

3.2 Publikation 2, Brandenburger et al. (2016), Manuskript in Vorbereitung 37

3.3 Publikation 3, Baccile et al. (2016), Nature Chemical Biology 77

4. Diskussion 161

4.1 Etablierung eines fungalen nichtribosomalen Codes 161

4.2 Diversität im Aufbau der NRPSs bedingt die strukturelle Vielfalt der Produkte 166

4.3 Neue Möglichkeiten durch besseres Verständnis zur Funktionsweise der NRPSs 171

5. Zusammenfassung 174

6. Summary 175

7. Referenzen 176

8. Anhang 185

Vektorkarten 185
Publikationen, Vorträge und Poster 186
Anteilsverteilung der Co-Autoren an den Publikationen 187
Abkürzungsverzeichnis 190
Abbildungsverzeichnis 191
Eigenständigkeitserklärung 192
Lebenslauf 193
Danksagung 194

1. Einleitung

1.1 Sekundärmetabolite – Ihre Produzenten und ihr breites Anwendungsspektrum

Zahlreiche bereits charakterisierte Naturstoffe, wie z. B. das durch Alexander Fleming entdeckte Penicillin (1) (Fleming, 1929), dienen in erster Linie nicht dem Überleben oder dem Wachstum des Produzenten (Williams et al., 1989), sondern erzeugen einen positiven Effekt u. a. in der Bekämpfung von Fraßfeinden und Pathogenen, beim Anlocken nützlicher Organismen, der Standortanpassung oder der Reproduktion. Diese Naturstoffe, welche häufig aus den Produkten des primären Stoffwechsels hervorgehen (z. B. Aminosäuren, Fettsäuren, andere organische Säuren oder Kohlenhydrate), werden dem Sekundärstoffwechsel zugeordnet, was wiederum eine eindeutige Trennung der Stoffwechselwege erschwert (Wang et al., 2013). Während primäre Naturstoffe ubiquitär vorkommen, beschränkt sich die Biosynthese der Sekundärmetabolite auf einzelne Familien oder Arten (Drew and Demain, 1977). Dennoch konnte die Biosynthese dieser Vorteil bringenden Moleküle bei Pflanzen, Tieren, Bakterien und zahlreichen Pilzen bereits nachgewiesen werden. Herausragend waren u. a. die Entdeckung des Morphins (2) aus *Papaver somniferum* durch Friedrich Wilhelm Adam Sertürner (1806) oder auch die strukturelle Aufklärung des Salicins (3) durch Hermann Kolbe (1859), welches zunächst durch Johann Buchner (1828) entdeckt wurde (Limmroth et al., 1999).

Zu den tierischen Naturstoffen zählen z. B. die Samandarin-Alkaloide (4) vom *Salamandra maculosa*, dem Feuersalamander (Shimizu, 1976). Diese werden über die Drüsen in der Haut bzw. am Kopf ausgeschüttet und dienen der Abwehr von Fraßfeinden aber auch dem Schutz vor Infektionen der Haut durch Bakterien und Pilze (Mebs and Pogoda, 2005).

Weitaus größere Anerkennung erfahren aus Bakterien isolierte Naturstoffe, wie das zytotoxische Antibiotikum Mitomycin C (5). Erstmals 1958 aus *Streptomyces caespitosus* aufgereinigt, konnte gezeigt werden, dass Mitomycin C DNA bakterieller Zellen degradiert. Darüber hinaus beeinflusst es die DNA-Synthese in Säugerzellen und hat den Abbau des Zellkerns zur Folge (Crooke and Bradner, 1976). Ein weiterer bakterieller Sekundärmetabolit von großer Bedeutung ist das Erythromycin (6), welches aus *Saccharopolyspora erythraea* isoliert wurde (McGuire et al., 1952; Cortes et al., 1990).

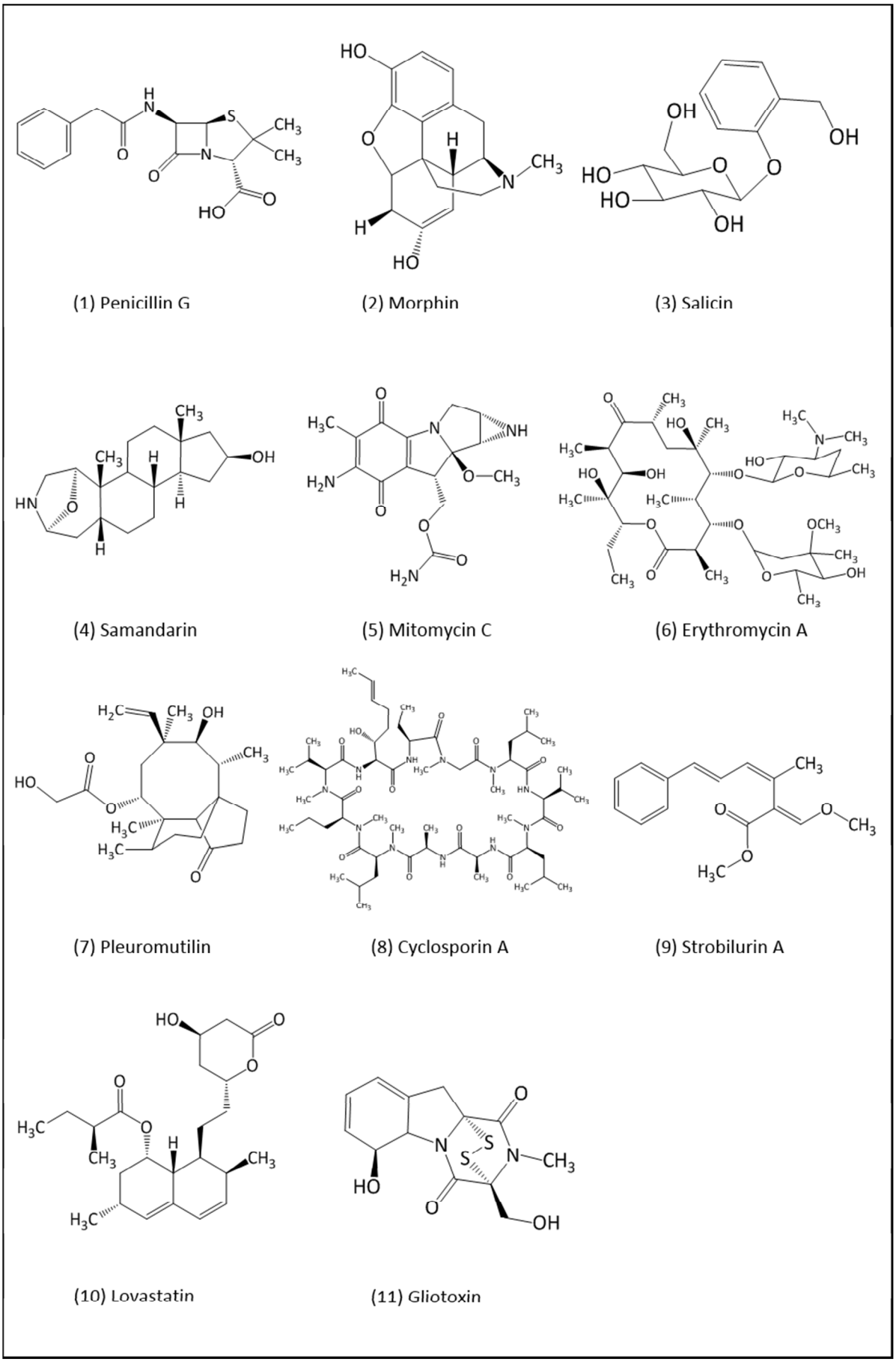

Abbildung 1: Strukturen ausgewählter Sekundärmetabolite aus Pflanzen, Tieren, Bakterien und Pilzen.

Spätestens mit der Entdeckung des Penicillins bekamen die Pilze als Produzenten von sekundären Naturstoffen eine größere Bedeutung. In den vergangenen Jahrzehnten wurden zahlreiche pilzliche Substanzen mit unterschiedlichsten Wirkmechanismen isoliert und charakterisiert. Das antibiotische Pleuromutilin (7) aus *Clitopilus passeckerianus* (zuvor beschrieben als *Pleurotus passeckerianus*) (Kavanagh et al., 1951), das immunsuppressiv wirkende Cyclosporin A (8), welches durch *Tolypocladium inflatum* (zuvor beschrieben als *Trichoderma polysporum*) produziert wird (Dreyfuss et al., 1976) oder das antifugal wirkende Strobilurin (9) aus *Strobilurus tenacellus* (Anke et al., 1977). Ein weiteres bedeutsames Beispiel stellt das Lovastatin (10) aus *Aspergillus terreus* dar, welches zur Behandlung von Hypercholesterinämie eingesetzt wird (Kennedy et al., 1999).

Trotz der großen Vielfalt der bereits bekannten sekundären Naturstoffe werden sie bezüglich ihrer Biosynthesewege häufig in Gruppen eingeordnet. In den meisten Fällen handelt es sich um Terpenoide, Polyketide oder Aminosäure-abgeleitete Metabolite. Letztere sollen in der folgenden Arbeit am Beispiel der nichtribosomalen Peptide (NRP) näher erläutert werden.

1.2 Die Biosynthese sekundärer Naturstoffe

Die Entwicklung neuer Analysetechniken wie z. B. die Massenspektrometrie (Fenn et al., 1989), die Kernspinresonanzspektroskopie (Bloch, 1946) oder die Hochleistungs-Flüssigkeitschromatografie (Okamura and Sawyer, 1972) ermöglichten die Isolierung und Charakterisierung einer Vielzahl neuer Naturstoffe. Weiterhin trugen die Sequenzierung zahlreicher Genome naturstoffproduzierender Organismen, sowie die Weiterentwicklung molekularbiologischer Methoden maßgeblich zur Aufklärung komplexer Biosynthesewege bei.

Diese Entwicklung lässt sich am Epipolythiodioxopiperazin Gliotoxin (11) anschaulich darstellen. Die Substanz wurde bereits 1936 aus *Trichoderma virens* isoliert (Weindling and Emerson, 1936). Die korrekte Struktur konnte allerdings erst 1958 veröffentlicht werden (Bell et al., 1958). Mit der Sequenzierung des Genoms von *Aspergillus fumigatus* (Nierman et al., 2005), ebenfalls ein Produzent des Gliotoxins, war dann die Identifizierung aller an der Biosynthese beteiligter Gene möglich. Nachfolgend konnten mehrere Arbeitsgruppen die Biosynthese vollständig aufklären (Balibar and Walsh, 2006a; Cramer et al., 2006; Kupfahl et

al., 2006; Scharf et al., 2010; Davis et al., 2011; Scharf et al., 2011; Scharf et al., 2012; Scharf et al., 2014).

Die vielfältige Gruppe der Terpene als nur ein Beispiel für eine Naturstoffklasse beinhaltet u. a. Steroide, Carotinoide oder Pflanzenfarbstoffe. Die Gemeinsamkeit aller ist der Aufbau aus Isopreneinheiten (2-Methyl-1,3-butadien) (Oldfield and Lin, 2012). Ein Vertreter ist z. B. das Pleuromutilin (7). Häufig treten Terpene auch durch die Verbindung mit Aminosäuren als Alkaloide auf (Facchini, 2001). Alkaloide, wie z. B. das Samandarin sind basische Verbindungen mit zyklisch gebundenem Stickstoff, abgeleitet von Aminosäuren, die ebenfalls als bioaktive Substanzen aus Pflanzen und Mikroorganismen bekannt sind.

Polyketide, welche sich aus formalen Acetateinheiten ableiten, werden durch Polyketid-synthasen (PKSs) gebildet. Dabei werden drei Typen unterschieden. Zum einen die Synthese über separate Enzyme, wo jedes Enzym einen Katalyseschritt übernimmt (Typ II PKS) und zum anderen die Synthese mithilfe sogenannter Megaenzyme (Typ I). Eine dritte Form der Polyketid-Synthese erfolgt mit Acyl-Carrier-Protein unabhängigen Typ III PKSs (Shen, 2003).

NRP werden ebenfalls von großen, multifunktionalen, modular aufgebauten Enzymen gebildet. Jedes Modul einer nichtribosomalen Peptidsynthetase (NRPS) aktiviert ein entsprechendes Substrat-Monomer, das wiederum, unter Bildung einer Peptidbindung, in die wachsende Peptidkette eingebaut wird (Schwarzer et al., 2003). Darüber hinaus konnten Naturstoffe (z. B. Fusarin C, isoliert aus *Fusarium graminearum*) nachgewiesen werden, deren Struktur auf das Zusammenspiel zweier Enzymklassen zurückzuführen ist. In diesem Fall erfolgt die Biosynthese durch einen PKS-NRPS Hybriden (ebenfalls möglich NRPS-PKS Hybrid) (Hoffmeister and Keller, 2007).

Einen weiteren Einfluss auf die strukturelle Diversität der bioaktiven Naturstoffe, haben die lange unbekannten ribosomal erzeugten Peptide (ribosomally-synthesized and post-translationally-modified peptides - RiPPs). Die in der Vergangenheit sowohl bei Prokaryoten als auch bei Eukaryoten entdeckten Sekundärmetabolite sind durch zahlreiche zusätzliche Modifikationen gekennzeichnet. Zu den Modifikationen zählen u. a. die Epimerisierung, die Makrozyklisierung oder die Ausbildung von Disulfidbrücken (Arnison et al., 2013).

1.2.1 Biosynthese nichtribosomaler Peptide

NRP sind aufgrund ihres breiten Anwendungsspektrums eine besonders interessante Klasse von Naturstoffen. Um die bereits charakterisierten Substanzen in ihrer Wirkung zu optimieren, war es jedoch notwendig, den Mechanismus der Biosynthese vollständig aufzuklären. So konnte in den vergangenen Jahrzehnten gezeigt werden, dass NRP durch modular aufgebaute Megaenzyme (NRPSs) produziert werden. Diese können wie z. B. bei der NRPS SimA in der Biosynthese von Cyclosporin A eine Größe von bis zu 1,6 MDa (Weber et al., 1994) oder wie bei der NRPS Kol in der Biosynthese von Kolossin A eine Größe von bis zu 1,8 MDa erreichen (Bode et al., 2015).

Jedes Modul einer NRPS, bestehend aus verschiedenen Domänen (Abbildung 2), ist für den Einbau eines Bausteins in die Oligopeptidkette verantwortlich. Bei diesen Bausteinen handelt es sich, anders als bei den ribosomal erzeugten Peptiden, nicht ausschließlich um proteinogene Aminosäuren. Denn zusätzlich wurden nichtproteinogene Aminosäuren, α-Hydroxy- und α-Ketosäuren oder auch Aryl- und Dicarbonsäuren als Substrate für die Synthese der NRP nachgewiesen (Marahiel et al., 1997; Mootz and Marahiel, 1999; Kalb et al., 2013). Diese Vielfalt an möglichen Substraten erklärt nicht nur die große Anzahl an verschiedenen NRP in der Natur, sondern auch deren strukturelle Diversität.

Ein Grundmodul einer NRPS zur Erkennung und Aktivierung eines Substrates sowie der nachfolgenden Amidbildung (Abbildung 2) besteht aus einer Adenylierungs-(A)-, einer Thiolierungs-(T)- (auch bekannt als Peptidyl-Carrier-Protein - PCP) und einer Kondensations-(C)-Domäne (Finking and Marahiel, 2004). Die Erkennung und Aktivierung des Substrates zum Aminoacyladenylat erfolgt unter ATP-Verbrauch durch die A-Domäne (ca. 550 Aminosäuren). Anhand der Kristallstruktur von PheA, der A-Domäne der Gramicidin S-Synthetase GrsA aus *Bacillus brevis* (Conti et al., 1997), konnten für die Bindung des Substrates wichtige Aminosäurepositionen identifiziert werden. Die vergleichende Analyse dieser Aminosäuren mit denen weiterer bekannter A-Domänen führte dann zur Beschreibung des sogenannten nichtribosomalen Codes. Dieser Code ermöglicht die Bestimmung der A-Domänen-Spezifität bereits auf Proteinebene. So steht die Asparaginsäure in der ersten Position des Codes (Asp235; bezogen auf PheA) für die Aktivierung einer Aminosäure. Die negative Ladung der Asp interagiert mit der positiven Ladung, die durch die Aminogruppe der Aminosäure zur Verfügung steht. Darüber hinaus

konnte gezeigt werden, dass Serin in dieser Position zur Bindung von Dicarbonsäuren (Steinchen et al., 2013), Glycin von Anthranilsäure (Ames and Walsh, 2010), Asparagin von Arylsäuren (May et al., 2002) und Valin zur Bindung von α-Ketosäuren (Kalb et al., 2013) durch die A-Domäne führt. Für bakterielle NRPSs gilt die *in silico* Spezifitätsbestimmung als etabliert (Röttig et al., 2011). Für eine entsprechende Vorhersage bei pilzlichen A-Domänen ist die biochemische Aufklärung weiterer NRPSs notwendig.

Das durch die A-Domäne aktivierte Substrat kann anschließend als Thioester an die T-Domäne (ca. 80-100 Aminosäuren) gebunden werden. Diese muss jedoch zunächst von der inaktiven *apo*-Form in die aktive *holo*-Form umgewandelt werden (Priming). Dafür wird ein 4'-Phosphopantethein-Cofaktor vom Coenzym A auf ein konserviertes Serin der T-Domäne übertragen (Stachelhaus et al., 1996). Diese Reaktion wird durch eine 4'-Phosphopantetheinyl-Transferase katalysiert (Lambalot et al., 1996).

Die C-Domäne (ca. 450 Aminosäuren) katalysiert die Peptidbindung von Substraten benachbarter Module und trägt somit zur Verlängerung des Oligopeptids bei. Die Anzahl der Module und deren Spezifität für ein Substrat-Monomer bestimmt daher die Größe und Struktur des Produktes. Die Produktfreisetzung erfolgt in den meisten Fällen über eine endständige Thioesterase-(TE)-Domäne in linearer, zyklischer oder verzweigter Form. Darüber hinaus wurde die Freisetzung ausgehend von endständigen C-Domänen beschrieben (Keating et al., 2001). Weitere Domänen, die zur Struktur des NRPs beitragen können, sind die Epimerisierungs-(E)-Domänen (Umwandlung von L-Aminosäuren zu D-Aminosäuren), die Methylierungs-(MT)-Domänen oder die Zyklisierungs-(Cy)-Domänen (Finking and Marahiel, 2004).

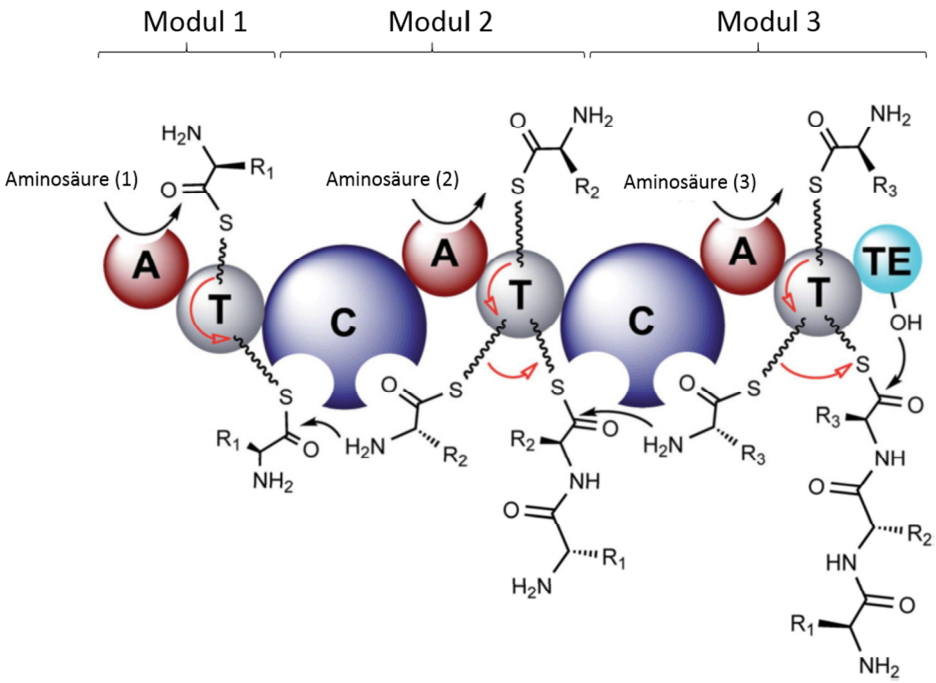

Abbildung 2: Darstellung der Funktionsweise einer NRPS (Winn et al., 2016); Modul 1 als Initiationsmodul, Modul 2 und 3 als Elongationsmodule, Aminosäuren werden durch die Adenylierungsdomäne aktiviert, auf die Thiolierungsdomäne übertragen, die Kondensationsdomäne verknüpft Substrate benachbarter Module, die Thioesterasedomäne dient der Produktfreisetzung, Abkürzungen: A: Adenylierungs-; T: Thiolierungs-, C: Kondensations- und TE: Thioesterase-Domäne.

1.3 Strukturelle Vielfalt der nichtribosomalen Peptidsynthetasen

Zusätzlich zu den oben erwähnten klassischen NRPSs sind weitere Formen bekannt, wie z. B. die monomodularen NRPSs, die auch als NRPS-ähnliche Enzyme bezeichnet werden (Abbildung 3). Diese setzen sich aus drei Domänen zusammen. Anders als bei einem klassischen Grundmodul befindet sich in der C-terminalen Position keine C-Domäne. Bereits mehrfach beschrieben sind NRPS-ähnliche Enzyme bestehend aus einer A-Domäne, einer T-Domäne und einer C-terminalen TE-Domäne. Charakteristisch für diese Enzyme ist die symmetrische Verbindung von zwei identischen α-Ketosäuren. Die Knüpfung von zwei C-C-Bindungen resultiert in der Bildung eines Chinons. Eine derartige Reaktion wird durch die Atromentinsynthetase AtrA aus *Tapinella panuoides* katalysiert (Schneider et al., 2008). Eine weitere Möglichkeit ist die Verknüpfung einer C-C- und einer C-O-Bindung wie bei der Furanonbiosynthese. Beispielhaft dafür ist die Furanonsynthetase RalA aus *Ralstonia solanacearum* zu nennen (Wackler et al., 2011).

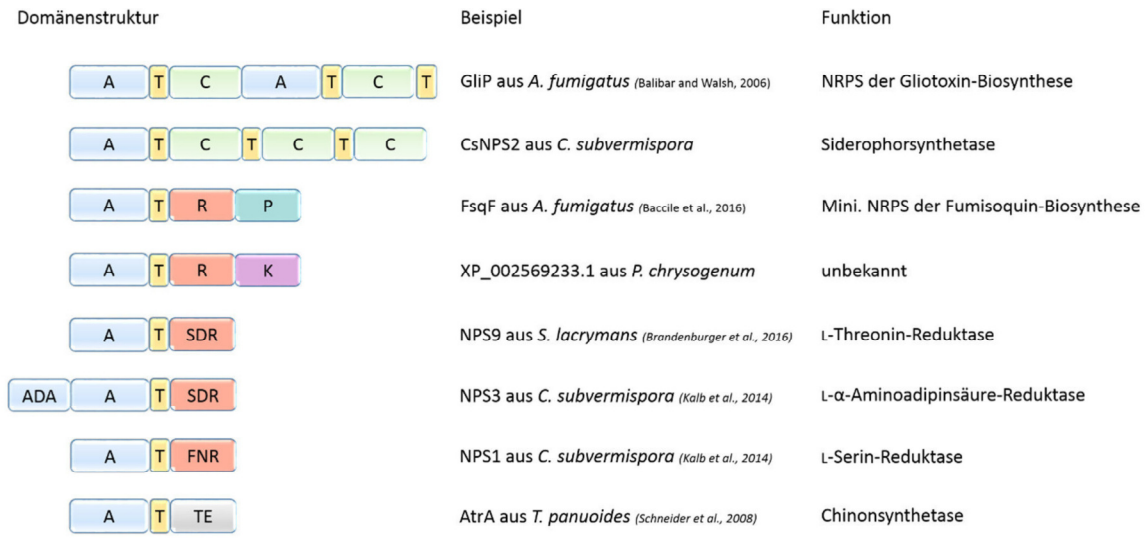

Abbildung 3: Beispielhafte Darstellung NRPS und NRPS-ähnlicher Enzyme; Abkürzungen: A: Adenylierungs-, T: Thiolierungs-, C: Kondensations-, R: Reduktase-, P: pyridoxalphosphatabhängige Aminotransferase-, K: Kinase-, TE: Thioesterase und ADA: Adenylierungs-aktivierende-Domäne, SDR: Kurzketten Dehydrogenase/Reduktase, FNR: Ferredoxin-$NADP^+$-Reduktase.

1.3.1 Monomodulare NRPSs mit C-terminaler Reduktasedomäne

Erstmals charakterisiert wurde ein NRPS-ähnliches Enzym mit C-terminaler Reduktasedomäne durch Walsh und Mitarbeiter (Ehmann et al., 1999). Lys2 aus *Saccharomyces cerevisiae* katalysiert die Reduktion von L-α-Aminoadipinsäure zu dem entsprechenden Semialdehyd, welcher weiter zu L-Lysin umgewandelt wird. Nachfolgende Arbeiten haben gezeigt, dass in verschiedenen Pilzen mehrere Gene vorhanden sind, die für Enzyme mit ähnlicher Domänenstruktur kodieren. Erst mit der biochemischen Charakterisierung wurde das umfangreiche Substratspektrum dieser adenylierenden Reduktasen deutlich. In Verbindung mit phylogenetischen Untersuchungen, ausgehend von den Adenylierungsdomänen, war es möglich, diese Reduktasen in vier Gruppen einzuteilen (Kalb et al., 2014). Lys2 aus *S. cerevisiae* oder auch NPS3 aus *Ceriporiopsis subvermispora* (Polyporales) vom Typ ADA-A-T-R (Klasse I) (Abbildung 4), wobei das ADA für eine Domäne steht, die an der Aktivierung des Substrates (L-α-Aminoadipinsäure) beteiligt ist (Kalb et al., 2015b), bilden die erste Gruppe. Darüber hinaus konnten Reduktasen charakterisiert werden, die L-Tyrosin als Substrat aktivieren (Klasse II), wie z. B. LnaA aus *Aspergillus flavus* (Forseth et al., 2013). Eine weitere Gruppe, zu der auch ATEG_03630 aus *A. terreus* gehört (Wang et al., 2014a), aktiviert Arylsäuren (Klasse III). Alle drei Klassen haben Reduktasedomänen, die strukturell zur SDR (short-chain dehydrogenase/reductase) Familie gehören und sich durch eine sogenannte Rossmann-Faltung auszeichnen. Zusätzlich dazu wurden NRPS-ähnliche Enzyme beschrieben, deren Reduktasedomänen zur Familie der

Ferredoxin-NADP$^+$-Reduktasen gehören. Diese Enzyme bilden die vierte Klasse der adenylierenden Reduktasen und sind charakterisiert durch die Aktivierung von L-Serin, was am Beispiel von NPS1 aus *C. subvermispora* biochemisch gezeigt wurde (Kalb et al., 2014).

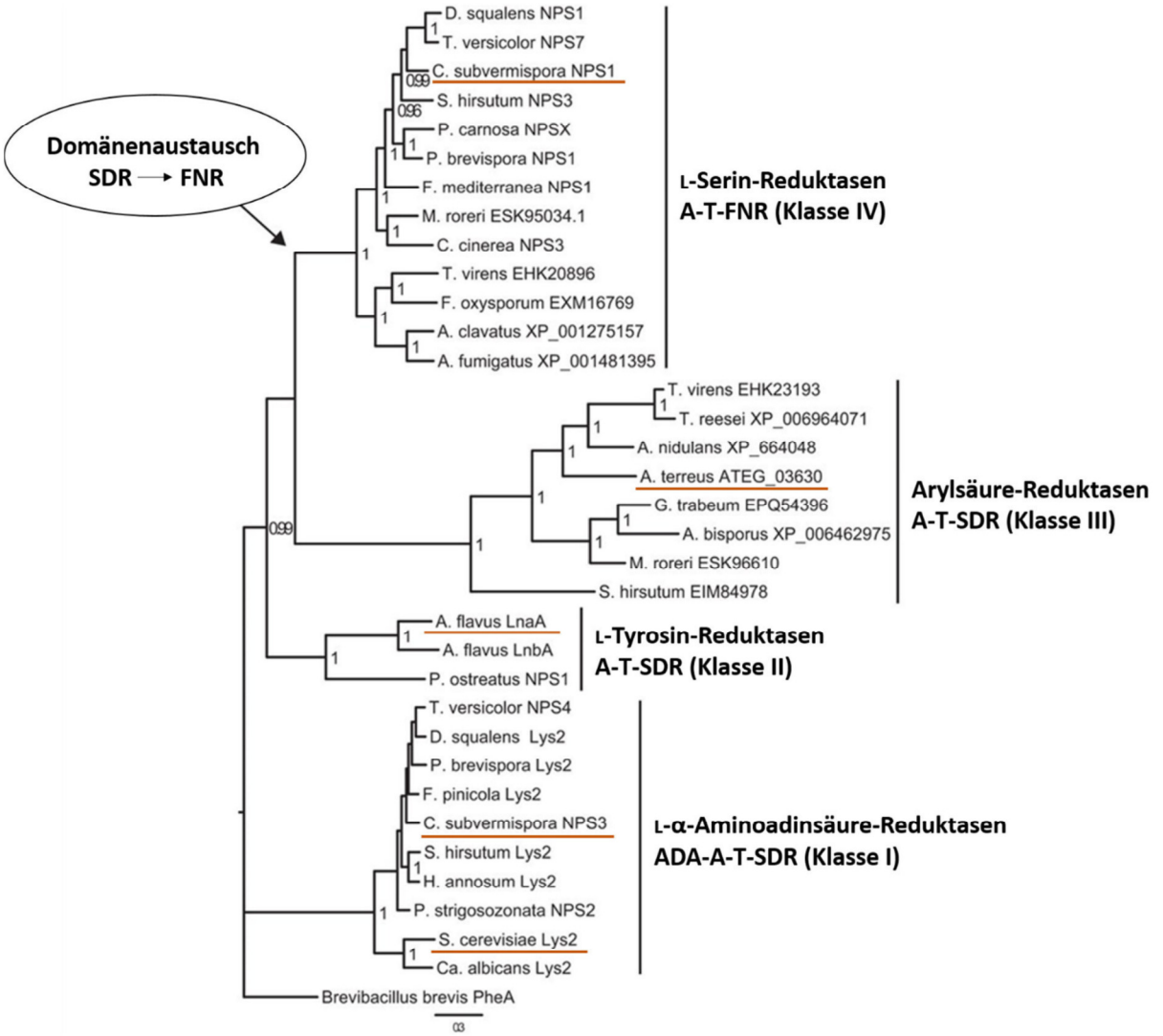

Abbildung 4: Phylogenie der A-Domänen pilzlicher adenylierender Reduktasen (modifiziert nach (Kalb et al., 2014)); Phylogenetische Unterteilung der A-Domänen in vier Klassen, gruppiert anhand der Substratspezifität und des Aufbaus, phylogenetische Abtrennung der adenylierenden Ferredoxin-NADP$^+$-Reduktasen lässt einen Domänenaustausch vermuten, Textbeispiele unterstrichen, Abkürzungen: A: Adenylierungs-, T: Thiolierungs- und ADA: Adenylierungs-aktivierende-Domäne, SDR: Kurzketten Dehydrogenase/Reduktase, FNR: Ferredoxin-NADP$^+$-Reduktase.

Um aufbauend auf den bisherigen Arbeiten weitere Organismengruppen einzubeziehen, sollten im Rahmen dieser Arbeit adenylierende Reduktasen aus verschiedenen monophyletischen Gruppen der Basidiomyceten bezüglich der Substratspezifität untersucht werden. Dafür wurden *Heterobasidion annosum* (Russulales) und *Serpula lacrymans* (Boletales) herangezogen.

Die zur Gruppe der Weißfäuleerreger gehörenden *H. annosum sensu lato* (Lind et al., 2005) sind in Nadelwäldern der nördlichen Halbkugel verbreitet. Als Pflanzenpathogene sind sie in der Lage, von einer saprotrophen in eine nekrotrophe Lebensweise überzugehen. Zunächst erfolgt die Infektion von frischem Holz, gefolgt von einer Verbreitung von Wurzel zu Wurzel, was dann zum Absterben ganzer Bäume führen kann. Anhand von Genomanalysen konnte gezeigt werden, das *H. annosum* drei Gene für die Biosynthese von Polyketiden, 13 für NRPS-ähnliche Enzyme und drei für Terpenzyklasen besitzt (Olson et al., 2012).

Serpula lacrymans ist ein Braunfäuleerreger. Als Kulturfolger wurde sein Auftreten in Gebäuden auf der ganzen Welt beobachtet. Als geografischer Ursprung für *S. lacrymans* wird das asiatische Festland angesehen (Kauserud et al., 2007). Mit der Sequenzierung des Genoms im Jahre 2011 konnten eine Vielzahl an Naturstoffgenen identifiziert werden (Eastwood et al., 2011). Unter anderem konnten acht Gene gefunden werden, die für NRPSs und 15 Gene, die für NRPS-ähnliche Enzyme kodieren.

1.3.2 NRPS-ähnliche Enzyme vom Typ A-T-R-X

Eine besondere und nahezu unbeschriebene Gruppe adenylierender Reduktasen bilden die aus vier Domänen aufgebauten NRPS-ähnlichen Enzyme vom Typ A-T-R-X. Die terminale Domäne (X) kann variieren. So handelt es sich bei FsqF aus *Aspergillus fumigatus* um eine pyridoxalphosphatabhängige Aminotransferase-Domäne. Darüber hinaus konnten mithilfe von Genomsequenzierungen Gene identifiziert werden, die für Reduktasen mit einer endständigen Kinasedomäne kodieren. XP_002569233.1 aus *Penicillium chrysogenum* (van den Berg et al., 2008) oder ASN170633 aus *Aspergillus niger* (Andersen et al., 2011) sind nur zwei Beispiele. Eine biochemische Charakterisierung bzw. das Produkt dieser Reduktasen wurde noch nicht beschrieben.

1.3.3 NRPS mit unvollständigen Modulen

Eine weitere Gruppe von NRPSs zeichnet sich durch unvollständige Module aus. Ein sehr prominentes Beispiel ist die NRPS GliP, welche den ersten Schritt in der Biosynthese des Epipolythiodioxopiperazins (ETP) Gliotoxin in *Aspergillus fumigatus* katalysiert (Balibar and Walsh, 2006b; Cramer et al., 2006; Kupfahl et al., 2006). Nicht zuletzt die biologischen Aktivitäten (u. a. antivirale, antibakterielle und immunsuppressive Eigenschaften) und die besondere Struktur (intramolekulare Disulfidbrücke) haben dazu beigetragen, dass die

Biosynthese bereits aufgeklärt wurde (Scharf et al., 2010; Davis et al., 2011; Scharf et al., 2011; Scharf et al., 2012; Scharf et al., 2014). Ausgehend von der trimodularen NRPS GliP (A_1-T_1-C_1-A_2-T_2-C_2-T_3), wobei das dritte Modul aufgrund der fehlenden A-Domäne unvollständig ist (C_2-T_3), wird ein Diketopiperazin durch die Verknüpfung von L-Phenylalanin (A_1) und L-Serin (A_2), gebildet. Es wird postuliert, dass die Zyklisierung des Dipeptids durch das dritte Modul katalysiert wird, wobei der exakte Reaktionsmechanismus noch unklar ist (Balibar and Walsh, 2006a). NRPSs mit diesem modularen Aufbau sind weit verbreitet. SirP aus *Leptosphaeria maculans* für die Biosynthese von Sirodesmin (Gardiner et al., 2004) oder AclA aus *Aspergillus flavus* (Arnaud et al., 2012) sind weiteren Beispiele aus Ascomyceten. Aber auch im Genom von *Serpula lacrymans*, als Vertreter der Basidiomyceten, konnte ein Gen (*nps1*) nachgewiesen werden, das für eine NRPS mit diesem Aufbau kodiert (Eastwood et al., 2011).

Noch ausgeprägter sind die scheinbar unvollständigen Module einer NRPS bei den Siderophorsynthetasen. Diese multimodularen Enzyme (Initiationsmodul und Elongationsmodule) haben charakteristischerweise zwei C-terminale C-T-Didomänen mit einer abschließenden C-Domäne (Schwecke et al., 2006). Diese Strukturen sind z. B. bekannt durch SidC (A-T-C-A-T-C-A-T-C-T-C-T-C) aus *Aspergillus fumigatus* für die Biosynthese von Ferricrocin (Reiber et al., 2005; Schrettl et al., 2007) oder durch Fer3 (A-T-C-A-T-C-A-T-C-T-C-T-C), die Ferrichrome A-Synthetase aus *Ustilago maydis* (Winterberg et al., 2010). Die Biosynthese der Siderophore, kleine Moleküle, die mit dreiwertigen Eisenionen Chelate bilden, ist für Bakterien und Ascomyceten umfangreich beschrieben (Haas, 2003; Schwecke et al., 2006; Haas, 2012; Dimpka, 2016). Siderophore aus Basidiomyceten sind allerdings wenig erforscht (Welzel et al., 2005; Haselwandter et al., 2006; Winterberg et al., 2010). Mithilfe von Sequenzanalysen, die für verschiedene Basidiomyceten durchgeführt wurden (Eastwood et al., 2011; Fernandez-Fueyo et al., 2012; Floudas et al., 2012; Shah et al., 2016), konnte ein hoch konserviertes Gen, welches für eine Siderophorsynthetase bestehend aus sieben Domänen kodiert (nur eine A-Domäne), identifiziert werden. Die Aufklärung der Biosynthese, ausgehend von dieser besonderen NRPS, und der damit verbundene tiefere Einblick in die Vielseitigkeit pilzlicher peptidischer Naturstoffe, soll im Rahmen dieser Arbeit erfolgen. Dafür wurde *Ceriporiopsis subvermispora* als Modellorganismus gewählt (Fernandez-Fueyo et al., 2012). Dieser Weißfäuleerreger ist von großem biotechnologischen Interesse, da er in der Lage ist, Lignin zu depolymerisieren und dabei wenig Cellulose

abzubauen. Als Modellorganismus attraktiv ist *C. subvermispora* aufgrund seines sehr kleinen Sets an Naturstoffgenen. Anhand von Sequenzanalysen konnten drei Gene, die für NRPSs bzw. NRPS-ähnliche Enzyme kodieren, zwei Gene, die für PKSs kodieren und ein Gen entschlüsselt werden, das für eine PKS-NRPS-Hybride kodiert.

2. Zielsetzung dieser Arbeit

Zum besseren Verständnis der Vielfalt der pilzlichen NRPSs wurden im Rahmen dieser Promotionsarbeit nichtkanonische NRPSs untersucht.

2.1 Untersuchung adenylierender Reduktasen aus *Heterobasidion annosum* (Russuales) und *Serpula lacrymans* (Boletales)

Adenylierende Reduktasen mit der Domänenarchitektur A-T-R wurden für verschiedene Ascomyceten und Basidiomyceten klassifiziert. Um die Klassifizierung biochemisch zu unterlegen, sollten verschiedene minimalen NRPS-ähnlichen Enzyme aus Basidiomyceten biochemisch charakterisiert werden. Ziele waren

1. Die biochemische Bestimmung der Substratspezifität.
2. Die Einordnung der untersuchten Reduktasen in die bereits bekannten Gruppen.

2.2 Charakterisierung der Siderophorsynthetase CsNPS2 aus *Ceriporiopsis subvermispora*

Anders als für Ascomyceten ist über Siderophorsynthetasen aus Basidiomyceten relativ wenig bekannt. Mit der steigenden Anzahl bekannter Basidiomyceten-Genomsequenzen konnte ein hoch konserviertes Gen identifiziert werden, welches vermutlich für eine Siderophorsynthetase kodiert. Folgende Fragen standen im Vordergrund:

1. Ist die Expression von Cs*NPS2* aus *Ceriporiopsis subvermispora* abhängig vom Eisengehalt im Medium und kann somit bestätigt werden, dass es sich bei CsNPS2 um eine Siderophorsynthetase handelt?
2. Kann die heterologe Expression von Cs*NPS2* in *Aspergillus niger* etabliert und die Substratspezifität sowie das Produkt *in vitro* bestimmt werden?
3. Kann das *in vitro* erzeugte Produkt auch *in vivo* nachgewiesen werden?

2.3 Charakterisierung der A-Domäne von FsqF aus *Aspergillus fumigatus*

In der Vergangenheit fokussierte sich die Naturstoffforschung hauptsächlich auf Gencluster, die Gene für multimodular aufgebaute Enzyme beinhalten. Das Cluster *fsq* aus *A. fumigatus* charakterisiert sich durch ein Gen *fsqF* für ein NRPS-ähnliches Enzym. Dieses sollte folgendermaßen analysiert werden:

> Kann FsqF heterolog produziert und mittels ATP-[^{32}P]-Pyrophosphat-Austausch-Assay die Substratspezifität der A-Domäne bestimmt werden?

Vergleichende Metabolomanalysen der Arbeitsgruppe um Frank C. Schroeder (Cornell University, Ithaca, NY) zeigten, dass ausgehend von diesem Gencluster verschiedene Isoquinolin-Alkaloide (Fumisoquine) produziert werden. So sollte diese Charakterisierung einen Beitrag zur Aufklärung der Biosynthese leisten.

3. Publikationen

3.1 Publikation 1, Brandenburger et al. (2016), *Fungal Genetics and Biology*

Multi-genome analysis identifies functional and phylogenetic diversity of basidiomycete adenylate-forming reductases.

Eileen Brandenburger, Daniel Braga, Anja Kombrink, Gerald Lackner, Julia Gressler, Markus Künzler, Dirk Hoffmeister.

Fungal Genet. Biol. (2016) DOI:10.1016/j.fgb.2016.1007.1008 (In Druck, akz. 14.7.2016)

Die Biosynthese nichtribosomal gebildeter Peptide (NRP), eine strukturell vielfältige Naturstoffklasse wird durch multimodulare nichtribosomale Peptidsynthetasen (NRPSs) katalysiert. Eine besondere Form bilden die adenylierenden Reduktasen mit monomodularem Aufbau, bestehend aus einer Adenylierungs-, einer Thiolierungs- und einer Reduktasedomäne. Phylogenetisch werden diese Reduktasen in vier Klassen eingeteilt. Es wurden adenylierende Reduktasen aus *Heterobasidion annosum* (Russulales) und *Serpula lacrymans* (Boletales) sowie *Coprinopsis cinerea (*Agaricales) heterolog erzeugt und *in vitro* Analysen zur Substratspezifitätsbestimmung eingesetzt. NPS9 und NPS11 aus *S. lacrymans* aktivieren L-Threonin bzw. Benzoesäure, NPS10 aus *H. annosum* aktiviert Phenylbrenztraubensäure. In den Reaktionen mit den Reduktasen 03009 und 06235 aus *C. cinerea* wurden Umsätze für die Substrate L-Serin, L-Alanin und L-Valin nachgewiesen. In der Klasse III der adenylierenden Reduktasen konnte somit ein zuvor unbekannter phylogenetischer Zweig identifiziert werden. Darüber hinaus zeigen die Ergebnisse sehr deutlich, dass diese Enzymklasse funktionell vielseitiger ist, als bisher angenommen.

Angaben zum Eigenanteil von E. Brandenburger (45 %)

Herstellung der Plasmide pEB05/06/18/20, Anleitung zur Herstellung der Plasmide pEB31/32, heterologe Genexpression, Produktion von NPS9, NPS11 und NPS10 in *E. coli*, Proteinaufreinigung und Analyse, Bestimmung der Substratspezifität sowie des pH- und Temperaturoptimums für NPS9 und NPS11, Mitarbeit an der Erstellung des Manuskriptes.

Fungal Genetics and Biology xxx (2016) xxx–xxx

Contents lists available at ScienceDirect

Fungal Genetics and Biology

journal homepage: www.elsevier.com/locate/yfgbi

Regular Articles

Multi-genome analysis identifies functional and phylogenetic diversity of basidiomycete adenylate-forming reductases

Eileen Brandenburger [a], Daniel Braga [a], Anja Kombrink [b], Gerald Lackner [c], Julia Gressler [a], Markus Künzler [b], Dirk Hoffmeister [a,*]

[a] Friedrich-Schiller-Universität Jena, Department Pharmaceutical Microbiology at the Hans-Knöll-Institute, Winzerlaer Strasse 2, 07745 Jena, Germany
[b] ETH Zürich, Institute of Microbiology, Vladimir-Prelog-Weg 4, 8093 Zürich, Switzerland
[c] Friedrich-Schiller-Universität Jena, Junior Research Group Synthetic Microbiology at the Hans-Knöll-Institute, Adolf-Reichwein-Strasse 23, 07745 Jena, Germany

ARTICLE INFO

Article history:
Received 22 April 2016
Revised 8 July 2016
Accepted 14 July 2016
Available online xxxx

Keywords:
Coprinopsis
Genome
Heterobasidion
Nonribosomal peptide synthetase
Reductase
Serpula

ABSTRACT

Among the invaluable benefits of basidiomycete genomics is the dramatically enhanced insight into the potential capacity to biosynthesize natural products. This study focuses on adenylate-forming reductases, which is a group of natural product biosynthesis enzymes that resembles non-ribosomal peptide synthetases, yet serves to modify one substrate, rather than to condense two or more building blocks. Phylogenetically, these reductases fall in four classes. The phylogeny of *Heterobasidion annosum* (Russulales) and *Serpula lacrymans* (Boletales) adenylate-forming reductases was investigated. We identified a previously unrecognized phylogenetic branch within class III adenylate-forming reductases. Three representatives were heterologously produced and their substrate preferences determined *in vitro*: NPS9 and NPS11 of *S. lacrymans* preferred L-threonine and benzoic acid, respectively, while NPS10 of *H. annosum* accepted phenylpyruvic acid best. We also investigated two class IV adenylate-forming reductases of *Coprinopsis cinerea*, which each were active with L-alanine, L-valine, and L-serine as substrates. Our results show that adenylate-forming reductases are functionally more diverse than previously recognized. As none of the natural products known from the species investigated in this study includes the identified substrates of their respective reductases, our findings may help further explore the diversity of these basidiomycete secondary metabolomes.

1. Introduction

Over the past years, genomic sequencing of Agaricomycotina species has greatly gained momentum. Only counting species included in the Joint Genome Institute's MycoCosm portal (Grigoriev et al., 2012), sequence data for more than 150 species have been released as of March of 2016. These efforts allowed for more profound understanding into plant biopolymer deconstruction and, consequently, use of basidiomycetes for bio-based industrial processes like bioethanol and renewable energy production (Fernandez-Fueyo et al., 2012; Hori et al., 2014). Given their relevance as heterotrophic partners in symbioses, genomic sequencing of (ecto-)mycorrhizal fungi vastly supports research into the ecology, e.g., of forest ecosystems (Kuo et al., 2014). Initially less evident, the basidiomycete post-genomic era also brought about another invaluable benefit: it taught us that the number of genetically encoded natural product pathways clearly exceeds the number of products or product families known from the respective species. For polyketide synthases (PKSs), an average of four genes per genome was found, based on 35 analyzed genomes. The sequenced Pucciniomycotina species lacked PKS genes, and as many as 11 PKS genes were found in the *Gloeophyllum trabeum* genome (Lackner et al., 2012).

Numerous available genome sequences have dramatically facilitated functional characterization of basidiomycete natural product genes and enzymes. Capitalizing on mainly basidiomycete sequence data, a recent phylogenetic study provided insight into the diversity of adenylate-forming reductases (Kalb et al., 2014). Featuring a tri-domain layout composed of an adenylation (A) a thiolation (T), and a terminal short chain dehydrogenase/reductase (SDR) domain (Fig. 1), these reductases resemble nonribosomal peptide synthetases (NRPSs), yet lack a condensation domain for amide bond formation. Instead, they adenylate and then covalently tether an amino or carboxylic acid as a thioester, which is then reductively released. Traditionally, adenylate-forming reductases, such as *S. cerevisiae* Lys2 (Ehmann et al., 1999) have been associated with L-α-aminoadipic acid reduction into its 6-semialdehyde

* Corresponding author.
E-mail address: dirk.hoffmeister@leibniz-hki.de (D. Hoffmeister).

http://dx.doi.org/10.1016/j.fgb.2016.07.008
1087-1845/

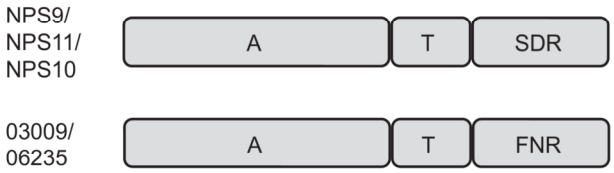

Fig. 1. Domain composition of basidiomycete adenylate-forming reductases NPS9 and NPS11 of *S. lacrymans*, and NPS10 of *H. annosum* (top), as well as of 03009 and 06325 of *C. cinerea* (bottom). Domain abbreviations: A, adenylation; FNR, ferredoxin-NADP$^+$ reductase; SDR, short chain dehydrogenase/reductase; T, thiolation.

during fungal L-lysine biosynthesis. However, closer inspection showed that four phylogenetically distinct classes exist (Kalb et al., 2014). Class I (Fig. 2) represents the above mentioned Lys2-type fungal L-lysine biosynthesis enzymes, class II comprises L-tyrosine reductases, while the class III has been described as aryl acid reductases, with the *Aspergillus terreus* orsellinic acid reductase ATEG_03630 being the only characterized representative (Wang et al., 2014). Unlike these three classes, the fourth class, exemplified by the *Ceriporiopsis subvermispora* L-serine reductase NPS1, possesses a ferredoxin: NADP$^+$ reductase (FNR) domain, rather than an SDR, as terminal reductive domain (Fig. 1).

Here, we report on a study that combines genomics with a biochemical *in vitro* investigation of basidiomycete adenylate-forming reductases. Our results demonstrate a previously unrecognized phylogenetic and functional diversity within class III. The newly characterized basidiomycete members in this class are represented by the *Serpula lacrymans* reductases NPS9 and NPS11, and by *Heterobasidion annosum* NPS10 (Table 1). These enzymes are dissimilar in their substrate preferences both among each other and from the prototypical class III enzyme ATEG_03630 of *A. terreus*. We also report biochemical characterization of two class IV adenylate-forming reductases of *Coprinopsis cinerea* Amut Bmut, encoded by genes orthologous to CC1G_06235 and CC1G_03009, respectively, in *C. cinerea* strain Okayama 7, and hereafter referred to as enzymes 06235 and 03009, Table 1). We provide evidence that the functional diversity in class IV is also greater than previously assumed and not restricted to L-serine reduction, as previously thought. Taken together, this study underscores how natural product research is supported by genomics-based discovery of biosynthesis enzymes to help explore the realm of basidiomycete metabolism.

2. Materials and methods

2.1. Microbial strains, culture conditions, and general methods

Serpula lacrymans S7 (Tlalka et al., 2008) was grown at 25 °C on MEP agar (per liter: 30 g malt extract, 3 g soy peptone, 18 g agar, pH = 5.6). *H. annosum* JMRC 9984 (Lind et al., 2005) was grown at 25 °C on 4% (w/v) Sabouraud solid medium, and *C. cinerea* AmutBmut (Swamy et al., 1984) was grown at 37 °C on 1.5% (w/v) YMG agar (0.4% (w/v) yeast extract, 1% (w/v) malt extract, 0.4% (w/v) glucose). *Escherichia coli* was routinely grown in LB medium, amended with carbenicillin (50 μg/ml) or kanamycin (50 μg/ml) when appropriate. Strain XL-1 blue was used for cloning and preparation of plasmid DNA, strains BL21(DE3) and KRX were used to produce reductases heterologously. DNA restriction, ligation, and other molecular genetics procedures were carried out following standard protocols (Sambrook and Russell, 2000) and in accordance with the manufacturer's instructions. Kits and enzymes were procured from Fermentas, NEB, Promega, Qiagen, Roche, Thermo Fisher Scientific, and Zymo Research. Chemicals were purchased from Sigma-Aldrich, BD, Roth and VWR, [^{32}P]pyrophosphate was purchased from PerkinElmer.

2.2. cDNA cloning and construction of expression plasmids

To prepare *S. lacrymans* and *H. annosum* for RNA extraction, they were grown on a sterile nylon membrane (Amersham Biosciences) placed on the respective agar media (see Section 2.1). To isolate total RNA from mycelium, the SV Total RNA isolation kit (Promega) was used. DNase treatment was repeated in the case of *H. annosum*. Total *C. cinerea* RNA was extracted using the RNeasy Lipid Tissue Mini Kit (Qiagen) according to manufacturer's protocol. First strand cDNA syntheses were performed in a total volume of 20 μl. The reactions were carried out at 42 °C for 60 min and consisted of the 18-mer oligo(dT)-primer (20 μM), 40 units of M-MuLV reverse transcriptase, 20 units of RiboLock RNase Inhibitor, deoxynucleoside triphosphates (dNTPs, 10 mM each) and the buffer supplied with the enzyme. An aliquot of the reaction (2 μl) was used as template in subsequent PCRs. The reaction (20 μl) consisted of 0.2 mM of each dNTP, 20 pmol (each) oligonucleotide primer (Table 2), 2 mM $MgCl_2$, and 0.4 U Phusion High Fidelity DNA polymerase in the supplied buffer.

For RNA isolation, vegetative mycelium of *C. cinerea* was grown on 5 mm glass beads submerged in liquid minimal medium as previously described (Essig et al., 2014). After harvesting, the mycelium was lyophilized. Qiazol (Qiagen) and 0.5 mm glass beads were added and the cells were lysed in three FastPrep steps. *C. cinerea* cDNA was synthesized using Transcriptor Universal cDNA Master (Roche) and used as template for the amplification of genes CC1G_06235 and CC1G_03009 by PCR with Phusion high fidelity DNA polymerase (Thermo Scientific), using primer pairs PF_06235/PR_06235 and PF_03009/PR_03009 (Table 2). PCR conditions were: 30 s at 98 °C; 30 cycles of 98 °C for 10 s, 65 °C for 15 s and 72 °C for 120 s and a final extension of 10 min at 72 °C. The PCR products were ligated to the pGEM-T vector (Promega) resulting in plasmids pGEM_03009 and pGEM_06235.

The *S. lacrymans* gene encoding NPS9 was amplified from cDNA with the primer pair oEB01/04. Thermal cycling parameters were: 30 s at 98 °C; 35 cycles of 98 °C for 10 s, 63 °C for 15 s and 72 °C for 105 s, followed by a terminal hold 5 min at 72 °C. The PCR product was ligated into the pJET1.2 vector to create pEB05. The *nps9* gene was then re-amplified in a second PCR, using the conditions above but 20 cycles and primers oEB33/34, and subsequently inserted into pET28b between the NcoI and SacI sites, to yield expression plasmid pEB18. The *nps11* gene was amplified using primers oEB19/oEB20 and the parameters described above but an annealing temperature of 54 °C to create pEB06. This plasmid was used to re-amplify the gene with primers oEB35/36 to introduce SalI and XhoI sites, using the above parameters. The PCR product was ligated into pET28b via these restriction sites to create expression plasmid pEB20. Plasmids pEB18 and pEB20 serve to produce *N*-terminally hexahistidine-tagged proteins.

The *H. annosum* gene encoding NPS10 was amplified from cDNA using the primer pair oEB72/73. Thermal cycling parameters were as described above for NPS9. The PCR product was inserted into the pJET1.2 cloning vector to yield pEB31. The insert was then released by NcoI and HindIII restriction and inserted into pET28b to yield pEB32 for production of a *C*-terminal NPS10-hexahistidine fusion protein.

The plasmids pGEM_03009 and pGEM_06235 encode the AT didomain of *C. cinerea* CC1G_06235 and the A domain of CC1G_03009, respectively. These genes were amplified with primer pairs oDB29/55 and oDB31/32, using the same PCR protocol, but with an annealing temperature of 63 °C and a polymerization time of 45 s at 72 °C. The primer pairs introduced NdeI/EcoRI and NheI/EcoRI sites, respectively, which were used to ligate the PCR

Please cite this article in press as: Brandenburger, E., et al. Multi-genome analysis identifies functional and phylogenetic diversity of basidiomycete adenylate-forming reductases. Fungal Genet. Biol. (2016), http://dx.doi.org/10.1016/j.fgb.2016.07.008

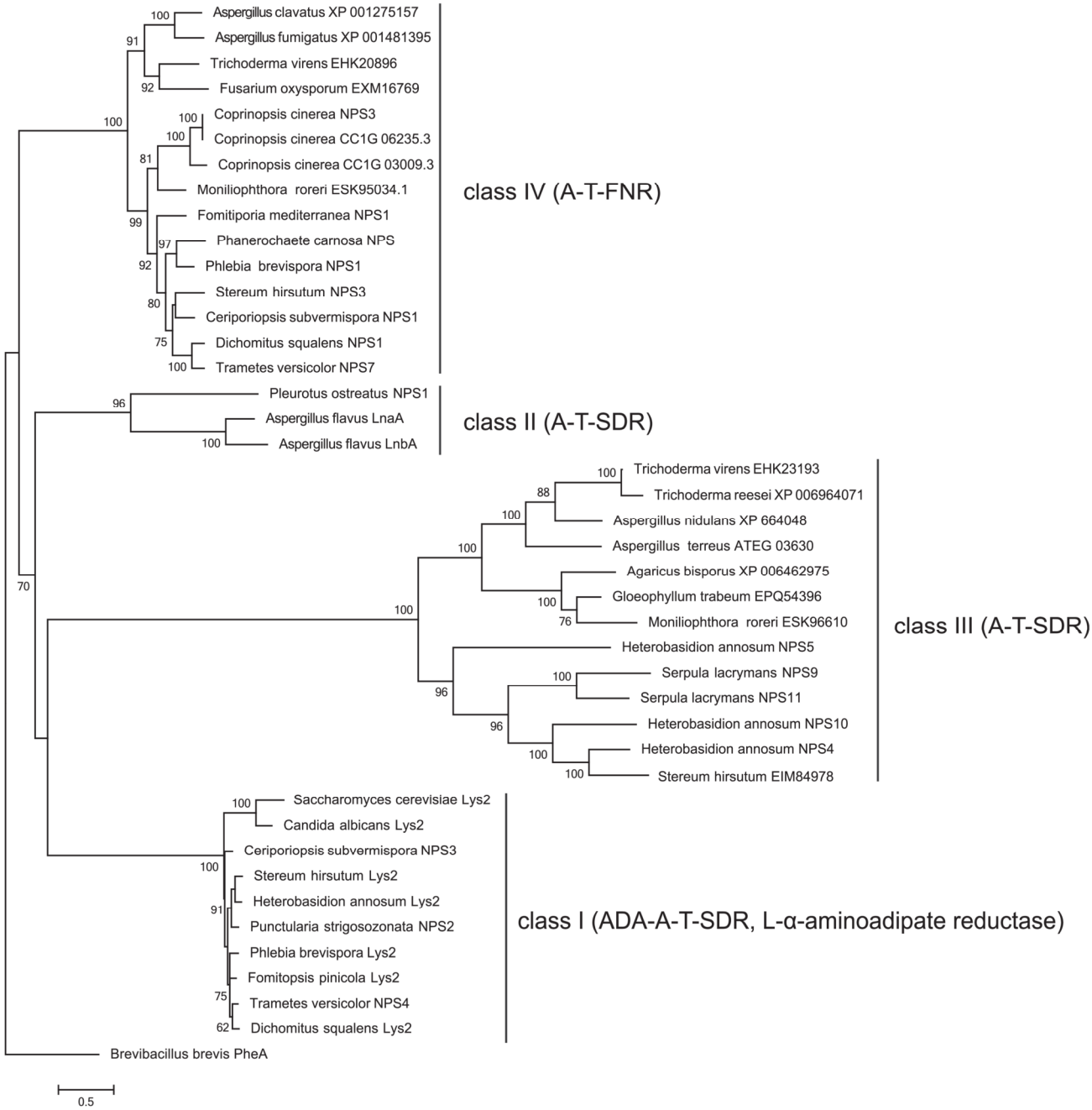

Fig. 2. Phylogenetic tree of adenylation domains taken from fungal adenylate-forming reductases. The percentage of trees in which the associated taxa clustered together is shown next to the branches. The tree is drawn to scale, with branch lengths measured in the number of substitutions per site. All positions with less than 95% site coverage were eliminated, that is, fewer than 5% alignment gaps, missing data, and ambiguous bases were allowed at any position. There were a total of 356 positions in the final dataset. Confirmed substrates of individual enzymes and the phylogenetically supported clades are indicated (reductase classes I–IV). The tree was rooted using the model adenylation domain PheA of *Brevibacillus brevis* as outgroup. Domain abbreviations: A, adenylation; FNR, ferredoxin-$NADP^+$ reductase; SDR, short chain dehydrogenase/reductase; T, thiolation, ADA, adenylation activating domain. Sequences were published by Goffeau et al., 1996; Suvarna et al., 1998; Galagan et al., 2005; Nierman et al., 2005; Martinez et al., 2008; Ma et al., 2010; Stajich et al., 2010; Eastwood et al., 2011; Kubicek et al., 2011; Arnaud et al., 2012; Fernandez-Fueyo et al., 2012; Floudas et al., 2012; Morin et al., 2012; Olson et al., 2012; Suzuki et al., 2012; Binder et al., 2013; Forseth et al., 2013; Meinhardt et al., 2014; Riley et al., 2014; Wang et al., 2014. Accession numbers are provided in Table S2.

products to the pET28a vector, restricted equally. The resulting plasmids (pDB035 and pDB036) encode the respective *N*-terminal hexahistidine fusions.

2.3. Heterologous protein production and purification

Escherichia coli BL21(DE3) was transformed with plasmids pEB18 and pEB20, respectively. *E. coli* KRX was individually transformed with pDB035, pDB036, and pEB32. Overnight pre-cultures (5 ml, 37 °C, 180 rpm) were used to inoculate the respective 400 ml production cultures, grown equally. Once an optical density (OD_{600} = 0.45) was reached, the temperature was lowered to 16 °C to express *S. lacrymans nps9*, *nps11*, *H. annosum nps10,* and *C. cinerea* CC1G_03009 and CC1G_06235 reductase genes, respectively. Gene expression was induced with 1 mM IPTG for 24 h (0.1% L-rhamnose for *C. cinerea* and *H. annosum* genes). Cells were

Table 1
Basidiomycete adenylate-forming reductases biochemically characterized in this study.

Enzyme	Accession [#a]	Length (aa)[b]	Species	Verified substrate(s)
NPS9	KX118590	1096	*Serpula lacrymans*	L-Threonine
NPS11	KX118591	1099	*Serpula lacrymans*	Benzoic acid
NPS10	KX118589	1088	*Heterobasidion annosum*	Phenylpyruvic acid
				Benzoic acid
03009	KX118593	1025	*Coprinopsis cinerea*	L-Alanine
				L-Valine
				L-Serine
06235	KX118592	1026	*Coprinopsis cinerea*	L-Alanine
				L-Valine
				L-Serine

[a] Refers to GenBank.
[b] Refers to the full-length native protein.

harvested by centrifugation (4 °C, 3200*g*, 20 min). After resuspending the cell paste in lysis buffer (50 mM $NaH_2PO_4{\cdot}H_2O$, 300 mM NaCl, 10 mM imidazole, pH 8.0), cells were disrupted with a Sonopuls ultrasonic sonifier (Bandelin). Cell debris was removed by centrifugation (4 °C, 17,000*g*, 20 min).

Protein purification was performed by nickel affinity chromatography on an Äkta Pure FPLC system, equipped with a His-Trap FF crude column (GE Healthcare). Buffer A was 50 mM NaH_2PO_4, 300 mM NaCl, pH 7.5, buffer B was 500 mM imidazole in buffer A. A step gradient 5–12% B (equivalent to 25–60 mM imidazole) within 10 min was used to separate proteins. Elution was performed at 100% B. Proteins were desalted on a PD-10 desalting column (GE Healthcare) and eluted with reaction buffer (100 mM Tris, pH = 7.5, 5 mM $MgCl_2$, 125 nM EDTA). Protein purification was verified by polyacrylamide gels, the protein concentration was determined by Bradford's assay (Bradford, 1976).

2.4. Biochemical assays

Substrate preferences of A domains were determined *in vitro* by the substrate-dependent ATP-[^{32}P]pyrophosphate exchange assay. All reactions were run in triplicates. The reactions were composed of reaction buffer (above), 1 mM substrate, either added as pools (Table S1), or individual pure compounds, 100 nM purified enzyme and 0.1 μM [^{32}P]pyrophosphate (50 Ci/mmol). *S. lacrymans* NPS9 (NPS11) was assayed at pH 7.0 (8.5) and 20 °C (25 °C) which were determined as optimum conditions. *H. annosum* NPS10 and *C. cinerea* enzymes were assayed at pH 7.5 and 25 °C, respectively. The reaction volume was 100 μl. The reactions were stopped after 30 min and further processed as described (Schneider et al., 2008). Radioisotope exchange was quantified on a PerkinElmer TriCarb 2910TR scintillation counter.

2.5. In silico methods and phylogeny

Analysis of the nonribosomal code *in silico* was performed with the NRPSpredictor2 (Röttig et al., 2011). The evolutionary history of A domains was inferred by using the Maximum Likelihood method based on the model by Le and Gascuel (1993). The tree with the highest log likelihood (−19906.0967) is shown. Evolutionary analyses were conducted in MEGA6 (Tamura et al., 2013).

3. Results and discussion

3.1. Phylogeny

We refined a prior phylogenetic tree (Kalb et al., 2014) of A domains of 35 asco- and basidiomycete adenylate-forming reductases whose coding sequences were identified in the respective genomes. Our objective was to represent the Boletales in this tree and to include more sequence data of the Russulales, which were only represented by two sequences of *Stereum hirsutum*, one thereof taken from an L-α-aminoadipate reductase. To this end, we included an additional five A domain sequences of *H. annosum* and *S. lacrymans*. The constructed tree was consistent with the previously identified four classes I through IV, along with PheA of *Brevibacillus brevis* as the outgroup (Fig. 2, Table S2). However, the class III clade was split in two major branches, with the *S. lacrymans*, *H. annosum*, and *S. hirsutum* sequences clustering on one branch. Surprisingly, this split did not correlate with the basidiomycete versus ascomycete origin of the sequences, as the second branch, in itself, had maintained the previously recognized diverging sub-branches of asco- and basidiomycete sequences. Given this

Table 2
Oligonucleotide primers used in this study.

Primer	Sequence (5′ to 3′)	Restriction site
oDB29	CGTAGCCATATGATGGGCAGCGATCTGCTTTCTC	NdeI
oDB31	CGTATAGCTAGCATGGCTTCTTCAGATCTCCTCTCG	NheI
oDB32	CGACTGAATTCTTAGGTGTTGGTTGAGCCGAGACTGTGG	EcoRI
oDB55	CGATTGAATTCTTAGCACCAGAATGGATACCACC	EcoRI
oEB01	TCC TTA CCA TGG CAC CGG GAC GTG	NcoI
oEB04	TCG ACG GAG CTC GAG AAC AAG CCT CTT GC	SacI
oEB06	CTA TTT ACC ATG GCA GAT CCC AGC	NcoI
oEB09	CTG GAT GCG GCC GCC ATA AAC ATT CCC TTT G	NotI
oEB19	CCT TGC ATT AGG CCC ATT AC	–
oEB20	CAG TCT GCT CAG ATT CCA TG	–
oEB33	ATT GAG CTC TAT GGC ACC GGG AG	SacI
oEB34	GAC GGA GCT CTC AGA ACA AGC CTC	SacI
oEB35	GGA GAG TCG ACA TGG CAG ATC CC	SalI
oEB36	GCT CGA CTC GAG TTA CAT AAA CAT TCC C	XhoI
oEB72	GAA CCA TGG GAA TGT CTT CCG TG	NcoI
oEB73	CGG AGA AGC TTA GCA GGA AAG AAC	HindIII
PF_06235	ATGGGCAGCGATCTGCTTTC	–
PR_06235	TTACGAATCCCAGATGGCACCAAAG	–
PF_03009	ATGGCTTCTTCAGATCTCCTCTC	–
PR_03009	TTAGGAGTCCCAGATGGCG	–

Please cite this article in press as: Brandenburger, E., et al. Multi-genome analysis identifies functional and phylogenetic diversity of basidiomycete adenylate-forming reductases. Fungal Genet. Biol. (2016), http://dx.doi.org/10.1016/j.fgb.2016.07.008

unexpected finding of a second branch within class III, that does not contain characterized members, we chose the genes that encode NPS9 and NPS11 in *S. lacrymans* (Table 1), as well as the gene coding for *H. annosum* NPS10 reductase for further investigation.

3.2. Analysis of the nonribosomal code

To initially predict the possible substrates of the selected *Heterobasidion* and *Serpula* reductases, their A domains were analyzed for the so-called nonribosomal code (Stachelhaus et al., 1999; May et al., 2002). This term describes a set of mostly non-adjacent residues within the A domain primary sequence that line its substrate binding pocket. The first position of this code is usually represented by an aspartate residue (D235 in the prototypical A domain PheA of *Brevibacillus brevis*, Stachelhaus et al., 1999), whose negatively charged side chain electrostatically interacts with the positive charge of the substrate's α-amino group. For A domains accepting substrates other than α-amino acids (α-keto acids, dihydroxybenzoic acid, orsellinic/anthranilic acid, fumaric acid) this aspartate residue is replaced by valine, asparagine, glycine, or serine, respectively (May et al., 2002; Cheng, 2006; Ames and Walsh, 2010; Steinchen et al., 2013; Wang and Zhao, 2014). Therefore, the first position of the code has predictive value regarding the substrate properties. The last position of the code is represented by a lysine residue (K517 in PheA) which counters the positive charge of the substrate carboxy group. Although essential for enzymatic function, this residue is not relevant for substrate prediction. Using NRPSpredictor2 software (Röttig et al., 2011), we attempted to extract the code of the three *H. annosum* and *S. lacrymans* reductases. However, this software did not recognize an A domain in the NPS9 and NPS11 sequences. An incomplete code was extracted from NPS10. In particular, the important positions equivalent to D235 and K517 in PheA were not identifiable. This outcome is likely due to the very limited data set that is available to optimize the software for fungal, and in particular, basidiomycete sequences. Hence, we aligned the sequences of characterized fungal A domains (Figs. S1 and S2), among them ATEG_03630, using ClustalW (Thompson et al., 1994). The alignment was inspected manually. However, no conclusive results were obtained either.

3.3. Substrate specificity profiling of class III adenylate-forming reductases

Given the non-recognizable, apparently highly deviating nonribosomal codes and, hence, unpredictable groups of substrates, we could not exclude a pseudogene scenario, even though reading frames did not seem corrupted. Thus, we sought further clarification and characterized the above class III reductases *in vitro*. cDNAs of *nps9*, *nps11*, and *nps10* were obtained that encode the intron-free genes 3291 bp, 3300 bp, and 3267 bp in length, respectively. The cloned genes were used to construct pET28-based expression vectors for heterologous production of hexahistidine fusion *apo*-proteins in *E. coli* BL21, transformed with pEB19 or pEB20, respectively, and in *E. coli* KRX, transformed with pEB32. The enzymes were purified by immobilized metal affinity chromatography (NPS9: 124.4 kDa, NPS11: 124.2 kDa, NPS10: 120.5 kDa). To identify substrate preferences, substrate pools (Table S1) were first used. They covered all proteinogenic α-amino acids (L- and D-configured), L-ornithin, L-α-aminoadipic acid, and 16 non-amino acid compounds. *In vitro* assays were based on ATP-[^{32}P]pyrophosphate radioisotope exchange reactions. In a subsequent step, individual substrates of positive pools were used to repeat the assays.

S. lacrymans NPS9 showed a clear preference for L-threonine (79,700 cpm, Fig. 3), while other substrates were only modestly accepted. Among them was L-valine with 18,400 cpm as second best substrate, others showed values below 15,000 cpm. The negative control, in which substrate was replaced by water, led to a value of 1800 cpm. The preference for L-threonine shows that a polar group is required at the β-carbon atom, rather than the non-polar methyl substituent of L-valine. All other tested compounds did not serve as substrate. Specifically, NPS9 rejected aryl acids (benzoic acid, 4-hydroxybenzoic acid, orsellinic acid, salicylic acid, 2,3-dihydroxybenzoic acid) evident by values of <6000 cpm, therefore contrasting the prototypical *A. terreus* orsellinic acid reductase ATEG_03630.

Serpula lacrymans NPS11 shares 50% identical amino acids with NPS9. However, its substrate preference turned out markedly different: amino acids, regardless of configuration, were only minimally turned over. Benzoic acid was identified as optimum substrate (55,600 cpm, Fig. 3), while none of its derivatives including orsellinic acid was accepted (<1000 cpm). Considering the dissimilar substrates of NPS11 and ATEG_03630 (benzoic acid and orsellinic acid, respectively), we extended the substrate screen for NPS11 and additionally tested 2,4-, 3,4-, and 3,5-dihydroxy benzoic acid, 2,4,6-trihydroxybenzoic acid, and 3,4,5-trihydroxybenzoic acid. Also, *trans*-cinnamic acid, *p*-coumaric acid, and caffeic acid were included. Except *p*-coumaric acid that resulted in a modest turnover (13,100 cpm) by NPS11, none of these compounds led to significant radiolabel exchange in our assay. We therefore conclude that NPS11 represents a benzoic acid reductase.

Next, we proceeded with *H. annosum* NPS10, whose primary sequence shares 34% identical amino acids with NPS11. In our assays, it did not turn over α-amino acids either (neither L- nor D-configured), yet showed clear activity both with phenylpyruvic acid and benzoic acid (74,400 and 63,200 cpm, Fig. 3) whereas turnover of 4-hydroxyphenylpyruvic acid, 4-hydroxybenzoic acid and all other α-keto and aryl acids was markedly lower (<15,000 cpm). While NPS11 clearly preferred benzoic acid over *p*-coumaric acid, i.e., a C6-C1 skeleton over a C6-C3 substrate backbone, NPS10 is remarkable in that it almost equally adenylated substrates with either type of scaffold structure. The slightly higher turnover with phenylpyruvic acid may point to this compound as the true physiological substrate.

3.4. Analysis of Coprinopsis cinerea class IV adenylate-forming reductase

Given the unexpected functional diversity among class III reductases, we then hypothesized that class IV enzymes, previously referred to as L-serine reductases, may be functionally more heterogeneous as well. Prior work included characterization of only one representative, i.e., *Ceriporiopsis subvermispora* NPS1 (Kalb et al., 2014). It was identified as L-serine reductase, yet accepted, at moderate levels, also L-alanine and L-threonine as substrates. Inspection of fungal genomes showed that class IV reductase genes are encoded by numerous asco- and basidiomycetes species of various phylogenetic groups. The majority of enzymes share an identical nonribosomal code (D-M-W-I-A-A-S-I-V-K) with *C. subvermispora* NPS1. However, two basidiomycete reductases, *C. cinerea* enzymes 06235 and 03009, whose deduced primary sequences share 78% identical amino acids, deviate in this respect and show the code D-F-W-F-V-A-A-I-A-K. According to the global phylogenomic survey on fungal NRPSs by Bushley and Turgeon (2010), these *C. cinerea* enzymes fall into the basidiomycete NPS12 group 1.

The above dissimilar nonribosomal code may point to a diverging substrate preference. Consequently, these two enzymes were included in this study as well and heterologously produced. As

Please cite this article in press as: Brandenburger, E., et al. Multi-genome analysis identifies functional and phylogenetic diversity of basidiomycete adenylate-forming reductases. Fungal Genet. Biol. (2016), http://dx.doi.org/10.1016/j.fgb.2016.07.008

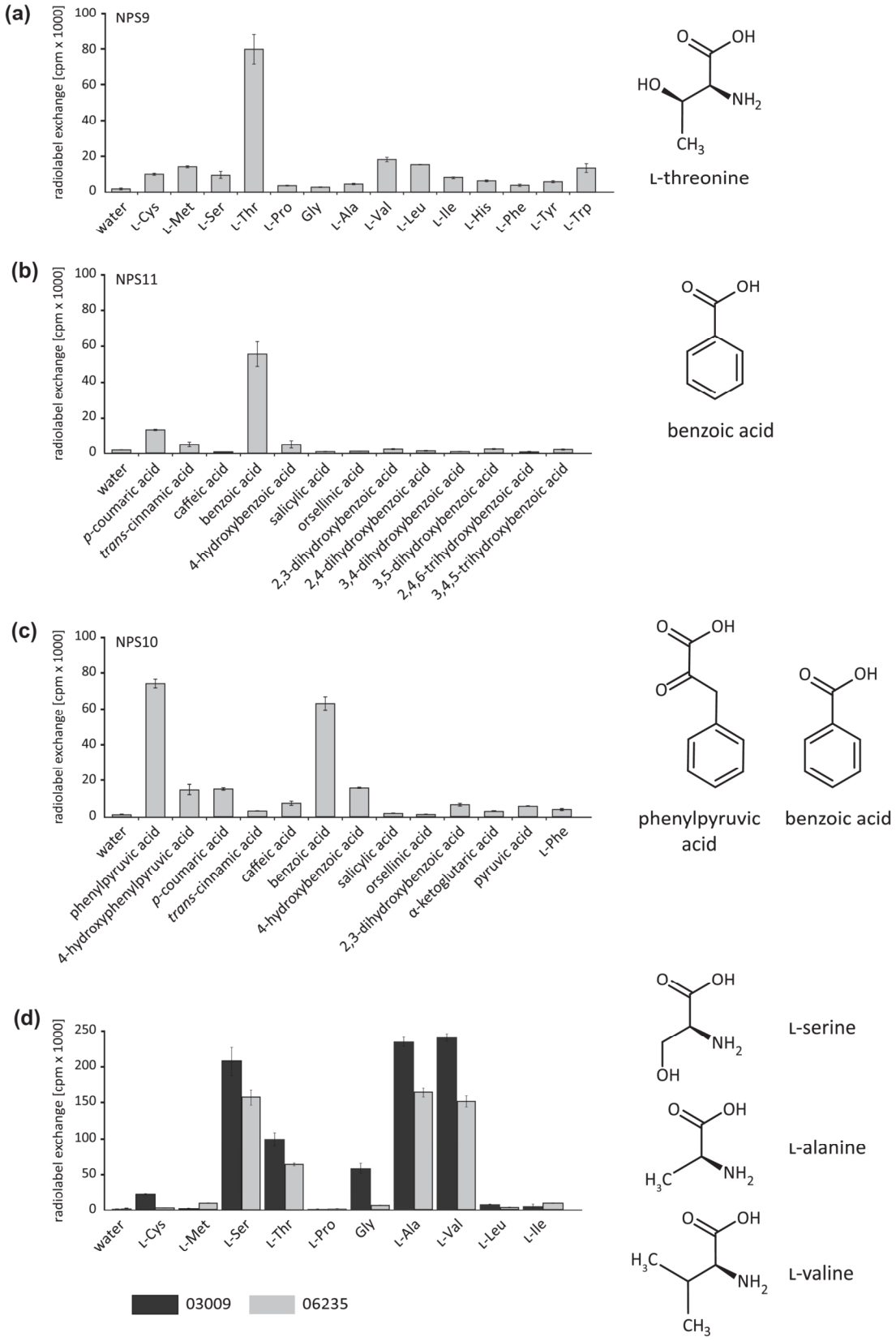

Fig. 3. Substrate specificities of adenylate-forming reductases NPS9 (A), NPS 11 (B), NPS10 (C), and 06325 and 03009 (D), as determined with the ATP-[^{32}P]pyrophosphate radiolabel exchange assay. The preferred substrate(s) are shown for each enzyme. Error bars indicate the standard deviation.

either full-length protein showed instabilities, we resorted to heterologous expression of partial genes in *E. coli* KRX as host, transformed with expression plasmids pDB035 or pDB36, respectively. They encode the A-T di-domain of 06235 and the A domain

Please cite this article in press as: Brandenburger, E., et al. Multi-genome analysis identifies functional and phylogenetic diversity of basidiomycete adenylate-forming reductases. Fungal Genet. Biol. (2016), http://dx.doi.org/10.1016/j.fgb.2016.07.008

of 03009 as *N*-terminally hexahistidine fusions (720 aa, 78.5 kDa and 585 aa, 62.8 kDa, respectively).

As with the above class III reductases, 06235 and 03009 were assayed in a two-step procedure with pools and individual substrates. Only two L-amino acid pools led to measurable turnover in the ATP-[^{32}P]pyrophosphate exchange assay. For both enzymes, single-substrate reactions showed almost equal preference for L-alanine, L-serine, and L-valine, as evident by the observed cpm values for 06235 (164,300, 158,100, and 151,900 cpm, respectively) and 03009 (235,100, 208,800, and 241,400 cpm, respectively, Fig. 3). In both cases, and as with *C. subvermispora* NPS1, L-threonine was accepted, too, but led to lower turnover (42,500 and 62,900 cpm). Unlike 06235, the reductase 03009 also used glycine (58,500 cpm). Taken together, these findings on the specificity of *C. cinerea* enzymes corroborate the notion of fungal adenylate-forming reductases being functionally more heterogeneous than previously recognized.

4. Conclusions

This study covers the analysis of adenylate-forming reductases that are encoded by from Boletales, Russulales, and Agaricales species: the dry rot fungus *S. lacrymans* (Boletales) is best known for its economic burden of timber structures as it has the potential to decompose wooden elements in buildings, while *H. annosum* (Russulales) is a serious pathogen in managed coniferous forests, causing root rot (Kauserud et al., 2012; Karlsson et al., 2003). Consequently, their metabolism including the structure of natural products has been analyzed in the past (Kepler et al., 1967; Bresinsky, 1973; Hirotani et al., 1977; Donnelly et al., 1987; Aqueveque et al., 2002). *Coprinopsis cinerea* (Agaricales) is a well-established model species to study development and other aspects of fungal biology, but has also been investigated for its capacity to synthesize natural products (Bu'Lock and Darbyshire, 1976; Lopez-Gallego et al., 2010). However, none of the reported secondary metabolites of the above species requires the incorporation or reduction of compounds that we identified as substrates of the respective five class III or IV reductases, which in themselves show heterogeneous substrate preferences. We identified structural elements of metabolites yet to be discovered from these three phylogenetically distant species. Hence, this report may promote research into mapping their secondary metabolome more profoundly and support efforts based on protein crystallization, to understand non-canonical and yet to be deciphered nonribosomal codes of the respective A domains. Eventually, this will help make predictive algorithms, computational substrate affinity searches, and functional annotations of basidiomycete genomic data more accurate.

Acknowledgment

This work was supported by the Deutsche Forschungsgemeinschaft (DFG grant HO2515/6-1 to D.H.). D.B. acknowledges a doctoral fellowship by the International Leibniz Research School (ILRS Mibintact), A.K. acknowledges a postdoctoral fellowship by the ETH Zürich. We thank Matthias Gube, Ph.D. (Georg-August-Universität Göttingen) for providing *Heterobasidion annosum* JMRC9984.

Appendix A. Supplementary material

Supplementary data associated with this article can be found, in the online version, at http://dx.doi.org/10.1016/j.fgb.2016.07.008.

References

Arnaud, M.B., Cerqueira, G.C., Inglis, D.O., Skrzypek, M.S., Binkley, J., Chibucos, M.C., Crabtree, J., Howarth, C., Orvis, J., Shah, P., Wymore, F., Binkley, G., Miyasato, S. R., Simison, M., Sherlock, G., Wortman, J.R., 2012. The *Aspergillus* Genome Database (AspGD): recent developments in comprehensive multispecies curation, comparative genomics and community resources. Nucleic Acids Res. 40, D653–D659.

Ames, B.D., Walsh, C.T., 2010. Anthranilate-activating modules from fungal nonribosomal peptide assembly lines. Biochemistry 49, 3351–3365.

Aqueveque, P., Anke, T., Sterner, O., 2002. The himanimides, new bioactive compounds from *Serpula himantoides* (Fr.) Karst. Z Naturforsch C. 57, 257–262.

Binder, M., Justo, A., Riley, R., Salamov, A., Lopez-Giraldez, F., Sjökvist, E., Copeland, A., Foster, B., Sun, H., Larsson, E., Larsson, K.H., Townsend, J., Grigoriev, I.V., Hibbett, D.S., 2013. Phylogenetic and phylogenomic overview of the Polyporales. Mycologia 105, 1350–1373.

Bradford, M., 1976. A rapid and sensitive method for the quantitation of microgram quantities of protein utilizing the principle of protein-dye binding. Anal. Biochem. 72, 248–254.

Bresinsky, A., 1973. On the chemical nature of some pigments of *Serpula lacrimans*. Z Naturforsch C. 28, 627.

Bu'Lock, J.D., Darbyshire, J., 1976. Lagopodin metabolites and artifacts in cultures of *Coprinus*. Phytochemistry 15, 2004.

Bushley, K.E., Turgeon, B.G., 2010. Phylogenomics reveals subfamilies of fungal nonribosomal peptide synthetases and their evolutionary relationships. BMC Evol. Biol. 10, 26.

Cheng, Y.Q., 2006. Deciphering the biosynthetic codes for the potent anti-SARS-CoV cyclodepsipeptide valinomycin in *Streptomyces tsusimaensis* ATCC 15141. ChemBioChem 7, 471–477.

Donnelly, D.M.X., ÓReilly, J., Polonsky, J., Sheridan, H., 1987. In vitro production and biosynthesis of fomajorin D and S by *Fomes annosus* (Fr.) Cooke. J. Chem. Soc. Perkin Trans. I, 1869–1872.

Eastwood, D.C., Floudas, D., Binder, M., Majcherczyk, A., Schneider, P., Aerts, A., Asiegbu, F.O., Baker, S.E., Barry, K., Bendiksby, M., Blumentritt, M., Coutinho, P. M., Cullen, D., de Vries, R.P., Gathman, A., Goodell, B., Henrissat, B., Ihrmark, K., Kauserud, H., Kohler, A., LaButti, K., Lapidus, A., Lavin, J.L., Lee, Y.H., Lindquist, E., Lilly, W., Lucas, S., Morin, E., Murat, C., Oguiza, J.A., Park, J., Pisabarro, A.G., Riley, R., Rosling, A., Salamov, A., Schmidt, O., Schmutz, J., Skrede, I., Stenlid, J., Wiebenga, A., Xie, X., Kües, U., Hibbett, D.S., Hoffmeister, D., Högberg, N., Martin, F., Grigoriev, I.V., Watkinson, S.C., 2011. The plant cell wall-decomposing machinery underlies the functional diversity of forest fungi. Science 333, 762–765.

Ehmann, D.E., Gehring, A.M., Walsh, C.T., 1999. Lysine biosynthesis in *Saccharomyces cerevisiae*: mechanism of alpha-aminoadipate reductase (Lys2) involves posttranslational phosphopantetheinylation by Lys5. Biochemistry 38, 6171–6177.

Essig, A., Hofmann, D., Münch, D., Gayathri, S., Künzler, M., Kallio, P.T., Sahl, H.G., Wider, G., Schneider, T., Aebi, M., 2014. Copsin, a novel peptide-based fungal antibiotic interfering with the peptidoglycan synthesis. J. Biol. Chem. 289, 34953–34964.

Fernandez-Fueyo, E., Ruiz-Duenas, F.J., Ferreira, P., Floudas, D., Hibbett, D.S., Canessa, P., Larrondo, L.F., James, T.Y., Seelenfreund, D., Lobos, S., Polanco, R., Tello, M., Honda, Y., Watanabe, T., San, R.J., Kubicek, C.P., Schmoll, M., Gaskell, J., Hammel, K.E., St John, F.J., Vanden Wymelenberg, A., Sabat, G., Splinter Bondurant, S., Syed, K., Yadav, J.S., Doddapaneni, H., Subramanian, V., Lavin, J. L., Oguiza, J.A., Perez, G., Pisabarro, A.G., Ramirez, L., Santoyo, F., Master, E., Coutinho, P.M., Henrissat, B., Lombard, V., Magnuson, J.K., Kues, U., Hori, C., Igarashi, K., Samejima, M., Held, B.W., Barry, K.W., Labutti, K.M., Lapidus, A., Lindquist, E.A., Lucas, S.M., Riley, R., Salamov, A.A., Hoffmeister, D., Schwenk, D., Hadar, Y., Yarden, O., de Vries, R.P., Wiebenga, A., Stenlid, J., Eastwood, D., Grigoriev, I.V., Berka, R.M., Blanchette, R.A., Kersten, P., Martinez, A.T., Vicuna, R., Cullen, D., 2012. Comparative genomics of *Ceriporiopsis subvermispora* and *Phanerochaete chrysosporium* provide insight into selective ligninolysis. Proc. Natl. Acad. Sci. USA 109, 5458–5463.

Floudas, D., Binder, M., Riley, R., Barry, K., Blanchette, R.A., Henrissat, B., Martínez, A. T., Otillar, R., Spatafora, J.W., Yadav, J.S., Aerts, A., Benoit, I., Boyd, A., Carlson, A., Copeland, A., Coutinho, P.M., de Vries, R.P., Ferreira, P., Findley, K., Foster, B., Gaskell, J., Glotzer, D., Górecki, P., Heitman, J., Hesse, C., Hori, C., Igarashi, K., Jurgens, J.A., Kallen, N., Kersten, P., Kohler, A., Kües, U., Kumar, T.K., Kuo, A., LaButti, K., Larrondo, L.F., Lindquist, E., Ling, A., Lombard, V., Lucas, S., Lundell, T., Martin, R., McLaughlin, D.J., Morgenstern, I., Morin, E., Murat, C., Nagy, L.G., Nolan, M., Ohm, R.A., Patyshakuliyeva, A., Rokas, A., Ruiz-Dueñas, F.J., Sabat, G., Salamov, A., Samejima, M., Schmutz, J., Slot, J.C., St John, F., Stenlid, J., Sun, H., Sun, S., Syed, K., Tsang, A., Wiebenga, A., Young, D., Pisabarro, A., Eastwood, D.C., Martin, F., Cullen, D., Grigoriev, I.V., Hibbett, D.S., 2012. The Paleozoic origin of enzymatic lignin decomposition reconstructed from 31 fungal genomes. Science 336, 1715–1719.

Forseth, R.R., Amaike, S., Schwenk, D., Affeldt, K.J., Hoffmeister, D., Schroeder, F.C., Keller, N.P., 2013. Homologous NRPS-like gene clusters mediate redundant small-molecule biosynthesis in *Aspergillus flavus*. Chem. Int. Ed. 52, 1590–1594.

Galagan, J.E., Calvo, S.E., Cuomo, C., Ma, L.J., Wortman, J.R., Batzoglou, S., Lee, S.I., Baştürkmen, M., Spevak, C.C., Clutterbuck, J., Kapitonov, V., Jurka, J., Scazzocchio, C., Farman, M., Butler, J., Purcell, S., Harris, S., Braus, G.H., Draht, O., Busch, S., D'Enfert, C., Bouchier, C., Goldman, G.H., Bell-Pedersen, D., Griffiths-Jones, S., Doonan, J.H., Yu, J., Vienken, K., Pain, A., Freitag, M., Selker, E.U., Archer, D.B.,

Peñalva, Oakley, B.R., Momany, M., Tanaka, T., Kumagai, T., Asai, K., Machida, M., Nierman, W.C., Denning, D.W., Caddick, M., Hynes, M., Paoletti, M., Fischer, R., Miller, B., Dyer, P., Sachs, M.S., Osmani, S.A., Birren, B.W., 2005. Sequencing of *Aspergillus nidulans* and comparative analysis with *A. fumigatus* and *A. oryzae*. Nature 438, 1105–1115.

Goffeau, A., Barrell, B.G., Bussey, H., Davis, R.W., Dujon, B., Feldmann, H., Galibert, F., Hoheisel, J.D., Jacq, C., Johnston, M., Louis, E.J., Mewes, H.W., Murakami, Y., Philippsen, P., Tettelin, H., Oliver, S.G., 1996. Life with 6000 genes. Science 274, 546.

Grigoriev, I.V., Nordberg, H., Shabalov, I., Aerts, A., Cantor, M., Goodstein, D., Kuo, A., Minovitsky, S., Nikitin, R., Ohm, R.A., Otillar, R., Poliakov, A., Ratnere, I., Riley, R., Smirnova, T., Rokhsar, D., Dubchak, I., 2012. The genome portal of the department of energy joint genome institute. Nucleic Acids Res. 40, D26–32.

Hirotani, M., ÓReilly, J.H., Donnelly, D.M.X., 1977. Fomannoxin – a toxic metabolite of *Fomes annosus*. Tetrahedron Lett. 7, 651–652.

Hori, C., Ishida, T., Igarashi, K., Samejima, M., Suzuki, H., Master, E., Ferreira, P., Ruiz-Dueñas, F.J., Held, B., Canessa, P., Larrondo, L.F., Schmoll, M., Druzhinina, I.S., Kubicek, C.P., Gaskell, J.A., Kersten, P., St. John, F., Glasner, J., Sabat, G., Splinter BonDurant, S., Syed, K., Yadav, J., Mgbeahuruike, A.C., Kovalchuk, A., Asiegbu, F. O., Lackner, G., Hoffmeister, D., Rencoret, J., Gutiérrez, A., Sun, H., Lindquist, E., Barry, K., Riley, R., Grigoriev, I.V., Henrissat, B., Kües, U., Berka, R.M., Martínez, A. T., Covert, S.F., Blanchette, R.A., Cullen, D., 2014. Analysis of the *Phlebiopsis gigantea* genome, transcriptome and secretome provides insight into its pioneer colonization strategies of wood. PLoS Genet. 10, e1004759.

Kalb, D., Lackner, G., Hoffmeister, D., 2014. Functional and phylogenetic divergence of fungal adenylate-forming reductases. Appl. Environ. Microbiol. 80, 6175–6183.

Karlsson, M., Olson, A., Stenlid, J., 2003. Expressed sequences from the basidiomycetous tree pathogen *Heterobasidion annosum* during early infection of scots pine. Fungal Genet. Biol. 39, 51–59.

Kauserud, H., Knudsen, H., Högberg, N., Skrede, I., 2012. Evolutionary origin, worldwide dispersal, and population genetics of the dry rot fungus *Serpula lacrymans*. Fungal Biol. Rev. 26, 84–93.

Kepler, J.A., Wall, M.E., Mason, J.E., Basset, C., McPhail, A.T., Sim, G.A., 1967. The structure of fomannosin, a novel sesquiterpene metabolite of the fungus *Fomes annosus*. J. Am. Chem. Soc. 89, 1260–1261.

Kubicek, C.P., Herrera-Estrella, A., Seidl-Seiboth, V., Martinez, D.A., Druzhinina, I.S., Thon, M., Zeilinger, S., Casas-Flores, S., Horwitz, B.A., Mukherjee, P.K., Mukherjee, M., Kredics, L., Alcaraz, L.D., Aerts, A., Antal, Z., Atanasova, L., Cervantes-Badillo, M.G., Challacombe, J., Chertkov, O., McCluskey, K., Coulpier, F., Deshpande, N., von Döhren, H., Ebbole, D.J., Esquivel-Naranjo, E.U., Fekete, E., Flipphi, M., Glaser, F., Gomez-Rodriguez, E.Y., Gruber, S., Han, C., Henrissat, B., Hermosa, R., Hernandez-Onate, M., Karaffa, L., Kosti, I., Le Crom, S., Lindquist, E., Lucas, S., Lubeck, M., Lubeck, P.S., Margeot, A., Metz, B., Misra, M., Nevalainen, H., Omann, M., Packer, N., Perrone, G., Uresti-Rivera, E.E., Salamov, A., Schmoll, M., Seiboth, B., Shapiro, H., Sukno, S., Tamayo-Ramos, J.A., Tisch, D., Wiest, A., Wilkinson, H.H., Zhang, M., Coutinho, P.M., Kenerley, C.M., Monte, E., Baker, S.E., Grigoriev, I.V., 2011. Comparative genome sequence analysis underscores mycoparasitism as the ancestral life style of *Trichoderma*. Genome Biol. 12, R40.

Kuo, A., Kohler, A., Martin, F.M., Grigoriev, I.V., 2014. Expanding genomics of mycorrhizal symbiosis. Front. Microbiol. 5, 582.

Lackner, G., Misiek, M., Braesel, J., Hoffmeister, D., 2012. Genome mining reveals the evolutionary origin and biosynthetic potential of basidiomycete polyketide synthases. Fungal Genet. Biol. 49, 996–1003.

Le, S.Q., Gascuel, O., 1993. An improved general amino acid replacement matrix. Mol. Biol. Evol. 25, 1307–1320.

Lind, M., Olson, A., Stenlid, J., 2005. An AFLP-marker based genetic linkage map of *Heterobasidion annosum* locating intersterility genes. Fungal Genet. Biol. 42, 519–527.

Lopez-Gallego, F., Agger, S.A., Abate-Pella, D., Distefano, M.D., Schmidt-Dannert, C., 2010. Sesquiterpene synthases Cop4 and Cop6 from *Coprinus cinereus*: catalytic promiscuity and cyclization of farnesyl pyrophosphate geometric isomers. ChemBioChem 11, 1093–1106.

Ma, L.J., van der Does, H.C., Borkovich, K.A., Coleman, J.J., Daboussi, M.J., Di Pietro, A., Dufresne, M., Freitag, M., Grabherr, M., Henrissat, B., Houterman, P.M., Kang, S., Shim, W.B., Woloshuk, C., Xie, X., Xu, J.R., Antoniw, J., Baker, S.E., Bluhm, B.H., Breakspear, A., Brown, D.W., Butchko, R.A., Chapman, S., Coulson, R., Coutinho, P. M., Danchin, E.G., Diener, A., Gale, L.R., Gardiner, D.M., Goff, S., Hammond-Kosack, K.E., Hilburn, K., Hua-Van, A., Jonkers, W., Kazan, K., Kodira, C.D., Koehrsen, M., Kumar, L., Lee, Y.H., Li, L., Manners, J.M., Miranda-Saavedra, D., Mukherjee, M., Park, G., Park, J., Park, S.Y., Proctor, R.H., Regev, A., Ruiz-Roldan, M.C., Sain, D., Sakthikumar, S., Sykes, S., Schwartz, D.C., Turgeon, B.G., Wapinski, I., Yoder, O., Young, S., Zeng, Q., Zhou, S., Galagan, J., Cuomo, C.A., Kistler, H.C., Rep, M., 2010. Comparative genomics reveals mobile pathogenicity chromosomes in *Fusarium*. Nature 464, 367–373.

Martinez, D., Berka, R.M., Henrissat, B., Saloheimo, M., Arvas, M., Baker, S.E., Chapman, J., Chertkov, O., Coutinho, P.M., Cullen, D., Danchin, E.G., Grigoriev, I. V., Harris, P., Jackson, M., Kubicek, C.P., Han, C.S., Ho, I., Larrondo, L.F., de Leon, A. L., Magnuson, J.K., Merino, S., Misra, M., Nelson, B., Putnam, N., Robbertse, B., Salamov, A.A., Schmoll, M., Terry, A., Thayer, N., Westerholm-Parvinen, A., Schoch, C.L., Yao, J., Barabote, R., Nelson, M.A., Detter, C., Bruce, D., Kuske, C.R., Xie, G., Richardson, P., Rokhsar, D.S., Lucas, S.M., Rubin, E.M., Dunn-Coleman, N., Ward, M., Brettin, T.S., 2008. Genome sequencing and analysis of the biomass-degrading fungus *Trichoderma reesei* (syn. *Hypocrea jecorina*). Nat. Biotechnol. 26, 553–560.

May, J.J., Kessler, N., Marahiel, M.A., Stubbs, M.T., 2002. Crystal structure of DhbE, an archetype for aryl acid activating domains of modular nonribosomal peptide synthetases. Proc. Natl. Acad. Sci. USA 99, 12120–12125.

Meinhardt, L.W., Costa, G.G., Thomazella, D.P., Teixeira, P.J., Carazzolle, M.F., Schuster, S.C., Carlson, J.E., Guiltinan, M.J., Mieczkowski, P., Farmer, A., Ramaraj, T., Crozier, J., Davis, R.E., Shao, J., Melnick, R.L., Pereira, G.A., Bailey, B.A., 2014. Genome and secretome analysis of the hemibiotrophic fungal pathogen, *Moniliophthora roreri*, which causes frosty pod rot disease of cacao: mechanisms of the biotrophic and necrotrophic phases. BMC Genom. 15, 164.

Morin, E., Kohler, A., Baker, A.R., Foulongne-Oriol, M., Lombard, V., Nagy, L.G., Ohm, R.A., Patyshakuliyeva, A., Brun, A., Aerts, A.L., Bailey, A.M., Billette, C., Coutinho, P.M., Deakin, G., Doddapaneni, H., Floudas, D., Grimwood, J., Hildén, K., Kües, U., Labutti, K.M., Lapidus, A., Lindquist, E.A., Lucas, S.M., Murat, C., Riley, R.W., Salamov, A.A., Schmutz, J., Subramanian, V., Wösten, H.A., Xu, J., Eastwood, D.C., Foster, G.D., Sonnenberg, A.S., Cullen, D., de Vries, R.P., Lundell, T., Hibbett, D.S., Henrissat, B., Burton, K.S., Kerrigan, R.W., Challen, M.P., Grigoriev, I.V., Martin, F., 2012. Genome sequence of the button mushroom *Agaricus bisporus* reveals mechanisms governing adaptation to a humic-rich ecological niche. Proc. Natl. Acad. Sci. USA 109, 17501–17506.

Nierman, W.C., Pain, A., Anderson, M.J., Wortman, J.R., Kim, H.S., Arroyo, J., Berriman, M., Abe, K., Archer, D.B., Bermejo, C., Bennett, J., Bowyer, P., Chen, D., Collins, M., Coulsen, R., Davies, R., Dyer, P.S., Farman, M., Fedorova, N., Fedorova, N., Feldblyum, T.V., Fischer, R., Fosker, N., Fraser, A., García, J.L., García, M.J., Goble, A., Goldman, G.H., Gomi, K., Griffith-Jones, S., Gwilliam, R., Haas, B., Haas, H., Harris, D., Horiuchi, H., Huang, J., Humphray, S., Jiménez, J., Keller, N., Khouri, H., Kitamoto, K., Kobayashi, T., Konzack, S., Kulkarni, R., Kumagai, T., Lafon, A., Latgé, J.P., Li, W., Lord, A., Lu, C., Majoros, W.H., May, G.S., Miller, B.L., Mohamoud, Y., Molina, M., Monod, M., Mouyna, I., Mulligan, S., Murphy, L., O'Neil, S., Paulsen, I., Peñalva, M.A., Pertea, M., Price, C., Pritchard, B.L., Quail, M. A., Rabbinowitsch, E., Rawlins, N., Rajandream, M.A., Reichard, U., Renauld, H., Robson, G.D., Rodriguez de Córdoba, S., Rodríguez-Peña, J.M., Ronning, C.M., Rutter, S., Salzberg, S.L., Sanchez, M., Sánchez-Ferrero, J.C., Saunders, D., Seeger, K., Squares, R., Squares, S., Takeuchi, M., Tekaia, F., Turner, G., Vazquez de Aldana, C.R., Weidman, J., White, O., Woodward, J., Yu, J.H., Fraser, C., Galagan, J. E., Asai, K., Machida, M., Hall, N., Barrell, B., Denning, D.W., 2005. Genomic sequence of the pathogenic and allergenic filamentous fungus *Aspergillus fumigatus*. Nature 438, 1151–1156.

Olson, A., Aerts, A., Asiegbu, F., Belbahri, L., Bouzid, O., Broberg, A., Canbäck, B., Coutinho, P.M., Cullen, D., Dalman, K., Deflorio, G., van Diepen, L.T., Dunand, C., Duplessis, S., Durling, M., Gonthier, P., Grimwood, J., Fossdal, C.G., Hansson, D., Henrissat, B., Hietala, A., Himmelstrand, K., Hoffmeister, D., Högberg, N., James, T.Y., Karlsson, M., Kohler, A., Kües, U., Lee, Y.H., Lin, Y.C., Lind, M., Lindquist, E., Lombard, V., Lucas, S., Lundén, K., Morin, E., Murat, C., Park, J., Raffaello, T., Rouzé, P., Salamov, A., Schmutz, J., Solheim, H., Ståhlberg, J., Vélëz, H., de Vries, R.P., Wiebenga, A., Woodward, S., Yakovlev, I., Garbelotto, M., Martin, F., Grigoriev, I.V., Stenlid, J., 2012. Insight into trade-off between wood decay and parasitism from the genome of a fungal forest pathogen. New Phytol. 194, 1001–1013.

Riley, R., Salamov, A.A., Brown, D.W., Nagy, L.G., Floudas, D., Held, B.W., Levasseur, A., Lombard, V., Morin, E., Otillar, R., Lindquist, E.A., Sun, H., LaButti, K.M., Schmutz, J., Jabbour, D., Luo, H., Baker, S.E., Pisabarro, A.G., Walton, J.D., Blanchette, R.A., Henrissat, B., Martin, F., Cullen, D., Hibbett, D.S., Grigoriev, I.V., 2014. Extensive sampling of basidiomycete genomes demonstrates inadequacy of the white-rot/brown-rot paradigm for wood decay fungi. Proc. Natl. Acad. Sci. USA 111, 9923–9928.

Röttig, M., Medema, M.H., Blin, K., Weber, T., Rausch, C., Kohlbacher, O., 2011. NRPSpredictor2-a web server for predicting NRPS adenylation domain specificity. Nucleic Acids Res. 39, W362–367.

Sambrook, J., Russell, D.W., 2000. Molecular Cloning: A Laboratory Manual, third ed. Cold Spring Harbor Laboratory Press, Cold Spring Harbor, NY.

Schneider, P., Bouhired, S., Hoffmeister, D., 2008. Characterization of the atromentin biosynthesis genes and enzymes in the homobasidiomycete *Tapinella panuoides*. Fungal Genet. Biol. 45, 1487–1496.

Stachelhaus, T., Mootz, H.D., Marahiel, M.A., 1999. The specificity-conferring code of adenylation domains in nonribosomal peptide synthetases. Chem. Biol. 6, 493–505.

Stajich, J.E., Wilke, S.K., Ahrén, D., Au, C.H., Birren, B.W., Borodovsky, M., Burns, C., Canbäck, B., Casselton, L.A., Cheng, C.K., Deng, J., Dietrich, F.S., Fargo, D.C., Farman, M.L., Gathman, A.C., Goldberg, J., Guigó, R., Hoegger, P.J., Hooker, J.B., Huggins, A., James, T.Y., Kamada, T., Kilaru, S., Kodira, C., Kües, U., Kupfer, D., Kwan, H.S., Lomsadze, A., Li, W., Lilly, W.W., Ma, L.J., Mackey, A.J., Manning, G., Martin, F., Muraguchi, H., Natvig, D.O., Palmerini, H., Ramesh, M.A., Rehmeyer, C. J., Roe, B.A., Shenoy, N., Stanke, M., Ter-Hovhannisyan, V., Tunlid, A., Velagapudi, R., Vision, T.J., Zeng, Q., Zolan, M.E., Pukkila, P.J., 2010. Insights into evolution of multicellular fungi from the assembled chromosomes of the mushroom *Coprinopsis cinerea* (*Coprinus cinereus*). Proc. Natl. Acad. Sci. USA 107, 11889–11994.

Steinchen, W., Lackner, G., Yasmin, S., Schrettl, M., Dahse, H.M., Haas, H., Hoffmeister, D., 2013. Bimodular peptide synthetase SidE produces fumarylalanine in the human pathogen *Aspergillus fumigatus*. Appl. Environ. Microbiol. 79, 6670–6676.

Suvarna, K., Seah, L., Bhattacherjee, V., Bhattacharjee, J.K., 1998. Molecular analysis of the LYS2 gene of *Candida albicans*: homology to peptide antibiotic synthetases and the regulation of the alpha-aminoadipate reductase. Curr. Genet. 33, 268–275.

Please cite this article in press as: Brandenburger, E., et al. Multi-genome analysis identifies functional and phylogenetic diversity of basidiomycete adenylate-forming reductases. Fungal Genet. Biol. (2016), http://dx.doi.org/10.1016/j.fgb.2016.07.008

Suzuki, H., MacDonald, J., Syed, K., Salamov, A., Hori, C., Aerts, A., Henrissat, B., Wiebenga, A., VanKuyk, P.A., Barry, K., Lindquist, E., LaButti, K., Lapidus, A., Lucas, S., Coutinho, P., Gong, Y., Samejima, M., Mahadevan, R., Abou-Zaid, M., de Vries, R.P., Igarashi, K., Yadav, J.S., Grigoriev, I.V., Master, E.R., 2012. Comparative genomics of the white-rot fungi, *Phanerochaete carnosa* and *P. chrysosporium*, to elucidate the genetic basis of the distinct wood types they colonize. BMC Genom. 13, 444.

Swamy, S., Uno, I., Ishikawa, T., 1984. Morphogenetic effects of mutations at the A and B incompatibility factors in *Coprinus cinereus*. J. Gen. Microbiol. 130, 3219–3224.

Tamura, K., Stecher, G., Peterson, D., Filipski, A., Kumar, S., 2013. MEGA6: molecular evolutionary genetics analysis version 6.0. Mol. Biol. Evol. 30, 2725–2729.

Thompson, J.D., Higgins, D.G., Gibson, T.J., 1994. CLUSTAL W: improving the sensitivity of progressive multiple sequence alignment through sequence weighting, position-specific gap penalties and weight matrix choice. Nucleic Acids Res. 22, 4673–4680.

Tlalka, M., Fricker, M., Watkinson, S., 2008. Imaging of long-distance alpha-aminoisobutyric acid translocation dynamics during resource capture by *Serpula lacrymans*. Appl. Environ. Microbiol. 74, 2700–2708.

Wang, M., Beissner, M., Zhao, H., 2014. Aryl-aldehyde formation in fungal polyketides: discovery and characterization of a distinct biosynthetic mechanism. Chem. Biol. 21, 257–263.

Wang, M., Zhao, H., 2014. Characterization and engineering of the adenylation domain of a NRPS-like protein: a potential biocatalyst for aldehyde generation. ACS Catal. 4, 1219–1225.

Please cite this article in press as: Brandenburger, E., et al. Multi-genome analysis identifies functional and phylogenetic diversity of basidiomycete adenylate-forming reductases. Fungal Genet. Biol. (2016), http://dx.doi.org/10.1016/j.fgb.2016.07.008

Supplementary material

Multi-genome analysis identifies functional and phylogenetic diversity of basidiomycete adenylate-forming reductases

Eileen Brandenburger[1], Daniel Braga[1], Anja Kombrink[2], Gerald Lackner[3], Julia Gressler[1], Markus Künzler[3], and Dirk Hoffmeister[1,*]

[1]Friedrich-Schiller-Universität Jena, Department Pharmaceutical Microbiology at the Hans-Knöll-Institute, Winzerlaer Strasse 2, 07745 Jena, Germany.

[2]ETH Zürich, Institute of Microbiology, Vladimir-Prelog-Weg 4, 8093 Zürich, Switzerland.

[3]Friedrich-Schiller-Universität Jena, Junior Research Group Synthetic Microbiology at the Hans-Knöll-Institute, Adolf-Reichwein-Strasse 23, 07745 Jena, Germany.

[*]Corresponding author. Tel.: +49 3641 949850; fax: +49 3641 949852. E-mail address: dirk.hoffmeister@leibniz-hki.de

Pool 1	Gly, L-Ala, L-Val, L-Leu, L-Ile
Pool 2	L-Cys, L-Met, L-Ser, L-Thr, L-Pro
Pool 3	L-His, L-Phe, L-Tyr, L-Trp
Pool 4	L-Asp, L-Asn, L-Glu, L-Gln
Pool 5	L-Lys, L-Arg, L-Orn
Pool 6	Pyruvic acid, α-ketoglutaric acid, phenylpyruvic acid, 4-hydroxyphenylpyruvic acid, indole-3-pyruvic acid
Pool 7	Benzoic acid, salicylic acid, 4-hydroxybenzoic acid, 2,3-dihydroxybenzoic acid
Pool 8	Fumaric acid, maleic acid, malic acid, malonic acid
Pool 9	Oxalic acid, succinic acid, citric acid, L-α-aminoadipic acid
Pool 10	D-Ala, D-Val, D-Leu, D-Ile
Pool 11	D-Cys, D-Met, D-Ser, D-Thr, D-Pro
Pool 12	D-His, D-Phe, D-Tyr, D-Trp
Pool 13	D-Asp, D-Asn, D-Glu, D-Gln, D-Lys, D-Arg

Table S1. Substrate pools used for initial characterization of adenylation domains using the substrate-dependent ATP-[^{32}P]pyrophosphate radiolabel exchange assay.

Table S2. Sequences used for the phylogenetic analyses of fungal adenylate-forming reductases. Accession numbers refer to entries in the NCBI database or the Mycocosm database (proteinIDs) of the Joint Genome Institute (http://genome.jgi.doe.gov/programs/fungi/index.jsf).

Organism	Accession	Length (aa)
Agaricus bisporus var. *bisporus* H97	XP_006462975	1092
Aspergillus clavatus NRRL 1	XP_001275157	996
Aspergillus flavus NRRL3357	XP_002384042.1	1042
Aspergillus flavus NRRL3357	XP_002384859.1	1029
Aspergillus fumigatus Af293	XP_001481395	994
Aspergillus nidulans FGSC A4	XP_664048	1039
Aspergillus terreus NIH2624	XP_001212808	1069
Candida albicans	Q12572	1391
Coprinopsis cinerea okayama	XP_001836648.2	1049
Coprinopsis cinerea Amut Bmut	KX118593 (03009)	1025
Coprinopsis cinerea Amut Bmut	KX118592 (06235)	1026
Ceriporiopsis subvermispora B	EMD40260.1	1049
Ceriporiopsis subvermispora B	EMD34789.1	1417
Dichomitus squalens LYAD-421 SS1	EJF63849.1	1428
Dichomitus squalens LYAD-421 SS1	EJF63449.1	1033
Fomitiporia mediterranea MF3/22	EJC98159.1	1045
Fusarium oxysporum f. sp. *vasinfectum* 25433	EXM16769	992
Fomitopsis pinicola FP-58527 SS1	EPS97414	1211
Gloeophyllum trabeum ATCC 11539	EPQ54396	1059
Heterobasidion irregulare TC 32-1	ETW75842	1419
Heterobasidion annosum	XP_009552374.1 (NPS4)	1092

Heterobasidion annosum	XP_009544373.1 (NPS5)	1011
Heterobasidion annosum	KX118589 (NPS10)	1088
Moniliophthora roreri MCA 2997	ESK96610	1086
Moniliophthora roreri MCA 2997	ESK96610	1086
Phlebia brevispora HHB-7030 SS6	ProteinID 161728	1428
Phlebia brevispora HHB-7030 SS6	ProteinID 137634	1022
Phanerochaete carnosa HHB-10118-sp	EKM49537.1	1024
Pleurotus ostreatus PC15	ProteinID 1062196	915
Punctularia strigosozonata HHB-11173 SS5	EIN08908	1443
Saccharomyces cerevisiae S288c	NP_009673.1	1392
Serpula lacrymans S7	KX118590 (NPS9)	1096
Serpula lacrymans S7	KX118591 (NPS11)	1099
Stereum hirsutum FP-91666 SS1	EIM84978	1086
Stereum hirsutum FP-91666 SS1	EIM82061.1	1425
Stereum hirsutum FP-91666 SS1	EIM85977.1	1048
Trichoderma reesei QM6a	XP_006964071	1052
Trametes versicolor FP-101664 SS1	EIW55513.1	1419
Trametes versicolor FP-101664 SS1	EIW59229.1	1035
Trichoderma virens Gv29-8	EHK20896	969
Trichoderma virens Gv29-8	EHK23193	1049

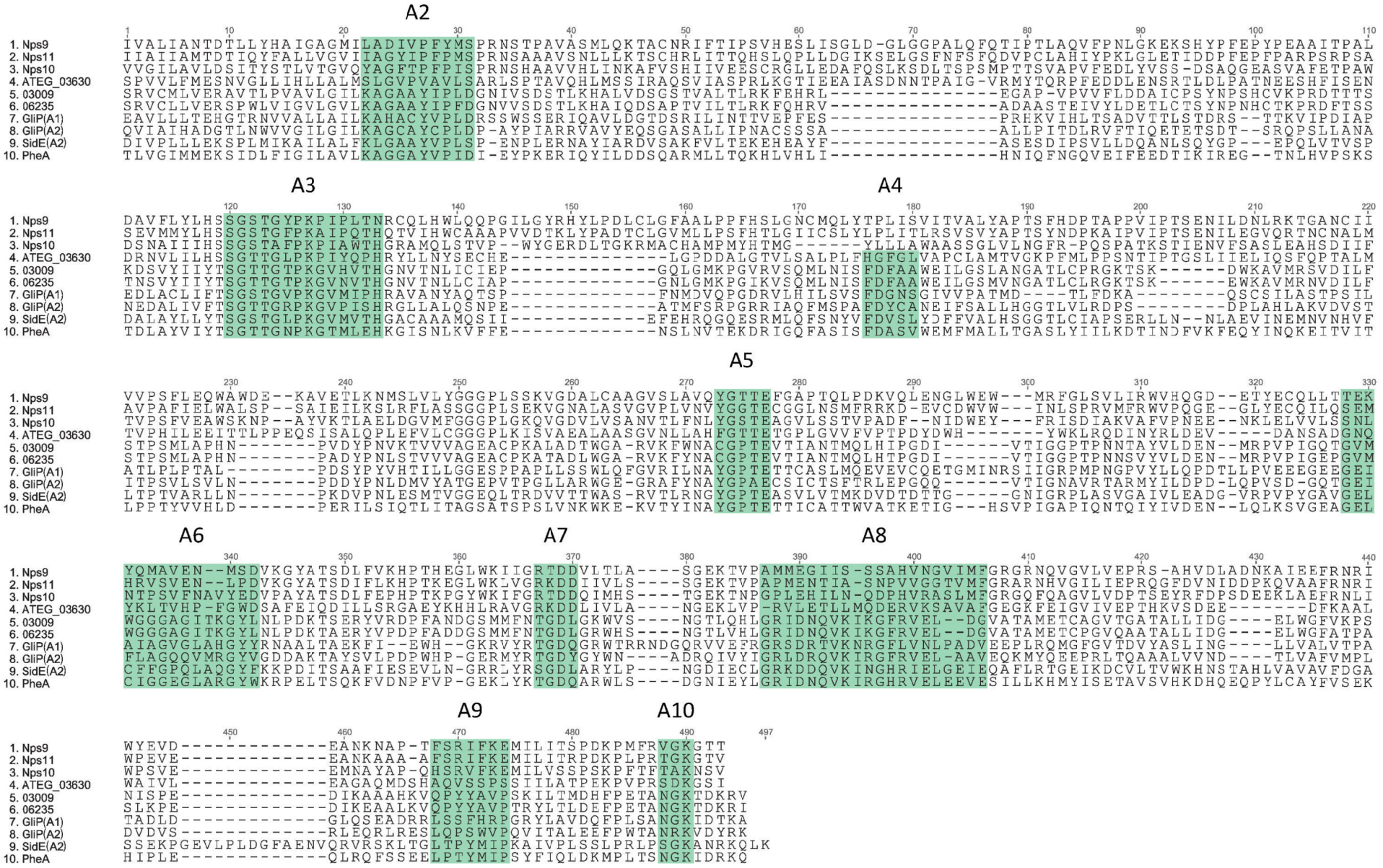

Figure S1. Alignment of amino acid sequences of adenylation domains. Core motifs A2-A10 according to Schwarzer et al. (2003) are highlighted in green. Note that motif A4 is not identifiable in the sequences of Nps9, Nps11, and Nps10. ATEG_03630: orsellinic acid reductase (Wang et al., 2014); GliP: gliotoxin synthetase (Balibar and Walsh, 2006); SidE: fumaryl-L-alanine synthetase (Steinchen et al., 2013); PheA: phenylalanine-accepting domain of the gramicidin S synthetase I (Stachelhaus et al., 1999).

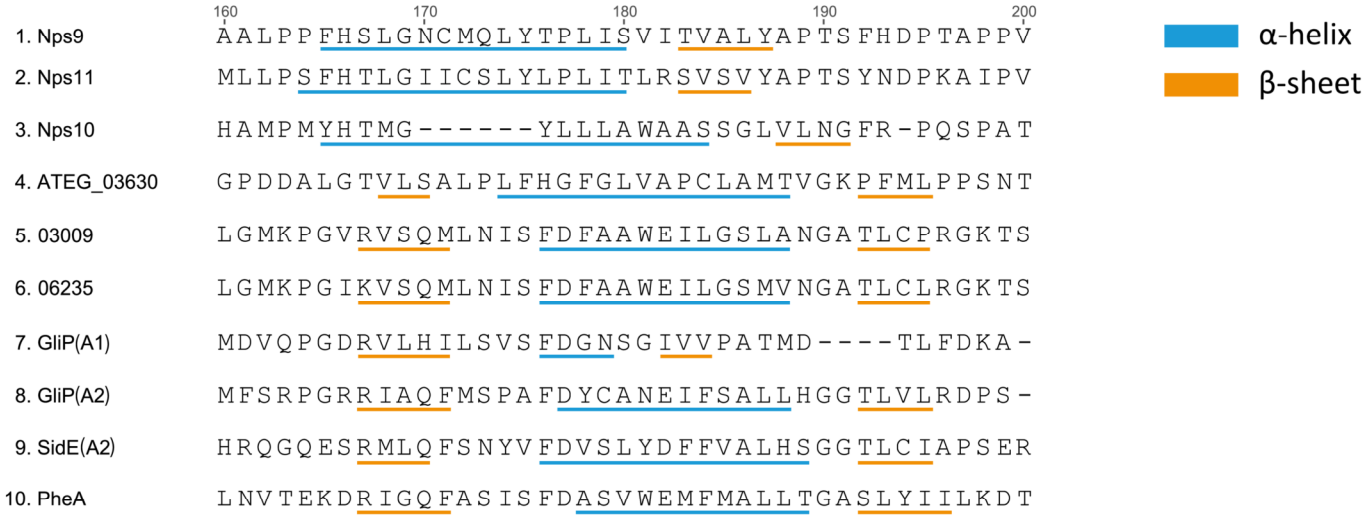

Figure S2. Secondary structure prediction around core motif A4 (FDxS), using the PSIPRED server (Buchan et al., 2013). Blue: α-helices, orange: β-sheets. Note that the beginning of the α-helices that comprise the indicative aspartic acid residue (D235 in PheA) in canonical adenylation domains does not align well with the beginning of the α-helix in reductases Nps9, Nps11, and Nps10.

References

Balibar, C.J., Walsh, C.T., 2006. GliP, a multimodular nonribosomal peptide synthetase in Aspergillus fumigatus, makes the diketopiperazine scaffold of gliotoxin. Biochemistry 45, 15029-15038.

Buchan D.W.A., Minneci F., Nugent T.C.O., Bryson K., Jones D.T., 2013. Scalable web services for the PSIPRED Protein Analysis Workbench. Nucleic Acids Res. 41 (W1): W340-W348.

Schwarzer, D., Finking, R., Marahiel, M.A., 2003. Nonribosomal peptides: from genes to products. Nat. Prod. Rep. 20, 275-287.

Stachelhaus, T., Mootz, H.D., Marahiel, M.A., 1999. The specificity-conferring code of adenylation domains in nonribosomal peptide synthetases. Chem. Biol. 6, 493-505.

Steinchen, W., Lackner, G., Yasmin, S., Schrettl, M., Dahse, H.M., Haas, H., Hoffmeister, D., 2013. Bimodular peptide synthetase SidE produces fumarylalanine in the human pathogen Aspergillus fumigatus. Appl. Environ. Microbiol. 79, 6670-6676.

Wang, M., Beissner, M., Zhao, H., 2014. Aryl-aldehyde formation in fungal polyketides: discovery and characterization of a distinct biosynthetic mechanism. Chem. Biol. 21, 257-263.

3.2 Publikation 2, Brandenburger et al. (2016), *Manuskript in Vorbereitung*

The basidiomycete peptide synthetase CsNPS2 catalyzes N^5-acetyl-N^5-hydroxy-L-ornithine trimerization for siderophore biosynthesis.

Eileen Brandenburger, Markus Gressler, Robin Leonhardt, Gerald Lackner, Andreas Habel, Christian Hertweck, Matthias Brock, Dirk Hoffmeister.

(Manuskript in Vorbereitung zum Einreichen bei Appl Environ Microbiol)

Die nichtribosomale Peptidsynthetase CsNPS2 aus *Ceriporiopsis subvermispora* bestehend aus einem Initiationsmodul (A-T), zwei unvollständigen Elongationsmodulen (C-T-Didomäne) und einer abschließenden C-Domäne. Orthologe Gene zu *CsNPS2* konnten in zahlreichen Basidiomyceten nachgewiesen werden. Die Domänenstruktur deutet auf die Funktionsweise einer Siderophorsynthetase. *CsNPS2* aus *C. subvermispora* wurde als repräsentatives Beispiel biochemisch untersucht. Die Expression des Gens erfolgte in Abhängigkeit vom Eisengehalt im Medium. Unter Eisenmangel konnte die Sekretion einer eisenbindenden Substanz detektiert werden. Das in *Aspergillus niger* tEB09 heterolog produzierte Histidin-markierte Protein CsNPS2 wurde *in vitro* charakterisiert. N^5-Acetyl-N^5-Hydroxy-L-Ornithin (L-AHO) wurde als Substrat der Adenylierungsdomäne identifiziert. Als Produkt von CsNPS2 konnte das lineare Trimer des L-AHO bezeichnet als Basidioferrin, nachgewiesen werden. In einem Assay mit Chrome Azurol S wurde die Fähigkeit des Basidioferrins Eisen zu binden bestätigt. Diese Daten bekräftigen die Hypothese, dass dieses in Basidiomyceten hoch konservierte Gen (*CsNPS2* und Orthologe) für eine Siderophorsynthetase kodiert.

Angaben zum Eigenanteil von E. Brandenburger (60 %)

Herstellung von pEB16 und der Transformante *Aspergillus niger* tEB09, heterologe Produktion von CsNPS2, Aufreinigung und Analyse, Substratspezifitätsbestimmung für CsNPS2, *in vitro* Produktbildungsassay, Aktivitätsnachweis des Produktes, HPLC-Analyse, Nachweis Siderophorsekretion durch *C. subvermispora*, Expressionsstudien für *CsNPS2*, *SMOI* und *MFS1*, Mitarbeit an der Erstellung des Manuskriptes.

The basidiomycete peptide synthetase CsNPS2 catalyzes N^5-acetyl-N^5-hydroxy-L-ornithine trimerization for siderophore biosynthesis

Eileen Brandenburger,[a] Markus Gressler,[b*] Robin Leonhardt,[a†] Gerald Lackner,[c] Andreas Habel,[d] Christian Hertweck,[d] Matthias Brock,[e] Dirk Hoffmeister[a#]

Department of Pharmaceutical Microbiology at the Hans-Knöll-Institute, Friedrich-Schiller-University, Jena, Germany[a]; Department Microbial Biochemistry and Physiology, Leibniz Institute for Natural Product Research and Infection Biology - Hans-Knöll-Institute, Jena, Germany[b]; Junior Group Synthetic Microbiology at the Hans-Knöll-Institute, Friedrich-Schiller-University, Jena, Germany[c]; Department Biomolecular Chemistry, Leibniz Institute for Natural Product Research and Infection Biology - Hans-Knöll-Institute, Jena, Germany[d]; School of Life Sciences, University of Nottingham, United Kingdom[e]

Present addresses:

*Markus Gressler, Department of Parasitology and Mycology at the Pasteur Institute, Paris, France

[†]Robin Leonhardt, Department of Food Chemistry, Leibniz-Universität Hannover, Germany

[#]Address correspondence to Dirk Hoffmeister, dirk.hoffmeister@leibniz-hki.de.

Running head: Basidiomycete siderophore synthetase

Abstract

The model white-rot basidiomycete *Ceriporiopsis subvermispora* encodes putative siderophore biosynthesis genes, among them the gene for the seven-domain nonribosomal peptide synthetase CsNPS2, which is a member of the so-called fungal type VI siderophore synthetases. The full-length enzyme (274.5 kDa) was heterologously produced as polyhistidine fusion in *Aspergillus niger* as soluble and active protein. Consistent with its hypothesized function in α-hydroxamate siderophore synthesis, N^5-acetyl-N^5-hydroxy-L-ornithine (L-AHO) and N^5-*cis*-anhydromevalonyl-N^5-hydroxy-L-ornithine (L-AMHO) were accepted as substrates, as assessed *in vitro* using the substrate-dependent [^{32}P]ATP-pyrophosphate radioisotope exchange assay. Full-length *holo*-CsNPS2 catalyzed the amide bond formation between L-AHO molecules to release trimeric basidioferrin as final product *in vitro*, as verified by LC-HRESIMS. In contrast, no oligomerization was observed with L-AMHO as substrate.

Importance: The basidiomycete nonribosomal peptide synthetase CsNPS2 represents the first characterized member of a widely distributed but previously uninvestigated class (type VI) of fungal siderophore synthetases. Genes orthologous to *CsNPS2* are highly conserved across various phylogenetic clades of the basidiomycetes. Hence, our work serves as a broadly applicable model for siderophore biosynthesis and iron metabolism in higher fungi. Also, our results on the amino acid substrate preference of CsNPS2 supports further understanding of the substrate selectivity of fungal adenylation domains. Methodologically, this report highlights the *Aspergillus niger*/SM-Xpress-based system as suitable platform to heterologously express

multimodular basidiomycete biosynthesis enzymes in the > 250 kDa range in soluble and active form.

Introduction

The transition element iron plays an essential role for numerous fundamental physiological processes, among them electron transport, e.g., during oxidative phosphorylation and nucleic acid biosynthesis [1,2]. To compensate for the very low bioavailability (e.g., the solubility product for $Fe(OH)_3$ is 10^{-39} M [2]), fungi primarily use high-affinity ferric iron-specific chelating natural products, referred to as siderophores, to acquire iron extracellularly from their environment and for intracellular iron storage and sequestration [1,3]. A second, less efficient acquisition strategy includes enzymatic reductive iron uptake [4]. Structurally, most fungal siderophores belong to the hydroxamate family of compounds (Figure 1). They share N^5-acyl-N^5-hydroxy-L-ornithine as monomers and chelate ferric iron through octahedral co-ordination to the oxygen atoms of the hydroxy and the acyl groups bound to these modified L-ornithine residues. Siderophores can structurally be further divided into i) the trimeric fusarinines, represented, e.g., by triacetylfusarinine C (TAFC), a secreted siderophore of *Aspergillus fumigatus* [5]), ii) the coprogens [6, 6a], iii), the ferrichromes, which include three N^5-acylated N^5-hydroxy-L-ornithine units in their usually hexameric structure, represented, e.g., by ferricrocin as intracellular storage siderophore of *Aspergilli* [5,7], and iv) rhodotorulic acid which is a dihydroxamate diketopiperazine [8,9].

Fungal siderophore biosynthesis has been studied extensively for *Aspergillus*, *Fusarium*, *Cochliobolus*, and other ascomycete genera [10-13]. The key enzymatic activity to assemble the backbone structure is provided by nonribosomal peptide synthetases (NRPSs). These are exceptionally large modular multi-domain enzymes which catalyze amide bond formation between proteinogenic or non-proteinogenic amino acids, or other monomers, that are covalently tethered to the enzyme via thioester bonds [14]. Depending on the domain architecture, siderophore-producing NRPSs are grouped into categories type I-VI [3]. Despite different products, all of them share a characteristic terminal thiolation (T)-/condensation (C) didomain duplication or, in most cases, triplication. Discrete enzymes catalyze the reaction to provide siderophore synthetases with monomeric substrates. These steps include hydroxylation and acylation of the nitrogen atom N^5 of L-ornithine. The monooxygenase gene may be located adjacent to the NRPS gene encoding the siderophore synthetase [4].

The impressive body of literature on ascomycete siderophores is starkly contrasted by the paucity of data on their basidiomycete congeners, whose genetic or enzymatic requisites for siderophore production are largely unknown. Merely two reports exist that pertain to ferrichrome and ferrichrome A biosynthesis in *Ustilago maydis* [15,16], alongside a report on the identification of ferrichrome A biosynthesis genes in the Jack O'Lantern mushroom *Omphalotus olearius* [17]. However, genomic sequencing of basidiomycetes of various phylogenetic clades [18-21] identified strongly conserved genes for a putative seven-domain type VI siderophore synthetase ($AT_1C_1T_2C_2T_3C_3$, Figure 2) in numerous species. Dissimilar to other fungal siderophore synthetases, type VI enzymes feature only one adenylation (A)

85 domain, plus the prototypical TC domain triple. Following the biosynthetic logic of NRPSs, this
86 domain configuration should result in a homotrimeric enzymatic product, making this most
87 conserved basidiomycete NRPS incompatible with the biosynthesis of the heterohexameric
88 ferrichromes.
89 The siderophore synthetase of the model white-rot basidiomycete *Ceriporiopsis subvermispora*,
90 CsNPS2, is representative of numerous type VI basidiomycete NRPSs. We here describe its
91 functional *in vitro* characterization, along with the *in vitro* identification of its product, the iron-
92 chelating linear trimer of N^5-acetyl-N^5-hydroxy-L-ornithine, now referred to as basidioferrin
93 (Figure 1).
94
95 **MATERIALS AND METHODS**
96 **General.** Standard molecular biology procedures were performed as described [22]. Isolation of
97 plasmid DNA from *Escherichia coli*, restriction and ligation followed the instructions of the
98 manufacturers of kits and enzymes (NEB, Promega, Fermentas, ThermoFisher Scientific, and
99 Zymo Research). Chemicals and media components were purchased from Becton-Dickinson,
100 Fisher, Fluka, Roth, Sigma-Aldrich, and Takara. The sodium salt of [^{32}P]pyrophosphate was from
101 PerkinElmer.
102
103 **Microorganisms and cultivation.** Routine cloning was done in *E. coli* XL1 blue. *E. coli* BL21(DE3)
104 and SoluBL were used for heterologous protein production. *E. coli* was cultured in LB- or auto-
105 induction medium, amended with kanamycin (50 µg/ml) or carbenicillin (50 µg/ml) for

106 selection. The basidiomycete *Ceriporiopsis subvermispora* [23] was grown at room temperature
107 on malt extract peptone (MEP) agar (per liter: 30 g malt extract, 3 g soy peptone, 18 g agar, pH
108 5.6). Seed cultures were grown in liquid MEP medium, for main cultures, low iron medium (LIM)
109 [24] was used. To induce siderophore biosynthesis, 200 µM bathophenanthroline disulfonic
110 acid (BPS) disodium salt was added. *Aspergillus niger* P2 [25] and its derivative tEB09
111 (*PamyB:terR; PterA:NPS2,* this study) were grown on *Aspergillus* minimal medium (AMM+50
112 mM D-glucose) [26] containing 2 % agar, or as liquid seed culture with 100 mM D-glucose, at 30
113 °C. Pyrithiamine hydrobromide (0.1 µg/ml) and phleomycin (80 µg/ml) were added, if
114 appropriate.
115
116 **cDNAs synthesis and plasmid construction.** RNA isolation was carried out with the SV Total
117 RNA Isolation kit (Promega). Reverse transcription PCR in a total volume of 20 µl (60 min; 42 °C)
118 was used to produce cDNA. To amplify a partial gene encoding the A_1-T_1-didomain of
119 *C. subvermispora CsNPS2* (putative siderophore synthetase gene), the first-strand synthesis
120 reaction was primed with oligonucleotide NPS2-1 (0.5 µM, Table S1), 2.5 mM $MgCl_2$, 0.5 mM
121 each dNTP, 1 µg total RNA, and ImProm-II reverse transcriptase (Promega). Subsequently, 1 µl
122 of the first strand reaction was used as template in a standard PCR. The reaction included 0.2
123 mM each dNTP, 1 µl (each) oligonucleotides NPS2fw and NPS2rev (Table S1), and 2 units *Pfu*
124 DNA-polymerase (Promega), in the buffer provided with the enzyme, in a total volume of 50 µl.
125 Thermocycling parameters were: initial denaturation, 30 s, 94 °C; amplification, 35 cycles (94 °C
126 for 30 s, 58 °C for 30 s, 72 °C for 6 min 30 s); terminal hold, 5 min at 72 °C. The purified PCR

product was restricted with *Bam*HI and *Eco*RI, whose recognition sites were introduced by the above primers, and ligated to the vector pBSK, restricted equally, to create plasmid pRL1 (see Figure S1 for plasmid construction). The insert was then ligated into vector pRSETb, using the same restriction sites, to create expression plasmid pRL3. The *CsNPS2* full-length gene was reconstituted by amplifying the portion between its naturally occurring *Sac*II site and the stop codon with primers oRL1 and oRL2 (Table S1, PCR parameters above), restriction of the amplicon by *Sac*II and *Mfe*I, and ligation into pRL3, restricted by *SacII* and *EcoRI*, to yield plasmid pRL5.

Full-length *CsNPS2* was then cloned into the SM-Xpress vector [25] by *in vitro* recombination, using the InFusion HD Cloning Kit (Clontech), to create plasmid pEB16. To this end, the gene was amplified by PCR (total volume 10 µl), using 20 ng pRL5 as template, 0.2 mM each dNTP, 0.5 µM each oligonucleotide (oEB28/oEB30, Table S1), and 1 unit Phusion DNA polymerase, in the buffer provided with the enzyme. Thermal speedcycling parameters were: initial denaturation at 98°C for 30 s; amplification with 33 cycles (98 °C for 7 s, 61 °C for 7 s, 72 °C for 125 s); terminal hold, 5 min at 72 °C.

Semi-quantitative PCR. Total RNA was isolated from *C. subvermispora* mycelia cultivated under high iron (10 µM $FeSO_4$) and iron deplete conditions (no iron, with 200 µM BPS). cDNA synthesis was performed with 500 ng template RNA per reaction. Semi-quantitative PCR was carried out with primer pairs (1 µM each) oRL3/oRL4 (*CsNPS2*), oEB48/oEB49 (*MFS1,* putative siderophore transporter gene, EMD31052.1), oEB54/oEB55 (*SMO1*, putative monooxygenase gene,

148 EMD38274.1) and oEB46/oEB47, (*GDH1*, glyceraldehyde-3-phosphate dehydrogenase gene,
149 EMD35149.1), in which the latter served as reference standard. Oligonucleotide sequences are
150 shown in Table S1. Thermal cycling parameters were: 30 s at 98 °C; 27 cycles of 98 °C for 10 s,
151 54 °C for 15 s and 72 °C for 105 s, followed by a terminal hold for 5 min at 72 °C. The PCR
152 products were separated by agarose gel electrophoresis.
153
154 ***Aspergillus niger* transformation and heterologous gene expression.** *A. niger* P2 (=FGSC
155 A1144_*PamyB:terR*) [25] was transformed with plasmid pEB16. Conidia (1×10^7 in 50 ml AMM)
156 were inoculated and incubated on an orbital shaker at 120 rpm and 30 °C overnight. Mycelium
157 was harvested and washed with 100 ml YAT buffer (0.6 M KCl, 50 mM maleic acid, pH 5.5). For
158 protoplast formation, mycelium was incubated with 100 mg Yatalase and 100 mg lysing enzyme
159 in 20 ml YAT buffer for approximately 2 h (30 °C, 70 rpm). Protoplasts were filtered and washed
160 three times with wash solution (0.6 M KCl, 0.1 M Tris-HCl, pH 7.0). Protoplasts were then
161 resuspended in solution A (0.6 M KCl, 50 mM $CaCl_2$, 10 mM Tris-HCl, pH 7.5) to give a final
162 concentration of 5×10^7 to 2×10^8 protoplasts/ml. To 100 µl protoplast suspension, 1 - 20 µg
163 plasmid DNA was added, followed by incubation on ice for 5 min. After addition of 25 µl PEG
164 solution (25 % (w/v) PEG 8000, 50 mM $CaCl_2$, 10 mM Tris-HCl, pH 7.5) the mixture was kept on
165 ice for further 20 min. Then, another 500 µl of PEG solution was added. After incubation on ice
166 for further 5 min, 1 ml solution A was added. 400 µl of the transformation reaction was mixed
167 with 12 ml top agar (AMM, 50 mM D-glucose, 1.2 M sorbitol, 80 µg/ml phleomycin, 2 % agar,
168 pH 6.5) and poured onto agar plates of the same composition. Plates were cultured at 30 °C for

169 3 - 5 days. Conidia from colonies were transferred four times to fresh plates. A PCR-based pre-
170 screen was used to test for full-length transgene integration (primer pair 2641/2644). Genomic
171 DNAs of nine pre-selected transformants were subsequently tested for single-integration
172 events of the *CsNPS2* cassette (*PterA:CsNPS2:trpC*^{T}) by Southern blotting, using a 0.9 kb
173 digoxigenin-labeled *CsNPS2*-specific probe (DIG high prime, Roche, Figure S2). For visualization,
174 blots were treated with CDP-star, according to the manufacturer's instruction (Roche). A
175 transformant (*A. niger* tEB09) with single integration of the expression construct in the genome
176 was used for further work.
177
178 **Protein purification.** Heterologous production of *Streptomyces verticillus* phosphopantetheinyl
179 transferase Svp in *E. coli* BL21(DE3) was performed as previously described [27]. Cells were
180 harvested by centrifugation (4 °C, 3,200 × g, 20 min), and the cell paste was resuspended in lysis
181 buffer (50 mM $NaH_2PO_4 \times H_2O$, 300 mM NaCl, 10 mM imidazole, pH 8.0), followed by sonication
182 to disrupt cells, centrifugation to remove debris, and FPLC-based purification (see below).
183 To produce full-length CsNPS2, conidia of *A. niger* tEB09 (1×10^6 in 50 ml) were used to
184 inoculate AMM+100 mM D-glucose, at 30 °C and 200 rpm, for 48 h. The mycelium was
185 harvested, ground under liquid nitrogen and resuspended in buffer (50 mM Tris, 150 mM NaCl,
186 pH 8.0). Cell debris was removed by centrifugation (4 °C, 14,000 × g, 20 min).
187 An Äkta Pure FPLC instrument (GE Healthcare) was used for immobilized metal affinity
188 chromatography. The instrument was equipped with a 1 ml His-Trap FF crude column (GE
189 Healthcare). Buffer A (50 mM NaH_2PO_4, 300 mM NaCl, pH 7.5) and buffer B (500 mM imidazole

190 in buffer A) were used as mobile phase. The wash was performed with a step gradient (5-12 %
191 B, equivalent to 25-60 mM imidazole) within 10 min. Elution of the histidine-tagged target
192 proteins (CsNPS2 full-length, Svp) was carried out at 100 % B. Proteins were desalted on a PD-
193 10 column (GE Healthcare) and eluted with buffer (80 mM Tris-HCl, 5 mM $MgCl_2$, 100 µM EDTA,
194 pH 7.5). Protein purification was verified on polyacrylamide gels, the protein concentration was
195 determined by Bradford's assay [28]. Additional MALDI-TOF/TOF MS analysis confirmed
196 authenticity of CsNPS2.
197
198 **Siderophore detection assay.** Siderophore activity was detected by the Chrome Azurol S (CAS)
199 agar diffusion method as described [29,30] and used to characterize the *in vitro* product of
200 CsNPS2. A 35 µl sample of the assay was filled into a 5 mm-diameter well. The plate was
201 incubated for 4 h at 37 °C. For analyses of siderophores produced *in vivo*, a split plate [31] was
202 used consisting of one half CAS agar for siderophore detection, and one half MEP agar, on
203 which the fungus was grown.
204
205 **Radiolabel exchange assay**. The substrate preferences of the CsNPS2 A domain was
206 determined by the substrate-dependent ATP-[^{32}P]pyrophosphate radiolabel exchange assay. All
207 reactions were run in triplicates. The reactions consisted of 80 mM Tris-buffer, 5 mM $MgCl_2$, 5
208 mM ATP, 1 mM substrate, 100 nM purified enzyme, and 0.1 µM [^{32}P]pyrophosphate (50
209 Ci/mmol). Substrates were: all proteinogenic L-amino acids, glycine, as well as L-ornithine,
210 N^5-hydroxy-L-ornithine, N^5-acetyl-N^5-hydroxy-L-ornithine (L-AHO), and N^5-*cis*-

anhydromevalonyl-N^5-hydroxy-L-ornithine (L-AMHO, fusarinine). First, substrates were added in pools (Table S2). Components of positive pools were added individually. The assays were kept at pH 7.5 and 28 °C in a total volume of 100 µl. After 30 min, the reactions were stopped and further processed as described [32]. Radiolabel exchange was quantified on a PerkinElmer TriCarb 2910TR scintillation counter.

Phosphopantetheinylation of CsNPS2. For CsNPS2-catalyzed product formation *in vitro*, the phosphopantetheinyl transferase Svp [27] was used to convert *apo*-CsNPS2 into its *holo*-form. 100 nM purified CsNPS2, 50 nM Svp, 250 µM coenzyme A in reaction buffer (80 mM Tris-HCl, pH 7.5, 5 mM $MgCl_2$, 100 µM EDTA) in a total volume of 3 ml were incubated for 30 min at 37 °C.

Basidioferrin synthesis *in vitro*. For basidioferrin formation, 5 mM ATP and 1 mM L-AHO, solved in Tris buffer (final volume 2 ml) were added. The reaction was carried out at 28 °C for 24 h, and stopped by lyophilization. The product was solved in methanol, filtered, and analyzed by the CAS agar diffusion assay, high performance liquid chromatography (HPLC) and mass spectrometry (LC-MS, see below). For negative control, an ATP-void reaction was run in parallel. For identification of iron coupled basidioferrin 1 mM $FeCl_3$ was added before LC-MS analysis.

Chemical analysis. HPLC and LC-MS with *in vitro* products were carried out on an Agilent Infinity 1260 liquid chromatograph equipped with a Zorbax Eclipse XDB-C18 column (150 × 4.6

232 mm, 5 µm particle size) and coupled to a 6130 single quad mass detector. Solvent A was 0.1 %
233 (v/v) formic acid in water, solvent B was acetonitrile. Diode array detection was at λ = 210 nm.
234 The gradient was: 10 % to 20 % B within 15 min, increase to 50 % B in 15 min, from 50 % to 60
235 % B in 10 min, and to 100 % B in another 10 min. For *in vivo* analyses, *Ceriporiopsis*
236 *subvermispora* culture supernatants were filtered and supplemented with Amberlite XAD-16
237 adsorber resin (10 % w/v). The beads were then washed with water, and the elution was
238 performed with 100 % MeOH. Subsequently, the solvent and residual water were removed by
239 rotary evaporation under reduced pressure. The dry extract was resuspended in MeOH. The
240 extract (5 ml) was further fractionated (2 min per fraction) by gel permeation chromatography
241 with Sephadex LH-20 (column 1.5 x 20 cm) as stationary phase and MeOH as mobile phase. CAS
242 assay-positive fractions were analyzed by LC-MS. High-resolution mass spectra were acquired
243 on a Thermo Accela liquid chromatograph with a C18 column (Grom-Sil 100 ODS-0 AB, 250 × 4.6
244 mm, 3 µm), interfaced to an Exactive Orbitrap spectrometer, operated in positive and negative
245 mode and by electrospray ionization. The following gradient was used: initial hold at 5% B for 1
246 min, followed by a linear gradient to 100% B within 15 min.
247
248 **Bioinformatic analyses.** The alignment and phylogenetic tree were created with MEGA5
249 software [33] using the built-in muscle alignment engine [34] and the neighbor-joining
250 algorithm. PheA from *Brevibacillus brevis* (pdb:1AMU) [35] was defined as an outgroup. The
251 muscle alignment was further used to determine the nonribosomal specificity codes by

252 extracting alignment positions corresponding to specificity-conferring residues of PheA or SidN3
253 [36].
254
255 **Chemical synthesis.** L-AHO was synthesized from N^2-benzyloxycarbonyl-L-ornithine as described
256 [37] and deprotected by hydrogenolysis. L-AMHO was obtained by mild alkaline hydrolysis of
257 fusarinine C. The identity of both compounds was confirmed using high resolution mass
258 spectrometry and NMR.
259
260 **RESULTS AND DISCUSSION**
261 **Identification of natural product biosynthesis genes.** The genomes of numerous
262 basidiomycetes of distinct phylogenetic clades encode type VI siderophore synthetases, making
263 these enzymes one of the most common (if not the most common) basidiomycete NRPS.
264 Among countless others, it is found in the white-rot model species *Ceriporiopsis subvermispora.*
265 Its genome sequence has been published [23]. Two adjacent genes encoding a 541 amino acid
266 (aa) putative monooxygenase (calculated mass 59.6 kDa) and a 2464 aa putative NRPS (270.8
267 kDa) hereafter referred to as SMO1 and CsNPS2, were identified (Figure 2, JGI protein IDs
268 113443 and 172109, respectively, GenBank accession number: KY287598). In addition, a gene
269 (*MFS1*) encodes a putative siderophore transporter of the major facilitator superfamily (MFS1,
270 protein ID 163556). However, *MFS1* is not clustered with *CsNPS2* and *SMO1*. The deduced
271 protein (600 aa, 64.4 kDa) shares 36.5 % identical amino acids with the characterized
272 transporter MirA of *A. nidulans* [38].

273 The *CsNPS2* gene is interrupted by 14, *SMO1* by five, and the *MFS* gene by 12 introns. A
274 comparably clustered arrangement of genes for a monooxygenase and an NRPS is found in
275 various fungi, e.g., for ferrichrome A biosynthesis in the basidiomycete *Omphalotus olearius*
276 [17]. Automatic annotation identified SMO1 as putative L-ornithine N^5-monooxygenase that
277 contains a Rossman-fold for NADPH+H^+ binding, similar to *Aspergillus fumigatus* SidA of the
278 ferricrocin/fusarinine C pathway [39]. CsNPS2 resembles a trimodular siderophore synthetase
279 that includes an adenylation domain and a triplicated thiolation-condensation di-domain
280 (Figure 2). Such triplications are also found with *Aspergillus fumigatus* SidC and numerous other
281 siderophore synthetases [3,40]. However, CsNPS2 and CsNPS2-like enzymes of other
282 basidiomycetes (Table 1) are dissimilar from SidC in that only one A domain is present.
283 Following the biosynthetic logic of NRPSs, through repetitive A-domain activity only one
284 monomeric substrate species would thus be loaded onto the T domains, followed by amide
285 bond formation between monomers. Consequently, this domain set-up makes a function as
286 synthetase for ferrichrome, ferricrocin, or ferrirhodin unlikely but points to a homotrimeric
287 compound, such as des(diserylglycl)ferrirhodin [41] or fusarinine B [42] (Figure 1). Given that
288 the relevant sequence portion (^{2136}LHHFQYDAWS^{2145}) of the terminal C domain of CsNPS2 does
289 not feature the signature motif typical for fungal C domain-like cyclization domains [43], a
290 linear CsNPS2 product was anticipated.
291
292 **Iron-dependent expression of natural product genes.** The expression of siderophore
293 biosynthesis genes is upregulated in response to iron limitation [4], e.g., shown for *sidC* and

294 *sidA* of *A. fumigatus* [44]. Our hypothesis that SMO1 and CsNPS2 serve siderophore
295 biosynthesis in *C. subvermispora*, was initially tested by a semi-quantitative reverse-
296 transcription PCR of *CsNPS2*, *SMO1*, and *MFS1*. We compared the transcriptional activity of
297 these genes under high iron conditions (that is, 10 µM Fe^{2+}) with iron depleted conditions (no
298 iron but 200 µM BPS added to chelate ferrous iron cations quantitatively and, thus, inhibit
299 reductive iron acquision). The constitutively expressed glyceraldehyde-3-phosphate
300 dehydrogenase gene (*GDH*) was used for reference. After RNA isolation and first strand cDNA
301 synthesis, the subsequent PCRs were then stopped after 27 cycles and the amplicons visually
302 evaluated after agarose gel electrophoresis (Figure S3). The *GDH* gene was equally intense, i.e.,
303 transcribed independently of iron availability. However, the cDNA amplicons of *CsNPS2*, *SMO1*,
304 and *MFS1* were stronger when cDNA was produced from mycelium grown under iron-deplete
305 conditions. This finding supports the hypothesis that CsNPS2, SMO1, and MFS1 may produce
306 and transport siderophores. Further evidence for siderophore secretion by *C. subvermispora*
307 came from the CAS-based siderophore detection assay. When the fungus was grown in the
308 modified CAS assay, using split plates (half CAS agar, half MEP, Figure S4), a pale yellow area on
309 the CAS side of the contact zone between the two media indicated siderophore secretion by *C.*
310 *subvermispora* under iron deplete conditions.
311
312 ***In silico* and *in vitro* analysis of CsNPS2 substrate specificity.** Prior to characterization of the
313 substrate specificity of CsNPS2 *in vitro*, we determined the so-called nonribosomal code, which
314 comprises ten mostly non-adjacent amino acids in adenylation domains that line the substrate-

315 binding pocket and, thus, impact substrate preference. It was identified as D-V-A-G-A-G-F-I-G-K
316 and present identically or near-identically in CsNPS2-like enzymes of other basidiomycete
317 species as well (Table 1). With an aspartic acid residue on the first position (D235, numbering
318 according to the bacterial reference enzyme PheA [35]) this code is indicative of an amino acid
319 as preferred CsNPS2 substrate as crystallography proved this aspartic acid residue as critical to
320 stabilize the α-amino group of the substrate [45]. Further, the CsNPS2 code resembles, to a
321 degree, the one for L-AHO-activating domains. For instance, the code D-V-L-D-I-G-F-I-G-K was
322 found with the N^5-acetyl-N^5-hydroxy-L-ornithine-activating A domain of the ferrichrome
323 synthetase Sib1 of S*chizosaccharomyces pombe* [40]. Notably, based on the crystal structure of
324 the *Neotyphodium lolii* epichloënin synthetase SidN (pdb:3ITE), an extended specificity code for
325 L-AHO activating domains was proposed [36]. However, the relevance for substrate prediction
326 by basidiomycete A domains remains still elusive.
327
328 Next, we determined the substrate specificity of the CsNPS2 A domain *in vitro*. A total of 24
329 amino acid substrates were tested, including N^5-hydroxy-L-ornithine, L-AHO, and L-AMHO.
330 Heterologous production of the full-length and *N*-terminally hexahistidine-tagged 274.5 kDa
331 CsNPS2 *apo*-protein was accomplished in *Aspergillus niger* tEB09. After purification by metal
332 affinity chromatography, pure CsNPS2 was assayed by substrate-dependent ATP-[^{32}P]-
333 pyrophosphate radiolabel exchange. High turnover was detected for monomeric siderophore
334 building blocks L-AHO (919,700 cpm, Figure 3) and L-AMHO (879,800 cpm). Contrastingly, poor
335 activity was observed for L-ornithine and L-alanine (3,640 and 4,050 cpm, respectively), i.e.,

values that come close to the negative control when water was offered as substrate (1,930 cpm). The result confirmed the above predictions made *in silico* and further supported the view that CsNPS2 acts as siderophore synthetase.

CsNPS2 product formation *in vitro*. *In vitro* product formation assays were subsequently performed with *holo*-CsNPS2, using either 1 mM L-AHO or L-AMHO as amino acid substrate. The reaction proceeded for 24 h and was then first analyzed by the CAS agar diffusion assay. Only the reaction with the substrate L-AHO resulted in a color change from blue to yellow which indicated the formation of a Fe(III)-chelating product (Figure S4). When L-AMHO was added as substrate or when ATP as left out (negative control), the CAS assay did not indicate iron chelation. Further analysis by HPLC and high-resolution mass spectrometry detected an additional signal at t_R = 8.3 min, which was not present in the negative control (Figure 4). High resolution mass spectrometry revealed the molecular mass of *m/z* 535.2722 $[M+H]^+$ which is consistent with the iron-void linear trimer of L-AHO (calculated *m/z* 535.2728 $[M+H]^+$). The linear trimer coupled to iron was also detected (*m/z* 588.1840 $[M+H]^+$). In the assay with L-AMHO as substrate, product formation was not detectable.

Chemical analysis of *C. subvermispora*. Mycelial extracts and the culture broth of *C. subvermispora,* grown under iron-limiting conditions, were chromatographically analyzed. Basidioferrin was not detectable, but the extract showed iron-chelating properties in the CAS agar diffusion assay. We therefore conclude that basidioferrin does not represent the ultimate

357 pathway product in *C. subvermispora*. Maybe it undergoes further post-NRPS modification, e.g.,
358 glycosylation, as shown for *Metarhizium robertsii* metachelins [46] or bacterial enterobactins
359 [47], or acetylation or hydroxylation which are found, e.g., with *Aspergillus fumigatus*
360 ferricrocins [48].
361
362 **Phylogeny of basidiomycete CsNPS2-like adenylation domains.** A sequence alignment was
363 produced using the MUSCLE algorithm [34]. The first set included A domains which adenylate L-
364 ornithine derivatives and which were taken from characterized asco- and basidiomycete
365 ferrichome synthetases. The second set represented A domains of CsNPS2-like enzymes with A-
366 T-C-T-C-T-C domain set-up. The phylogenetic clustering analysis (Figure 5) supported the
367 assumption that all CsNPS2-like A domains would group together, and represented a
368 monophyletic sub-branch of the tree. This phylogeny extends previous results by Turgeon and
369 coworkers, who categorized a single CsNPS2-like protein (EAU88504.2 of *Coprinopsis cinerea*)
370 as representative of type VI of siderophore synthetases [3]. Though CsNPS2 is likely to share a
371 common ancestor with N^5-acyl-N^5-hydroxy-L-ornithine-activating enzymes, it is only remotely
372 related to the ferrichrome A synthetase of the basidiomycete *Omphalotus olearius* [17].
373
374 **Conclusion**. The enzymatic and genetic basis of basidiomycete siderophore biosynthesis is little
375 explored yet, compared to ascomycetes. Besides the above-mentioned results on *Ustilago* and
376 *Omphalotus* ferrichromes, trimeric N^5-(3-methyl-*cis*-glutaconyl)-N^5-hydroxy-L-ornithine,
377 referred to as basidiochrome, was reported from *Ceratobasidium* and *Rhizoctonia* species [23].

For the ectomycorrhiza fungus *Suillus granulatus*, production and secretion of fusarinines B and C, ferrichrome, coprogen, and TAFC is reported. The closely related species *Suillus luteus* was found to release fusarinines B and C (= linear and cyclic fusigen, respectively), ferricrocin and coprogen [49] (Figure 1). These findings are incompatible with genomic data on the potential repertoire of natural product biosynthesis in either species. None of them encodes a ferrichrome synthetase, a SidC-like enzyme that would provide the catalytic capacity to synthesize TAFC, or an enzyme that is consistent with coprogen biosynthesis. The origin of this remarkable siderophore diversity in a fungal species remains unclear as is the case with *Laccaria bicolor* and *L. laccata*, found to produce ferricrocine, coprogen, triacetylfusarinine C, and fusarinine B [50]. *Suillus* or *Laccaria* siderophore biosynthesis has not been investigated biochemically. However, either above *Suillus* species encodes a type VI siderophore synthetase, whereas available genomic sequence data of *L. bicolor* does not indicate any siderophore synthetase gene [51]. The situation for *Laccaria* remains cryptic. However, in the light of our findings for CsNPS2, only a slightly altered activity for the *Suillus* synthetases needs to be assumed. Whereas both L-AHO and L-AMHO are adenylated by the CsNPS2 A domain, our results prove that only the former is trimerized. Assuming equal A domain preferences in the *Suillus* synthetases, but L-AMHO as building block that undergoes trimerization, our biochemical data could be well reconciled with the previously observed fusarinine B production. Fusarinine B biosynthesis also appears plausible, as in all cases, a linear trimeric N^5-acylated N^5-hydroxy-L-ornithine with chelating properties represents the immediate product of the respective enzyme.

Numerous basidiomycete genomes of various phylogenetic clades and lifestyles code for seven-domain type VI siderophore synthetases. Hence, our work on CsNPS2 has pilot character and helps investigate iron metabolism in basidiomycetes more thoroughly and broadly.

SUPPLEMENTAL MATERIAL

ACKNOWLEDGMENTS

We gratefully acknowledge Julia Gressler (Friedrich-Schiller-University Jena), Maria Poetsch, and Andrea Perner (both Leibniz Institute for Natural Product Research and Infection Biology - Hans-Knöll-Institute, Jena) for excellent technical assistance. Fusarinine C was kindly provided by Professor Hubertus Haas, Ph.D. (Innsbruck Medical University, Innsbruck, Austria).

FUNDING INFORMATION

This work was supported by the Deutsche Forschungsgemeinschaft (DFG grant HO2515/6-1).

FIGURE LEGENDS

Figure 1. Chemical structures of fungal siderophores, including basidioferrin, the newly described product of the peptide synthetase CsNPS2. Abbreviations: DDF: des(diserylglycl)ferrirhodin; TAFC: triacetylfusarinine C.

Figure 2. Physical map of basidioferrin biosynthetic genes in *Ceriporiopsis subvermispora*. The black arrows represent the transcriptional direction of the *CsNPS2* and *SMO1* genes. Intron positions within the genes are indicated by spaces between arrow segments. Below: domain setup of CsNPS2. Domain abbreviations are: A, adenylation; C, condensation; T, thiolation.

Figure 3. Adenylation domain substrate specificity of *Ceriporiopsis subvermispora* CsNPS2 siderophore synthetase, determined with the ATP-[^{32}P]pyrophosphate radioisotope exchange assay. Abbreviations: cpm: counts per minute; L-AHO, N^5-acetyl-N^5-hydroxy-L-ornithine; L-AMHO, N^5-*cis*-anhydromevalonyl-N^5-hydroxy-L-ornithine; Error bars indicate the standard deviation of three independent experiments.

Figure 4. HPLC analysis (λ = 210 nm) of CsNPS2-dependent basidioferrin production *in vitro*. Negative control: ATP-omitted reaction. The inset refers to the basidioferrin signal at t_R = 8.3 min and represents the respective high-resolution mass spectrum.

Figure 5. Phylogenetic tree of A-domains taken i) from basidiomycete NPS2-like proteins, ii) N^5-acyl-N^5-hydroxy-L-ornithine (AHO)-activating A-domains of known siderophore synthetases and iii) select non-siderophore A-domains. A sequence alignment was produced using the MUSCLE algorithm. PheA from *Brevibacilus brevis* was defined as outgroup.

REFERENCES

1. **Haas H**. 2003. Molecular genetics of fungal siderophore biosynthesis and uptake: the role of siderophores in iron uptake and storage. Appl Microbiol Biotechnol **62**:316-330.

2. **Hider RC, Kong X.** 2010. Chemistry and biology of siderophores. Nat Prod Rep 2010 27:637-657.
3. **Bushley KE, Ripoll DR, Turgeon BG.** 2008. Module evolution and substrate specificity of fungal nonribosomal peptide synthetases involved in siderophore biosynthesis. BMC Evol Biol **8**:328.
4. **Haas H.** 2012. Iron - A Key Nexus in the Virulence of *Aspergillus fumigatus*. Front Microbiol **3:**28.
5. **Schrettl M, Bignell E, Kragl C, Sabiha Y, Loss O, Eisendle M, Wallner A, Arst HN, Jr., Haynes K, Haas H.** 2007. Distinct roles for intra- and extracellular siderophores during *Aspergillus fumigatus* infection. PLoS Pathog **3:**1195-1207.
6. **Winkelmann G, Barnekow A, Ilgner D, Zähner H.** 1973. Metabolic products of microorganisms. 120. Uptake of iron by *Neurospora crassa*. Arch Mikrobiol **92**:285-300.
6a. **Gressler M, Meyer F, Heine D, Hortschansky P, Hertweck C, Brock M.** 2015. Phytotoxin production in Aspergillus terreus is regulated by independent environmental signals. Elife **4**: doi: 10.7554/eLife.07861.
7. **Eisendle M, Oberegger H, Zadra I, Haas H.** 2003. The siderophore system is essential for viability of *Aspergillus nidulans*: functional analysis of two genes encoding L-ornithine N^5-monooxygenase (*sidA*) and a non-ribosomal peptide synthetase (*sidC*). Mol Microbiol **49**:359-375.
8. **Atkin CL, Neilands JB.** 1968. Rhodotorulic acid, a diketopiperazine dihydroxamic acid with growth-factor activity. I. Isolation and characterization. Biochemistry **7**:3734-3739.
9. **Anke T, Diekmann H.** 1972. Biosynthesis of sideramines in fungi. Rhodotorulic acid synthetase from extracts of *Rhodotorula glutinis*. FEBS Lett 27:259-262.
10. **Haas H, Eisendle M, Turgeon BG.** 2008. Siderophores in fungal physiology and virulence. Annu Rev Phytopathol **46**:149-187.
11. **Haas H**. 2014. Fungal siderophore metabolism with a focus on *Aspergillus fumigatus*. Nat Prod Rep **31**:1266-1276.
12. **Munawar A, Marshall JW, Cox RJ, Bailey AM, Lazarus CM**. 2013. Isolation and characterisation of a ferrirhodin synthetase gene from the sugarcane pathogen *Fusarium sacchari*. Chembiochem **14**:388-394.
13. **Turgeon BG, Oide S, Bushley K.** 2008. Creating and screening *Cochliobolus heterostrophus* non-ribosomal peptide synthetase mutants. Mycol Res **112**:200-206.
14. **Finking R, Marahiel MA.** 2004. Biosynthesis of nonribosomal peptides. Annu Rev Microbiol **58:**453-488.
15. **Yuan WM, Gentil GD, Budde AD, Leong SA.** 2001. Characterization of the *Ustilago maydis sid2* gene, encoding a multidomain peptide synthetase in the ferrichrome biosynthetic gene cluster. J Bacteriol **183**:4040-4051.
16. **Winterberg B, Uhlmann S, Linne U, Lessing F, Marahiel MA, Eichhorn H, Kahmann R, Schirawski J.** 2010. Elucidation of the complete ferrichrome A biosynthetic pathway in *Ustilago maydis*. Mol Microbiol **75**:1260-1271.

17. **Welzel K, Eisfeld K, Antelo L, Anke T, Anke H.** 2005. Characterization of the ferrichrome A biosynthetic gene cluster in the homobasidiomycete *Omphalotus olearius*. FEMS Microbiol Lett **249:**157-163.
18. **Floudas D, Binder M, Riley R, Barry K, Blanchette RA, Henrissat B, Martinez AT, Otillar R, Spatafora JW, Yadav JS, Aerts A, Benoit I, Boyd A, Carlson A, Copeland A, Coutinho PM, de Vries RP, Ferreira P, Findley K, Foster B, Gaskell J, Glotzer D, Gorecki P, Heitman J, Hesse C, Hori C, Igarashi K, Jurgens JA, Kallen N, Kersten P, Kohler A, Kues U, Kumar TK, Kuo A, LaButti K, Larrondo LF, Lindquist E, Ling A, Lombard V, Lucas S, Lundell T, Martin R, McLaughlin DJ, Morgenstern I, Morin E, Murat C, Nagy LG, Nolan M, Ohm RA, Patyshakuliyeva A, Rokas A, Ruiz-Dueñas FJ, Sabat G, Salamov A, Samejima M, Schmutz J, Slot JC, St John F, Stenlid J, Sun H, Sun S, Syed K, Tsang A, Wiebenga A, Young D, Pisabarro A, Eastwood DC, Martin F, Cullen D, Grigoriev IV, Hibbett DS.** 2012. The Paleozoic origin of enzymatic lignin decomposition reconstructed from 31 fungal genomes. Science **336:**1715-1719.
19. **Eastwood DC, Floudas D, Binder M, Majcherczyk A, Schneider P, Aerts A, Asiegbu FO, Baker SE, Barry K, Bendiksby M, Blumentritt M, Coutinho PM, Cullen D, de Vries RP, Gathman A, Goodell B, Henrissat B, Ihrmark K, Kauserud H, Kohler A, LaButti K, Lapidus A, Lavin JL, Lee YH, Lindquist E, Lilly W, Lucas S, Morin E, Murat C, Oguiza JA, Park J, Pisabarro AG, Riley R, Rosling A, Salamov A, Schmidt O, Schmutz J, Skrede I, Stenlid J, Wiebenga A, Xie X, Kües U, Hibbett DS, Hoffmeister D, Högberg N, Martin F, Grigoriev IV, Watkinson SC.** 2011. The plant cell wall-decomposing machinery underlies the functional diversity of forest fungi. Science **333:**762-765.
20. **Stajich JE, Wilke SK, Ahrén D, Au CH, Birren BW, Borodovsky M, Burns C, Canbäck B, Casselton LA, Cheng CK, Deng J, Dietrich FS, Fargo DC, Farman ML, Gathman AC, Goldberg J, Guigó R, Hoegger PJ, Hooker JB, Huggins A, James TY, Kamada T, Kilaru S, Kodira C, Kües U, Kupfer D, Kwan HS, Lomsadze A, Li W, Lilly WW, Ma LJ, Mackey AJ, Manning G, Martin F, Muraguchi H, Natvig DO, Palmerini H, Ramesh MA, Rehmeyer CJ, Roe BA, Shenoy N, Stanke M, Ter-Hovhannisyan V, Tunlid A, Velagapudi R, Vision TJ, Zeng Q, Zolan ME, Pukkila PJ**. 2010. Insights into evolution of multicellular fungi from the assembled chromosomes of the mushroom *Coprinopsis cinerea* (*Coprinus cinereus*). Proc Natl Acad Sci USA **107**: 11889-11894.
21. **Shah F, Nicolás C, Bentzer J, Ellström M, Smits M, Rineau F, Canbäck B, Floudas D, Carleer R, Lackner G, Braesel J, Hoffmeister D, Henrissat B, Ahrén D, Johansson T, Hibbett DS, Martin F, Persson P, Tunlid A.** 2016. Ectomycorrhizal fungi decompose soil organic matter using oxidative mechanisms adapted from saprotrophic ancestors. New Phytol **209**:1705-1719.
22. **Sambrook J, Russell DW.** 2000. Molecular Cloning: A Laboratory Manual, 3rd ed., Cold Spring Harbor Laboratory Press, Cold Spring Harbor.
23. **Fernandez-Fueyo E, Ruiz-Duenas FJ, Ferreira P, Floudas D, Hibbett DS, Canessa P, Larrondo LF, James TY, Seelenfreund D, Lobos S, Polanco R, Tello M, Honda Y, Watanabe T, Watanabe T, Ryu JS, Kubicek CP, Schmoll M, Gaskell J, Hammel KE, St John FJ, Vanden Wymelenberg A, Sabat G, Splinter BonDurant S, Syed K, Yadav JS,**

Doddapaneni H, Subramanian V, Lavin JL, Oguiza JA, Perez G, Pisabarro AG, Ramirez L, Santoyo F, Master E, Coutinho PM, Henrissat B, Lombard V, Magnuson JK, Kues U, Hori C, Igarashi K, Samejima M, Held BW, Barry KW, LaButti KM, Lapidus A, Lindquist EA, Lucas SM, Riley R, Salamov AA, Hoffmeister D, Schwenk D, Hadar Y, Yarden O, de Vries RP, Wiebenga A, Stenlid J, Eastwood D, Grigoriev IV, Berka RM, Blanchette RA, Kersten P, Martinez AT, Vicuna R, Cullen D. 2012. Comparative genomics of *Ceriporiopsis subvermispora* and *Phanerochaete chrysosporium* provide insight into selective ligninolysis. Proc Natl Acad Sci USA **109:**5458-5463.

24. **Haselwandter K, Passler V, Reiter S, Schmid DG, Nicholson G, Hentschel P, Albert K, Winkelmann G.** 2006. Basidiochrome - a novel siderophore of the Orchidaceous Mycorrhizal Fungi *Ceratobasidium* and *Rhizoctonia* spp. Biometals **19:**335-343.

25. **Gressler M, Hortschansky P, Geib E, Brock M.** 2015. A new high-performance heterologous fungal expression system based on regulatory elements from the *Aspergillus terreus* terrein gene cluster. Front Microbiol **6:**184.

26. **Shimizu K, Keller NP.** 2001. Genetic involvement of a cAMP-dependent protein kinase in a G protein signaling pathway regulating morphological and chemical transitions in *Aspergillus nidulans*. Genetics **157:**591-600.

27. **Sanchez C, Du L, Edwards DJ, Toney MD, Shen B.** 2001. Cloning and characterization of a phosphopantetheinyl transferase from *Streptomyces verticillus* ATCC15003, the producer of the hybrid peptide-polyketide antitumor drug bleomycin. Chem Biol **8:**725-738.

28. **Bradford MM.** 1976. A rapid and sensitive method for the quantitation of microgram quantities of protein utilizing the principle of protein-dye binding. Anal Biochem **72:**248-254.

29. **Schwyn B, Neilands JB.** 1987. Universal CAS assay for the detection and determination of siderophores. Anal Biochem **160:**47-60.

30. **Shin SH, Lim Y, Lee SE, Yang NW, Rhee JH.** 2001. CAS agar diffusion assay for the measurement of siderophores in biological fluids. J Microbiol Methods **44:**89-95.

31. **Milagres AM, Machuca A, Napoleao D.** 1999. Detection of siderophore production from several fungi and bacteria by a modification of chrome azurol S (CAS) agar plate assay. J Microbiol Methods **37:**1-6.

32. **Schneider P, Weber M, Rosenberger K, Hoffmeister D.** 2007. A one-pot chemoenzymatic synthesis for the universal precursor of antidiabetes and antiviral bis-indolylquinones. Chem Biol **14:**635-644.

33. **Tamura K, Peterson P, Peterson N, Stecher G, Nei M, Kumar S.** 2011. MEGA5: molecular evolutionary genetics analysis using maximum likelihood, evolutionary distance, and maximum parsimony methods. Mol Biol Evol **28**:2731-2739.

34. **Edgar RC.** 2004. MUSCLE: multiple sequence alignment with high accuracy and high throughput. Nucleic Acids Res **32**:1792-1797.

35. **Conti E, Stachelhaus T, Marahiel MA, Brick P**. 1997. Structural basis for the activation of phenylalanine in the non-ribosomal biosynthesis of gramicidin S. EMBO J **16**:4174-4183.

36. **Lee TV, Johnson LJ, Johnson RD, Koulman A, Lane GA, Lott JS, Arcus VL.** 2010. Structure of a eukaryotic nonribosomal peptide synthetase adenylation domain that activates a large hydroxamate amino acid in siderophore biosynthesis. J Biol Chem **285:**2415-2427.
37. **Lin YM, Miller MJ.** 1999. Practical synthesis of hydroxamate-derived siderophore components by an indirect oxidation method and syntheses of a DIG-siderophore conjugate and a biotin-siderophore conjugate. J Org Chem **64**:7451-7458.
38. **Oberegger H, Schoeser M, Zadra I, Abt B, Haas H.** 2001. SREA is involved in regulation of siderophore biosynthesis, utilization and uptake in *Aspergillus nidulans*. Mol Microbiol **41:**1077-1089.
39. **Schrettl M, Haas H.** 2011. Iron homeostasis--Achilles' heel of *Aspergillus fumigatus*? Curr Opin Microbiol **14:**400-405.
40. **Schwecke T, Göttling K, Durek P, Duenas I, Kaufer NF, Zock-Emmenthal S, Staub E, Neuhof T, Dieckmann R, von Döhren H.** 2006. Nonribosomal peptide synthesis in *Schizosaccharomyces pombe* and the architectures of ferrichrome-type siderophore synthetases in fungi. ChemBioChem **7:**612-622.
41. **Jalal MAF, Galles JL, Vanderhelm D.** 1985. Structure of Des(Diserylglycyl)Ferrirhodin, Ddf, a Novel Siderophore from *Aspergillus ochraceous*. J Org Chem **50:**5642-5645.
42. **Diekmann H**. 1967. Stoffwechselprodukte von Mikroorganismen. 56. Mitteilung. Fusigen – ein neues Sideramin aus Pilzen. Arch Microbiol **58**:1-5.
43. **Gao X, Haynes SW, Ames BD, Wang P, Vien LP, Walsh CT, Tang Y.** 2012. Cyclization of fungal nonribosomal peptides by a terminal condensation-like domain. Nat Chem Biol **8:**823-830.
44. **Schrettl M, Bignell E, Kragl C, Sabiha Y, Loss O, Eisendle M, Wallner A, Arst HN, Jr., Haynes K, Haas H.** 2007. Distinct roles for intra- and extracellular siderophores during *Aspergillus fumigatus* infection. PLoS Pathog **3:**1195-1207.
45. **Stachelhaus T, Mootz HD, Marahiel MA**. 1999. The specificity conferring code of adenylation domains in nonribosomal peptide synthetases. Chem Biol **6**:493-505.
46. **Krasnoff SB, Keresztes I, Donzelli BG, Gibson DM**. 2014. Metachelins, mannosylated and *N*-oxidized coprogen-type siderophores from *Metarhizium robertsii*. J Nat Prod **77**: 1685-1692.
47. **Fischbach MA, Lin H, Liu DR, Walsh CT**. 2006. How pathogenic bacteria evade mammalian sabotage in the battle for iron. Nat Chem Biol **2**:132-138.
48. **Blatzer M, Schrettl M, Sarg B, Lindner HH, Pfaller K, Haas H**. 2011. SidL, an *Aspergillus fumigatus* transacetylase involved in biosynthesis of the siderophores ferricrocin and hydroxyferricrocin. Appl Environ Microbiol **77**:4959-4966.
49. **Haselwandter K, Häninger G, Ganzera M.** 2011. Hydroxamate siderophores of the ectomycorrhizal fungi *Suillus granulatus* and *S. luteus*. Biometals **24**:153-157.
50. **Haselwandter K, Häninger G, Ganzera M, Haas H, Nicholson G, Winkelmann G**. 2013. Linear fusigen as the major hydroxamate siderophore of the ectomycorrhizal Basidiomycota *Laccaria laccata* and *Laccaria bicolor*. Biometals **26**:969–979.
51. **Martin F**, **Selosse MA.** 2008. The *Laccaria* genome: a symbiont blueprint decoded. New Phytol **180**:296-310.

52. **Lee BN, KrokenS, Chou DY, Robbertse B, Yoder OC, Turgeon BG**. 2005. Functional analysis of all nonribosomal peptide synthetases in *Cochliobolus heterostrophus* reveals a factor, NPS6, involved in virulence and resistance to oxidative stress. Eukaryot Cell **4**:545-555.

53. **Kohler A, Kuo A, Nagy LG, Morin E, Barry KW, Buscot F, Canbäck B, Choi C, Cichocki N, Clum A, Colpaert J, Copeland A, Costa MD, Doré J, Floudas D, Gay G, Girlanda M, Henrissat B, Herrmann S, Hess J, Högberg N, Johansson T, Khouja HR, LaButti K, Lahrmann U, Levasseur A, Lindquist EA, Lipzen A, Marmeisse R, Martino E, Murat C, Ngan CY, Nehls U, Plett JM, Pringle A, Ohm RA, Perotto S, Peter M, Riley R, Rineau F, Ruytinx J, Salamov A, Shah F, Sun H, Tarkka M, Tritt A, Veneault-Fourrey C, Zuccaro A; Mycorrhizal Genomics Initiative Consortium., Tunlid A, Grigoriev IV, Hibbett DS, Martin F.** 2015. Convergent losses of decay mechanisms and rapid turnover of symbiosis genes in mycorrhizal mutualists. Nat Genet **47**:410-415.

Table1: Comparison of fungal siderophore synthetases mentioned in this study with CsNPS2 and like enzymes. For synthetases featuring more than one A domain, it is indicated in brackets to which A domain the NRPS code and substrate specificity refer. Abbreviations: L-AHO, N^5-acetyl-N^5-hydroxy-L-ornithine; L-AMHO, N^5-*cis*-anhydromevalonyl-N^5-hydroxy-L-ornithine; L-MGHO, N^5-*trans*-(α-methyl)-glutaconyl-N^5-hydroxy-L-ornithine. Domain abbreviations: A, adenylation; dA, degenerate adenylation; C, condensation; T, thiolation. The siderophore synthetase categories described by Turgeon and co-workers [3] are given in the column "synthetase type".

Organism	NRPS (A domain)	Synthetase domain structure	NRPS code	Substrate	Synthetase type	Ref.
Ustilago maydis	Sid2 (A2)	A-T-C-A-T-C-A-T-C-T-C	DVLSIGAIGK	L-AHO	I	[15]
Ustilago maydis	Sid2 (A3)	A-T-C-A-T-C-A-T-C-T-C	DVIDMGAIGK	L-AHO	I	[15]
Neotyphodium lolii	SidN (A3)	A-T-C-A-T-C-A-T-C-T-C-T-C	DVGGGGVIGK	L-AMHO	II	[36]
Aspergillus fumigatus	SidC (A3)	A-T-C-A-T-C-A-T-C-T-C-T-C	DVLSSGAIGK	L-AHO	II	[7]
Omphalotus olearius	Fso1 (A3)	A-T-C-A-T-C-A-T-C-T-C-T-C	DIITITATLR	L-MGHO	II	[17]
Ustilago maydis	Fer3 (A3)	A-T-C-A-T-C-A-T-C-T-C-T-C	DVSSGGAIMK	L-MGHO	II	[16]
Schizosaccharomyces pombe	Sib1 (A3)	A-T-C-T-C-dA-T-C-A-T-C-T-C-T-C	DVLDIGFIGK	L-AHO	III	[40]
Cochliobolus heterostrophus	NPS2 (A4)	A-T-C-A-T-C-A-T-C-A-T-C-T-C-T-C	DVLDIGGIGK	L-AHO	V	[3,52]
Coniophora puteana	NPS1	A-T-C-T-C-T-C	DVSGAGFIGK	?	VI	[18]
Serpula lacrymans	NPS4	A-T-C-T-C-T-C	DVCGGGFIGK	?	VI	[19]
Coprinopsis cinerea	EAU88504.2	A-T-C-T-C-T-C	DVCGGGFIGK	?	VI	[20]
Suillus luteus	Sid1	A-T-C-T-C-T-C	DVAGAGFIGK	?	VI	[53]
Stereum hirsutum	EIM88654.1	A-T-C-T-C-T-C	DVSGVGFVGK	?	VI	[18]
Fomitiporia mediterranea	EJD05778.1	A-T-C-T-C-T-C	DVAGAGFIGK	?	VI	[18]
Ceriporiopsis subvermispora	CsNPS2	A-T-C-T-C-T-C	DVAGAGFIGK	L-AHO	VI	[23, this work]

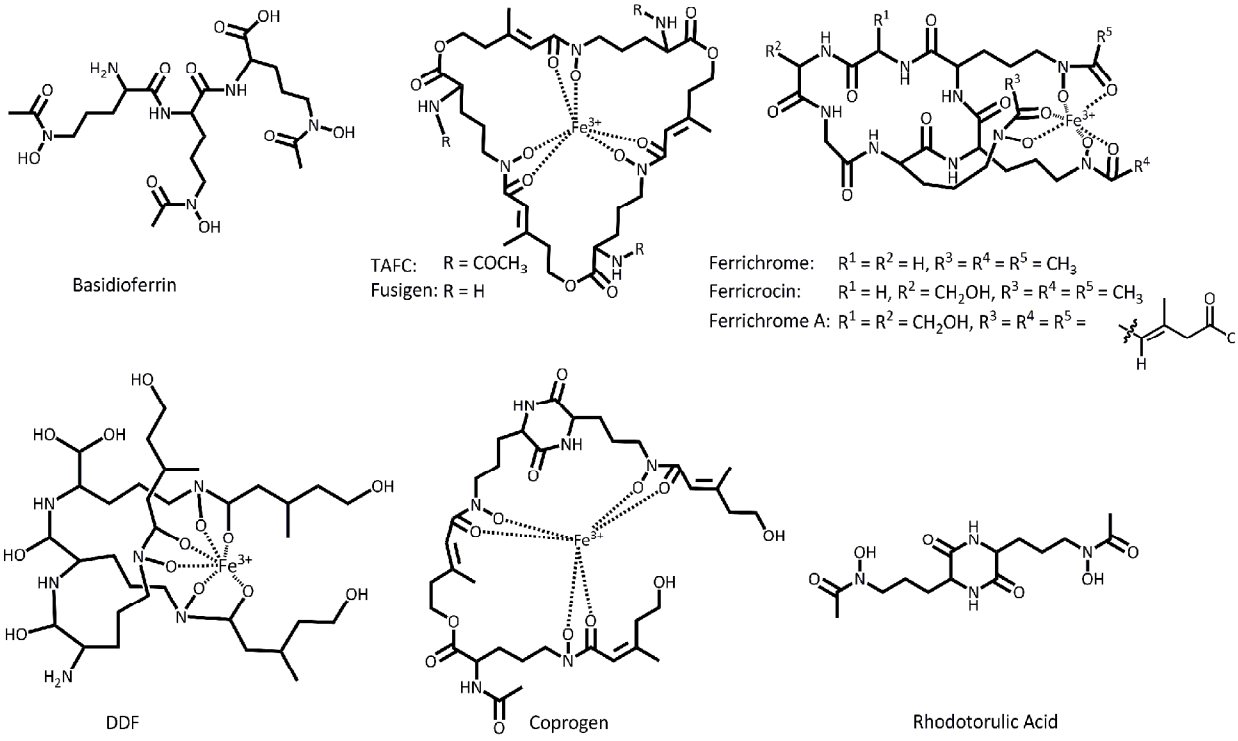

Figure 1. Chemical structures of fungal siderophores

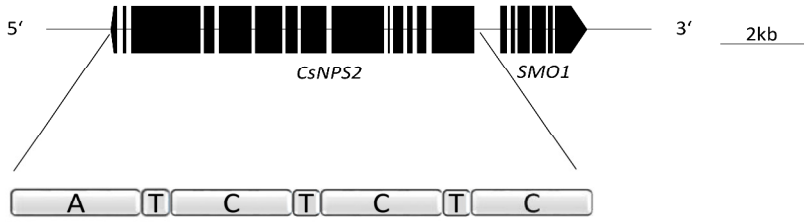

Figure 2. Physical map of basidioferrin biosynthetic genes in C*eriporiopsis subvermispora*

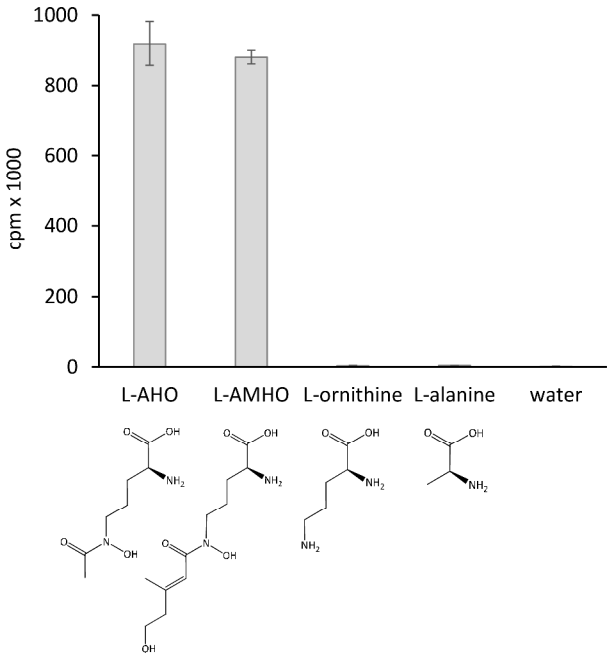

Figure 3. Adenylation domain substrate specificity of C*eriporiopsis subvermispora* CsNPS2

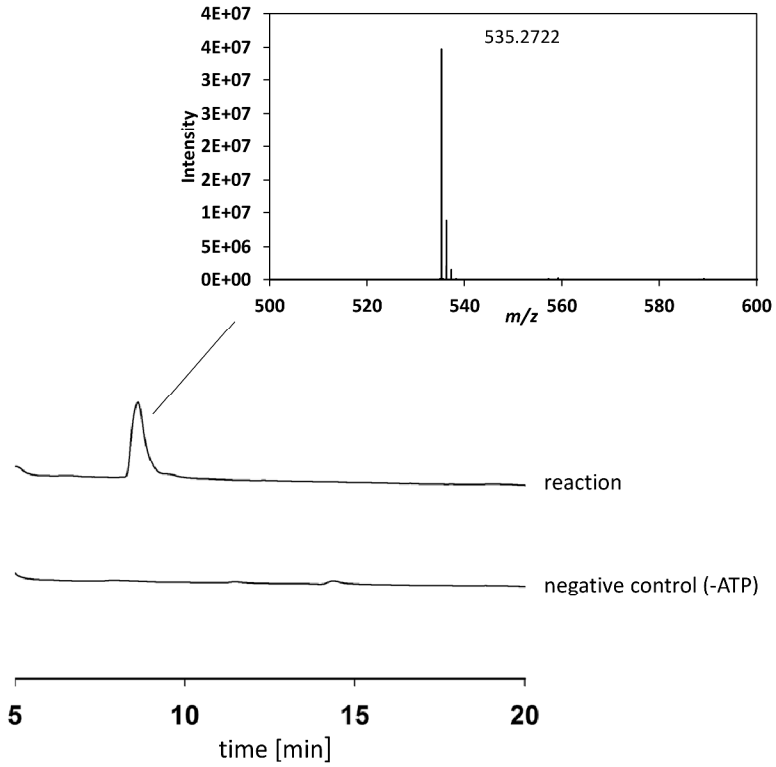

Figure 4. HPLC analysis (λ = 210 nm) of CsNPS2-dependent basidioferrin production *in vitro.*

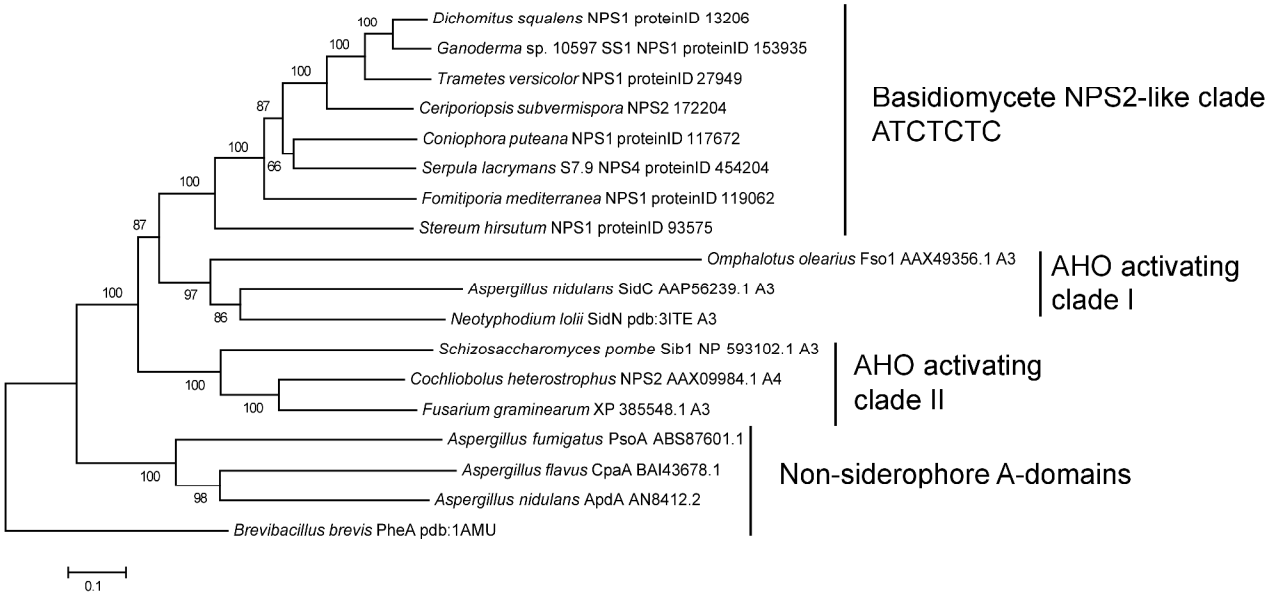

Figure 5. . Phylogenetic tree of A-domains

Supplemental Material

The basidiomycete peptide synthetase CsNPS2 catalyzes N^5-acetyl-N^5-hydroxy-L-ornithine trimerization for siderophore biosynthesis

Eileen Brandenburger,[a] Markus Gressler,[b*] Robin Leonhardt,[a†] Gerald Lackner,[c] Andreas Habel,[d] Christian Hertweck,[d] Matthias Brock,[e] Dirk Hoffmeister[a#]

Department of Pharmaceutical Microbiology at the Hans-Knöll-Institute, Friedrich-Schiller-University, Jena, Germany[a]; Department Microbial Biochemistry and Physiology, Leibniz Institute for Natural Product Research and Infection Biology - Hans-Knöll-Institute, Jena, Germany[b]; Junior Group Synthetic Microbiology at the Hans-Knöll-Institute, Friedrich-Schiller- University, Jena, Germany[c]; Department Biomolecular Chemistry, Leibniz Institute for Natural Product Research and Infection Biology - Hans-Knöll-Institute, Jena, Germany[d]; School of Life Sciences, University of Nottingham, United Kingdom[e]

Present addresses:

*Markus Gressler, Department of Parasitology and Mycology at the Pasteur Institute, Paris, France

[†]Robin Leonhardt, Department of Food Chemistry, Leibniz-Universität Hannover, Germany

[#]Address correspondence to Dirk Hoffmeister, dirk.hoffmeister@leibniz-hki.de.

Table of contents

Table S1 (Oligonucleotide primers) 3

Table S2 (Pools of substrates) 4

Figure S1 (Plasmid construction) 5

Figure S2 (Southern Blots) 6

Figure S3 (Gel electrophoresis) 7

Figure S4 (Chrome Azurol S agar diffusion assay) 8

Figure S5 (SDS-polyacrylamide gel electrophoresis) 9

Table S1. Sequences (5´to 3´) of oligonucleotide primers.

Primer	Sequence
NPS2-1	CGGAGCCAGCTCTAAGAGAAC
NPS2fw	TTATGGCGGATCCAATGAGCGCACAC
NPS2rev	GTGTCTGAATTCACGGAGCGTTATAGGATTCC
2641	GACGGCCAGTGAATTCGATCCTCTCTCTGATATTGTCG
2644	TACCGAGCTCGAATTCGAGTGAGGGTTGAGTACGAG
oRL1	CTAGAAGTGATTGGCCGTATCG
oRL2	CTAACCCGCGACTCAATTGATTCTG
oEB28	CATCACAGCACCATGCGGGGTTCTCATCATCATCATC
oEB30	ATCACTGCTGCCATGGCTAAGCAAGGCACTCCTTGAC
oRL3	CATACCGAACTGGCGATCTC
oRL4	CGGAGCCAGCTCTAAGAGAAC
oEB46	TCAAGTACGACTCCGTCCAC
oEB47	GTACCACGAGATGAGCTTG
oEB48	GTGTGAAGAAGGTCGAGG
oEB49	GTCTGCGTAGACGAGAAG
oEB54	GGAAGCACAAGATCCTCTG
oEB55	GTTGCGGAGTCTGTTTCG
oRL5	CATACCGAACTGGCGATCTC
oRL6	CGGAGCCAGCTCTAAGAGAAC

Table S2. Pools of amino acid substrates used for the ATP-[^{32}P]pyrophosphate radiolabel exchange assay. Non-standard abbreviations: L-AHO, N^5-hydroxy-L-ornithine, N^5-acetyl-N^5-hydroxy-L-ornithine; L-AMHO, N^5-*cis*-anhydromevalonyl-N^5-hydroxy-L-ornithine.

Pool	Compounds
1	Gly, L-Ala, L-Val, L-Leu, L-Ile
2	L-Cys, L-Met, L-Ser, L-Thr, L-Pro
3	L-His, L-Phe, L-Tyr, L-Trp
4	L-Asp, L-Asn, L-Glu, L-Gln
5	L-Lys, L-Arg
6	L-AHO, L-AMHO, L-Orn, N^5-hydroxy-L-ornithine

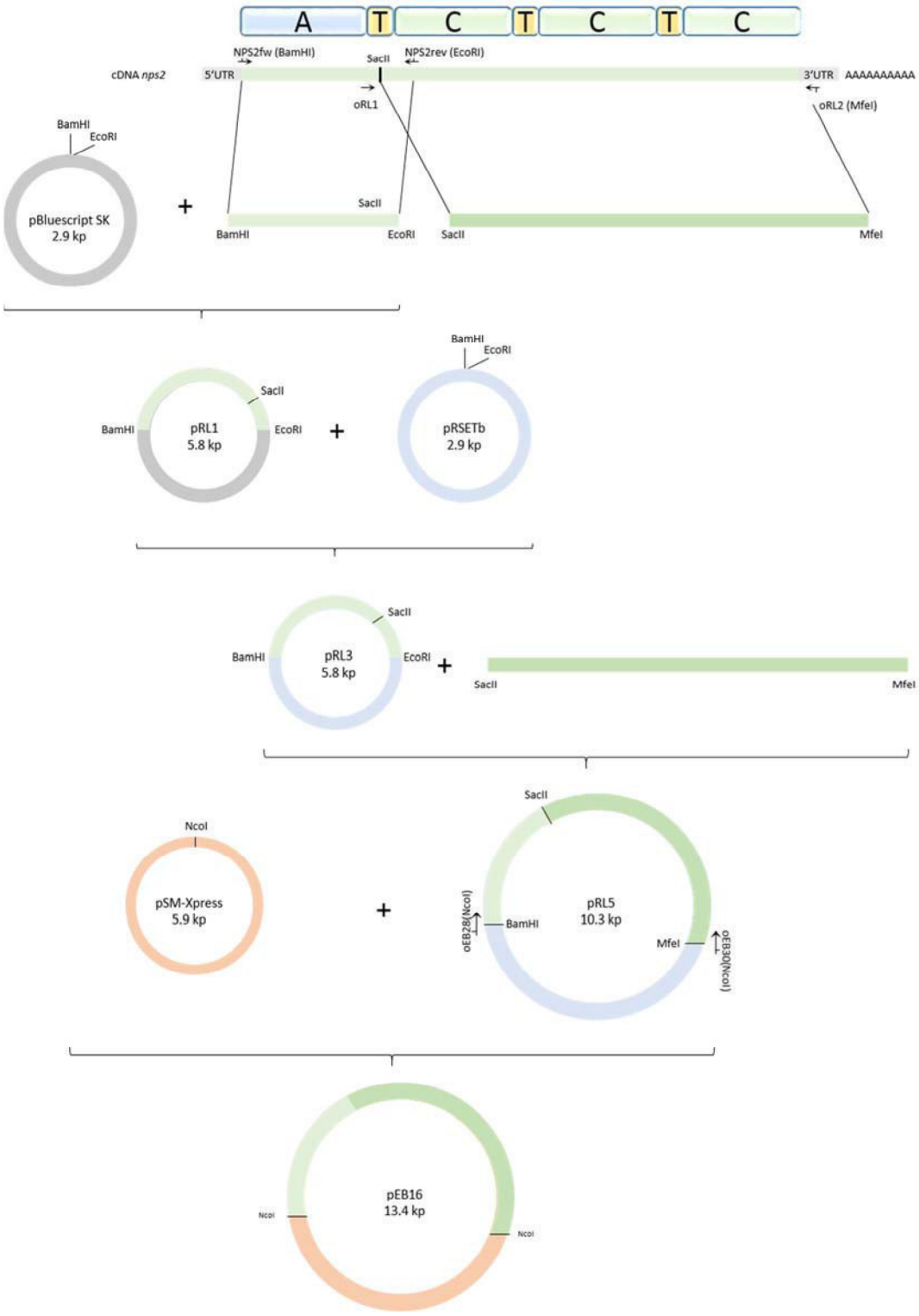

Figure S1. Strategy to construct expression plasmid pEB16 for heterologous expression of the siderophore synthetase gene *CsNPS2* in *A. niger*.

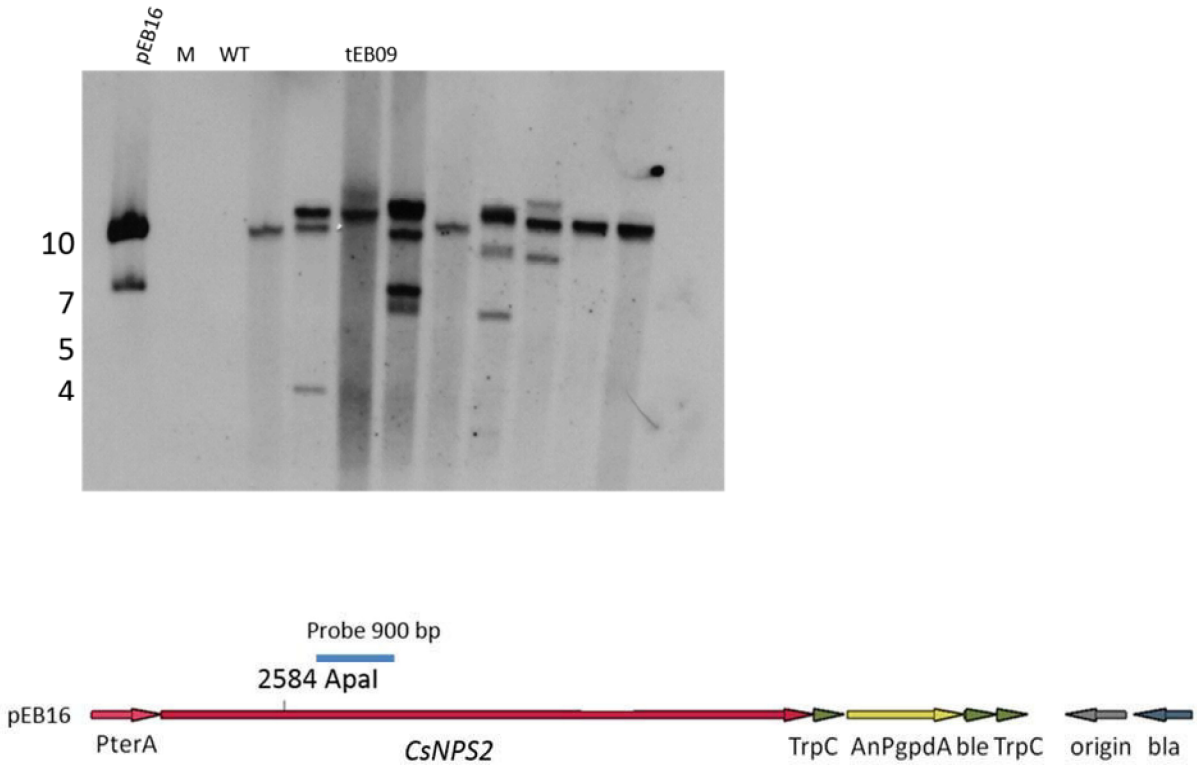

Figure S2. Southern blot analysis of *Aspergillus niger* transformants. pEB16: positive control, that is, *CsNPS2* expression plasmid pEB16 linearized (see schematic) and in circular form. WT: Negative control, i.e., *A. niger* P2 (wild type) genomic DNA, cut with ApaI. The other lanes represent ApaI-treated genomic DNA of nine transformants. Single-integration transformant tEB09 was used for this study. The blot was probed with a 0.9 kb *CsNPS2* fragment (blue bar in the schematic), PCR-amplified from *C. subvermispora* genomic DNA using oligonucleotides oRL5 and oRL6.

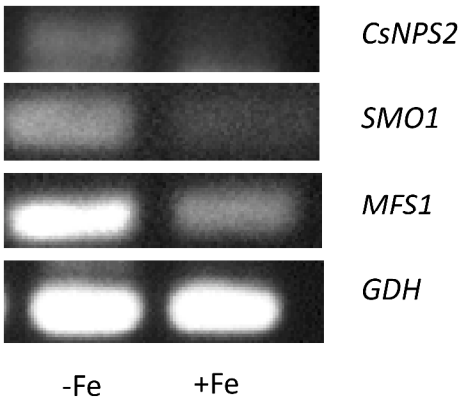

Figure S3. Gel electrophoresis of reverse transcription PCR products (27 cycles) of siderophore biosynthesis-related genes *CsNPS2*, *SMO1*, and *MFS1* of cultures grown under iron deplete conditions (-Fe) and iron availability (+Fe). The constitutively expressed glyceraldehyde-3-phosphate dehydrogenase gene *GDH* served as reference.

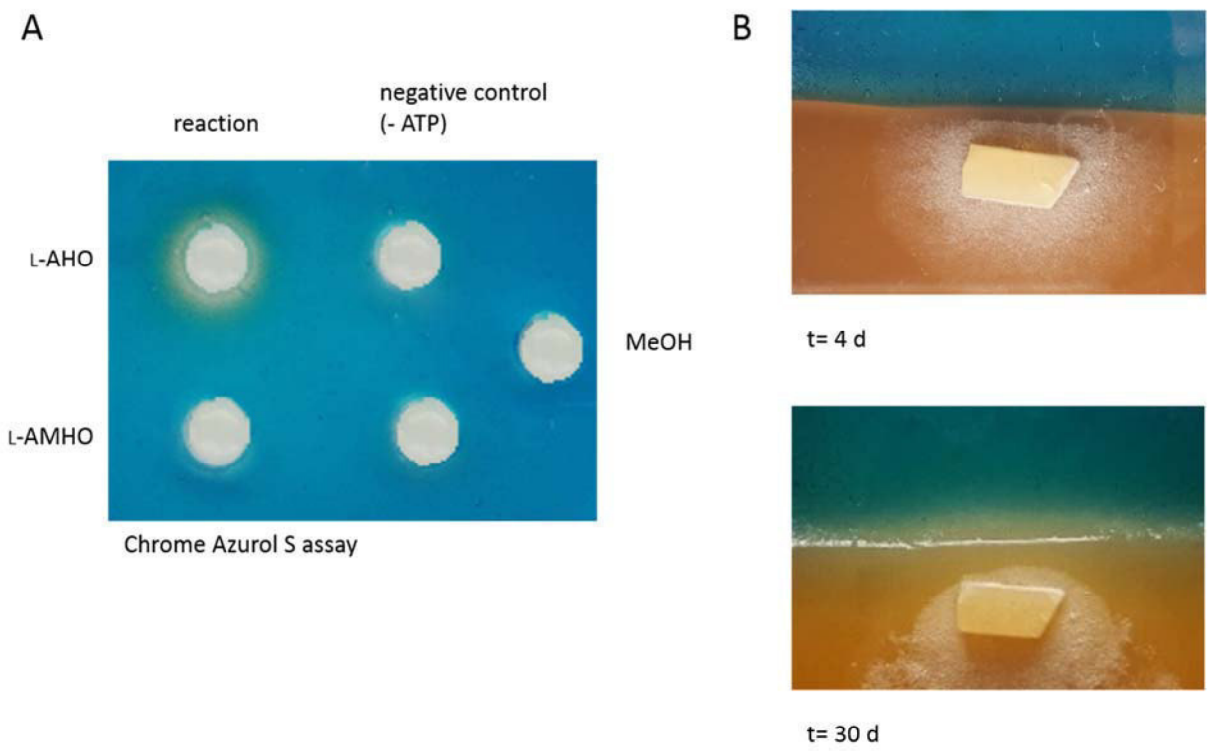

Figure S4. Chrome Azurol S agar diffusion assays to test for iron chelation. A) Test of CsNPS2-based *in vitro* product formation reactions, using either L-AHO (top, left) or L-AMHO (bottom, left) as monomers for the synthetase reaction. Negative controls (center) included ATP-free reactions. Solvent control (right) was with methanol. Right panel: *Ceriporiopsis subvermispora* inoculated on split plates after 4 and 30 days of growth. Top sector (blue): CAS-agar, bottom sector (ochre): malt extract peptone agar.

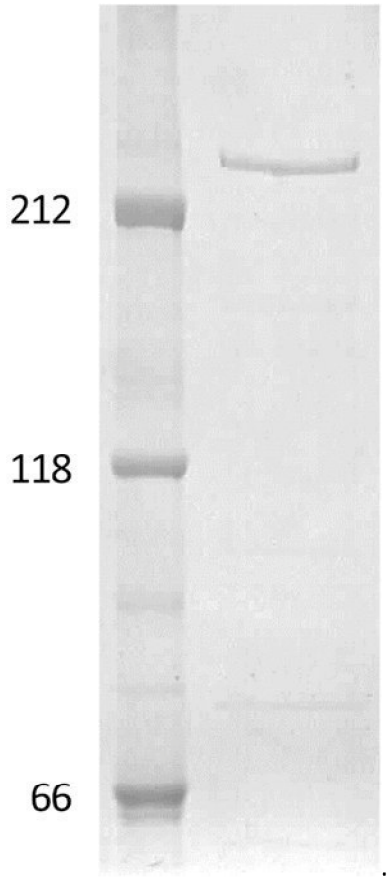

Figure S5. SDS-polyacrylamide gel electrophoresis of hexahistidine-tagged CsNPS2 that was heterologously produced in *Aspergillus niger*. Molecular weight of the protein standard is given in kDa.

3.3 Publikation 3, Baccile et al. (2016), *Nature Chemical Biology*

Plant-like biosynthesis of isoquinoline alkaloids in *Aspergillus fumigatus.*

Joshua A. Baccile, Joseph E. Spraker, Henry H Le, Eileen Brandenburger, Christian Gomez, Jin Woo Bok, Juliane Macheleidt, Axel A. Brakhage, Dirk Hoffmeister, Nancy P. Keller, Frank C. Schroeder.

Nature Chemical Biology *12*, 419-424.

Mit vergleichenden Metabolomanalysen wurde in *Aspergillus fumigatus* das Gencluster *fsq* identifiziert. Dieses Cluster kodiert für Biosyntheseenzyme, die für die Produktion neuer Isoquinolin-Alkaloide (Fumisoquine) erforderlich sind und beinhaltet ein Gen für ein NRPS-ähnliches Enzym ohne Kondensationsdomäne. Dieser Syntheseweg, welcher auf der Verknüpfung von Kohlenstoffatomen zwischen zwei Aminosäureeinheiten basiert, ähnelt der Biosynthese der Isoquinolin-Alkaloide in Pflanzen. Für die Fumisoquin-Synthese wird die *N*-Methyltransferase FsqC und die FAD-abhängige Oxidase FsqB benötigt. Funktionelle Analoga dazu sind die Coclaurin *N*-Methyltransferase und die Berberin-Brückenenzyme in Pflanzen. Diese Ergebnisse tragen zu einer neuen Sichtweise hinsichtlich biosynthetischer Gencluster mit unvollständigen NRPSs bei und lassen vermuten, dass Biosynthesewege wie für die pflanzlichen Isoquinoline auch bei Pilzen zu finden sind.

Angaben zum Eigenanteil von E. Brandenburger (10 %)

Heterologe Produktion und Aufreinigung und Analyse von FsqF, Durchführung der ATP-[^{32}P]-Pyrophosphat-Austauschassays.

nature chemical biology

ARTICLE

PUBLISHED ONLINE: 11 APRIL 2016 | DOI: 10.1038/NCHEMBIO.2061

Plant-like biosynthesis of isoquinoline alkaloids in *Aspergillus fumigatus*

Joshua A Baccile[1,8], Joseph E Spraker[2,8], Henry H Le[1], Eileen Brandenburger[3], Christian Gomez[1], Jin Woo Bok[4], Juliane Macheleidt[4,5], Axel A Brakhage[4,5], Dirk Hoffmeister[3], Nancy P Keller[6,7]* & Frank C Schroeder[1]*

Natural product discovery efforts have focused primarily on microbial biosynthetic gene clusters (BGCs) containing large multimodular polyketide synthases and nonribosomal peptide synthetases; however, sequencing of fungal genomes has revealed a vast number of BGCs containing smaller NRPS-like genes of unknown biosynthetic function. Using comparative metabolomics, we show that a BGC in the human pathogen *Aspergillus fumigatus* named *fsq*, which contains an NRPS-like gene lacking a condensation domain, produces several new isoquinoline alkaloids known as the fumisoquins. These compounds derive from carbon-carbon bond formation between two amino acid–derived moieties followed by a sequence that is directly analogous to isoquinoline alkaloid biosynthesis in plants. Fumisoquin biosynthesis requires the *N*-methyltransferase FsqC and the FAD-dependent oxidase FsqB, which represent functional analogs of coclaurine *N*-methyltransferase and berberine bridge enzyme in plants. Our results show that BGCs containing incomplete NRPS modules may reveal new biosynthetic paradigms and suggest that plant-like isoquinoline biosynthesis occurs in diverse fungi.

One major source of medicinally important small molecules are microbial BGCs that encode PKSs and NRPSs, two classes of multifunctional mega-enzymes that are usually accompanied by sets of tailoring enzymes. The recent surge in the sequencing of fungal genomes has revealed large numbers of BGCs that do not appear to encode enzymes involved in the production of any known metabolites ('orphan BGCs') and thus may harbor new biosynthetic capabilities[1–3].

In our search for new biosynthetic mechanisms, we focused on orphan BGCs that contain small NRPS-like genes that diverge from canonical NRPSs in their domain structure. Canonical NRPSs include, at minimum, one adenylation domain that selects and activates an amino acid (or related building block), one thiolation domain for covalent attachment of the activated amino acid and a condensation domain that catalyzes formation of a peptide bond between the tethered amino acid and another substrate[4–6]. However, sequencing of fungal genomes has additionally revealed numerous genes that encode only a subset of these domains[1,2]. Such noncanonical NRPS-like genes may feature adenylation and thiolation domains but lack condensation domains and thus most likely do not function as peptide synthetases[7,8]. We hypothesized that analyzing BGCs, including small NRPS-like genes encoding incomplete modules, would most likely reveal new biosynthetic functions.

Here we show that the *fsq* gene cluster in *A. fumigatus*, which features an NRPS-like gene, *fsqF*, produces a series of new isoquinoline alkaloids known as the fumisoquins. We then demonstrate that FsqF, which lacks a canonical condensation domain, is required for carbon-carbon bond formation between L-serine– and L-tyrosine–derived building blocks in the fumisoquin biosynthetic pathway. Two additional enzymes encoded by the *fsq* cluster, the *N*-methyltransferase FsqC and the FAD-dependent oxidase FsqB, catalyze the formation of the isoquinoline ring system in the fumisoquins via a sequence that we show is directly analogous to the biosynthesis of a prominent group of plant isoquinoline alkaloids, one of the largest families of medicinally important natural products[9,10].

RESULTS

FsqF encodes an incomplete NRPS module

The expression of many fungal orphan BGCs is under the control of the nuclear protein LaeA, a global regulator of morphogenesis and virulence factor in *A. fumigatus* and other pathogenic fungi[11,12]. Among LaeA-regulated orphan BGCs in the human pathogen *A. fumigatus*, the *fsq* cluster features a small NRPS-like gene, *fsqF*, which encodes an adenylation, thiolation, reductase and pyridoxal phosphate–dependent aminotransferase domain (**Fig. 1a**). Notably, FsqF lacks the condensation domain that is essential for canonical peptide bond formation, and bioinformatic analysis of the vicinity of *fsqF* did not reveal any genes that could code for a second NRPS or free-standing condensation domain[13]. We found that expression of *fsqF* is regulated by the $Zn(II)_2Cys_6$–type transcriptional activator FsqA (**Fig. 1a** and **Supplementary Results**, **Supplementary Fig. 1**). $Zn(II)_2Cys_6$ transcription factors are unique to fungi and have been shown to regulate many metabolic pathways, such as aflatoxin biosynthesis in *A. flavus*[14]. In addition to FsqF, the transcription factor FsqA was found to regulate expression of five adjacent genes, annotated as ABC transporter (*fsqE*), fructosyl amino acid oxidase (*fsqB*), *N*-methyltransferase (*fsqC*), phenol 2-monooxygenase (*fsqG*) and ATP-grasp enzyme (*fsqD*), defining the boundaries of the *fsq* cluster (**Supplementary Fig. 1**)[13].

[1]Boyce Thompson Institute and Department of Chemistry and Chemical Biology, Cornell University, Ithaca, New York, USA. [2]Department of Plant Pathology, University of Wisconsin–Madison, Madison, Wisconsin, USA. [3]Department of Pharmaceutical Microbiology at the Hans-Knöll-Institute, Friedrich Schiller University, Jena, Germany. [4]Institute for Microbiology, Friedrich Schiller University, Jena, Germany. [5]Molecular and Applied Microbiology, Leibniz Institute for Natural Product Research and Infection Biology (HKI), Jena, Germany. [6]Department of Bacteriology, University of Wisconsin–Madison, Madison, Wisconsin, USA. [7]Department of Medical Microbiology and Immunology, University of Wisconsin–Madison, Madison, Wisconsin, USA. [8]These authors contributed equally to this work. *e-mail: schroeder@cornell.edu or npkeller@wisc.edu

Identification of *fsq* cluster-derived metabolites

Overexpression of *fsqA* was associated with accumulation of a characteristic brown pigment in the surrounding medium (**Supplementary Fig. 2**), suggesting secretion of a colored metabolite (or metabolites). To identify *fsq*-derived metabolites, we used two-dimensional NMR-based comparative metabolomics (differential analysis by two-dimensional NMR spectroscopy (DANS)), which facilitates comprehensive and largely unbiased detection of new metabolites associated with gene cluster overexpression[15,16]. DANS-based comparison of whole metabolome extracts from overexpression (OE::*fsqA*) and deletion (Δ*fsqA*) strains revealed several differential signals, most prominently two sets of OE-dependent doublets between 4.6 p.p.m. and 5.0 p.p.m. with large coupling constants of 18–20 Hz (**Fig. 1b**), suggesting a diastereotopic benzylic CH_2 group within a bi- or oligocyclic structure. The OE::*fsqA*–dependent metabolites were characterized further following partial purification via reversed-phase chromatography using a standard suite of two-dimensional NMR spectra and high-resolution MS (HRMS) (**Supplementary Table 1** and **Supplementary Note**). These analyses revealed two new tricyclic isoquinoline derivatives as major metabolites associated with *fsq* overexpression: the pyrido[1,2-*b*] isoquinolines fumisoquin A (**1**; **Fig. 1c**) and fumisoquin B (**2**; **Fig. 1c**). Fumisoquin A and B decompose gradually during chromatography, most likely as a result of the oxidation-prone hydroquinone moiety. We further noted a deeply purple OE-dependent metabolite that was not captured by DANS because it decomposed during sample preparation. Optimization of extraction conditions and reverse-phase fractionation, followed by two-dimensional NMR spectroscopic and HRMS analysis, allowed us to identify a third isoquinoline, fumisoquin C (**3**; **Fig. 1c**), as the deeply purple colored metabolite (**Supplementary Fig. 3** and **Supplementary Note**). While standing or during chromatography, fumisoquin C decomposes into **4** and **5**, which are more stable and were isolated (**Fig. 1c**, **Supplementary Fig. 4a** and **Supplementary Note**). Treatment of partially purified fumisoquin C with trimethylsilyldiazomethane furnished the corresponding dimethyl derivative (**Supplementary Fig. 4b**), which is much less prone to decomposition and provided additional NMR spectroscopic data to confirm the structure and relative configuration of fumisoquin C (**Supplementary Note**).

A plant-analogous isoquinoline formation pathway

Isoquinoline alkaloids are rare among known fungal natural products, and the tricyclic ring systems of the fumisoquins, to the best of our knowledge, are unprecedented in fungi. However, the identified dihydroxylated isoquinolines are reminiscent of a large and diverse family of plant-derived isoquinoline alkaloids (pyrido[1,2-*b*]isoquinolines such as scoulerine (**6**); **Fig. 1d**), whose biosynthetic pathways have been studied extensively[17–19]. Plant pyrido[1,2-*b*]isoquinoline biosynthesis proceeds via N-methylation of a tyrosine-derived catechol precursor, followed by oxidative cyclization via the FAD-dependent berberine bridge enzyme (BBE; **Fig. 1d**)[17], a member of a large group of flavin-dependent amine oxidases[20,21]. The cyclization most likely proceeds via a two-step mechanism, beginning with FAD-dependent oxidation of the methyl group to an iminium species followed by electrophilic attack on the deprotonated phenol, although earlier studies suggested an alternative, concerted mechanism[17,19]. Because of the manifold pharmaceutical uses of plant isoquinoline alkaloids, there is considerable interest in developing microbial-based production approaches[22–24], and yeast-based expression systems for several groups of plant isoquinoline alkaloids, including the berberines, have been developed[25–30]. We noted that the *fsq* cluster features a set of genes that may encode functional analogs of the berberine biosynthetic enzymes, including the putative phenol 2-monooxygenase FsqG, *N*-methyltransferase FsqC and FAD-dependent oxidase FsqB. Bioinformatic analysis revealed several orphan gene clusters in fungi

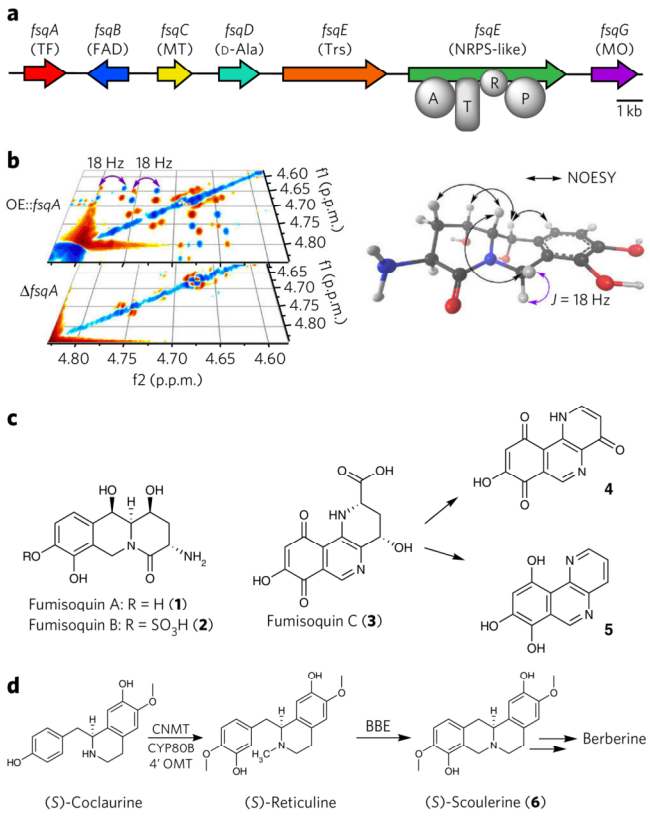

Figure 1 | Analysis of the *fsq* gene cluster and metabolite production. (**a**) *fsq* gene cluster and putative assignments of encoded proteins. TF, transcription factor; FAD, FAD-binding domain protein; MT, *N*-methyltransferase; D-ala, ATP-grasp enzyme (D-alanine ligase); Trs, transporter; A, adenylation; T, thiolation; R, short-chain dehydrogenase/reductase domain; P, pyridoxal phosphate binding domain; MO, phenol 2-monooxygenase. (**b**) Section of the double quantum filtered COSY spectra of OE::*fsqA* and Δ*fsqA* metabolite extracts used for comparative metabolomics (DANS). NOESY, nuclear Overhauser effect spectroscopy. (**c**) The *fsq*-dependent compounds fumisoquin A and B (**1** and **2**), including stereochemical assignments via NOESY for **1** (**Supplementary Note**) as well as the structure of fumisoquin C (**3**), which decomposes to **4** and **5**. (**d**) Biosynthesis of structurally related isoquinoline alkaloids in plants via coclaurine *N*-methyltransferase (CNMT), *N*-methylcoclaurine 3′-monooxygenase (CYP80B), 3′-hydroxy-*N*-methyl-(*S*)-coclaurine 4′-*O*-methyltransferase (4′OMT) and berberine bridge enzyme (BBE).

that feature homologous sets of genes (**Supplementary Table 2** and **Supplementary Fig. 5**). Moreover, the only other known fungal isoquinolines have been linked to a gene cluster containing homologs for these three genes[31].

To investigate the biosynthesis of the fumisoquins, we created deletion strains in the OE::*fsqA* background for all of the genes in the *fsq* cluster except for *fsqD* and the putative transporter *fsqE*, which we were unable to delete, possibly because of a protective function of these proteins that has been found in several other fungal BGCs[1]. We then compared the metabolomes of each of these deletion strains with those of OE::*fsqA* and Δ*fsqA* via DANS and HPLC/MS (**Fig. 2a–d**). We found that deletion of the *N*-methyltransferase FsqC, phenol 2-monooxygenase FsqG or FAD-dependent oxidase FsqB in the OE::*fsqA* background led to complete abolishment of isoquinoline alkaloid production and accumulation of a series of benzyl pyrroles (**7** and **8**; **Figs. 2c** and **3**), including the previously reported fumipyrrole, **7** (where the *fsq* cluster was referred to as *fmp*[32]), smaller amounts of which were also produced in the

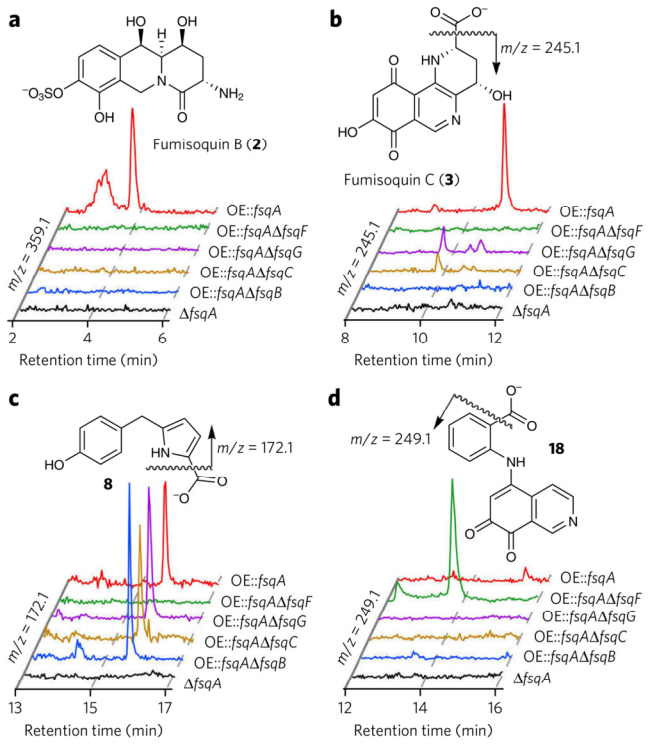

Figure 2 | Comparative metabolomics of *fsq* gene cluster mutants by HPLC/MS. (**a**–**d**) HPLC/MS analysis of *fsq* gene deletion strains in the OE::*fsqA* background shows ion chromatograms representing major products and shunt metabolites.

OE::*fsqA* control strain (**Fig. 2c**). Comparison of the carbon skeletons of the pyrroles (**7** and **8**; **Fig. 3**) with those of the fumisoquins provided support for the predicted *N*-methyltransferase and phenol 2-monooxygenase functions of FsqC and FsqG, respectively, and suggested that the fumisoquins form from an open-chain precursor such as **9** (**Fig. 3**) in a manner very similar to that of plant benzophenanthridine alkaloid biosynthesis[18].

The structure of the putative open-chain precursor **9** suggested that it may be derived from tyrosine and a dehydroalanine equivalent (**10**; **Fig. 3**), which could be produced from serine or cysteine via the pyridoxal-phosphate dependent aminotransferase domain of the NRPS-like protein FsqF[10,33]. By growing the OE::*fsqA* strain in medium supplemented with different amino acids labeled with stable isotopes, we found that L-tyrosine and L-serine are incorporated into the fumisoquins and pyrroles (**1**–**3** and **8**) in a manner consistent with the biosynthetic model shown in **Figure 3**, whereas L-cysteine is not incorporated (**Fig. 4a**,**b**, **Supplementary Figs. 6** and **7b**–**d** and Online Methods). Furthermore, we showed that the L-methionine methyl group is incorporated into the fumisoquin ring systems at the predicted position, in agreement with the putative function of FsqC as an *S*-adenosyl methionine–dependent *N*-methyltransferase (**Fig. 4c** and **Supplementary Fig. 8**).

FsqB is a functional analog of plant BBE

To test whether FsqB catalyzes isoquinoline ring formation in **1**–**3** and thus acts as a functional ortholog of plant BBE, we recombinantly produced polyhistidine-tagged FsqB in *E. coli* (**Supplementary Fig. 9**). We then assayed its activity on a range of potential substrates that mimicked the tyrosine-derived portion of putative intermediate **9**. Whereas *N*-methyl dopamine did not react, we found that FsqB converts *N*-methyl DOPA (**11**), prepared via a simple one-step procedure, directly into isoquinoline **12** (**Fig. 5a** and **Supplementary Figs. 10** and **12a**). We first tested FsqB activity on **11** on a small scale suitable for LC/MS, which yielded near-quantitative conversion to **12** within 3–4 h (100 mM phosphate buffer, pH 7, K_M = 142.5 ± 42.9 µM (mean ± s.d.)) (**Fig. 5b** and **Supplementary Fig. 11**). Next we demonstrated isoquinoline formation from **11** on a milligram scale by conducting the reaction in an NMR tube using deuterated phosphate buffer (**Fig. 5c** and **Supplementary Note**). Notably, FsqB-catalyzed formation of **12** proceeds with complete regioselectivity, as the alternative cyclization product, 6,7-dihydroxy-1,2,3,4-tetrahydroisoquinoline-3-carboxylic acid (**13**), which does form alongside **12** in a nonenzymatic reaction of DOPA with formaldehyde, was not observed (**Supplementary Fig. 10** and **Supplementary Note**). In contrast, we observed no cyclized products when incubating FsqB with *N*-methyl-L-tyrosine, *N*,*N*-dimethyl DOPA or the BBE-substrate (*S*)-reticuline, suggesting that both a catechol moiety and a secondary β-*N*-methylamine are required for FsqB activity (**Supplementary Fig. 12b**–**d**).

Next we asked whether the mechanism of isoquinoline formation as catalyzed by FsqB is directly analogous to that of the extensively studied plant enzyme, BBE[9,17,19,34]. Fluorescence analysis of

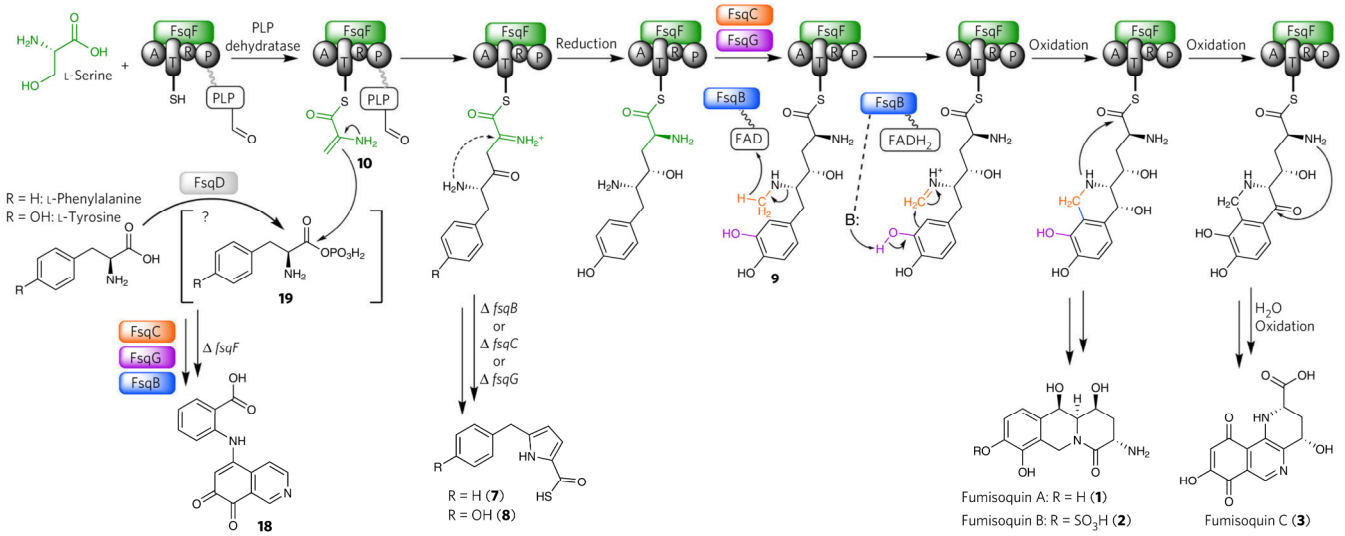

Figure 3 | Model for fumisoquin biosynthesis. The proposed mechanism for FsqB-mediated isoquinoline formation is based on its functional similarity to plant BBE[17–19] (detailed in **Fig. 5**). The role of the ATP-grasp enzyme FsqD in activating tyrosine to form **19** is putative. A, adenylation; T, thiolation; R, short-chain dehydrogenase/reductase domain; P, pyridoxal phosphate binding domain.

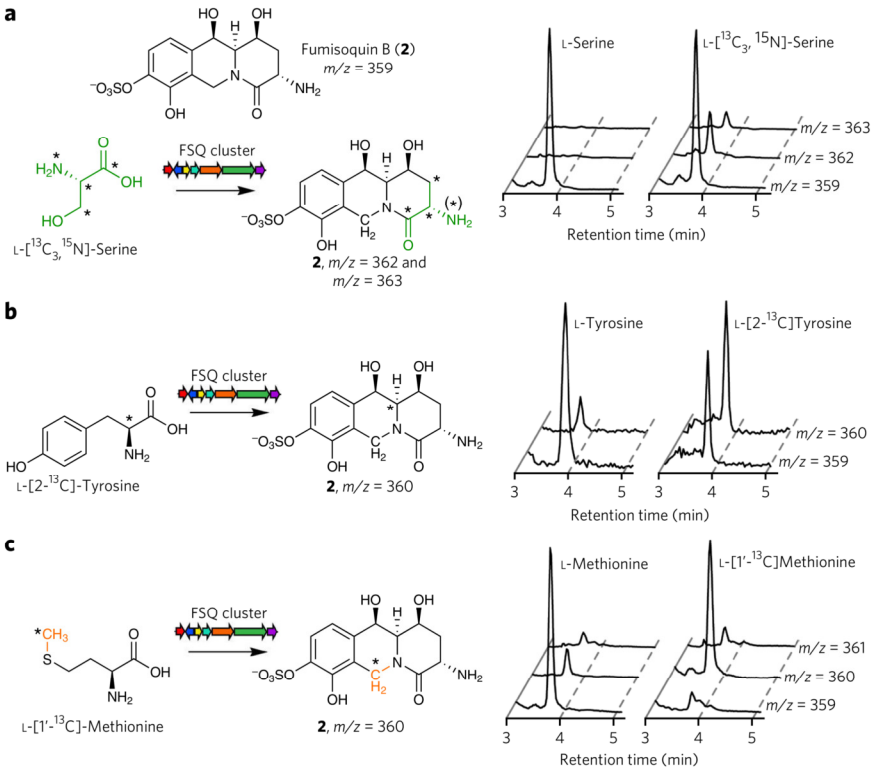

Figure 4 | The fumisoquins incorporate L-serine, L-tyrosine and an L-methionine–derived methyl group. (**a**–**c**) HPLC/MS ion chromatograms derived from fungal cultures grown with L-serine or L-[$^{13}C_3$,^{15}N]-serine (**a**), L-tyrosine or L-[2-^{13}C]-tyrosine (**b**) and L-methionine or L-[1′-^{13}C]-methionine (**c**). In contrast, L-cysteine is not incorporated (**Supplementary Fig. 6**). Mass spectra are shown in **Supplementary Figure 7**. Asterisks denote labeled isotopes. In the case of L-[$^{13}C_3$,^{15}N]-serine, loss of ^{15}N due to partial deamination or amination contributes to an increased *m/z* of 362.

recombinant FsqB showed excitation and emission maxima at 461 nm and 530 nm, respectively (**Supplementary Fig. 9**), suggesting that FsqB uses a flavin cofactor, as predicted[35]. Further proteomic analysis of FsqB confirmed the presence of FAD, which was found to be covalently bound to Cys414 (**Supplementary Fig. 13a** and **Supplementary Table 3**). FAD is also part of BBE, where it is bound to a histidine residue[17]. Flavin reduction during catalytic cycling of BBE is recovered with molecular oxygen–generating hydrogen peroxide[17], a characteristic that was also observed with FsqB using an Amplex Red assay (**Supplementary Fig. 13b**). Isoquinoline formation as catalyzed by BBE most likely proceeds via an imine intermediate in a two-step mechanism[19]. To test whether isoquinoline formation via FsqB also involves an imine intermediate, we incubated FsqB with *N*-methyl-L-tyrosine (**14**), which we hypothesized may represent an oxidation-competent substrate for FsqB but, as shown below, does not get cyclized in the presence of the electrophile trapping agent dimedone (**15**). This reaction produced the adduct **16** as well as free tyrosine, consistent with capture of an imine intermediate (**17**) by dimedone or water (**Fig. 5d**). Therefore, the fungal enzyme FsqB appears to catalyze isoquinoline formation via a two-step mechanism that is analogous to that of plant-derived BBE.

Carbon-carbon bond formation requires FsqF

Next we recombinantly produced the FsqF adenylation domain to test whether it activates L-tyrosine or L-serine, as suggested by the stable isotope labeling study, using the ATP-[^{32}P]pyrophosphate exchange activity[36]. However, neither enantiomer of serine or tyrosine showed any activity in the *in vitro* assay nor did any other tested standard amino acid (**Supplementary Fig. 14**). These results may indicate that the recombinantly expressed FsqF adenylation domain was not functional or that the true substrate is not a standard amino acid. Given the homology of the PLP-dependent domain in FsqF to other serine dehydrogenases[13,33], we hypothesized that L-serine may first be converted into dehydroalanine, which is then activated and tethered to the thiolation domain (**Fig. 3**).

To further investigate the role of the NRPS-like enzyme FsqF in fumisoquin biosynthesis, we analyzed the effect of *fsqF* deletion on the OE::*fsqA* metabolome. As anticipated, production of the fumisoquins (**1**–**3**) as well as the pyrroles (**7** and **8**) was completely abolished in OE::*fsqA*-Δ*fsqF* (**Fig. 2d**). Notably, we also observed production of a single, brightly red shunt metabolite, the anthranilic acid–substituted isoquinoline **18** (**Figs. 2d** and **3**). Feeding experiments of the OE::*fsqA*-Δ*fsqF* mutant with stable isotope–labeled L-tyrosine confirmed that the isoquinoline ring system in **18** is derived from tyrosine, as in the case of the fumisoquins (**Supplementary Fig. 15**). Incubation of **12**, obtained *in vitro* from recombinant FsqB, with anthranilic acid (**19**) led to formation of the shunt metabolite **18**, consistent with a model in which **18** forms nonenzymatically from **12** via oxidation to the corresponding *o*-quinone, subsequent capture of anthranilic acid and decarboxylation (**Supplementary Fig. 16**). Compound **12** was not observed in any of the analyzed OE::*fsqA*-Δ*fsqF* extracts, most likely because of its high susceptibility to oxidize to the reactive *o*-quinone, which is rapidly captured by anthranilic acid (**Supplementary Fig. 16**).

The identification of the shunt metabolite **18** indicates that the NRPS-like protein FsqF is only required for addition of a serine-derived dehydroalanine moiety to activated tyrosine but is not essential for the subsequent steps leading to isoquinoline formation and that a different enzyme, most likely the ATP-grasp enzyme FsqD, is responsible for activation of tyrosine (**Fig. 3**). The production of shunt metabolite **7** would then indicate that FsqD is also capable of activating phenylalanine; however, phenylalanine-derived intermediates only lead to the production of **7**, as expected given the predicted function of FsqG as a phenol 2-monooxygenase[13] and the observation that recombinantly produced FsqB requires a catechol as a substrate. FsqD has homology to carboxylate-amine ligases that furnish aminoacyl phosphate from ATP and amino acid precursors[37,38]. In a recent example, the FsqD homolog PGM1 was shown to activate nonproteinogenic amino acids for peptide bond formation in pheganomycin biosynthesis[39]. In contrast, FsqD appears to activate tyrosine (or phenylalanine) for subsequent condensation with serine-derived dehydroalanine (**Fig. 3**), providing what is to our knowledge the first example for a new strategy for forming carbon-carbon bonds in fungi.

DISCUSSION

Our analysis of the *fsq* cluster revealed a plant-like strategy for the biosynthesis of oligocyclic alkaloids in fungi. The biosynthetic steps of phenol hydroxylation, *N*-methylation and oxidative cyclization seem to be the same in plants and fungi, and thus the corresponding enzymes can be considered functionally equivalent. Sequence

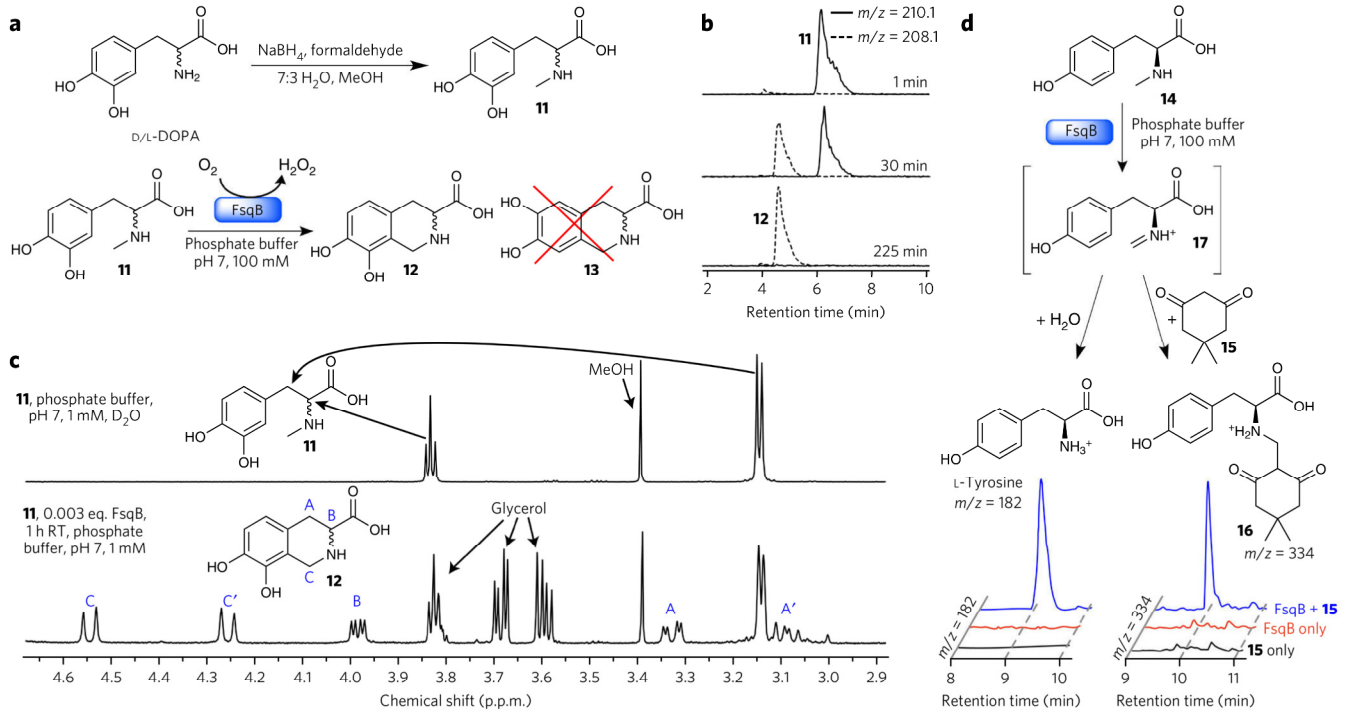

Figure 5 | Enzymatic activity of recombinant FsqB. (**a**) Synthesis of *N*-methyl-3′,4′-dihydroxy-D/L-phenylalanine **11** (top) and regioselective conversion of **11** into **12** by purified recombinant FsqB (bottom). The isomer **13** does not form. (**b**) Ion chromatograms at indicated time points for the FsqB-catalyzed *in vitro* conversion of **11** to **12** (100 mM phosphate buffer, pH 7, 100:1 substrate to enzyme). (**c**) ^{1}H NMR spectra of a sample of **11** (1 mM phosphate buffer in D_2O) before FsqB addition (top) and 1 h after FsqB addition (333:1 substrate to enzyme), showing selective conversion of **11** into **12** (bottom). RT, room temperature. (**d**) Ion chromatograms showing the formation of tyrosine and **16** resulting from the capture of intermediate **17** by H_2O or dimedone, **15** (1.5 μM FsqB and 400 μM *N*-methyl-L-tyrosine in 100 mM phosphate buffer, pH 7).

analysis does not suggest homology for these proteins, though it is notable that cyclization proceeds via analogous two-step mechanisms that are catalyzed by FAD-dependent oxidases in both fungi and plants[19], presenting a marked case of convergent evolution of specialized metabolic pathways. Given that analysis of available fungal genomes[13] revealed many co-occurrences of homologs of the *N*-methyltransferase *fsqC* and FAD-dependent oxidase *fsqB* (**Supplementary Fig. 5**), it seems likely that fungi are capable of producing a diverse range of as-yet-undiscovered isoquinoline alkaloids. For example, in addition to *Aspergillus* spp., the genomes of plant pathogenic *Fusarium* spp. feature BGCs that include homologs for most *fsq* genes[40].

Together with other recent examples[7,8], the fumisoquins show that analysis of gene clusters containing incomplete NRPS modules can reveal intriguing new structures and biosynthetic strategies. It remains unclear, however, whether the biosynthetic roles of NRPS-like enzymes can be predicted as current examples, though few, hint at considerable functional diversity. For example, two NRPS-like enzymes in *A. flavus*, named LnaA and LnaB, have been shown to produce a series of tyrosine-derived piperazines, pyridines and morpholines[7], whereas an NRPS-like enzyme from *Aspergillus terreus* was shown to reduce products of an accompanying non-reducing PKS[8]. The *fsq* pathway example demonstrates that NRPS-like enzymes lacking condensation domains may nonetheless contribute to ligating amino acids, albeit via the formation of carbon-carbon bonds. Characterization of BGCs featuring small NRPS-like genes may thus reveal new types of alliances of NRPS-like enzymes with other amino acid–activating proteins, for example, ATP-grasp enzymes such as FsqD.

This work supports a mining strategy of assessing fungal natural products that applies not only to canonical NRPS but also PKS-like genes and even those fungal clusters lacking NRPS or PKS-like domain genes altogether. Recent examples have focused on cyclic ribosomal peptides[41], but a bioinformatic scan of fungal genomes and expression data shows the existence of yet more alternative biosynthetic clusters lacking NRPS-like, PKS-like and canonical ribosomal peptides, suggesting unexplored chemical diversity[42]. Efforts to characterize such alternative clusters may yield even more unique fungal chemistry.

Received 23 July 2015; accepted 22 February 2016;
published online 11 April 2016

METHODS

Methods and any associated references are available in the online version of the paper.

References

1. Keller, N.P. Translating biosynthetic gene clusters into fungal armor and weaponry. *Nat. Chem. Biol.* **11**, 671–677 (2015).
2. Sanchez, J.F., Somoza, A.D., Keller, N.P. & Wang, C.C. Advances in *Aspergillus* secondary metabolite research in the post-genomic era. *Nat. Prod. Rep.* **29**, 351–371 (2012).
3. Brakhage, A.A. Regulation of fungal secondary metabolism. *Nat. Rev. Microbiol.* **11**, 21–32 (2013).
4. Fischbach, M.A. & Walsh, C.T. Assembly-line enzymology for polyketide and nonribosomal peptide antibiotics: logic, machinery, and mechanisms. *Chem. Rev.* **106**, 3468–3496 (2006).
5. Jenke-Kodama, H. & Dittmann, E. Bioinformatic perspectives on NRPS/PKS megasynthases: advances and challenges. *Nat. Prod. Rep.* **26**, 874–883 (2009).
6. Walsh, C.T., O'Brien, R.V. & Khosla, C. Nonproteinogenic amino acid building blocks for nonribosomal peptide and hybrid polyketide scaffolds. *Angew. Chem. Int. Edn Engl.* **52**, 7098–7124 (2013).
7. Forseth, R.R. *et al.* Homologous NRPS-like gene clusters mediate redundant small-molecule biosynthesis in *Aspergillus flavus*. *Angew. Chem. Int. Edn Engl.* **52**, 1590–1594 (2013).

8. Wang, M., Beissner, M. & Zhao, H. Aryl-aldehyde formation in fungal polyketides: discovery and characterization of a distinct biosynthetic mechanism. *Chem. Biol.* **21**, 257–263 (2014).
9. Hagel, J.M. & Facchini, P.J. Benzylisoquinoline alkaloid metabolism: a century of discovery and a brave new world. *Plant Cell Physiol.* **54**, 647–672 (2013).
10. Bentley, K.W. β-Phenylethylamines and the isoquinoline alkaloids. *Nat. Prod. Rep.* **23**, 444–463 (2006).
11. Bok, J.W. *et al.* LaeA, a regulator of morphogenetic fungal virulence factors. *Eukaryot. Cell* **4**, 1574–1582 (2005).
12. Bok, J.W. & Keller, N.P. LaeA, a regulator of secondary metabolism in Aspergillus spp. *Eukaryot. Cell* **3**, 527–535 (2004).
13. Marchler-Bauer, A. *et al.* CDD: NCBI's conserved domain database. *Nucleic Acids Res.* **43**, D222–D226 (2015).
14. MacPherson, S., Larochelle, M. & Turcotte, B. A fungal family of transcriptional regulators: the zinc cluster proteins. *Microbiol. Mol. Biol. Rev.* **70**, 583–604 (2006).
15. Forseth, R.R. & Schroeder, F.C. NMR-spectroscopic analysis of mixtures: from structure to function. *Curr. Opin. Chem. Biol.* **15**, 38–47 (2011).
16. Forseth, R.R. & Schroeder, F.C. Correlating secondary metabolite production with genetic changes using differential analysis of 2D NMR spectra. *Methods Mol. Biol.* **944**, 207–219 (2012).
17. Kutchan, T.M. & Dittrich, H. Characterization and mechanism of the berberine bridge enzyme, a covalently flavinylated oxidase of benzophenanthridine alkaloid biosynthesis in plants. *J. Biol. Chem.* **270**, 24475–24481 (1995).
18. Winkler, A. *et al.* A concerted mechanism for berberine bridge enzyme. *Nat. Chem. Biol.* **4**, 739–741 (2008).
19. Gaweska, H.M., Roberts, K.M. & Fitzpatrick, P.F. Isotope effects suggest a stepwise mechanism for berberine bridge enzyme. *Biochemistry* **51**, 7342–7347 (2012).
20. Scrutton, N.S. Chemical aspects of amine oxidation by flavoprotein enzymes. *Nat. Prod. Rep.* **21**, 722–730 (2004).
21. Dunn, R.V., Munro, A.W., Turner, N.J., Rigby, S.E. & Scrutton, N.S. Tyrosyl radical formation and propagation in flavin dependent monoamine oxidases. *ChemBioChem* **11**, 1228–1231 (2010).
22. Leonard, E., Runguphan, W., O'Connor, S. & Prather, K.J. Opportunities in metabolic engineering to facilitate scalable alkaloid production. *Nat. Chem. Biol.* **5**, 292–300 (2009).
23. Glenn, W.S., Runguphan, W. & O'Connor, S.E. Recent progress in the metabolic engineering of alkaloids in plant systems. *Curr. Opin. Biotechnol.* **24**, 354–365 (2013).
24. Nakagawa, A. *et al.* A bacterial platform for fermentative production of plant alkaloids. *Nat. Commun.* **2**, 326 (2011).
25. DeLoache, W.C. *et al.* An enzyme-coupled biosensor enables (*S*)-reticuline production in yeast from glucose. *Nat. Chem. Biol.* **11**, 465–471 (2015).
26. Hawkins, K.M. & Smolke, C.D. Production of benzylisoquinoline alkaloids in *Saccharomyces cerevisiae*. *Nat. Chem. Biol.* **4**, 564–573 (2008).
27. Fossati, E. *et al.* Reconstitution of a 10-gene pathway for synthesis of the plant alkaloid dihydrosanguinarine in *Saccharomyces cerevisiae*. *Nat. Commun.* **5**, 3283 (2014).
28. Thodey, K., Galanie, S. & Smolke, C.D. A microbial biomanufacturing platform for natural and semisynthetic opioids. *Nat. Chem. Biol.* **10**, 837–844 (2014).
29. Galanie, S. & Smolke, C.D. Optimization of yeast-based production of medicinal protoberberine alkaloids. *Microb. Cell Fact.* **14**, 144–156 (2015).
30. Galanie, S., Thodey, K., Trenchard, I.J., Filsinger Interrante, M. & Smolke, C.D. Complete biosynthesis of opioids in yeast. *Science* **349**, 1095–1100 (2015).
31. Imamura, K. *et al.* Identification of a gene involved in the synthesis of a dipeptidyl peptidase IV inhibitor in *Aspergillus oryzae*. *Appl. Environ. Microbiol.* **78**, 6996–7002 (2012).
32. Macheleidt, J. *et al.* Transcriptome analysis of cyclic AMP-dependent protein kinase A–regulated genes reveals the production of the novel natural compound fumipyrrole by *Aspergillus fumigatus*. *Mol. Microbiol.* **96**, 148–162 (2015).
33. Yamada, T. *et al.* Crystal structure of serine dehydratase from rat liver. *Biochemistry* **42**, 12854–12865 (2003).
34. Wallner, S. *et al.* Catalytic and structural role of a conserved active site histidine in berberine bridge enzyme. *Biochemistry* **51**, 6139–6147 (2012).
35. Mukherjee, A., Walker, J., Weyant, K.B. & Schroeder, C.M. Characterization of flavin-based fluorescent proteins: an emerging class of fluorescent reporters. *PLoS One* **8**, e64753 (2013).
36. Schneider, P., Weber, M., Rosenberger, K. & Hoffmeister, D. A one-pot chemoenzymatic synthesis for the universal precursor of antidiabetes and antiviral bis-indolylquinones. *Chem. Biol.* **14**, 635–644 (2007).
37. Fawaz, M.V., Topper, M.E. & Firestine, S.M. The ATP-grasp enzymes. *Bioorg. Chem.* **39**, 185–191 (2011).
38. Fan, C., Moews, P.C., Shi, Y., Walsh, C.T. & Knox, J.R. A common fold for peptide synthetases cleaving ATP to ADP: glutathione synthetase and D-alanine:D-alanine ligase of *Escherichia coli*. *Proc. Natl. Acad. Sci. USA* **92**, 1172–1176 (1995).
39. Noike, M. *et al.* A peptide ligase and the ribosome cooperate to synthesize the peptide pheganomycin. *Nat. Chem. Biol.* **11**, 71–76 (2015).
40. Tobiasen, C. *et al.* Nonribosomal peptide synthetase (NPS) genes in *Fusarium graminearum*, *F. culmorum* and *F. pseudograminearium* and identification of NPS2 as the producer of ferricrocin. *Curr. Genet.* **51**, 43–58 (2007).
41. Nagano, N. *et al.* Class of cyclic ribosomal peptide synthetic genes in filamentous fungi. *Fungal Genet. Biol.* **86**, 58–70 (2016).
42. Wiemann, P. *et al.* Perturbations in small molecule synthesis uncovers an iron-responsive secondary metabolite network in *Aspergillus fumigatus*. *Front. Microbiol.* **5**, 530 (2014).

Acknowledgments

This research was funded in part by NIH R01GM112739-01 (to N.P.K. and F.C.S.), NIH CBI training grant T32GM008500 (J.A.B.) and an NSF Graduate Research Fellowship under grant DGE-1256259 (to J.E.S.). A.A.B. and D.H. were supported by the Deutsche Forschungsgemeinschaft (CRC ChemBioSys 1127). The authors would like to thank D. Kiemle for his kind assistance in operating the Bruker Avance III HD 800 MHz NMR spectrometer.

Author contributions

J.A.B. and F.C.S. characterized and identified metabolites and biosynthetic pathways. J.E.S. and J.W.B. created all of the *A. fumigatus* mutants used. J.A.B. and C.G. performed stable-isotope labeling experiments. H.H.L., E.B. and D.H. contributed biochemical assays. J.M. and A.A.B. contributed to the identification of new metabolites. J.A.B., J.E.S., D.H., N.P.K. and F.C.S. wrote the manuscript.

Competing financial interests

The authors declare no competing financial interests.

Additional information

Any supplementary information, chemical compound information and source data are available in the online version of the paper. Reprints and permissions information is available online at http://www.nature.com/reprints/index.html. Correspondence and requests for materials should be addressed to F.C.S. or N.P.K.

ONLINE METHODS

Strains, media and growth conditions. The fungal strains used in this study are listed in **Supplementary Table 4**. All strains were grown at 37 °C on glucose minimal medium (GMM)[43] and, when appropriate, were supplemented with 0.56 g/l uracil, 1.26 g/l uridine and 1.0 g/l arginine and maintained as glycerol stocks at −80 °C. *Escherichia coli* strain DH5α was propagated in LB medium with the appropriate antibiotics for plasmid DNA.

Gene cloning, plasmid construction and genetic manipulations. The plasmids used in this study are listed in **Supplementary Table 4**. The oligonucleotide sequences for PCR primers are given in **Supplementary Table 5**. PCR amplification was carried out on a C1000™ Thermal Cycler (Bio-Rad). To create the *fsqA* overexpression (OE) strain (TJES1.18), the OE cassette was constructed by amplifying the *fsqA* open reading frame (ORF) from *Af293* genomic DNA using primers Afu6g03430_NcoI_For and Afu6g03430_NotI_Rev, which introduced a 5′ NcoI restriction site and a 3′ NotI restriction site. This PCR product was purified with a QIAquick gel extraction kit (Qiagen), quantified and digested with the appropriate restriction enzymes before being cloned into pJMP8.12 (ref. 44), resulting in plasmid pJES 1.2. Subsequently, *A. fumigatus argB* was transferred from pJMP4.1 (ref. 45) by digesting with EcoRI and introduced into pJES1.2, resulting in plasmid pJES2.7 (*A. fumigatus argB::gpdA(p)::fsqA*). All of the PCR steps were carried out with Pfu Ultra II DNA Polymerases (Agilent), and all of the digestion reactions were carried out with NEB enzymes (New England BioLabs). The correctness of the inserted DNA was then confirmed by sequencing.

Construction of the *fsq* gene knockout cassettes were generated using standard double-joint PCR procedures[46]. Briefly, *Aspergillus parasiticus pyrG* (*A.ppyrG)* was amplified from pJMP9.1. Then, an approximately 1 kb fragment upstream and downstream of each *fsq* gene was amplified from genomic DNA of *A. fumigatus* Af293 using designated primers, respectively. These three amplified PCR products were purified with a QIAquick gel extraction kit, quantified and fused using standard double-joint PCR procedures. The final PCR product was amplified with the bottom primer pairs *gene*_5′F_flank and _3′R_flank, confirmed with endonuclease digestion and purified for fungal transformation. The first two rounds of PCR were done with Pfu Ultra II DNA Polymerases (Agilent), and the final PCR step used the Expand long template PCR system (Roche) according to the manufacturer's instructions. Af293.6 (double auxotroph *A. fumigatus, pyrG*$^{-}$, *argB*$^{-}$) was used to make the *OE::fsqA, pyrG*$^{-}$ auxotroph, TJES1.18. This strain was used as the recipient host strain for subsequent deletions of *fsq* genes as well as the ectopic complementation of *pyrG1* with plasmid pJMP9.1 (containing *A.ppyrG*), resulting in prototrophic strain TJES3.1 (OE::*fsqA, A.ppyrG*). Similarly Δ*fsqA* auxotrophic strains (TJES2.20) were made by transforming Af293.6 with deletion cassettes and complemented with ectopically integrated pJMP4 to make Δ*fsqA* prototroph TJES8.2.

For the creation of deletion mutants in OE::*fsqA* TJES1.18 background, a deletion cassette of each cluster gene (*fsqB* to *fsqG*) was constructed by using double-joint PCR with *A. parasiticus pyrG* (*A.ppyrG*) for replacement of target genes. The *A.ppyrG* gene was amplified from the plasmid pJMP9.1 as template. Five micrograms of the double-joint PCR cassette were used to delete each *fsq* cluster gene by using TJES1.18 (*A.fargB::gpdA(p):: fsqA, pyrG1*) as the recipient host. After transformation, transformants were grown on minimal medium plates without supplements for screening. All of the strains were verified by PCR and Southern blot analysis (**Supplementary Fig. 17**). Multiple confirmed strains for each mutant were stored at −80 °C with 33% glycerol for future use.

Heterologous protein production and biochemical assays. The expression vectors for the *fsqF* (NRPS-like) adenylation domain (pJES13.2) were constructed by amplifying bases 1–1968 of the coding DNA sequence (CDS) of the gene Afu6g03480 from Af293 using primers fqsF_Adomain_xp_5′F and fqsF_Adomain_xp_3′R introducing 5′ NotI and 3′ XhoI restriction sites, respectively. These products were gel purified and digested with the appropriate enzymes before being cloned into pET30-a(+) (EMD Biosciences) to create an expression plasmid with a His_6-tagged *fsqF* adenylation domain. The plasmid was introduced into chemically competent *E. coli* DH5α, selected on LB agar with Kanamycin and confirmed by sequencing. Subsequently, they were extracted from DH5α cells and used to transform expression host *E. coli* BL21. Protein purification was carried out as described[47]. All reactions were carried out in triplicate. Reaction parameters for the ATP-[^{32}P]pyrophosphate exchange assay were as follows: total assay volume of 100 µl at 25 °C in 100 mM phosphate buffer, 5 mM $MgCl_2$, 125 nM EDTA, 5 mM ATP, 100 nM purified FsqF adenylation domain, 0.1 µM [^{32}P]pyrophosphate (50 Ci/mmol) and 1 mM amino acid substrate. The reaction proceeded for 30 min before it was stopped (1% (w/v) activated charcoal, 4.5% (w/v) tetrasodium pyrophosphate, 3.5% (v/v) perchloric acid) and further processed as described[48]. Pyrophosphate exchange was quantified on a scintillation counter (PerkinElmer TriCarb 2910TR).

The expression vector for *fsqB* (fructosyl amino acid oxidase) was constructed using the CDS of the gene Afu6g03440 from OE::*fsqA* using primers pet28_fsqB_3′_fwd and fsqB_5′_pet28_rev. These products were gel purified and cloned into pET28-b(+) using ligase-free PCR cloning to create an expression plasmid with a His_6-tagged FsqB. The plasmid was introduced into chemically competent *E. coli* DH5α, selected on LB agar with kanamycin and confirmed by sequencing. Subsequently, they were extracted from DH5α cells and used to transform expression host *E. coli* BL21(DE3) (New England BioLabs). BL21(DE3) pET28-b(+) *fsqB* containing *E. coli* were grown in LB containing 50 µg/ml kanamycin at 37 °C to an OD of ~0.6 and cooled to 18 °C, and expression was induced with 250 µM IPTG for 15 h. Four liters of LB containing *E. coli* were harvested at 6,000*g* for 20 min, yielding 10.6 g of wet weight pellet that was stored at −80 °C. Protein purification was carried out at 4 °C by resuspending the pellet in lysis buffer containing 100 mM phosphate buffer, pH 7.8, 10 mM imidazole, 10% (v/v) glycerol, 1 mM PMSF, 0.1 mg/ml lysozyme and 0.1 mg/ml Benzonase (EMD Millipore) and sonicated. All following steps were performed in low light to avoid detrimental flavin-mediated reactions. Lysed cells were centrifuged at 20,000*g* for 20 min and loaded onto TALON affinity resin (Clontech) pre-equilibrated with lysis buffer and incubated for 30 min with stirring. Resin was loaded onto a column and washed with two column volumes of lysis buffer without lysosome or Benzonase. FsqB was eluted with 100 mM phosphate buffer, pH 7.8, 150 mM imidazole, 10% (v/v) glycerol with eight column volumes, concentrated and buffer exchanged with an Amicon Ultra-15 centrifugal filter with a 30-kDa cutoff with 100 mM phosphate buffer, pH 7.8, 25% (v/v) glycerol and stored at −80 °C. Activity assays were performed in total assay volumes of 100 µl at 37 °C in 100 mM phosphate buffer, pH 7.0, in the dark. Reaction products were identified on a Thermo Scientific-Dionex Ultimate3000 UHPLC system equipped with a diode array detector and connected to a Thermo Scientific Q Exactive Orbitrap operated in electrospray negative (ESI^{-}) ionization mode. UV-visible absorbance spectra were obtained on a Cary 5000 UV-Vis-NIR spectrophotometer, and fluorescence emission was obtained on a HORIBA Nanolog Spectrofluorometer.

FsqB steady-state kinetic analysis and imine capture. Steady-state kinetics were carried out at 25 °C in 100 mM phosphate buffer, pH 7.0, with 100 nM FsqB at final volumes of 500 or 1,000 µl at various initial concentrations of *N*-methyl-3,4-dihydroxy-D/L-phenylalanine (**11**). Imine capture was carried out at 25 °C in 100 mM phosphate buffer, pH 7.0, with 1.5 µM FsqB, 400 µM *N*-methyl-L-tyrosine (**14**) and 1 mM dimedone (**15**) (Sigma-Aldrich) with <0.5% (v/v) methanol for dimedone solubility. Both kinetics and imine capture were monitored with low-resolution HPLC/MS performed on an Agilent 1100 series HPLC system equipped with a diode array detector and connected to a Quattro II mass spectrometer (Micromass/Waters) operated in electrospray negative ionization (ESI^{-}) mode for kinetic analysis and positive electrospray ionization (ESI^{+}) mode for imine capture. Kinetic data analysis was performed using GraphPad Prism version 6.00 for Windows (GraphPad Software).

FsqB Amplex Red assay. 100 µM *N*-methyl- D/L-DOPA or D/L-DOPA, either with or without 15 µM FsqB, were incubated in 100 mM, pH 7.0 potassium phosphate buffer at 25 °C in 100 µL total reaction volume in the dark in a 96-well plate with gentle shaking. After 1.5 h of incubation, 100 µL of hydrogen peroxide detection mixture (containing 50 mM potassium phosphate, pH 7.0, 100 µM Amplex Red (Thermo Scientific), 0.2 units/ml HRP) was added and incubated at 25 °C in the dark for 10 min. Readings were performed on a BioTek Synergy 2 96-well plate reader using a 500 ± 27 nm excitation filter

and a 615 ± 15 nm emission filter and normalized to 0 and 100 µM hydrogen peroxide standards. All conditions were performed in triplicate.

FsqB trypsinization analysis. Eighty micrograms of recombinant FsqB was buffer exchanged into 55 µl of 50 mM ammonium bicarbonate. Three microliters of 0.33 µg/µl sequencing-grade porcine trypsin (Promega) was added to FsqB and incubated at 37 °C for 12 h. Five microliters of 50 mM TCEP was added, and the mixture was further incubated at 37 °C for 10 min. The solution was cooled to 25 °C, and 5 µl of 100 mM iodoacetamide was added and incubated at 25 °C in the dark for 1 h. Formic acid was added to 1% (v/v), and peptides were prepared with 100-µl Pierce C_{18} Tips (Thermo Scientific) per the manufacturer's protocol using 100 µl of the elution solution. Peptides were identified via UHPLC-MS/MS using a Thermo Scientific Dionex Ultimate 3000 UHPLC system equipped with a diode array detector and connected to a Thermo Scientific Q Exactive Orbitrap operated in positive electrospray (ESI^+) ionization mode.

Nucleic acid analysis. Preparation of plasmids, restriction enzyme digestions, gel electrophoresis, blotting, probe preparation and hybridization were carried out by standard protocols. *Aspergillus* DNA was extracted using a previously described method[49]. Sequence data were analyzed using the LASERGENE software package from DNASTAR.

Northern analysis. Fifty milliliters of liquid GMM[43] were inoculated with 1.0×10^6 spores (asexual) per ml of all of the appropriate strains in this study and incubated with shaking at 250 r.p.m. at 25 °C. After 48 h, the mycelium was collected, and total RNA was extracted by using Isol-RNA Lysis Reagent according to the manufacturer's instructions (5 Prime).

To determine the boundaries of the *fsq* gene cluster, gene fragments of potential cluster genes used as probes were amplified individually from Af293 genomic DNA with appropriate primers. The wild type, OE::*fsqA* (TJES3.1) and Δ*fsqA* (TJES8.2) were used for this experiment. About 40 µg of total RNA were used for RNA blot analysis. RNA blots were hybridized with designated DNA fragments. All of the experiments were performed in duplicate. Detection of signals was carried out with a Storm 860 phosphoimager (Molecular Dynamics).

Fermentation and metabolome extraction for comparative metabolomics by DANS and HPLC-UV-MS. Preparation for NMR spectroscopic analysis: *A. fumigatus* strains were inoculated (1.0×10^6 spores per ml) into 1 l GMM[43] in a 2-l Erlenmeyer flask at 37 °C with shaking at 220 rpm. After 4 d, liquid fungal cultures including fungal tissue and medium were frozen using a dry ice acetone bath and lyophilized. The lyophilized residues were extracted with 500 ml of 10% methanol in ethyl acetate for 3.5 h with vigorous stirring. Extracts were filtered over cotton, evaporated to dryness and stored in 8-ml glass vials at −20 °C. Prior to NMR spectroscopic analysis, the crude extracts (~30–50 mg) were suspended in 0.15 ml of methanol-d_4. The resulting suspension was evaporated to dryness, the residue was re-suspended in 0.6 ml of methanol-d_4 and centrifuged to remove insoluble materials, and the supernatant was transferred into a 5-mm NMR tube.

Preparation for HPLC-MS analysis: *A. fumigatus* strains were inoculated (1.0×10^6 spores per ml) into 50 ml GMM[43] in a 125-ml Erlenmeyer flask at 37 °C with shaking at 220 r.p.m. After 4 d, liquid fungal cultures including fungal tissue and medium were frozen using a dry ice acetone bath and lyophilized. The lyophilized residues were extracted with 30 ml of MeOH for 1.5 h with vigorous stirring. Extracts were filtered over cotton, evaporated to dryness and stored in 4-ml vials. Crude extracts were suspended in 0.5 ml of MeOH and centrifuged to remove insoluble materials, and the supernatant was subjected to HPLC/MS analysis.

Fermentation and metabolome extraction for 3–5. *A. fumigatus* strains were inoculated (1.0×10^6 spores ml^{-1}) into 1 l GMM[43] in a 2-l Erlenmeyer flask at 37 °C with shaking at 220 r.p.m. After 3.5 d, liquid fungal cultures including fungal tissue and medium were frozen using a dry ice acetone bath and lyophilized. The lyophilized residues were extracted with 500 ml of MeOH for 1 h with vigorous stirring. Extracts were filtered over cotton and evaporated on Celite-545 (Acros Organics) to dryness. The dry Celite was then loaded into a 25-g solid phase cartridge (Isco) and subjected to large-scale reverse phase chromatography (detailed below). Compounds **4** and **5** are also minor components of the culture medium.

Analytical methods and equipment overview. (a) NMR spectroscopy: NMR spectroscopic instrumentation: a Varian INOVA 600 MHz NMR spectrometer (600 MHz ^1H reference frequency, 151 MHz for ^{13}C) equipped with an HCN indirect-detection probe or a Bruker Avance III HD (800 MHz ^1H reference frequency, 201 MHz for ^{13}C) equipped with a 5-mm CPTCI ^1H-$^{13}C/^{15}N$ cryo probe. Nongradient phase-cycled dqfCOSY spectra were acquired using the following parameters: 0.6 s acquisition time; 400–600 complex increments; 8, 16 or 32 scans per increment. Nongradient HSQC, HMQC and HMBC spectra were acquired with these parameters: 0.25 s acquisition time, 200–500 increments, 8–64 scans per increment. ^1H, ^{13}C-HMBC spectra were optimized for $J_{H,C}$ = 6 Hz. HSQC spectra were acquired with or without decoupling. Susceptibility-matched NMR tubes (Shigemi) were used for sample amounts smaller than 1 mg. NMR spectra were processed and baseline corrected using MestreLabs MNOVA software packages. (b) MS: high-resolution UHPLC-MS was performed on a Thermo Scientific-Dionex Ultimate3000 UHPLC system equipped with a diode array detector and connected to a Thermo Scientific Q Exactive Orbitrap operated in electrospray positive (ESI^+) or electrospray negative (ESI^-) ionization mode. Low-resolution HPLC/MS was performed on an Agilent 1100 series HPLC system equipped with a diode array detector and connected to a Quattro II mass spectrometer (Micromass/Waters) operated in ESI^+ or ESI^- mode. Data acquisition and processing for the LC/HRMS was controlled by Thermo Scientific Xcalibur software. Data acquisition and processing for the HPLC-MS was controlled by Waters MassLynx software. (c) Chromatography: flash chromatography was performed using a Teledyne ISCO CombiFlash system. For semi-preparative HPLC Agilent Zorbax Eclipse XDB-C18 or XDB-C8 columns (25 cm × 10 mm, 5 µm particle diameter) were used. An Agilent Zorbax RRHD Eclipse XDB-C18 column (2.1 × 100 mm, 1.8 µm particle diameter) was used in the LC/HRMS *A. fumigatus* mutant profiling analysis. An Agilent Zorbax Eclipse XDB-C18 column (4.6 × 250 mm, 5 µm particle diameter) was used in the HPLC-MS *A. fumigatus* mutant profiling analysis.

Chromatographic enrichment of compounds 1, 3, dimethyl-3, 7, 8, 11–13 and 18. Methanol extracts derived from 1-2 l of *A. fumigatus* cultures were fractionated using large-scale reverse-phase flash chromatography on a Teledyne ISCO CombiFlash with a Teledyne C18 gold (100 g) column with acetonitrile (organic phase) and 0.1% acetic acid in water (aqueous phase) as solvents at a flow rate of 60 ml/min. A linear ramp from 0% organic to 100% organic over 30 min was used, and fractions containing compounds of interest were collected, evaporated to dryness and stored in 8-ml glass vials at −20 °C. Fractions containing compounds **1**, **3**, dimethyl-**3**, **7**, **8**, **11–13** and **18** were further purified via semi-preparative HPLC using an Agilent XDB C-18 or C-8 column (25 cm × 10 mm, 5 µm particle diameter) acetonitrile (organic phase) and 0.1% acetic acid in water (aqueous phase) as solvents at a flow rate of 3.6 ml/min. A solvent gradient scheme was used, starting at 5% organic for 3 min, followed by a linear increase to 100% organic over 27 min, holding at 100% organic for 5 min, decreasing back to 5% organic for 0.1 min and holding at 5% organic for the final 4.9 min, for a total of 40 min.

***In vivo* stable isotope labeling experiments.** Deuterium-labeled and ^{13}C-labeled amino acids were purchased from Cambridge Isotopes Inc. Each amino acid (labeled or unlabeled control) was added to 50 ml (2 mM) of GMM[43] media in 125-ml Erlenmeyer flasks. Each flask was inoculated with OE::*fsqA* or OE::*fsqA*-Δ*fsqF* (1.0×10^6 spores per ml) and grown for 4 d at 37 °C with shaking at 220 r.p.m. After 4 d, liquid fungal cultures including fungal tissue and medium were frozen using a dry ice acetone bath and lyophilized. The lyophilized residues were extracted with MeOH (25 ml) for 1.5 h with vigorous stirring. Extracts were filtered over cotton, evaporated to dryness and stored in 4-ml vials at −20 °C. Crude extracts were suspended in 0.5 ml of MeOH and centrifuged to remove insoluble materials, and the supernatant was subjected to HPLC-MS analysis.

doi:10.1038/nchembio.2061

Conversion of 3 into dimethyl-3 for NMR spectroscopic analysis. To a solution of a partially purified fumisoquin C (**3**) in 3:2 toluene/MeOH (2 ml) was added trimethylsilyldiazomethane (Sigma-Aldrich) (20 µL, 0.04 mmol) as a 2.0 M diethyl ether solution. After stirring at room temperature for 30 min, the mixture was quenched with glacial acetic acid (10 µl) and dried by rotary evaporation. The mixture was resuspended in MeOH (100 µl), and dimethyl-**3** was purified by semi-preparative HPLC (detailed above).

Synthesis of FsqB substrates. All reagents were purchased and used as is from Sigma-Aldrich. All solvents were purchased and used as is from Fischer Scientific. To produce *N*-methyl-3,4-dihydroxy-D/L-phenylalanine (**11**), a 100-ml Schlenk flask under argon at room temperature was charged with 3,4-dihydroxy-D/L-tyrosine (394 mg, 2.0 mmol), dissolved in 50 ml of a 7:3 mixture of water and MeOH. To this $NaBH_4$ (228 mg, 6.6 mmol) was added, followed by immediate addition of formaldehyde (0.5 ml of a 37% solution in H_2O, 6.0 mmol). The reaction was stirred for 1 h at room temperature then quenched by addition of glacial acetic acid (10 ml). The solvents were removed by rotary evaporation, and the product was isolated by reverse-phase HPLC. See **Supplementary Note** for full NMR spectroscopic data of (**12**). *N*-methyl-dopamine was prepared according to the literature procedure[50].

43. Shimizu, K. & Keller, N.P. Genetic involvement of a cAMP-dependent protein kinase in a G protein signaling pathway regulating morphological and chemical transitions in *Aspergillus nidulans*. *Genetics* **157**, 591–600 (2001).
44. Sekonyela, R. *et al.* RsmA regulates *Aspergillus fumigatus* gliotoxin cluster metabolites including cyclo(L-Phe-L-Ser), a potential new diagnostic marker for invasive aspergillosis. *PLoS One* **8**, e62591 (2013).
45. Palmer, J.M. *et al.* Loss of CclA, required for histone 3 lysine 4 methylation, decreases growth but increases secondary metabolite production in *Aspergillus fumigatus*. *PeerJ* **1**, e4 (2013).
46. Yu, J.H. *et al.* Double-joint PCR: a PCR-based molecular tool for gene manipulations in filamentous fungi. *Fungal Genet. Biol.* **41**, 973–981 (2004).
47. Kalb, D., Lackner, G. & Hoffmeister, D. Functional and phylogenetic divergence of fungal adenylate-forming reductases. *Appl. Environ. Microbiol.* **80**, 6175–6183 (2014).
48. Schneider, P., Bouhired, S. & Hoffmeister, D. Characterization of the atromentin biosynthesis genes and enzymes in the homobasidiomycete *Tapinella panuoides*. *Fungal Genet. Biol.* **45**, 1487–1496 (2008).
49. Bok, J.W. *et al.* Chromatin-level regulation of biosynthetic gene clusters. *Nat. Chem. Biol.* **5**, 462–464 (2009).
50. Carpenter, J.F. An improved synthesis of 5,6-diacetoxy-*N*-methylindole and of epinine. *J. Org. Chem.* **58**, 1607–1609 (1993).

Supplementary Information

Plant-like biosynthesis of isoquinoline alkaloids in *Aspergillus fumigatus*

Joshua A. Baccile[1,#], Joseph E. Spraker[2,#], Henry H. Le[1], Eileen Brandenburger[3], Christian Gomez[1], Jin Woo Bok[4], Juliane Macheleidt[5], Axel A. Brakhage[5], Dirk Hoffmeister[3], Nancy P. Keller[4,6*], Frank C. Schroeder[1,*]

[1]Boyce Thompson Institute and Department of Chemistry and Chemical Biology, Cornell University, Ithaca, NY, United States

[2]Department of Plant Pathology, University of Wisconsin-Madison, WI, United States

[3]Department of Pharmaceutical Microbiology at the Hans-Knöll-Institute, Friedrich Schiller University, Jena, Germany

[4]Department of Bacteriology, University of Wisconsin-Madison, WI, United States

[5]Molecular and Applied Microbiology, Leibniz Institute for Natural Product Research and Infection Biology (HKI), and Institute for Microbiology, Friedrich Schiller University, Jena, Germany

[6]Department of Medical Microbiology and Immunology, University of Wisconsin-Madison, WI, United States

[#]These authors contributed equally
*To whom correspondence should be directed

Nature Chemical Biology: doi:10.1038/nchembio.2061

Supplementary Results

Supplemetary Table 1. LC-HRMS data of reported compounds

Compound	HR-ESI(+/-) observed (*m/z*)	Ion	Calculated ion formula	Calculated *m/z*	Retention time [min]	Yield of compound (per L culture)*
1	281.1137	$[M+H]^+$	$C_{13}H_{17}N_2O_5^+$	281.1132	0.74	~1–5 mg
2	359.0557	$[M-H]^-$	$C_{13}H_{15}N_2O_8S^-$	359.0555	0.81	~1–5 mg
3	289.0471	$[M-H]^-$	$C_{13}H_9N_2O_6^-$	289.0466	4.31	~10–50 mg
4	241.0255	$[M-H]^-$	$C_{12}H_5N_2O_4^-$	241.0255	4.38	
5	227.0462	$[M-H]^-$	$C_{12}H_7N_2O_3^-$	227.0462	6.58	
7	200.0727	$[M-H]^-$	$C_{12}H_{10}NO_2^-$	200.0717	7.46	~0.5–2 mg
8	216.0676	$[M-H]^-$	$C_{12}H_{10}NO_3^-$	216.0666	5.98	~0.5–2 mg
11	210.0772	$[M-H]^-$	$C_{10}H_{12}NO_4^-$	210.0772	1.71	
12	208.0615	$[M-H]^-$	$C_{10}H_{10}NO_4^-$	208.0165	1.38	
18	293.0565	$[M-H]^-$	$C_{16}H_9N_2O_4^-$	293.0568	5.46	~1–5 mg
21	343.0941	$[M-H]^-$	$C_{17}H_{15}N_2O_6^-$	343.0936	4.31	
22	337.0473	$[M-H]^-$	$C_{17}H_9N_2O_6^-$	337.0466	5.13	

*Numbers indicate estimated production of each compound prior to sample treatment, where significant losses are incurred at each chromatographic step.

Nature Chemical Biology: doi:10.1038/nchembio.2061

Supplementary Table 2. Predicted homologs of *fsqB*, *fsqC*, and *fsqG* that are clustered in other *Aspergilli*.

Protein	Identity* (%) to genes of				Putative function
A. fumigatus 293	*N. fischeri*	*A. parasiticus*	*A. oryzae*	*A. flavus*	
fsqB	474/497 (95%)	234/501 (47%)	232/501 (46%)	228/501 (46%)	FAD binding domain protein
fsqC	338/365 (93%)	157/321 (49%)	160/343 (47%)	158/325 (49%)	methyltransferase
fsqG	557/598 (93%)	329/619 (53%)	326/619 (53%)	330/619 (53%)	cytochrome P450 monooxygenase

*Percentage similarity values of the *A. fumigatus* 293 ORFs to *N. fischeri, A. parasiticus, A. oryzae,* and *A. flavus* clusters are given in parentheses.

Supplementary Table 3. Amino acid sequence of polyhistidine-tagged FsqB and software-aided[1] identification of tryptic FsqB peptides analyzed with UHPLC-MS/MS.

MGSSHHHHHHSSGLVPRGSHMSIPNSFIIVGSGVFGLSLAYALSLDDRFADKKIILVDRWNFEPPNATGSVHNPAAAN
ADTSRVIRRDYPHGPYASLALEAMKHWRGKFGENNRYVNQRLLFSGEGSSLTTPPKALETVNYIKKAYAISCELTPGG
RDAVQVLDSLDEVRAFLGNTPSHPPHLPVNKDPAARDLRGYVSNDCGWADAGASIEWLRQEVLRLGRVECVVGEVE
SLVYSDDQRAVKGVKLVDGKVLTAELTVIAAGARSSHILGIPKLCDVYSEFVAYIQLTKEEADELRRRQWPILVNCHRG
VFAVGPDHDNCLKFGHFSYSGIVDVLREASIQVPTRPDGWEAQQKYWSDPRFAFGGEVKVSALGDVDDYENPAAQR
ALADYRLFLLELLGPTGLQGVDTLGLDQSDNLLNNIANRPFTRVRKCWYNDTPALDFVVDYHPSYGKTLFVATGGCD
HAFKFLPIIGEKTLALILRNRGDSAVSLPAGVEPSLEELSELWRFPVELLQDN

Peptide	observed	expected	z	Δ
MGSSHHHHHHSSGLVPR	590.2879	633.9679	3	-131.0400
GSHMSIPNSFIIVGSGVFGLSLAYALSLDDRFADKKIILVDR	1075.2218	1075.2200	3	0.0254
WNFEPPNATGSVHNPAAANADTSR	842.0560	842.0509	3	-0.0066
DYPHGPYASLALEAMK	881.9266	881.9198	2	-0.0010
FGENNR	736.3424	736.3373	1	0.0051
LLFSGEGSSLTTPPK	767.4106	767.4043	2	-0.0020
ALETVNYIK	1050.5813	1050.5757	1	-0.0017
AYAISCELTPGGR	697.8393	697.8330	2	-0.0020
DAVQVLDSLDEVR	1458.7411	1458.7362	1	-0.0024
FLGNTPSHPPHLPVNK	457.2478	457.2409	4	-0.0015
GYVSNDCGWADAGASIEWLR	1113.9964	1113.9900	2	-0.0018
VECVVGEVESLVYSDDQR	1041.9851	1041.9788	2	-0.0020
VLTAELTVIAAGAR	462.2763	462.2695	3	-0.0014
SSHILGIPK	951.5615	951.5549	1	-0.0007
LCDVYSEFVAYIQLTK	974.9887	974.9826	2	-0.0023
EEADELR	431.2024	431.1938	2	0.0027
QWPILVNCHR	661.8428	661.8357	2	-0.0003
GVFAVGPDHDNCLK	764.8631	764.8570	2	-0.0024
FGHFSYSGIVDVLR	798.9108	798.9048	2	-0.0026

Nature Chemical Biology: doi:10.1038/nchembio.2061

EASIQVPTRPDGWEAQQK	1020.5093	1020.5036	2	-0.0032
YWSDPR	412.1909	412.1903	2	0.0012
FAFGGEVK	854.4397	854.4334	1	-0.0009
VSALGDVDDYENPAAQR	910.4254	910.4192	2	-0.0022
LFLLELLGPTGLQGVDTLGLDQSDNLLNNIANRPFTR	1346.7254	1346.7195	3	-0.0042
KCWYNDTPALDFVVDYHPSYGK	1134.4530	892.7407	3	725.1369
TLFVATGGCDHAFK	762.3686	762.3620	2	-0.0013
FLPIIGEK	916.5490	916.5429	1	-0.0012
TLALILR	799.5390	799.5327	1	-0.0009
GDSAVSLPAGVEPSLEELSELWR	1221.1133	1221.1061	2	-0.0002
FPVELLQDN	1074.5451	1074.5393	1	-0.0015
KC(FAD)WYNDTPALDFVVDYHPSYGK	1134.4530	1134.4454	3	0.0009

Nature Chemical Biology: doi:10.1038/nchembio.2061

Supplementary Table 4. Fungal strains and plasmids used in this study

Strain/plasmid	Description	Reference
***Aspergillus fumigatus* 293 background strains**		
Af293	Wild type	2
Af293.1	*pyrG1*	2
Af293.6	*pyrG1, argB1*	2
TJES1.18	*A.fargB::gpdA(p):: fsqA, pyrG1*	This study
TJES2.20	*ΔfsqA::A.ppyrG, argB1*	This study
TJES3.1	*A.fargB::gpdA(p):: fsqA, A.ppyrG*	This study
TJES4.10	*A.fargB::gpdA(p):: fsqA, ΔfsqF::A.ppyrG*	This study
TJES8.2	*ΔfsqA::A.ppyrG, A.fargB*	This study
TJES13.61	*A.fargB::gpdA(p):: fsqA, ΔfsqB::A.ppyrG*	This study
TJES14.68	*A.fargB::gpdA(p):: fsqA, ΔfsqC::A.ppyrG*	This study
TJES15.91	*A.fargB::gpdA(p):: fsqA, ΔfsqG::A.ppyrG*	This study
***Aspergillus flavus* NRRL3357 background strains**		
NRRL3357.5	*pyrG1*	3
TJW149.27	*Δku70::pyrG*	This study
TJES19.1	*ΔpyrG, Δku70*	This study
TJES 23.3	*A.ppyrG::gpdA(p)::imqA, Δku70*	This study
TJES 27.1	*ΔimqA::A.ppyrG, Δku70*	This study
Plasmids		
pJMP4	*A. fumigatus argB*	4
pJMP8.1	*A. nidulans* gpdA promoter (truncated to 1.5 kb) in pBluescript	5
pJMP9.1	*A. nidulans gpdA(p) + A parasiticus pyrG*	6
pJES1.2	*gpdA(p):: fsqA* in *pJMP8.1*	This study
pJES2.7	*A. fumigatus argB::gpdA(p):: fsqA*	This study
pJES13.2	C-terminal 6His tagged *fsqF* A-domain in pET30a vector	This study
pJW24	*A parasiticus pyrG* in pBluescript	7

pXX = plasmid, TXX = original transformant

Nature Chemical Biology: doi:10.1038/nchembio.2061

Supplementary Table 5. PCR primer sets used in this study

Name of the primer	Oligonucleotide sequence (5'-3')	Uses
Afu6g03380_FOR_Nprobe	CTTTCACGTGGACACTGCGC	Northern probe
Afu6g03380_REV_Nprobe	TACTGCTCCAACCAGCACCG	Northern probe
Afu6g03390_FOR_Nprobe	TCAGGGAGATATGGTGGCG	Northern probe
Afu6g03390_REV_Nprobe	CAACGCAGCAGGTAGTCACG	Northern probe
Afu6g03400_FOR_Nprobe	CTTCCAAGCCCAACAAGCC	Northern probe
Afu6g03400_REV_Nprobe	AATCTCGTAGGCCTCCAGCG	Northern probe
Afu6g03430_FOR_Nprobe	TGGCCTATCACACCAGTGGC	Northern probe
Afu6g03430_REV_Nprobe	GTGCAGCCTGAATCTCACGG	Northern probe
Afu6g03420_FOR_Nprobe	GAGCTCGACAATGGTGAGCG	Northern probe
Afu6g03420_REV_Nprobe	CAATCACATCGGCATGCGG	Northern probe
Afu6g03440_FOR_Nprobe	GATGGAACTTCGAGCCACCC	Northern probe
Afu6g03440_REV_Nprobe	GGCGATAATCTGCCAACGCC	Northern probe
Afu6g03450_FOR_Nprobe	CTACATCGCCTGCGATGTGG	Northern probe
Afu6g03450_REV_Nprobe	TAGCACACGCGCCAGATACC	Northern probe
Afu6g03460_FOR_Nprobe	GCGACTTCGCGACTCGGAAT	Northern probe
Afu6g03460_REV_Nprobe	CCATCACAAACTCGGTCCCG	Northern probe
Afu6g03470_FOR_Nprobe	AACTGCGCTCCAAAACCGCC	Northern probe
Afu6g03470_REV_Nprobe	ATCCACAAGGGCGATCTGGC	Northern probe
Afu6g03490_FOR_Nprobe	GTTCTCAGGGGATGTGACCG	Northern probe
Afu6g03490_REV_Nprobe	ACAAGTTCGCCCTTCGCTCCG	Northern probe
Afu6g03500_FOR_Nprobe	GGTGCTCAAGGAACAGAGGG	Northern probe
Afu6g03500_REV_Nprobe	GCCAAGAGGTCATTCTGCCC	Northern probe
Afu6g03510_FOR_Nprobe	AACACCCGATACCAGCTCGC	Northern probe
Afu6g03510_REV_Nprobe	ATGGGCCACCCATTGATGGC	Northern probe
Afu6g03520_FOR_Nprobe	ATGCCATCATCACCGGTGCC	Northern probe
Afu6g03520_REV_Nprobe	CGAGCATGGACAATAGCC	Northern probe
A.ppyrG_T7 FOR	CGTAATACGACTCACTATAGGG	Amplification of A.ppyrG from pJMP9.1
A.ppyrGR_Rev	ATTCGACAATCGGAGAGGCTGC	Amplification of A.ppyrG from pJMP9.1
Afu6g03430_3'F_flank	CTGTCGCTGCAGCCTCTCCGATTGTCG AATGCTTCAGCTGGAGTGTCTCC	Amplification of *fsqA* 3' flanking region
Afu6g03430_3'R_flank	TACAGCGACGACCAACGAGC	Amplification of *fsqA* 3' flanking region
Afu6g03430_5'F_flank	TAAGAGCGGAGACTGGTGGC	Amplification of *fsqA* 5' flanking region
Afu6g03430_5'R_flank	CCAATTCGCCCTATAGTGAGTCGTATT ACGTCTGCAAGGGTTTACGAGGG	Amplification of *fsqA* 5' flanking region
Afu6g03440_3'F_flank	CTGTCGCTGCAGCCTCTCCGATTGTCG AATTCGGAACTCTGGAGGTTCCC	Amplification of *fsqB* 3' flanking region
Afu6g03440_3'R_flank	ACTGCGCGACAAATGCAGCC	Amplification of *fsqB* 3' flanking region
Afu6g03440_5'F_flank	GTCTCGTCACTTACCCTGCC	Amplification of *fsqB* 5'

Nature Chemical Biology: doi:10.1038/nchembio.2061

		flanking region
Afu6g03440_5'R_flank	CCAATTCGCCCTATAGTGAGTCGTATT ACGAAAGAGACAGCCGGGATCCG	Amplification of *fsqB* 5' flanking region
Afu6g03450_3'F_flank	CTGTCGCTGCAGCCTCTCCGATTGTCG AATCTTGCTGCGGAAATCGAGCG	Amplification of *fsqC* 3' flanking region
Afu6g03450_3'R_flank	CACGGTAAAAGCCCAGTCCG	Amplification of *fsqC* 3' flanking region
Afu6g03450_5'F_flank	GATGTAGGCCACGAACTCGC	Amplification of *fsqC* 5' flanking region
Afu6g03450_5'R_flank	CCAATTCGCCCTATAGTGAGTCGTATT ACGAGGATGCCAAAAGCCCACCG	Amplification of *fsqC* 5' flanking region
Afu6g03480_3'F_flank	CTGTCGCTGCAGCCTCTCCGATTGTCG AATCGCGGGCATCTAGTATTCGG	Amplification of *fsqF* 3' flanking region
Afu6g03480_3'R_flank	ACTTGCGCAACCAGCTGTGC	Amplification of *fsqF* 3' flanking region
Afu6g03480_5'F_flank	GAATCTGAGCGCTTGTCGCG	Amplification of *fsqF* 5' flanking region
Afu6g03480_5'R_flank	CCAATTCGCCCTATAGTGAGTCGTATT ACGAAGAAAGGCGAAACGGAGCG	Amplification of *fsqF* 5' flanking region
Afu6g03490_3'F_flank	CTGTCGCTGCAGCCTCTCCGATTGTCG AATATGGACTCCAGTCAGGACCG	Amplification of *fsqG* 3' flanking region
Afu6g03490_3'R_flank	ATCCACCTCGTGGAGAAGCC	Amplification of *fsqG* 3' flanking region
Afu6g03490_5'F_flank	TGTGTCACGAAGGCAGTGCG	Amplification of *fsqG* 5' flanking region
Afu6g03490_5'R_flank	CCAATTCGCCCTATAGTGAGTCGTATT ACGGTGCCCATCGTCCAATACGG	Amplification of *fsqG* 5' flanking region
fqsF_Adomain_xp_5'F	AATAA**GCGGCCGC**ACCTGGAACACCG TGGTTGC	Amplification of *fsqF* A-domain **(NotI cut site)**
fqsF_Adomain_xp_3' R	ATTAGC**CTCGAG**TTCGTTGCCCCGAGT GTGC	Amplification of *fsqF* A-domain **(XhoI cut site)**
fsqD_xp_5' F	GTAGGCTA**GAATTC**TCACACCAGCCTC TCTTGGC	Amplification of *fsqD* ORF **(EcoRI cut site)**
fsqD_xp_3' R	CATTAT**AAGCTT**GAGAAAGGAGTAGC GGACCTCTTCCC	Amplification of *fsqD* ORF **(HindIII cut site)**
Afu6g03430_NcoI_FOR	CAGATG**CCATGG**ACGACAAGCATGGC C	Amplification of *fsqA* ORF **(NcoI cut site)**
Afu6g03430_NotI_REV	GCAACC**GCGGCCGC**AGACAGCGCGGT ATCACTG	Amplification of *fsqA* ORF **(NotI cut site)**
flvku70F5	ACATCTCTTCCGTCAAAGGCGC	Amplification of *ku70* 5' flanking region
flavku70R5	CGATATCAAGCTATCGATACCTCGACT CTGTGTTGAGAGTCGTAAGTCATGAAT TGCG	Amplification of *ku70* 5' flanking region
flvku70F3	GTCGCTGCAGCCTCTCCGATTGTCGAA TGACAACGCTAGTATTGGTTACGAGAG	Amplification of *ku70* 3' flanking region

Nature Chemical Biology: doi:10.1038/nchembio.2061

flavku70R3	ACAG AGAATGGCTACGTCAACCTCCG	Amplification of *ku70* 3' flanking region
Fku70IF	ATGAGGAAGAGGAGGAGACCG	Amplification of Δ*ku70* cassette
Fku70IR	CACTTTTCAATCGTGCGAGCCG	Amplification of Δ*ku70* cassette
pet28_fsqB_3'_fwd	TGGTGCCGCGCGGCAGCCATATGTC TATCCCTAACTCTTTCATCATTGT	Amplification of fsqB, pET28b+ 3' destination
fsqB_5'_pet28_rev	CTCAGCTTCCTTTCGGGCTTTGTTACTA GTTGTCCTGTAGTAGTTCCACGG	Amplification of fsqB pET28b+ 5' destination

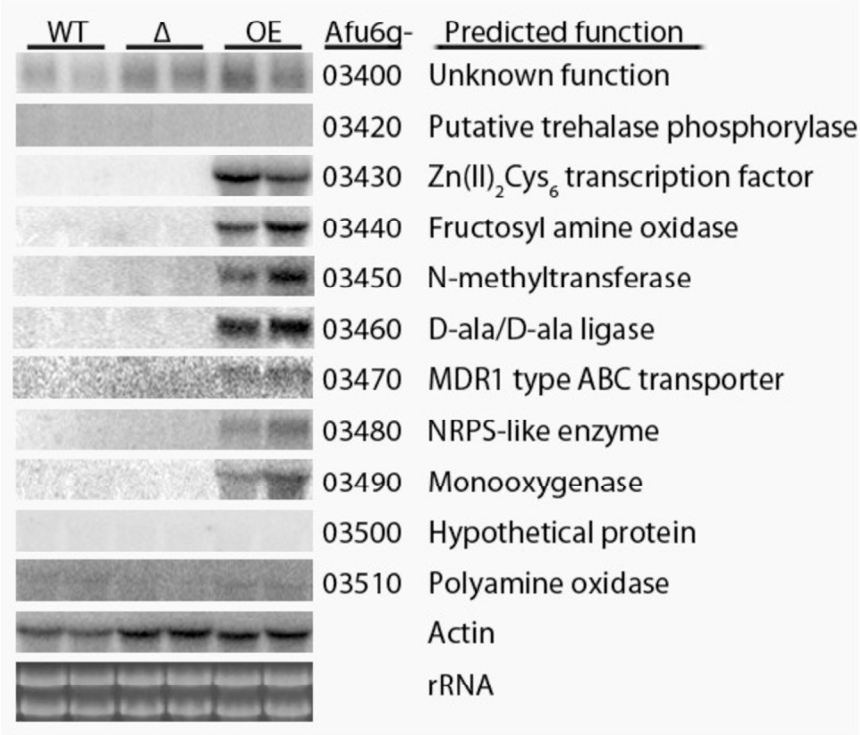

Supplementary Figure 1. Northern blot analysis of WT (Af293) left, Δ*fsqA* middle, and OE::*fsqA*, right. Overexpression of *fsqA* causes specific up-regulation of AFUA6g_03430 – AFUA6g_03490, defining the boundaries of the *fsq* cluster.

Nature Chemical Biology: doi:10.1038/nchembio.2061

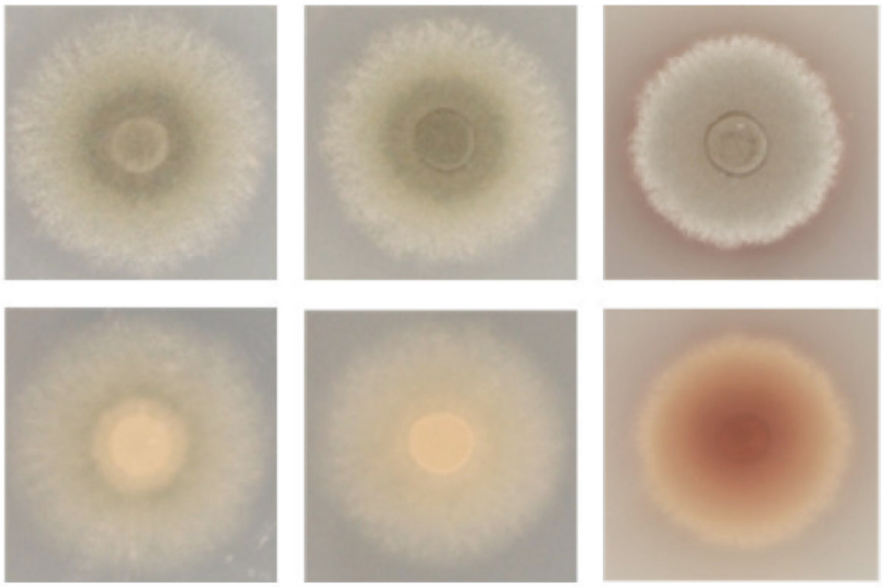

Supplementary Figure 2. Phenotype of WT (Af293) left, Δ*fsqA* middle, and OE::*fsqA* right grown on GMM at 37ºC for 72 hours. OE::*fsqA* decreases radial growth and shows characteristic brown pigmentation diffusing into the media.

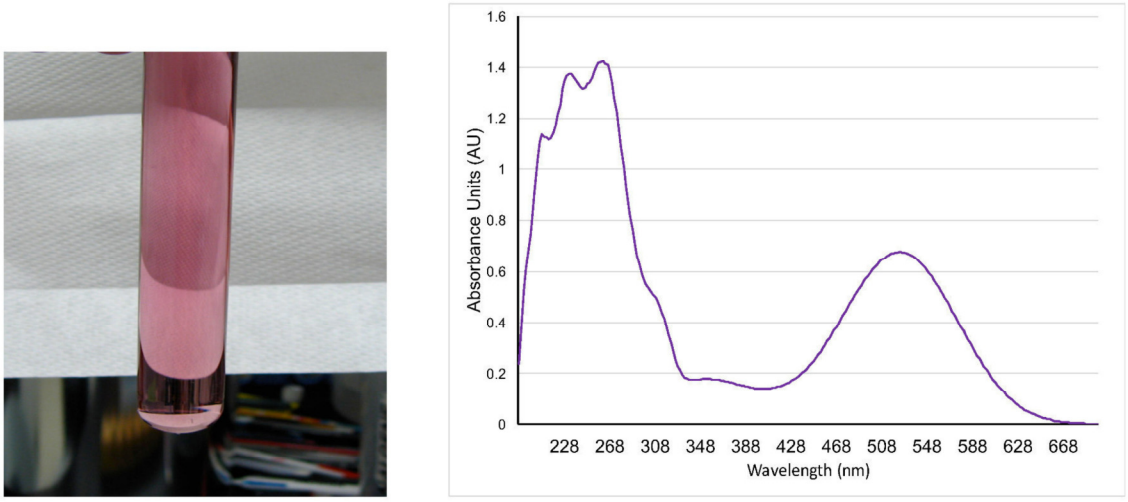

Supplementary Figure 3. Color of fumisoquin C. Photograph of a test tube (18 x 150 mm) from large-scale reverse-phase chromatography containing ~0.02 mg/mL of fumisoquin C, **3**, (left) and UV-Vis spectrum from HPLC-UV-MS analysis (right).

Nature Chemical Biology: doi:10.1038/nchembio.2061

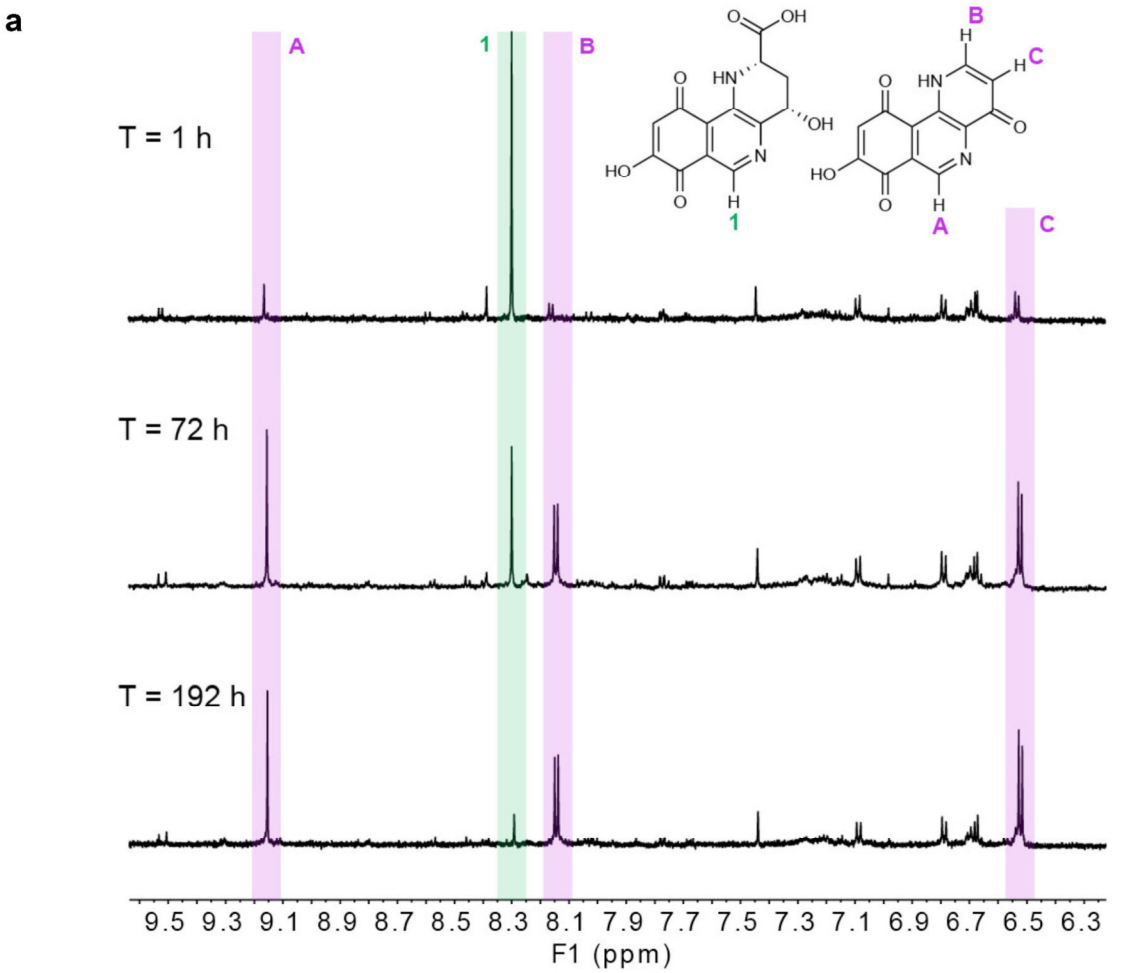

Supplementary Figure 4. Fumisoquin C decomposition and derivatization. (**a**) ^{1}H NMR spectra in CD_3OD at T = 2 h (top), T = 72 h (middle), and T = 192 h (bottom) after chromatographic purification, showing conversion of fumisoquin C, **3**, into **4**. (**b**) Conversion of fumisoquin C (**3**) into dimethyl fumisoquin C**.** See Online Methods for experimental procedure.

Nature Chemical Biology: doi:10.1038/nchembio.2061

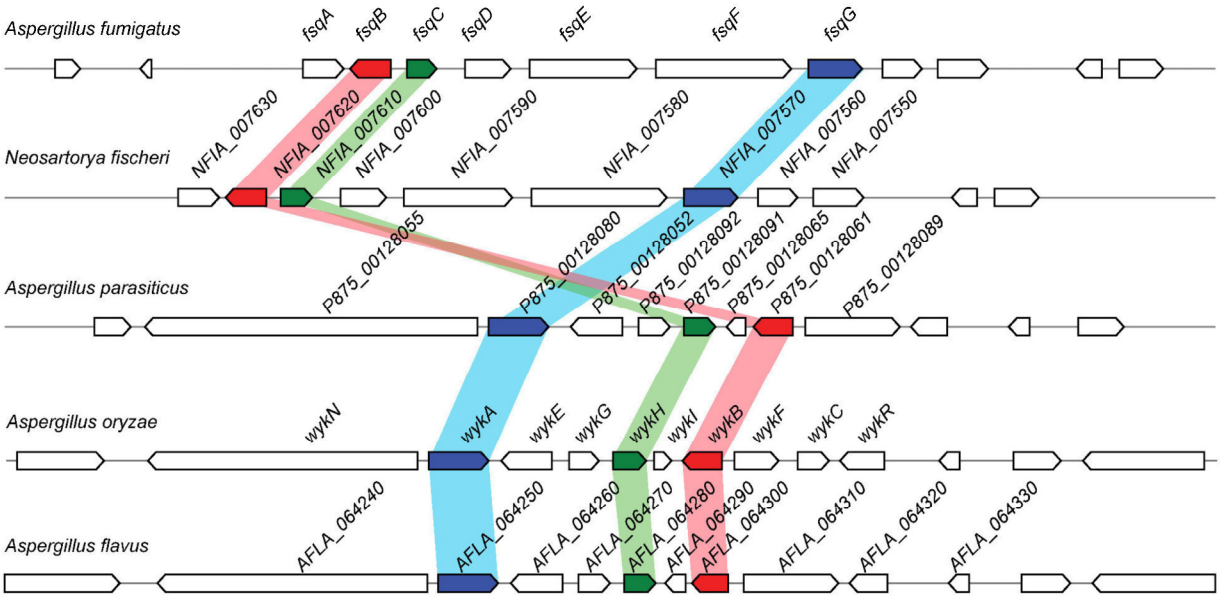

Supplementary Figure 5. Synteny analysis of *fsq* cluster in indicated *Aspergillus* and *Neosartorya* species. The analysis shows conservation of *fsqB* (red), *fsqC* (green), and *fsqG* (blue), which encode the enzymes responsible for the incorporation of the isoquinoline ring in **1-5**, and **18**. For % identity of these genes in each species shown, see **Supplementary Table 2**.

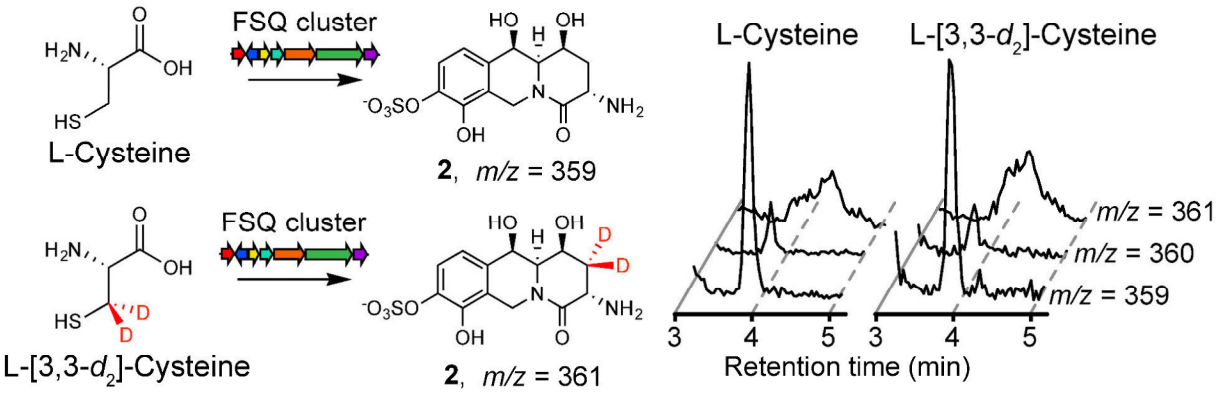

Supplementary Figure 6. L-cysteine is not incorporated into the fumisoquins. Ion chromatograms from HPLC-MS analysis of extracts from OE::*fsqA* fed with L-cysteine or L-[3,3-d_2]-cysteine. Indicated *m/z* values correspond to isotopomers of **2** with or without heavy atom incorporation.

Nature Chemical Biology: doi:10.1038/nchembio.2061

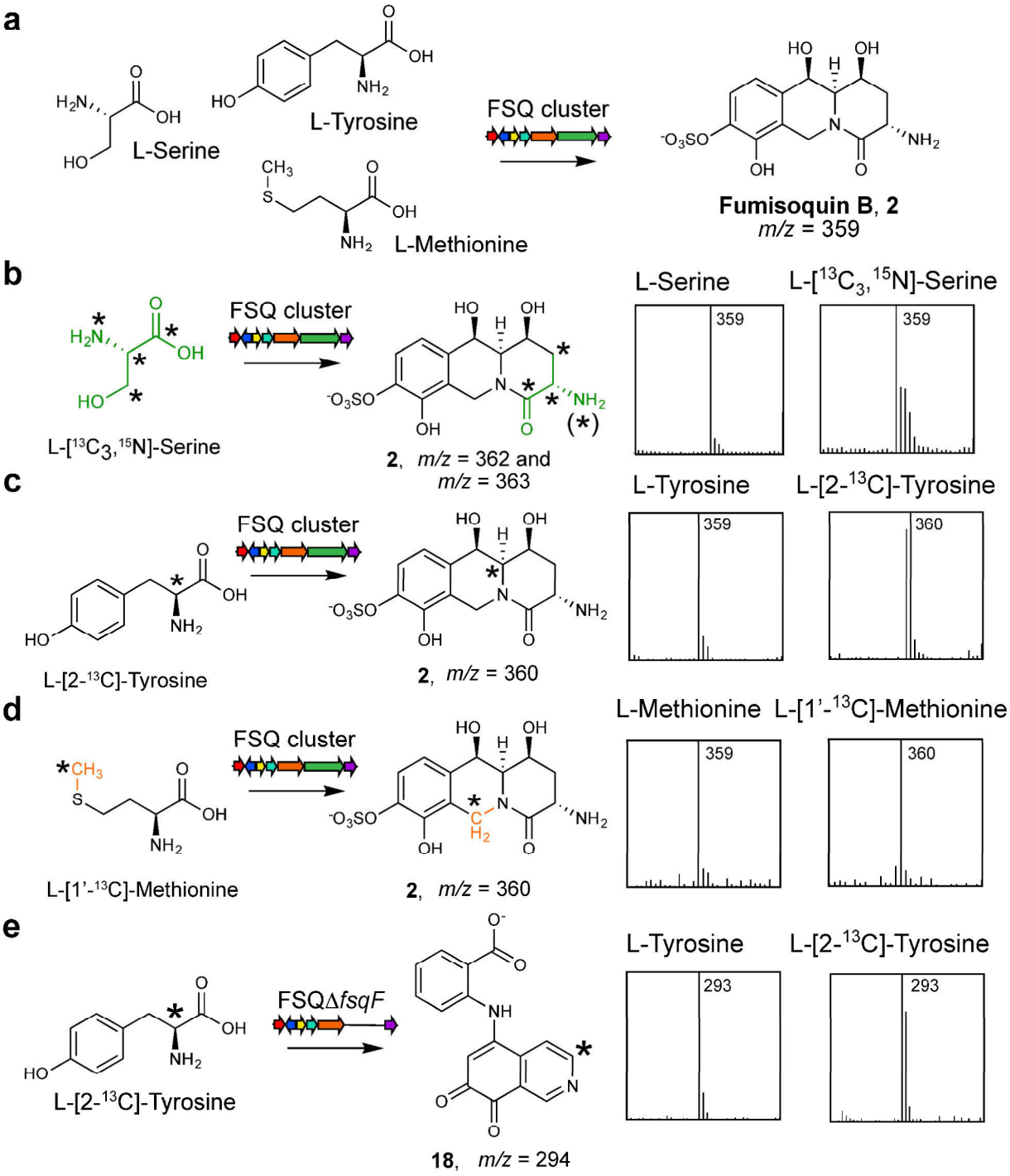

Supplementary Figure 7. **Mass spectra of FSQ cluster metabolites with and with out heavy atom incorporation**. (**a**) L-serine, L-tyrosine, and L-methionine are incorporated into the fumisoquins. (**b**) Mass spectrum of **2** with L-serine incorporated (left) and mass spectrum of **2** with L-[$^{13}C_3$, ^{15}N]-serine incorporated (right). Increased M+1 and M+2 peaks likely result from amination/deamination and use of abundant labeled serine for methionine production. (**c**) Mass spectrum of **2** with L-tyrosine incorporated (left) and mass spectrum of **2** with L-[2-^{13}C]-tyrosine incorporated (right). (**d**) Mass spectrum of **2** with L-methionine incorporated (left) and mass spectrum of **2** with L-[1'-^{13}C]-methionine incorporated (right). (**e**) Mass spectrum of **18** with L-tyrosine incorporated (left) and mass spectrum of **18** with L-[2-^{13}C]-tyrosine incorporated (right).

Nature Chemical Biology: doi:10.1038/nchembio.2061

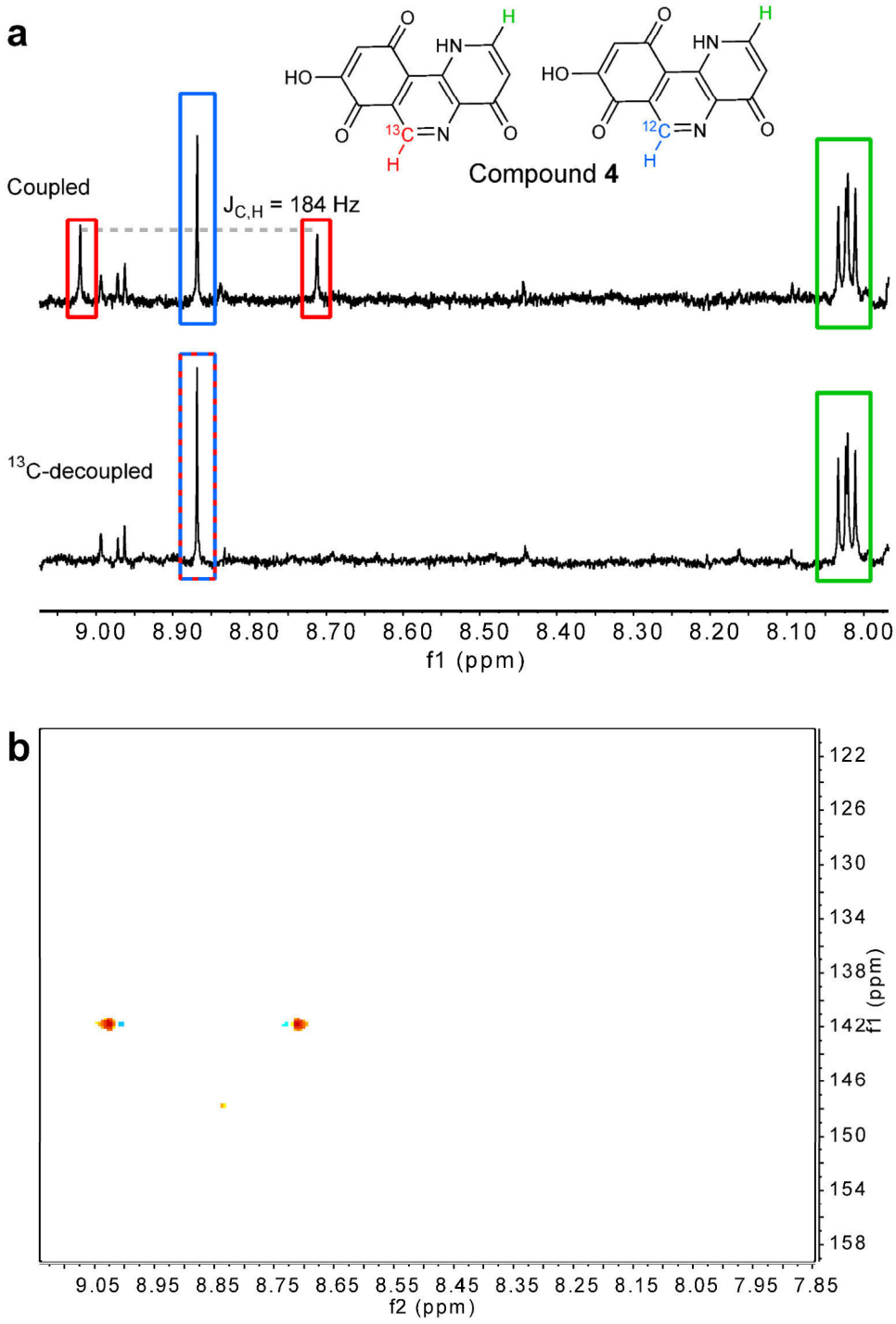

Supplementary Figure 8. **NMR spectra of ^{13}C-enriched 4** (a) ^{1}H-^{13}C coupled ^{1}H NMR spectrum of a sample of **4** obtained from fumisoquin C (**3**) isolated from a fungal culture grown with L-[1'-^{13}C]-methionine (top) and ^{1}H-^{13}C *decoupled* ^{1}H NMR spectrum of the same sample of **4** (bottom), showing selective incorporation of the methionine methyl group. In the decoupled spectrum, the intensity of the signal of the proton attached to the labeled carbon does not increase proportionally due to partial signal loss and line shape changes during decoupling. (**b**) ^{1}H-^{13}C coupled HSQC spectrum of this sample of **4**. Spectra were acquired using the 600 MHz Varian INOVA spectrometer, using DMSO-d_6 as solvent.

Nature Chemical Biology: doi:10.1038/nchembio.2061

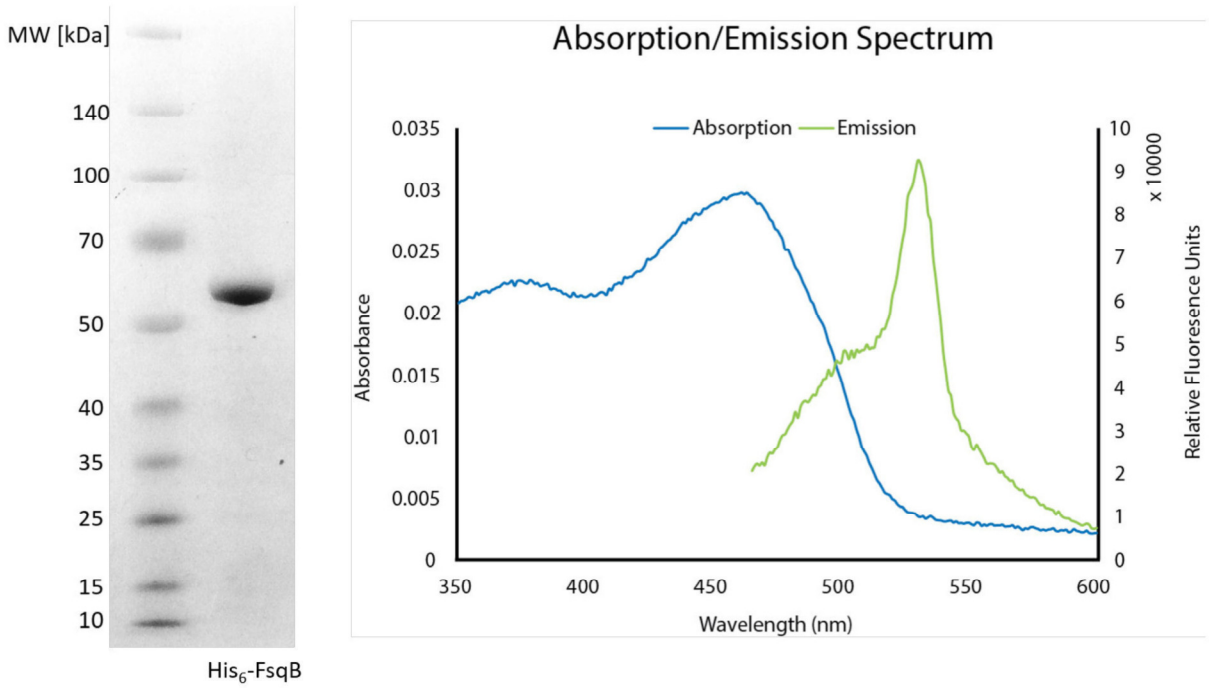

Supplementary Figure 9. **Purification and spectra of FsqB.** SDS-polyacrylamide gel of the polyhistidine-tagged FsqB (left), and UV-Vis absorption and fluorescence spectra (right) of FsqB. Spectra were acquired in 100 mM potassium phosphate buffer at pH 7.0, and fluorescence spectrum was acquired using an excitation wavelength of 450 nm.

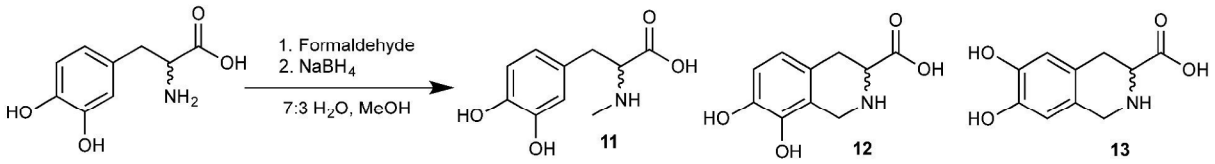

Supplementary Figure 10. Reaction of DL-DOPA with formaldehyde followed by addition of sodium borohydride produces a 7:3 mixture of cyclized products **12** and **13**, respectively, in addition to variable amounts of uncyclized **11**, as determined by HPLC-MS**.**

Nature Chemical Biology: doi:10.1038/nchembio.2061

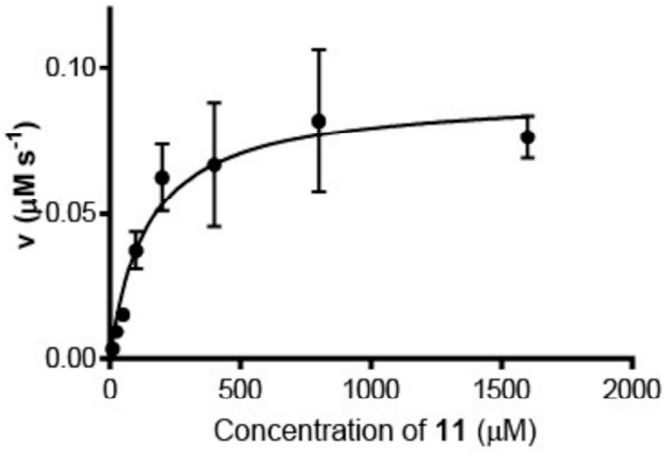

Supplementary Figure 11. **Enzymatic activity of FsqB.** Steady-state kinetics evaluated for FsqB on model substrate **11**. The observed apparent steady-state kinetic parameters of FsqB operating on **11** were K_M: 142.5 ± 42.9 μM and k_{cat}: 0.9 ± 0.1 s^{-1} at 25 °C. Each initial concentration of **11** was sampled twice for kinetic analysis, and displayed as the mean ± s.d.

Nature Chemical Biology: doi:10.1038/nchembio.2061

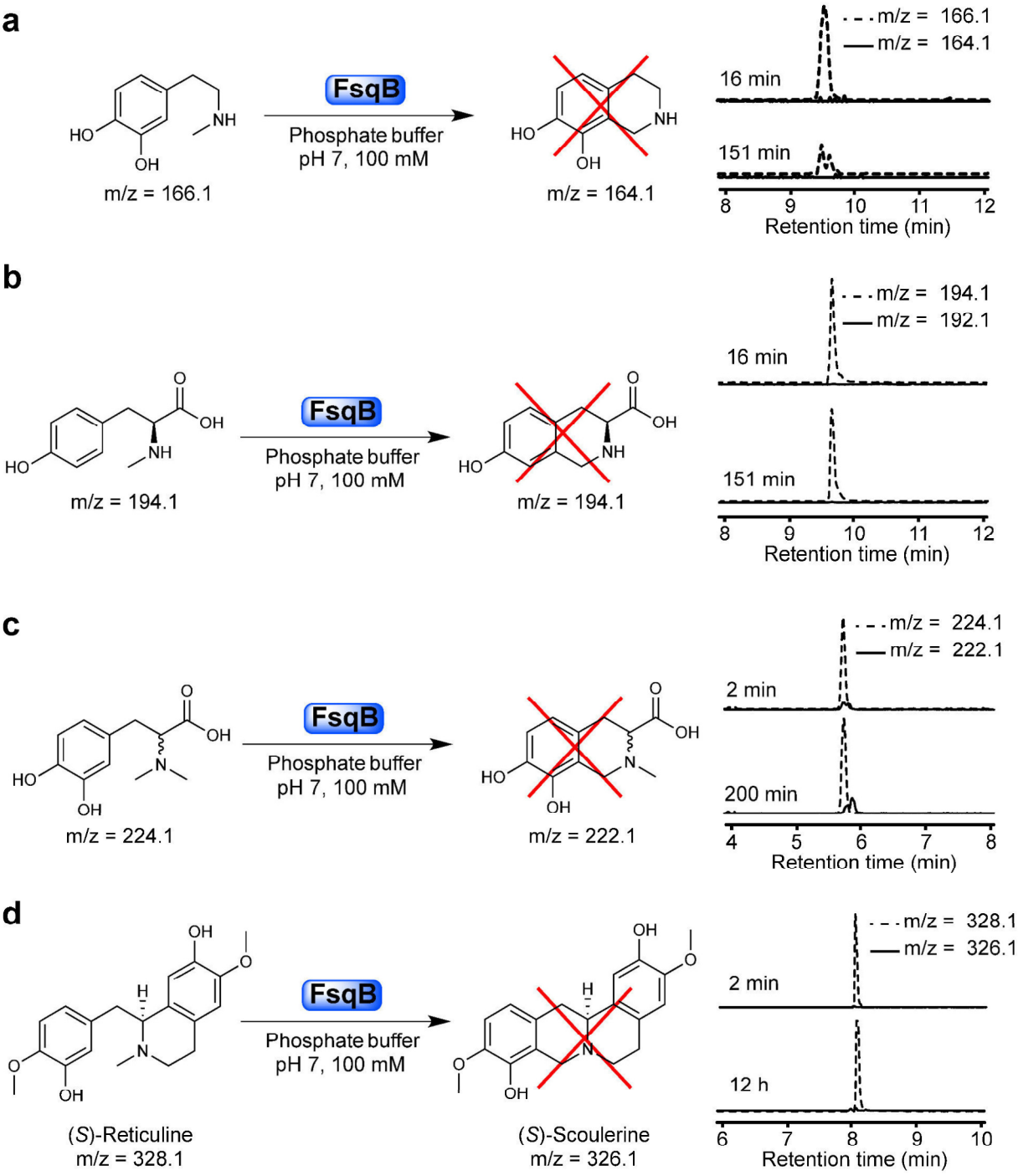

Supplementary Figure 12. Substrate specificity of FsqB. (**a**) Ion chromatograms for *N*-methyl dopamine (*m/z* = 166.1) and cyclic product (*m/z* = 164.1), showing no product formation after 151 min. (**b**) FsqB does not catalyze the cyclization of *N*-methyl-L-tyrosine. Ion chromatograms for *N*-methyl-L-tyrosine (*m/z* = 194.1) and cyclic product (*m/z* = 192.1) obtained after 151 min show no product formation. (**c**) FsqB does not catalyze the cyclization of *N,N*-dimethyl DOPA. Ion chromatograms for *N,N*-dimethyl DOPA (*m/z* = 224.1) and putative cyclic product (*m/z* = 222.1) obtained after 200 min show no product formation. Validating FsqB preference toward secondary β-*N*-methylamine substrates. (**d**) FsqB does not catalyze the cyclization of (*S*)-reticuline. Ion chromatograms for (*S*)-reticuline (*m/z* = 328.1) and cyclic product (*m/z* = 326.1) obtained after 12 h show no product formation.

Nature Chemical Biology: doi:10.1038/nchembio.2061

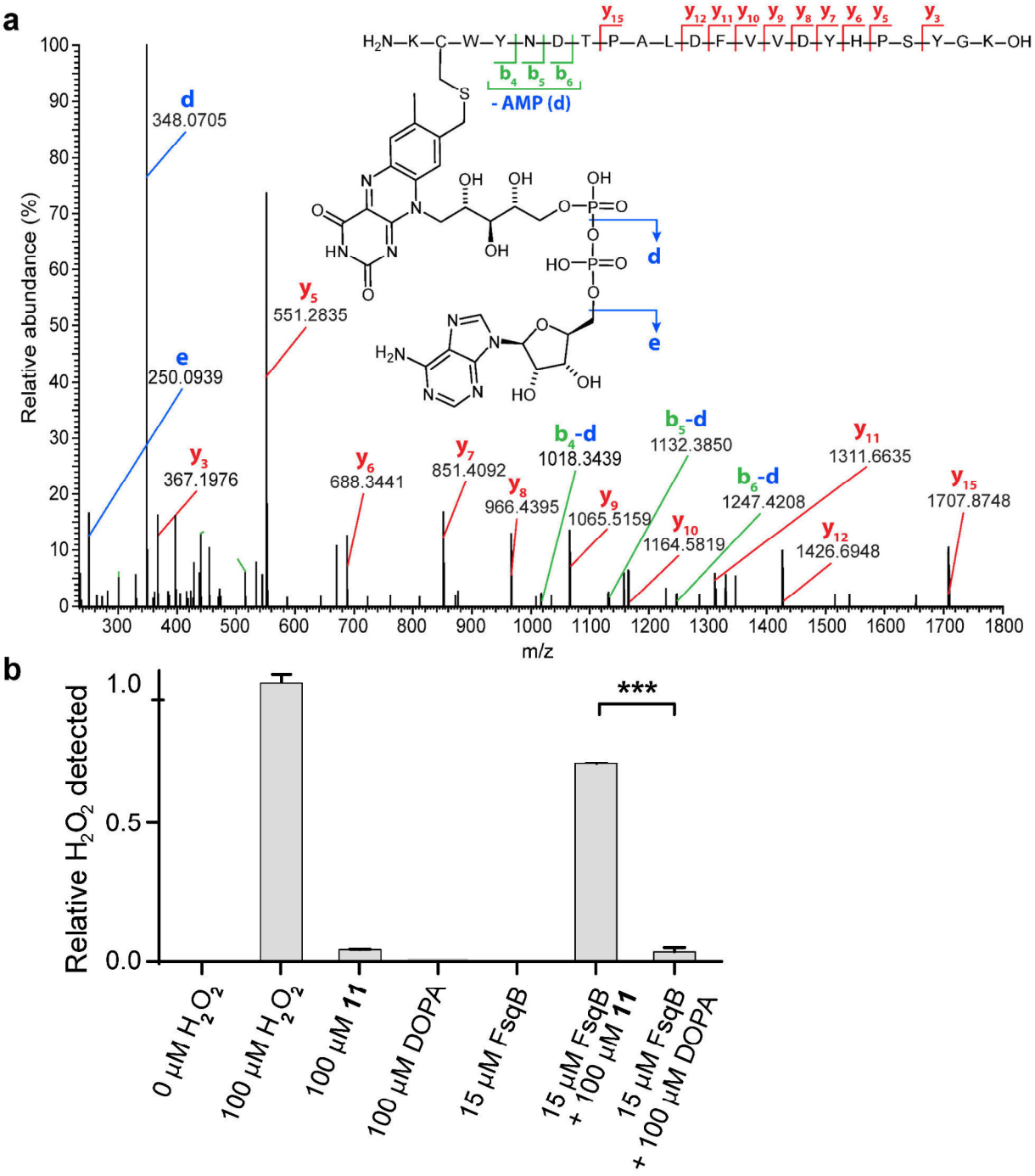

Supplementary Figure 13. **FsqB features a covalently bound FAD cofactor and produces H_2O_2 in the presence of substrate** (**a**) Collision-induced dissociation mass spectrum of tryptic FsqB peptide, revealing covalently bound FAD. Amino acid sequence and location of FAD attachment were inferred from indicated *b*- (green) and *y*-type (red) ion series and diagnostic FAD fragmentation (blue). (**b**) Amplex Red H_2O_2 assay of 15 μM FsqB with or without **11**, or 3,4-dihydroxy-DL-phenylalanine (DOPA) (100 mM phoshate buffer, pH 7, 1.5 h). Values were normalized to 0 and 100 μM H_2O_2 and presented as mean ± s.d. (n = 3), where * $P < 0.05$, ** $P < 0.001$, *** $P < 0.0001$, determined using Student's *t*-test.

Nature Chemical Biology: doi:10.1038/nchembio.2061

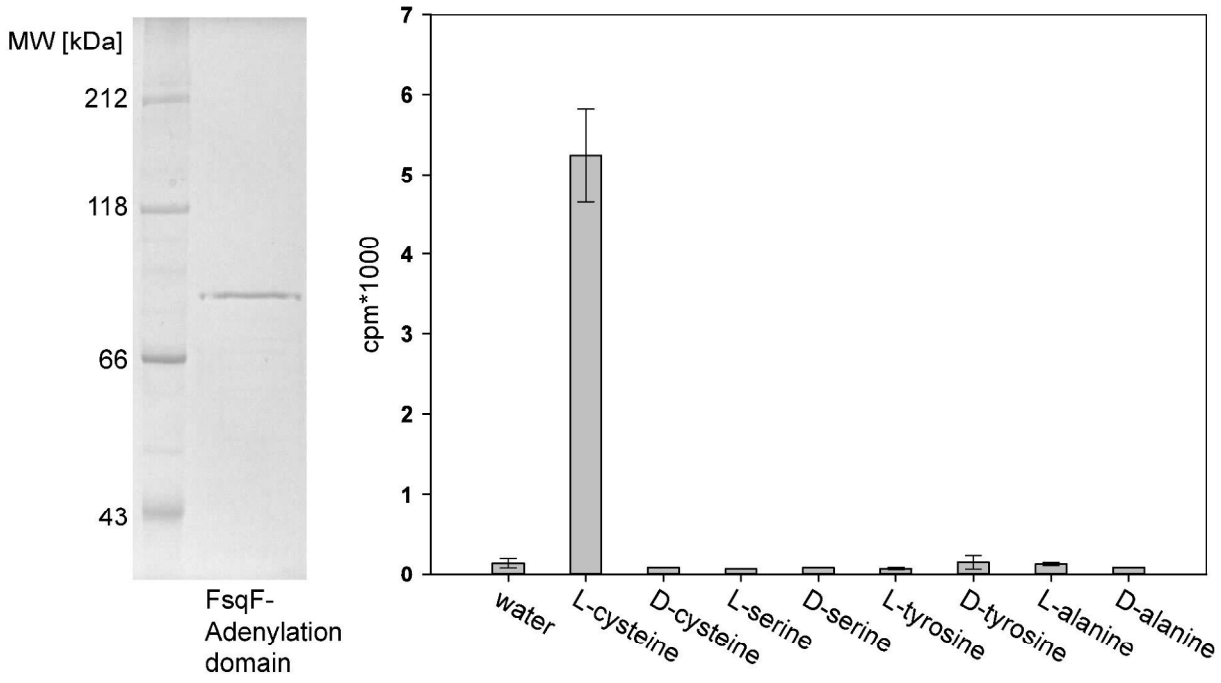

Supplementary Figure 14. **Properties of recombinant FsqF adenylation domain.** SDS-polyacrylamide gel showing the purity of the FsqF adenylation domain (left), and ATP-[^{32}P]pyrophosphate exchange assay results (right) for amino acids selected based on results from the stable-isotope labeling experiments (see **Fig. 4a-c** and **Supplementary Fig. 6** and Online Methods). The exchange assay shows none or minimal (in the case of L-cysteine) activation for all tested amino acids. Collectively, the assay results suggest that no standard amino acid is the true substrate, but rather a derivative of an amino acid, such as dehydroalanine, as proposed in the biosynthetic model shown in main text **Fig. 3**.

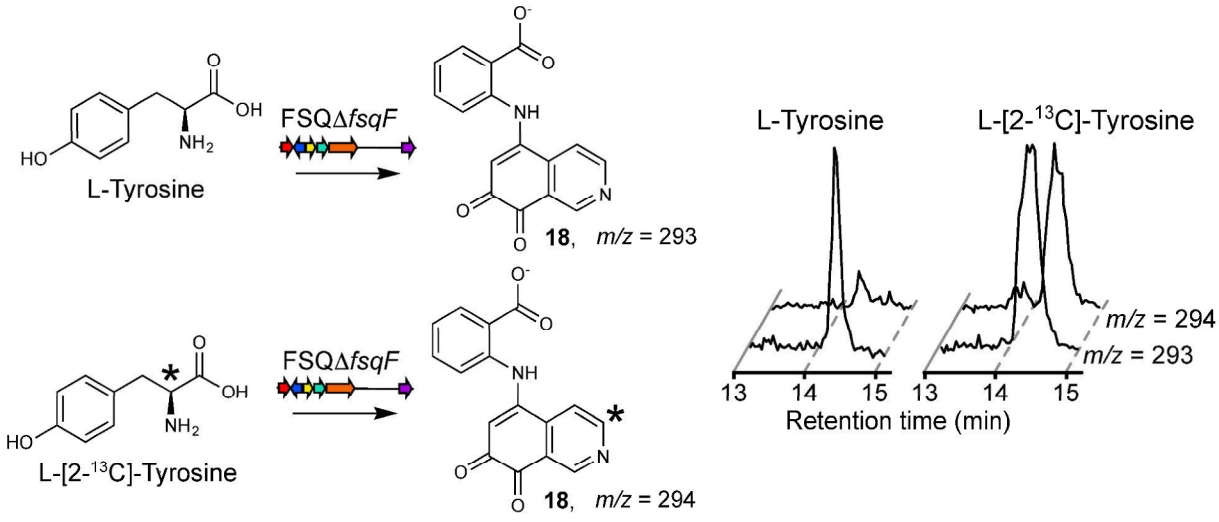

Supplementary Figure 15. **L-tyrosine is incorporated into shunt metabolite 18.** Ion chromatograms extracted from HPLC-MS analysis of extracts from OE::*fsqA*-Δ*fsqF* fed with L-tyrosine or L-[2-^{13}C]-tyrosine. The indicated *m/z* values correspond to **18** with or without heavy atom incorporation. The data support the hypothesis that FsqD is responsible for incorporation of L-tyrosine and not FsqF, as shown in main text **Fig 3.**

Nature Chemical Biology: doi:10.1038/nchembio.2061

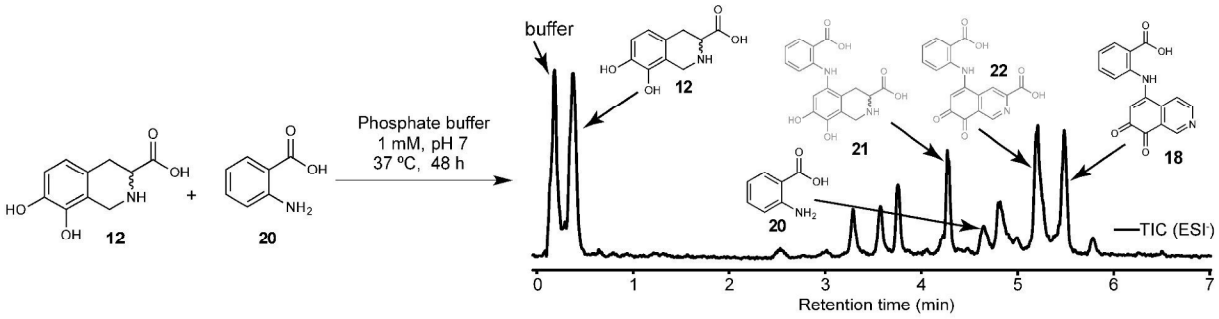

Supplementary Figure 16. Shunt metabolite 18 is produced non-enzymatically from 12 and anthranilic acid, 20. High-resolution UHPLC-MS total ion chromatogram for a reaction mixture of **12** and **20** reveals formation of **18**, along with two intermediates, **21** and **22** (proposed structures shown in gray). See **Supplementary Table 1** for HRMS data.

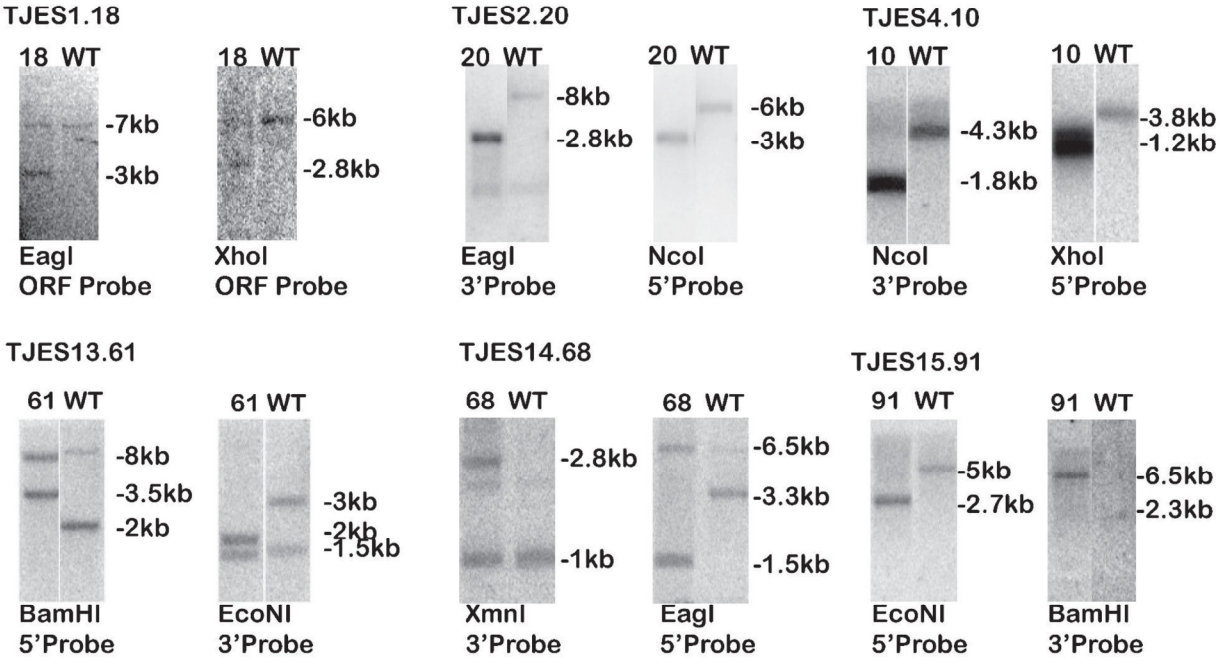

Supplementary Figure 17. Southern analysis confirmation of all mutants used in this study. Mutant (number) lanes are on the left of each image and the parental strain ("WT") is shown on the right. Expected band sizes correlating with those seen in the images are marked accordingly. Under each image is the enzymes used in the restriction digest as well as the nucleic acid probe us

Nature Chemical Biology: doi:10.1038/nchembio.2061

Supplementary References

1. Clauser, K. R., Baker, P. & Burlingame, A. L. Role of accurate mass measurement (+/- 10 ppm) in protein identification strategies employing MS or MS/MS and database searching. *Anal Chem* **71,** 2871–82 (1999).

2. Xue, T., Nguyen, C. K., Romans, A., Kontoyiannis, D. P. & May, G. S. Isogenic auxotrophic mutant strains in the Aspergillus fumigatus genome reference strain AF293. *Arch Microbiol* **182,** 346-353 (2004).

3. He, Z., Price, M.S., OBrian, G.R., Georgianna, D.R. & Payne, G.A. Improved protocols for functional analysis in the pathogenic fungus Aspergillus flavus. *BMC Microbiology* **7**, 104 (2007).

4. Palmer, J. M. *et al.* Loss of CclA, required for histone 3 lysine 4 methylation, decreases growth but increases secondary metabolite production in Aspergillus fumigatus. *PeerJ* **1**, e4 (2013).

5. Sekonyela, R. *et al.* RsmA regulates Aspergillus fumigatus gliotoxin cluster metabolites including cyclo(L-Phe-L-Ser), a potential new diagnostic marker for invasive aspergillosis. *PLoS One* **8**, e62591 (2013).

6. Lim, F.Y., *et al.* Genome-Based Cluster Deletion Reveals an Endocrin Biosynthetic Pathway in Aspergillus fumigatus. *Appl Environ Microbiol* **78**, 4117-4125 (2012).

7. Calvo, A.M., Bok, J.W., Brooks, W. & Keller, N.P. LeA Is Required for Toxin and Sclerotial Production in Aspergillus parasiticus. *Appl Environ Microbiol* **70**, 4733-4739 (2004)

Nature Chemical Biology: doi:10.1038/nchembio.2061

Supplementary Note

^{1}H (800 MHz) and ^{13}C (200 MHz) NMR spectroscopic data for fumisoquin A, 1, in methanol-d_4.

Chemical shifts were referenced to δ(C<u>H</u>D_2OD) = 3.31 and δ(^{13}<u>C</u>HD_2OD) = 49.0.^{13}C chemical shifts were determined via HMBC and HSQC spectra. ^{1}H, ^{1}H-*J*-coupling constants were determined from the acquired ^{1}H or dqfCOSY spectra. NOESY correlations were observed using a mixing time of 400 ms. HMBC correlations are from the proton(s) stated to the indicated ^{13}C atom.

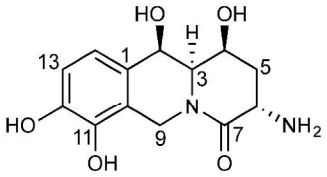

No.	δ_c	Proton	δH (J_{HH}[Hz])	HMBC	NOESY
1	128.03				
2	70.99	2-H	4.94 ($J_{2,3}$ = 1.9)	1, 3, 4, 7, 10, 11, 14	3, 4, 14
3	60.44	3-H	3.73 ($J_{3,2}$ = 1.9, $J_{3,4}$ = 8.7)	1, 7	2, 4, 5b
4	67.19	4-H	4.65 ($J_{4,3}$ = 8.7, $J_{4,5a}$ = 7.6, $J_{4,5b}$ < 1)	5	2, 5a, 5b
5	33.67	5-H_a	2.46 ($J_{5a,4}$ = 7.6, $J_{5a,5b}$ = 13.0, $J_{5a,6}$ = 5.7)	3, 4, 6, 7	4, 6, 5b
		5-H_b	2.06 ($J_{5b,4}$ < 1, $J_{5b,5a}$ = 13.0, $J_{5b,6}$ = 12.4)	3, 4, 6, 7	3, 4, 5a
6	47.88	6-H	4.29 ($J_{6,5a}$ = 5.7, $J_{6,5b}$ = 12.4)	5, 7	5a
7	169.75				
8					
9	42.35	9-H_a	4.66 ($J_{9Ha,9Hb}$ = 18.0)	1, 2, 3, 6, 7, 10, 11, 12, 13	
		9-H_b	4.78 ($J_{9Hb,9Ha}$ = 18.0)	1, 2, 3, 6, 7, 10, 11, 12, 13	3
10	119.92				
11	142.82				
12	146.06				
13	114.23	13-H	6.73 ($J_{13,14}$ = 8.0)	1, 10, 11, 12	14
14	120.04	14-H	6.70 ($J_{14,13}$ = 8.0)	1, 2, 4, 9, 10, 12, 13	2,1 3

Nature Chemical Biology: doi:10.1038/nchembio.2061

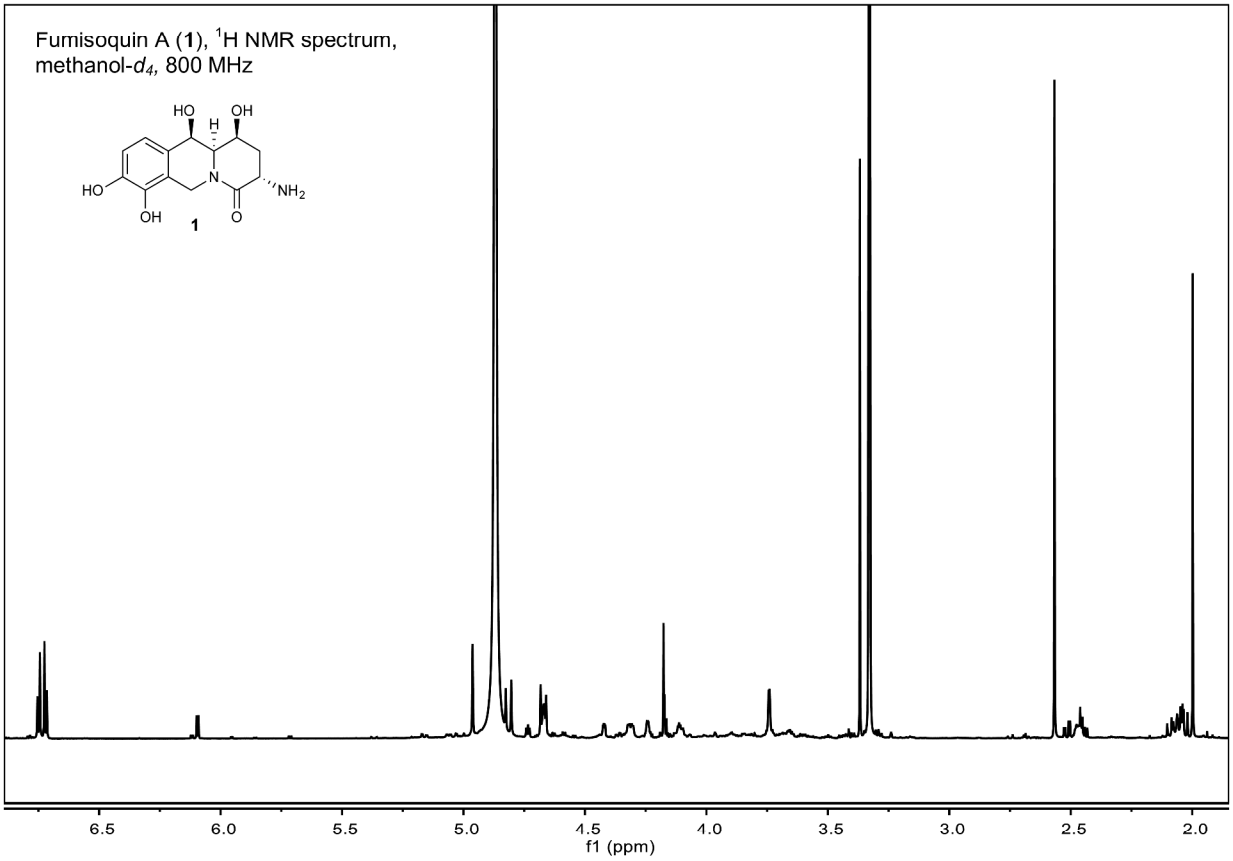

Nature Chemical Biology: doi:10.1038/nchembio.2061

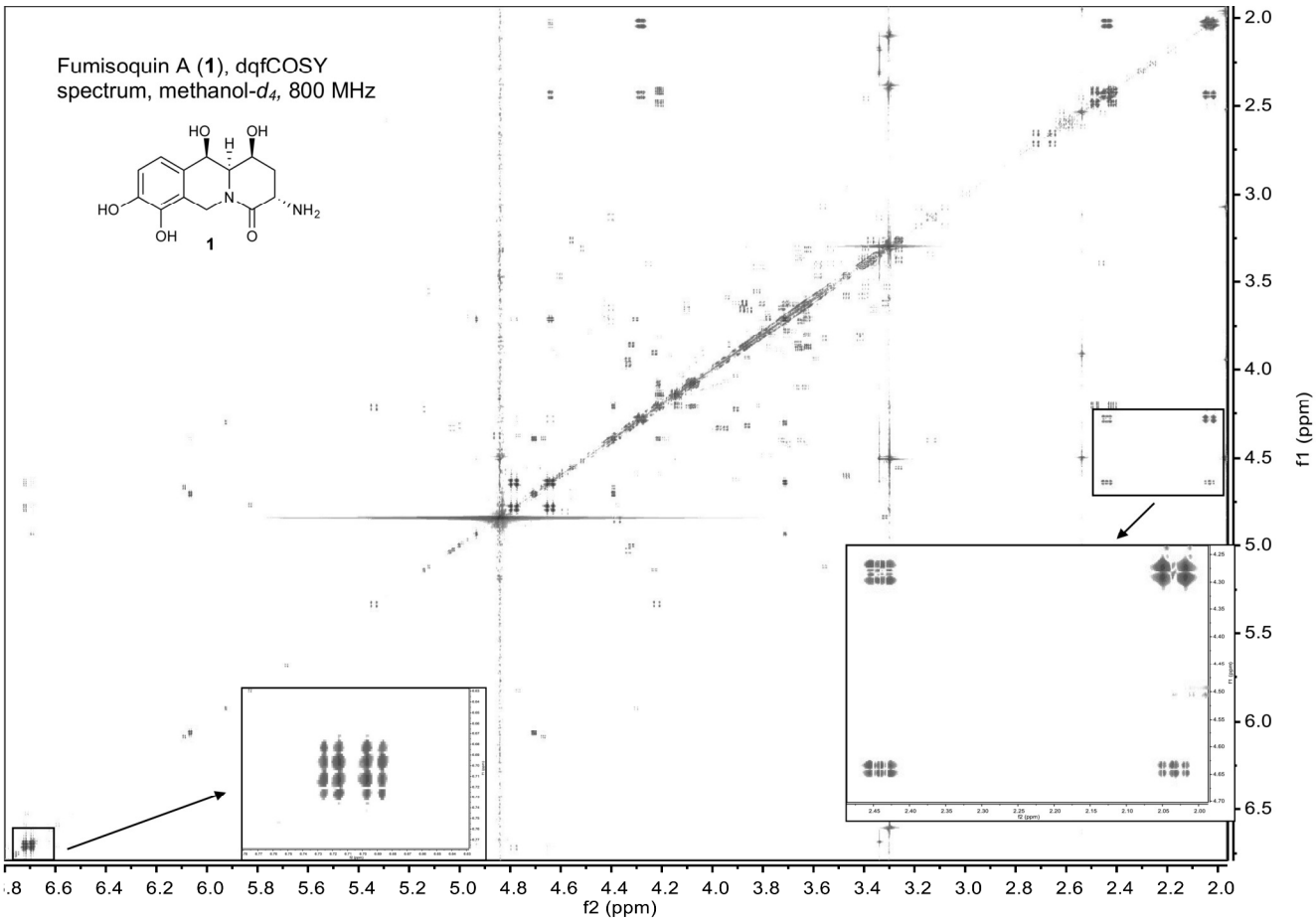

Nature Chemical Biology: doi:10.1038/nchembio.2061

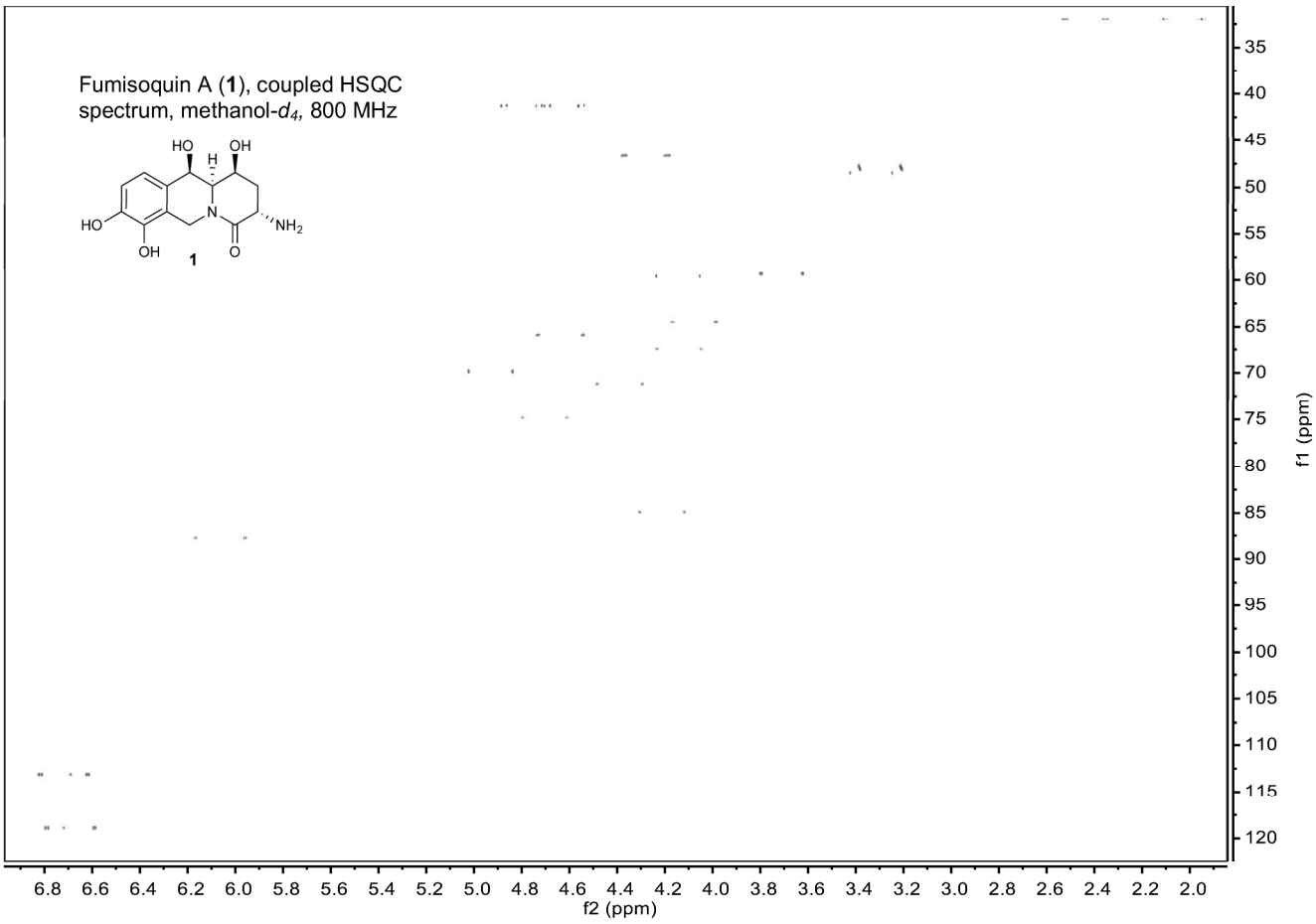

Nature Chemical Biology: doi:10.1038/nchembio.2061

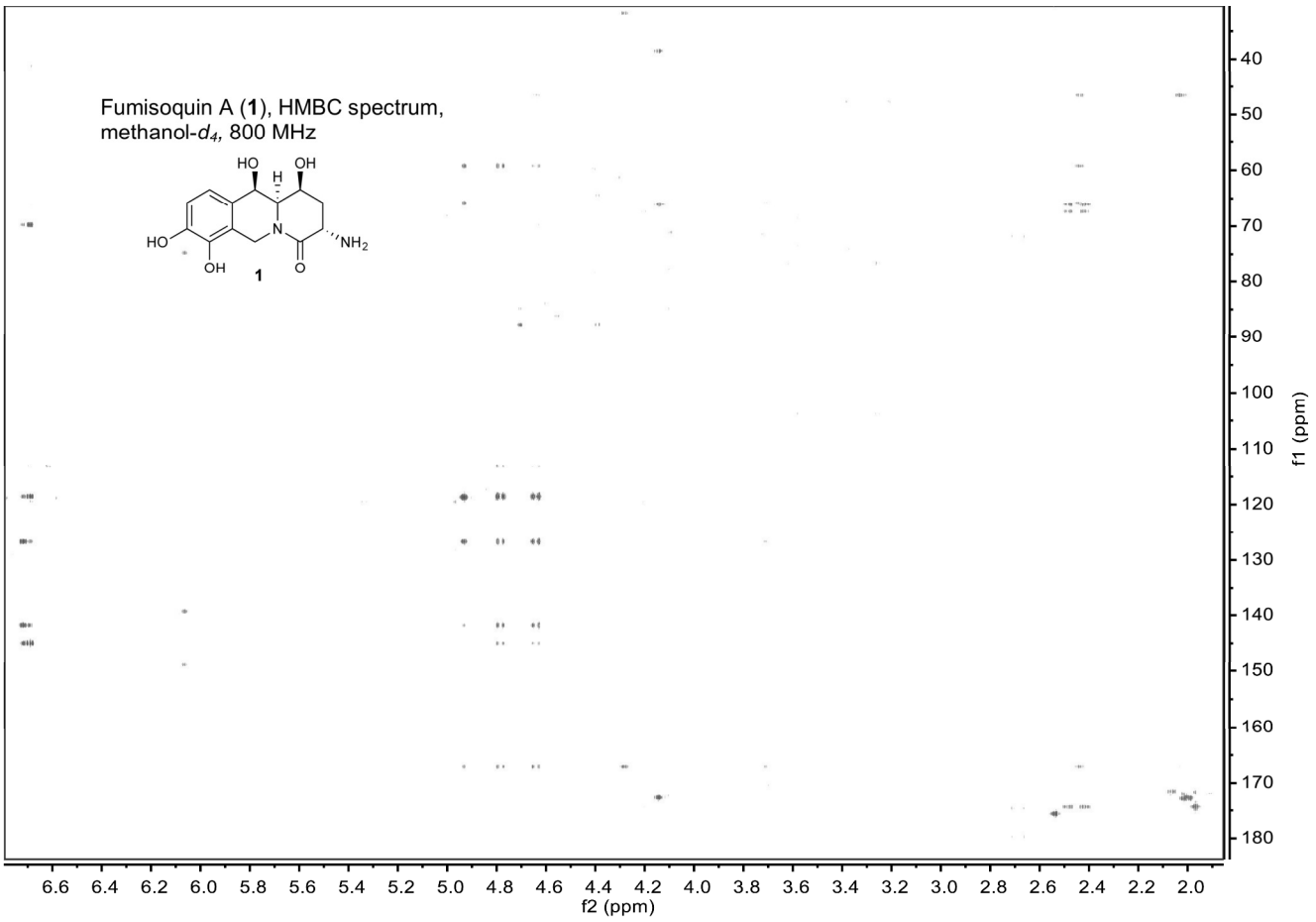

Nature Chemical Biology: doi:10.1038/nchembio.2061

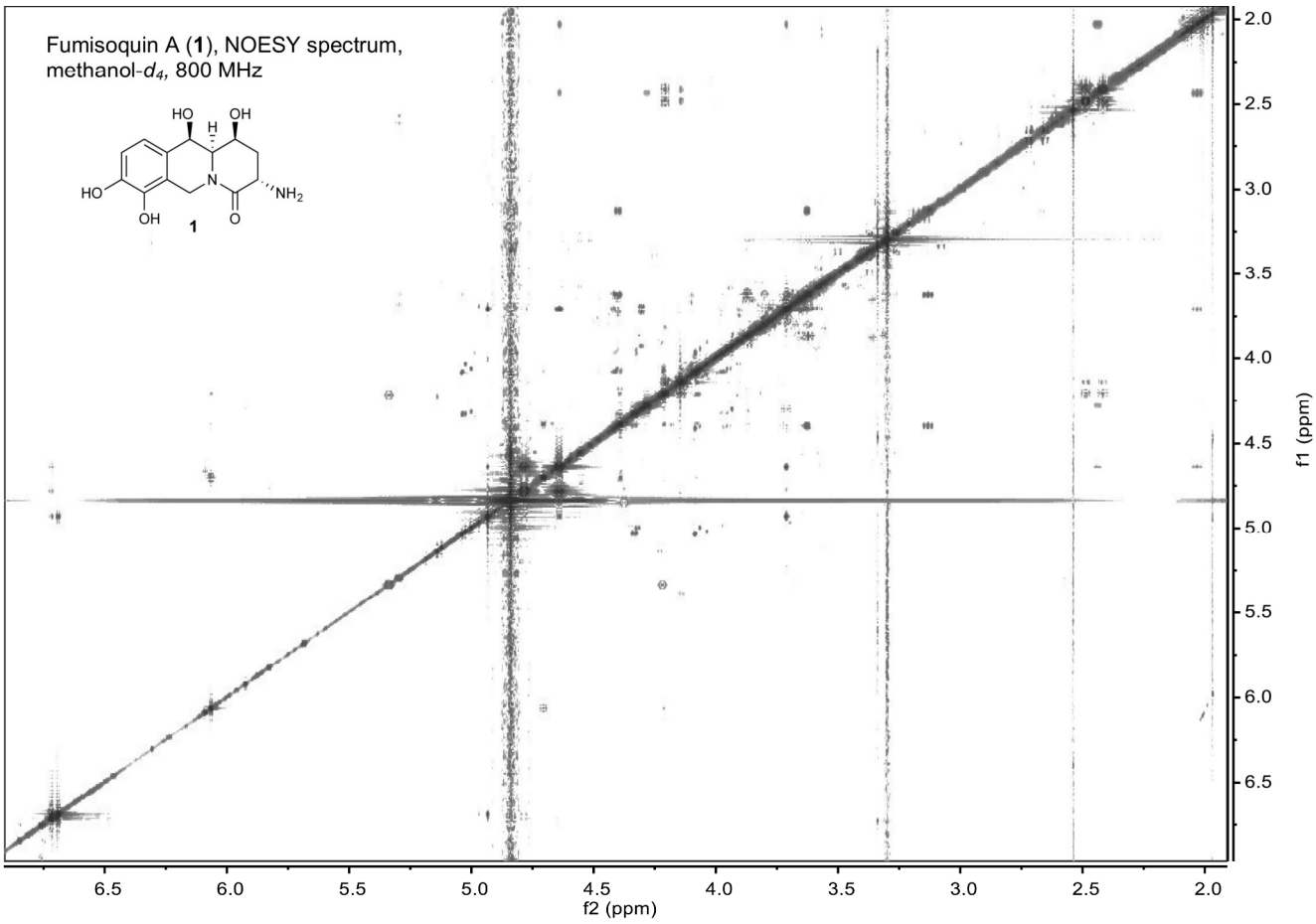

Nature Chemical Biology: doi:10.1038/nchembio.2061

^{1}H (600 MHz) and ^{13}C (151 MHz) NMR spectroscopic data for fumisoquin B, 2, in methanol-d_4.

Chemical shifts were referenced to δ(C<u>H</u>D$_2$OD) = 3.31 and δ(^{13}<u>C</u>HD$_2$OD) = 49.0.^{13}C chemical shifts were determined via HMBC and HSQC spectra. ^{1}H, ^{1}H-*J*-coupling constants were determined from the acquired ^{1}H or dqfCOSY spectra. ROESY correlations were observed using a mixing time of 500 ms. HMBC correlations are from the proton(s) stated to the indicated ^{13}C atom.

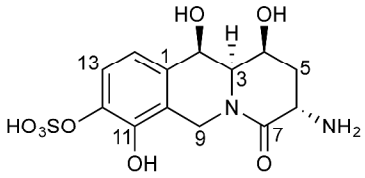

No.	δ_c	Proton	δH (J_{HH}[Hz])	HMBC[a]	ROESY
1	134.03				
2	70.75	2-H	4.98 ($J_{2,3}$ = 2.0)	1, 3, 10	4, 14
3	60.19	3-H	3.71 ($J_{3,2}$ = 2.0, $J_{3,4}$ = 9.2)		5a
4	67.30	4-H	4.62 ($J_{4,3}$ = 9.2, $J_{4,5a}$ = 6.9, $J_{4,5b}$ = 7.9)	6	2
5	34.69	5-H$_a$	1.94 ($J_{5a,4}$ = 6.9, $J_{5a,5b}$ = 13.0, $J_{5a,6}$ = 11.5)	4, 6, 7	3
		5-H$_b$	2.43 ($J_{5b,4}$ = 7.9, $J_{5b,5a}$ = 13.0, $J_{5b,6}$ = 5.8)	4, 6, 7	
6	47.88	6-H	4.02 ($J_{6,5a}$ =11.5, $J_{6,Hb}$ = 5.8)	5, 7	
7	171.61				
8					
9	42.26	9-H$_a$	4.63 ($J_{9Ha,9Hb}$ = 18.5)	3	
		9-H$_b$	4.81 ($J_{9Hb,9Ha}$ = 18.5)	10, 11	
10	121.61				
11	147.05				
12	140.92				
13	122.08	13-H	7.23 ($J_{13,14}$ = 8.1)	1, 11, 12w	
14	119.96	14-H	6.83 ($J_{14,13}$ = 8.1)	2, 10, 12, 13	2

[a]w: weak correlation (less than ~10% of the intensity of strongest signal)

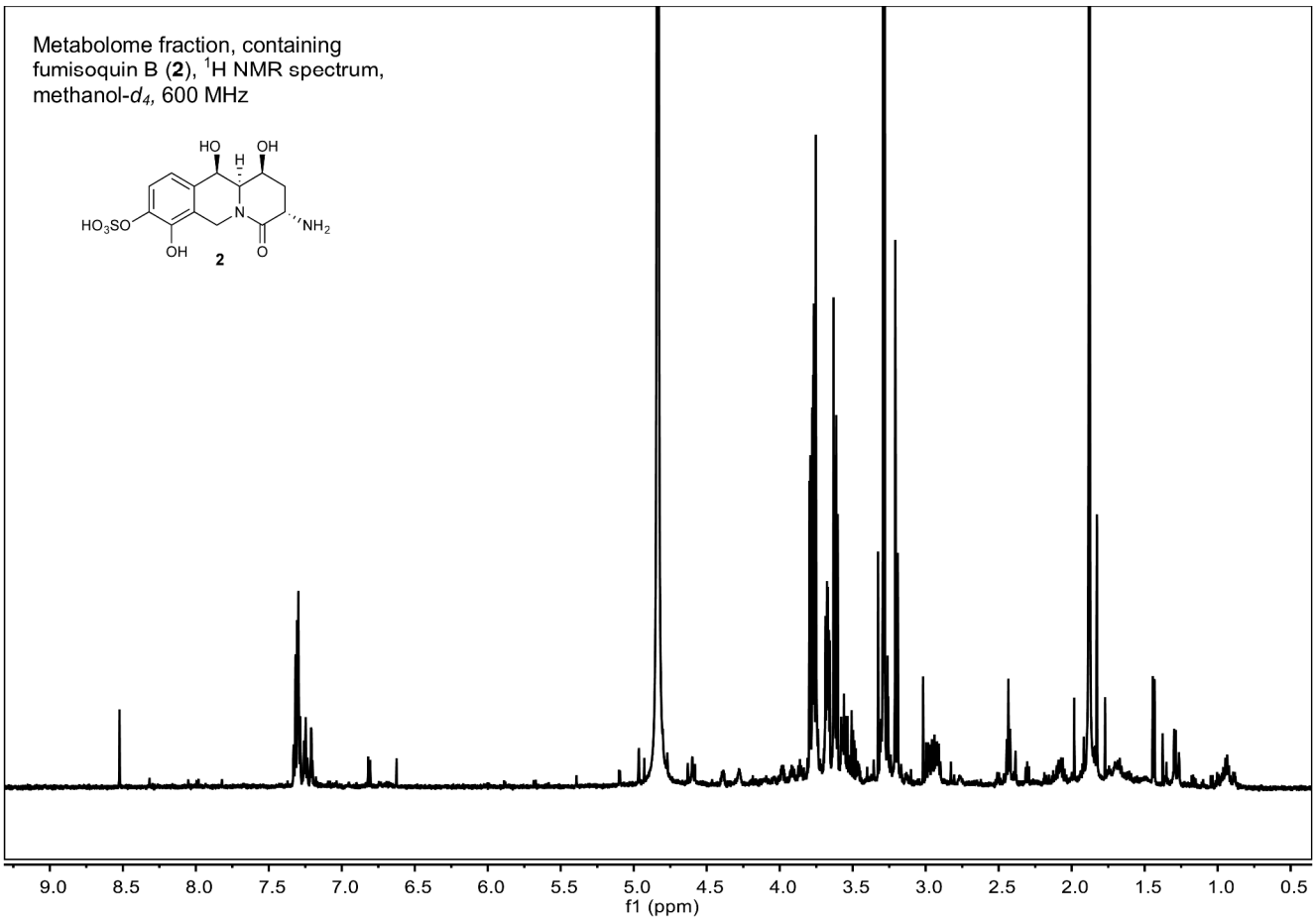

Nature Chemical Biology: doi:10.1038/nchembio.2061

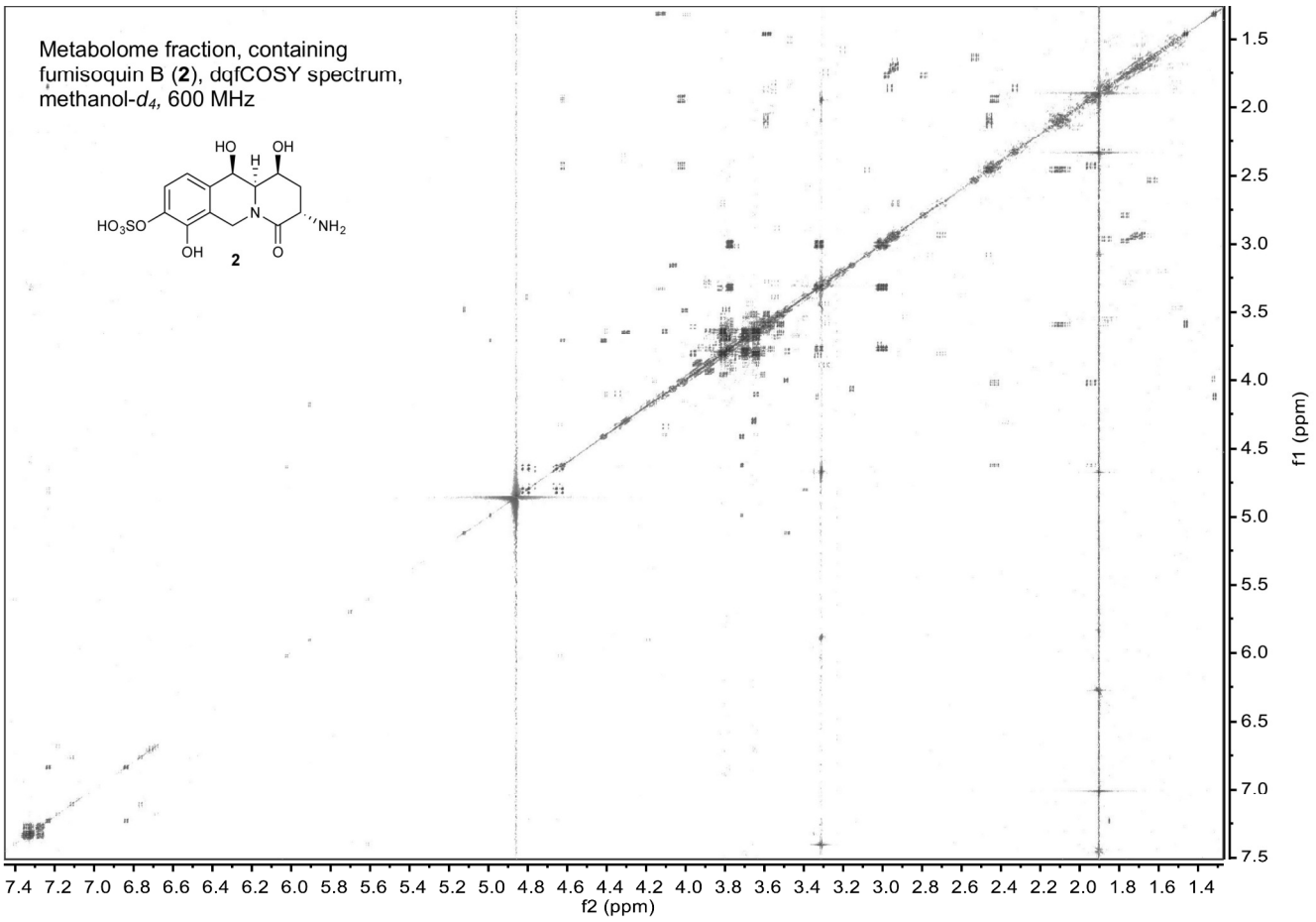

Nature Chemical Biology: doi:10.1038/nchembio.2061

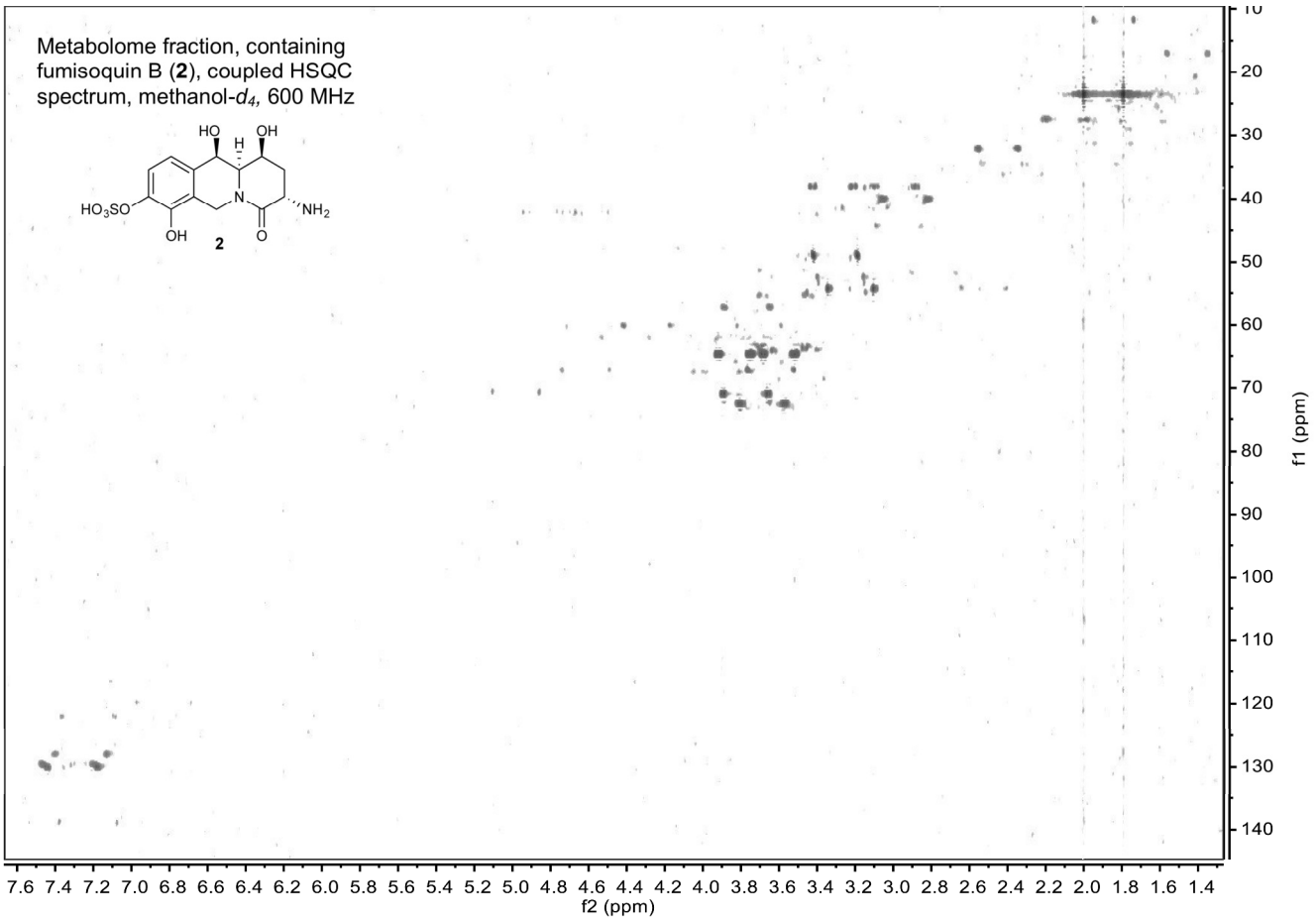

Nature Chemical Biology: doi:10.1038/nchembio.2061

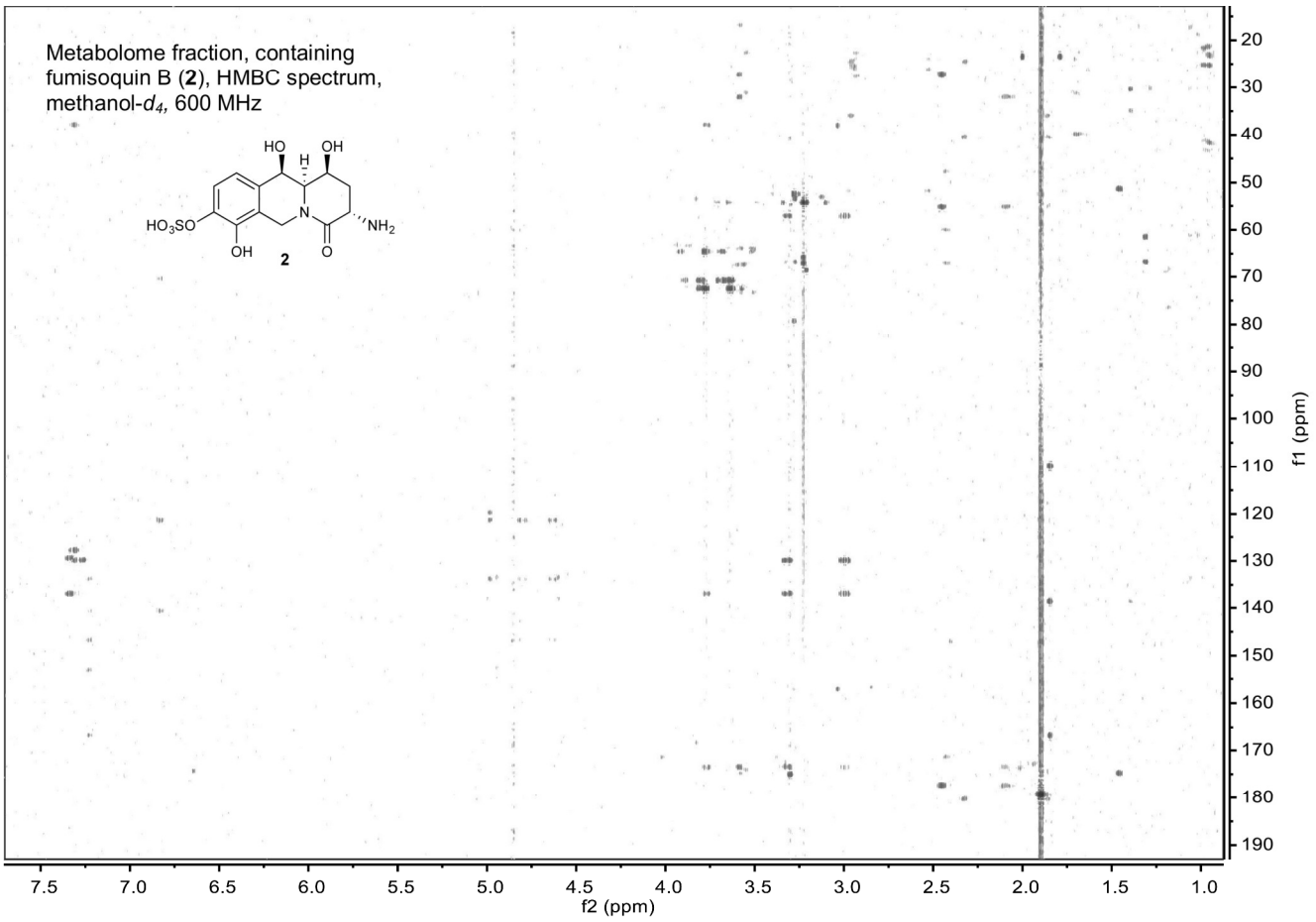

Nature Chemical Biology: doi:10.1038/nchembio.2061

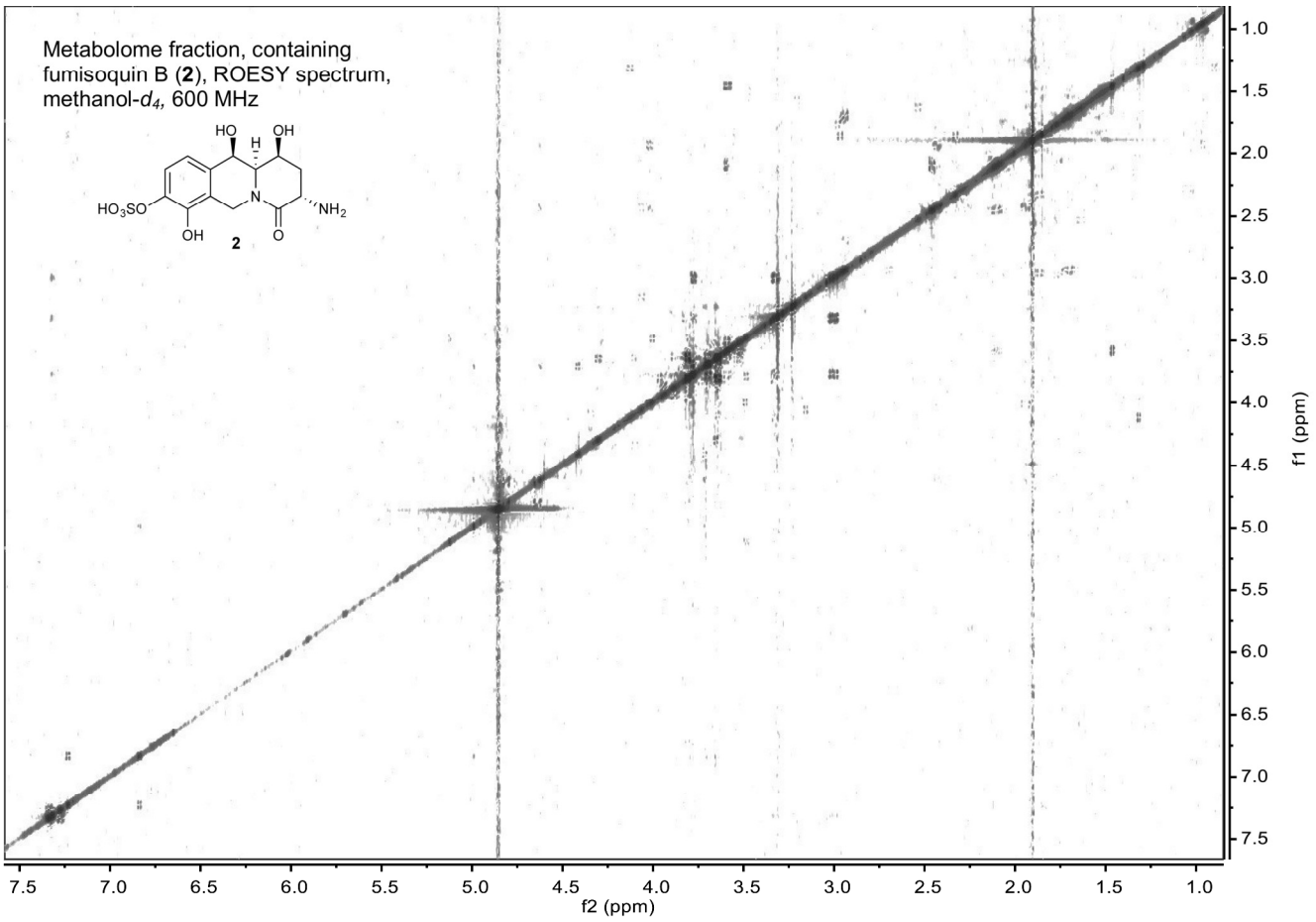

Nature Chemical Biology: doi:10.1038/nchembio.2061

^{1}H and ^{13}C spectroscopic data for fumisoquin C, 3, in DMSO-d_6.

Chemical shifts were referenced to δ($C\underline{H}D_2SOCD_3$) = 2.50 and δ($^{13}\underline{C}HD_2SOCD_3$) = 39.52. ^{13}C chemical shifts were determined via HMBC and HSQC spectra. Spectra were acquired using the Varian INOVA 600 spectrometer, except for the HSQC, which was acquired using the Bruker Avance 800 spectrometer. ^{1}H, ^{1}H-*J*-coupling constants were determined from the acquired ^{1}H spectrum. NOESY correlations were observed using a mixing time of 600 ms. HMBC correlations are from the proton(s) stated to the indicated ^{13}C atom.

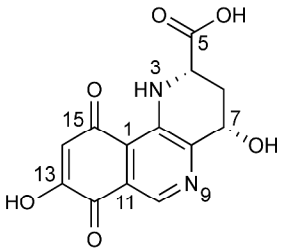

No.	δ_c	Proton	δH (J_{HH}[Hz])	HMBC	NOESY
1	115.62				
2	138.33				
3		3-NH	9.46 ($J_{3,4}$ = 1.5)	1, 4, 5, 6, 8	4
4	53.27	4-H	3.73 ($J_{4,3}$ = 1.5, $J_{4,6a}$ =9.6, $J_{4,6b}$ = 5.4)	2, 5, 6, 7	3, 7
5	173.40				
6	32.31	6-Ha	1.69 ($J_{6a,4}$ =12, $J_{6a,6b}$ = 12.8, $J_{6a,7}$ = 9.5)	4, 5, 7, 8	
		6-Hb	2.38 ($J_{6b,4}$ =12, $J_{6a,6b}$ = 12.8, $J_{6b,7}$ = 5.3)	4, 5, 7, 8	
7	66.85	7-H	4.57 ($J_{7,6a}$ = 9.5, $J_{7,6b}$ = 5.3)	2, 4, 6, 8	4
8	152.69				
9					
10	130.73	10-H	7.98	1, 8, 11, 12, 13, 15	
11	124.93				
12	188.04				
13[a]	184.60				
14	107.92	14-H	5.24	1, 12, 13, 15	
15[a]	170.85				

[a]Position 13 and 15 carbon chemical shifts are interchangeable

Nature Chemical Biology: doi:10.1038/nchembio.2061

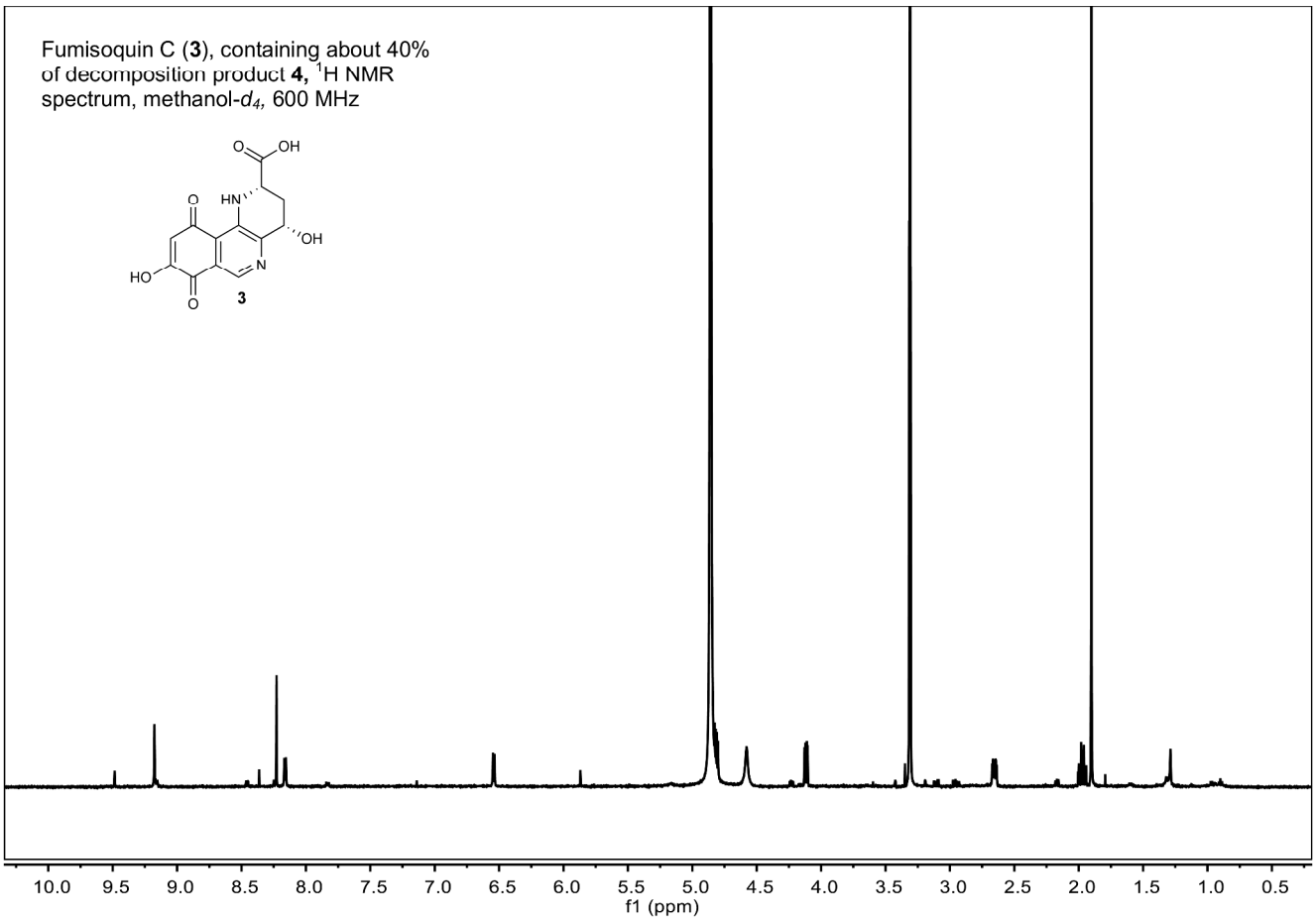

Nature Chemical Biology: doi:10.1038/nchembio.2061

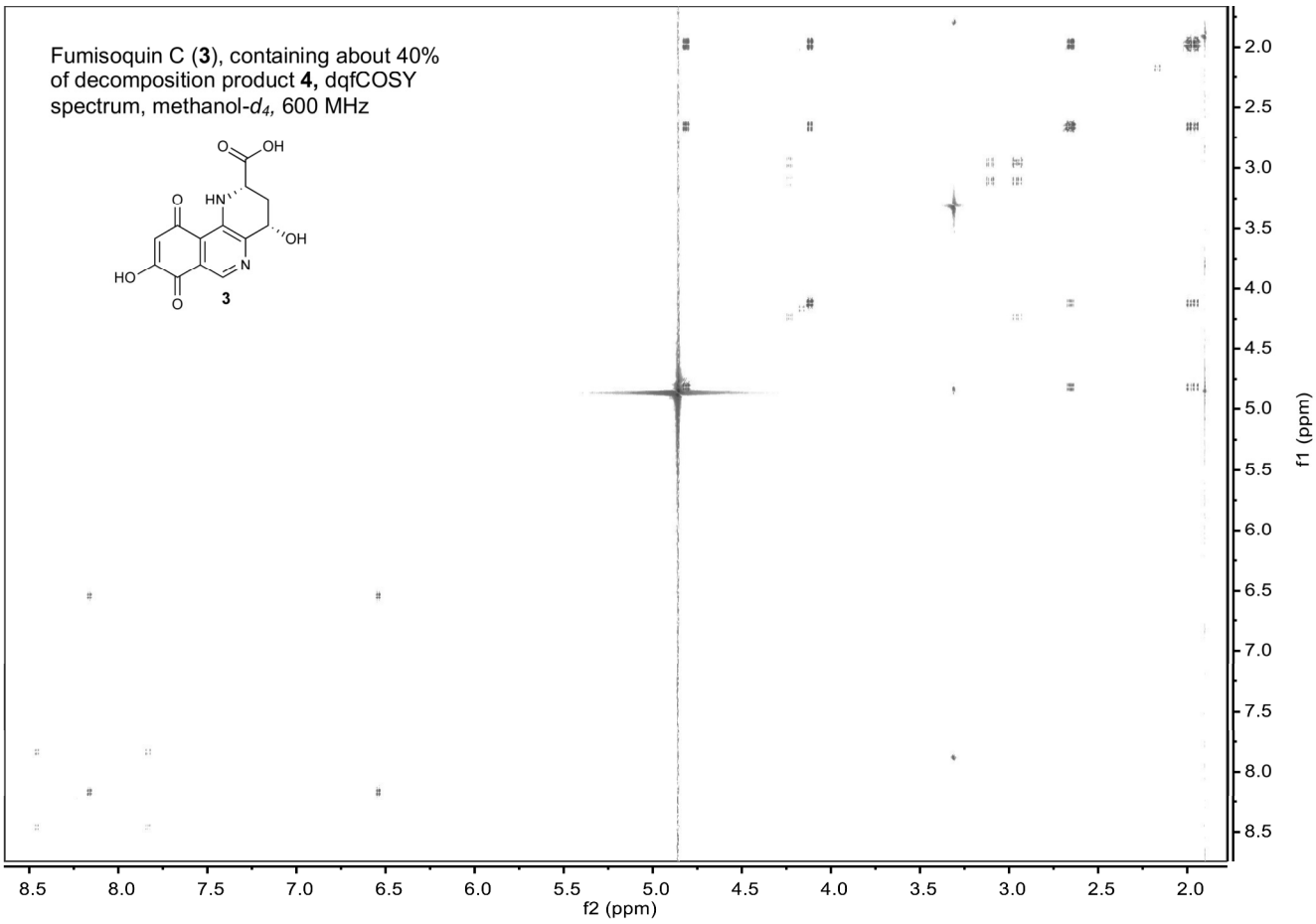

Nature Chemical Biology: doi:10.1038/nchembio.2061

Fumisoquin C (**3**), containing about 40% of decomposition product **4,** ^{1}H NMR spectrum, DMSO-d_6, 600 MHz

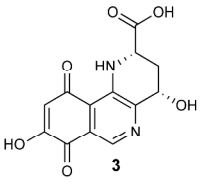

3

Nature Chemical Biology: doi:10.1038/nchembio.2061

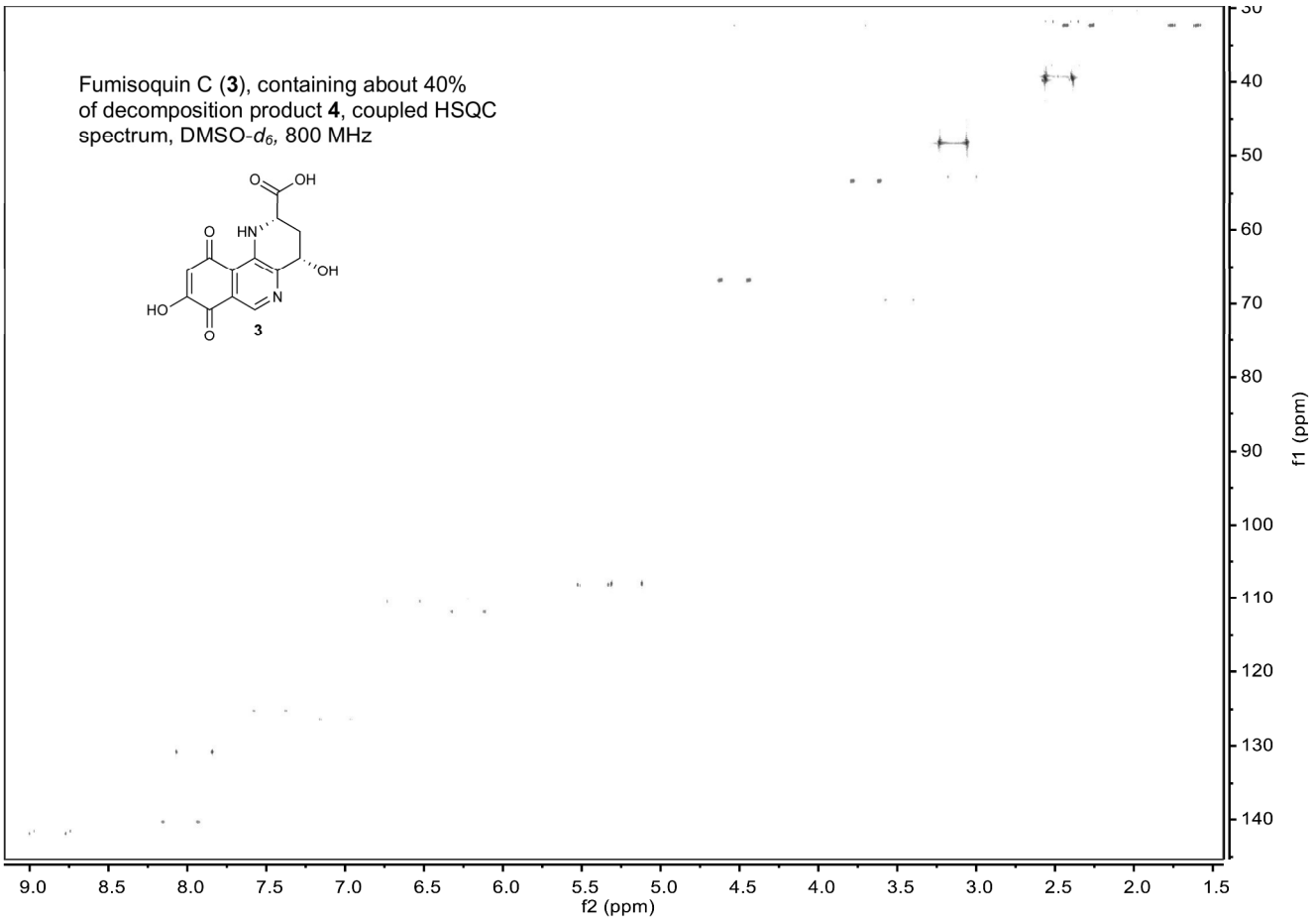

Nature Chemical Biology: doi:10.1038/nchembio.2061

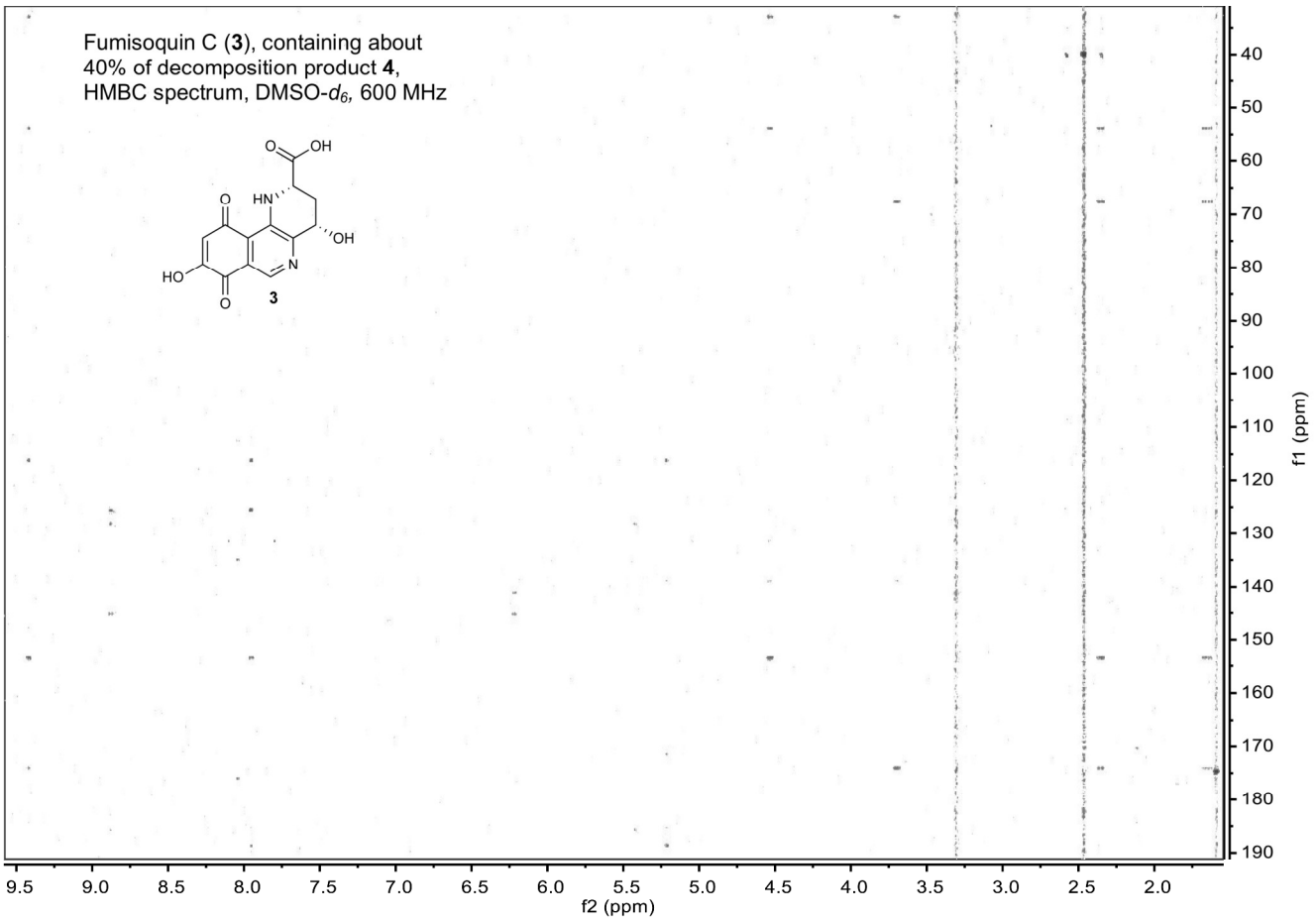

Nature Chemical Biology: doi:10.1038/nchembio.2061

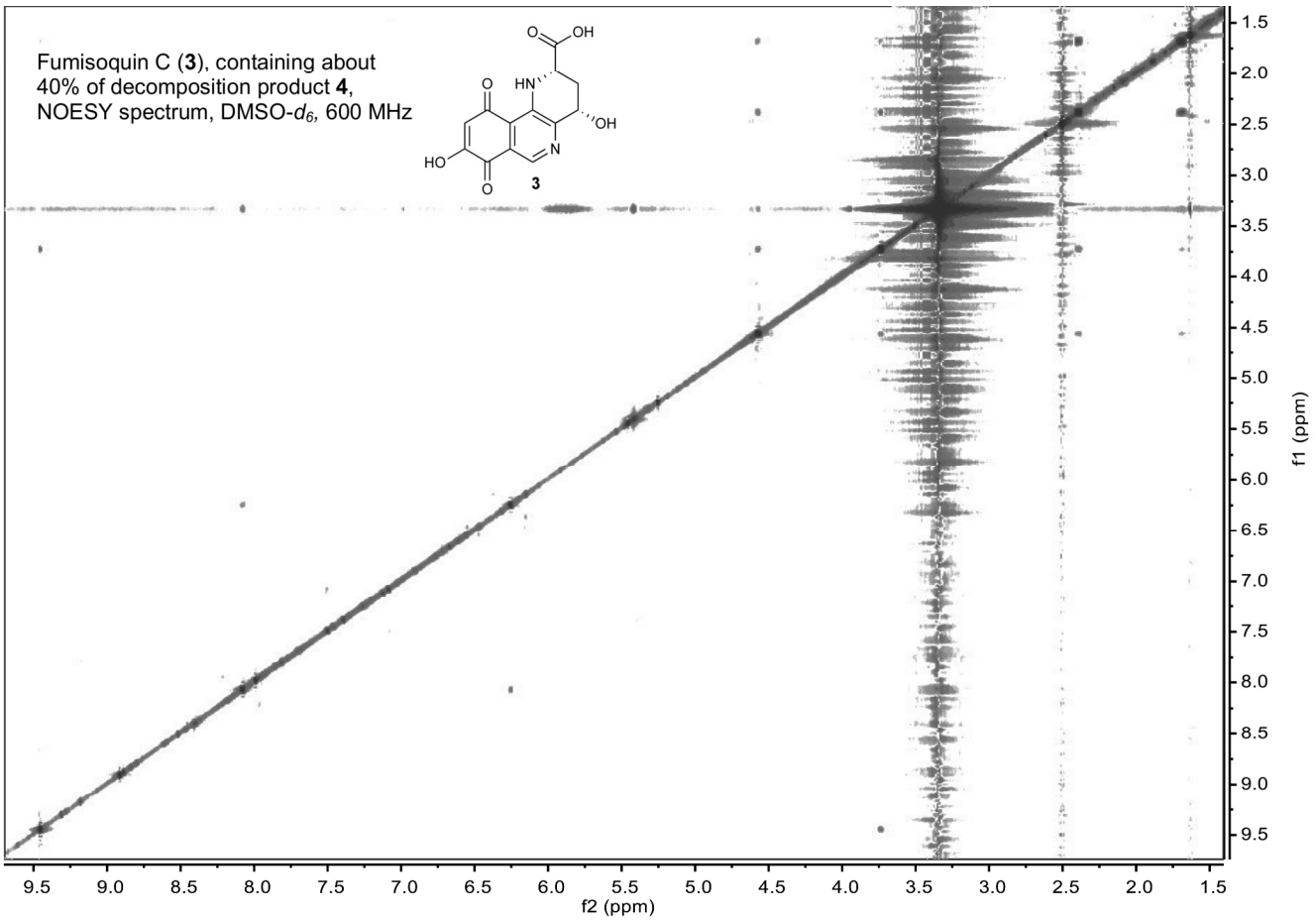

Nature Chemical Biology: doi:10.1038/nchembio.2061

^{1}H (800 MHz) and ^{13}C (200 MHz) NMR spectroscopic data for dimethyl-fumisoquin C (dimethyl-3) in DMSO-d_6.

Chemical shifts were referenced to δ($C\underline{H}D_2SOCD_3$) = 2.50 and δ($^{13}\underline{C}HD_2SOCD_3$) = 39.52. ^{13}C chemical shifts were determined via HMBC and HSQC spectra. ^{1}H, ^{1}H-*J*-coupling constants were determined from the acquired ^{1}H spectrum. ROESY correlations were observed using a mixing time of 600 ms. HMBC correlations are from the proton(s) stated to the indicated ^{13}C atom.

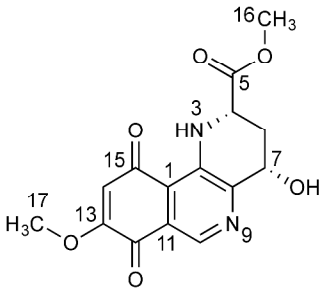

No.	δ_c	Proton	δH (J_{HH}[Hz])	HMBC[a]	ROESY
1	112.56				
2	138.34				
3		3-NH	9.22 ($J_{3,4}$ = 3.8)	1,2,4,6,8	4
4	49.12	4-H	4.49 ($J_{4,3}$ = 3.8, $J_{4,6a}$ = 6.3) ($J_{4,6b}$ = 12.2)	2,5,6,7,8	3, 6a, 6b, 7
5	172.07				
6	30.13	6-Ha	2.24 ($J_{6a,4}$ =6.3, $J_{6a,6b}$ = 13.5, $J_{6a,7}$ = 3.6)	4,5,7,8	4, 6b, 7
		6-Hb	2.38 ($J_{6b,4}$ =12.2, $J_{6a,6b}$ = 13.5) ($J_{6b,7}$ = 9.0)	4,5,7,8	4, 6a, 7
7	65.09	7-H	4.69 ($J_{7,6a}$ = 3.6, $J_{7,6b}$ = 9.0)		4, 6a, 6b, 7OH
7		7-OH	5.61 ($J_{7OH,7}$ = 4.2)	2,4,8	7
8	153.51				
9					
10	132.52	10-H	8.31	1,2w,8,11,12,13,15	
11	123.43				
12	179.63				
13	159.07				
14	111.20	14-H	6.32	1,2,12,13,15	17
15	187.38				
16	51.58	16-H3	3.63	5	4
17	56.24	17-H3	3.86	13,14	14

[a]w: weak correlation (less than ~10% of the intensity of strongest signal)

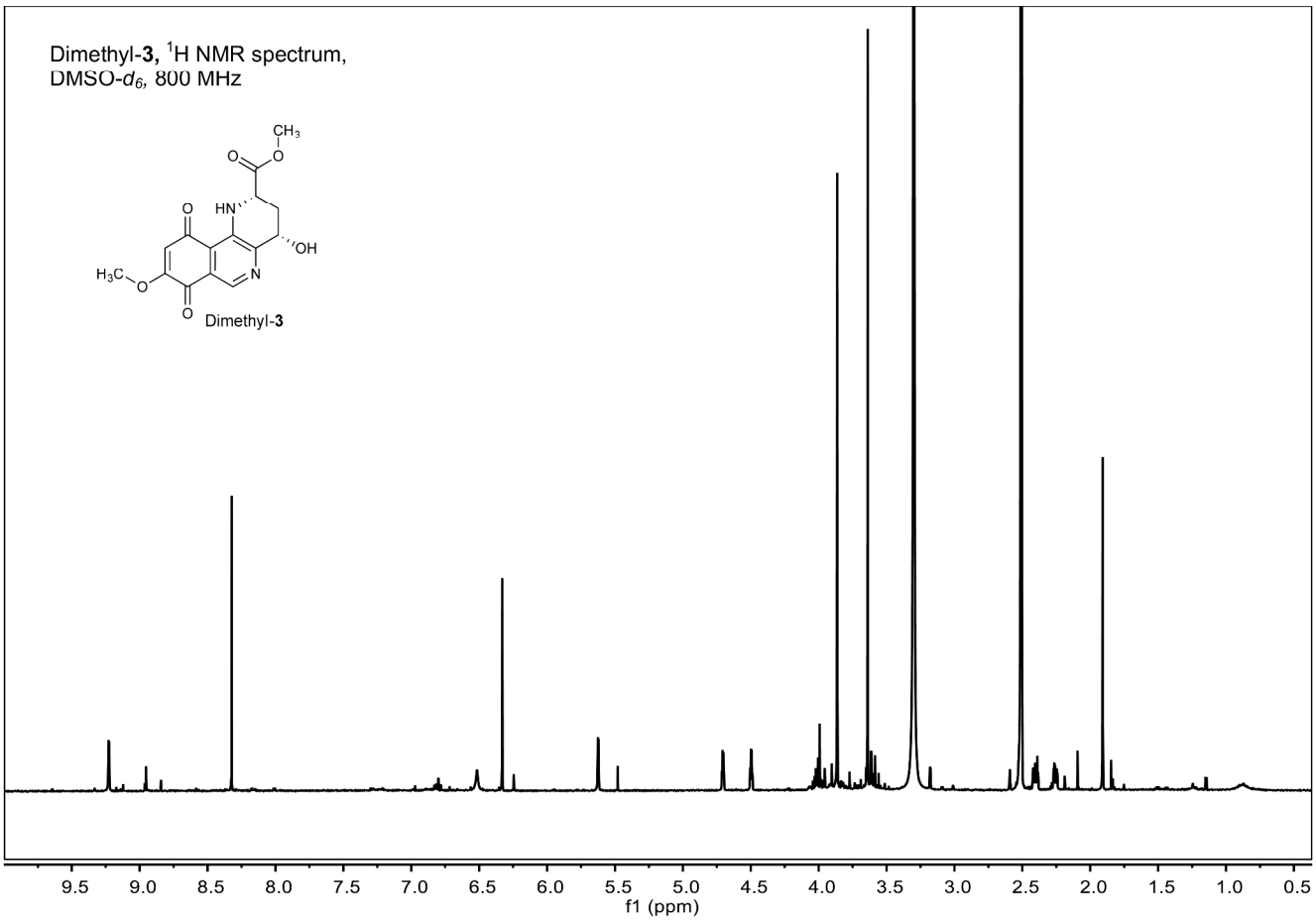

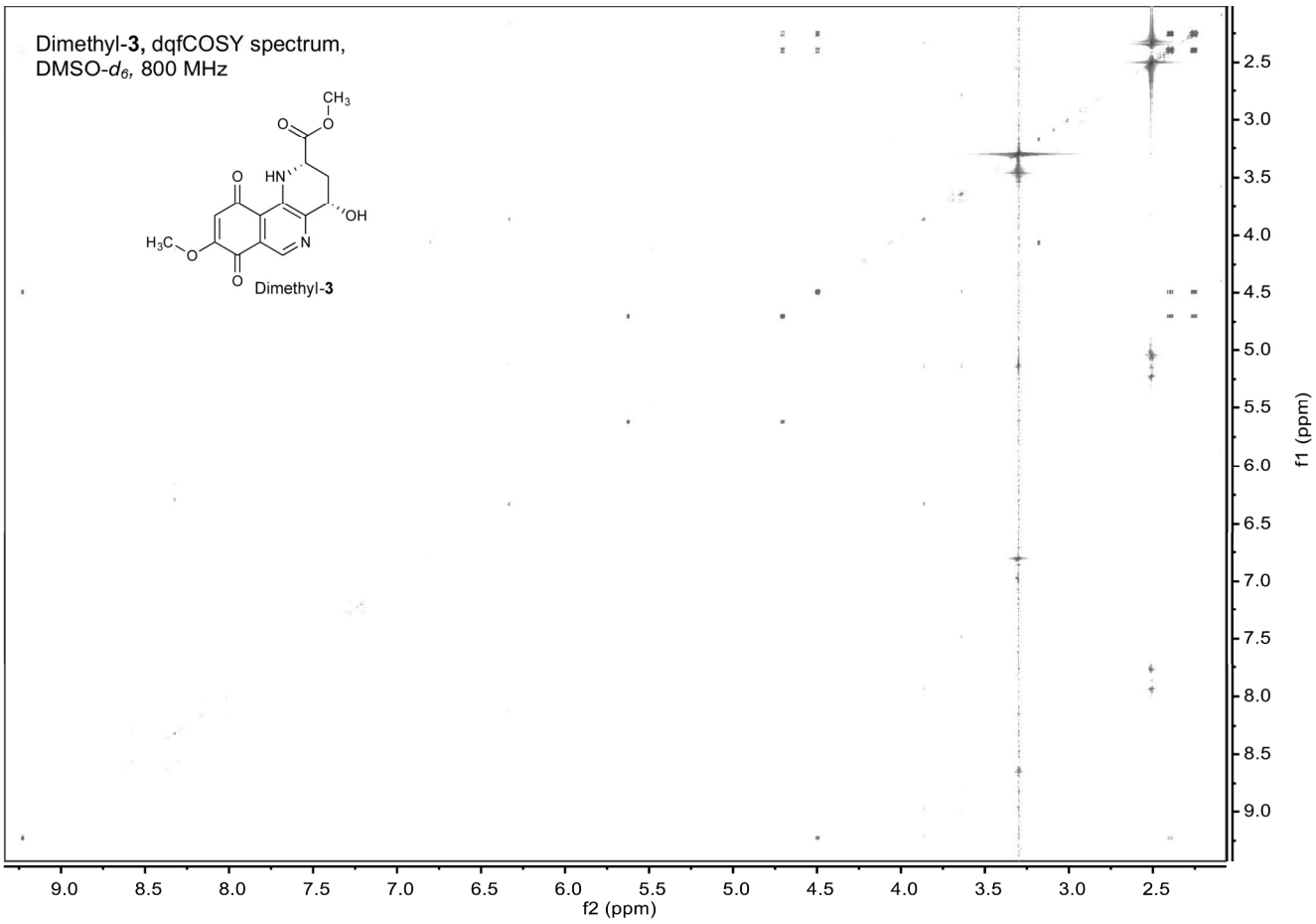

Nature Chemical Biology: doi:10.1038/nchembio.2061

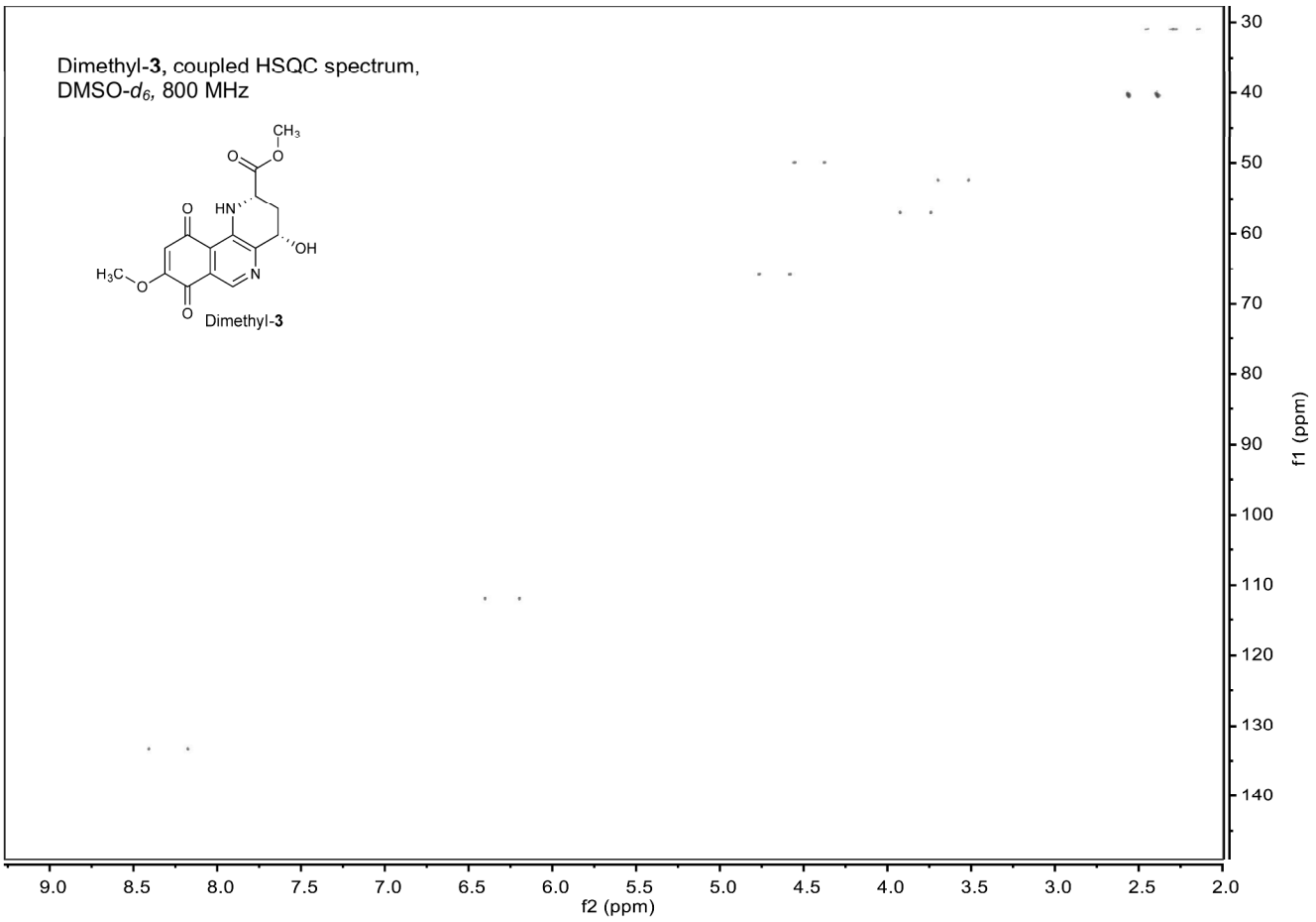

Nature Chemical Biology: doi:10.1038/nchembio.2061

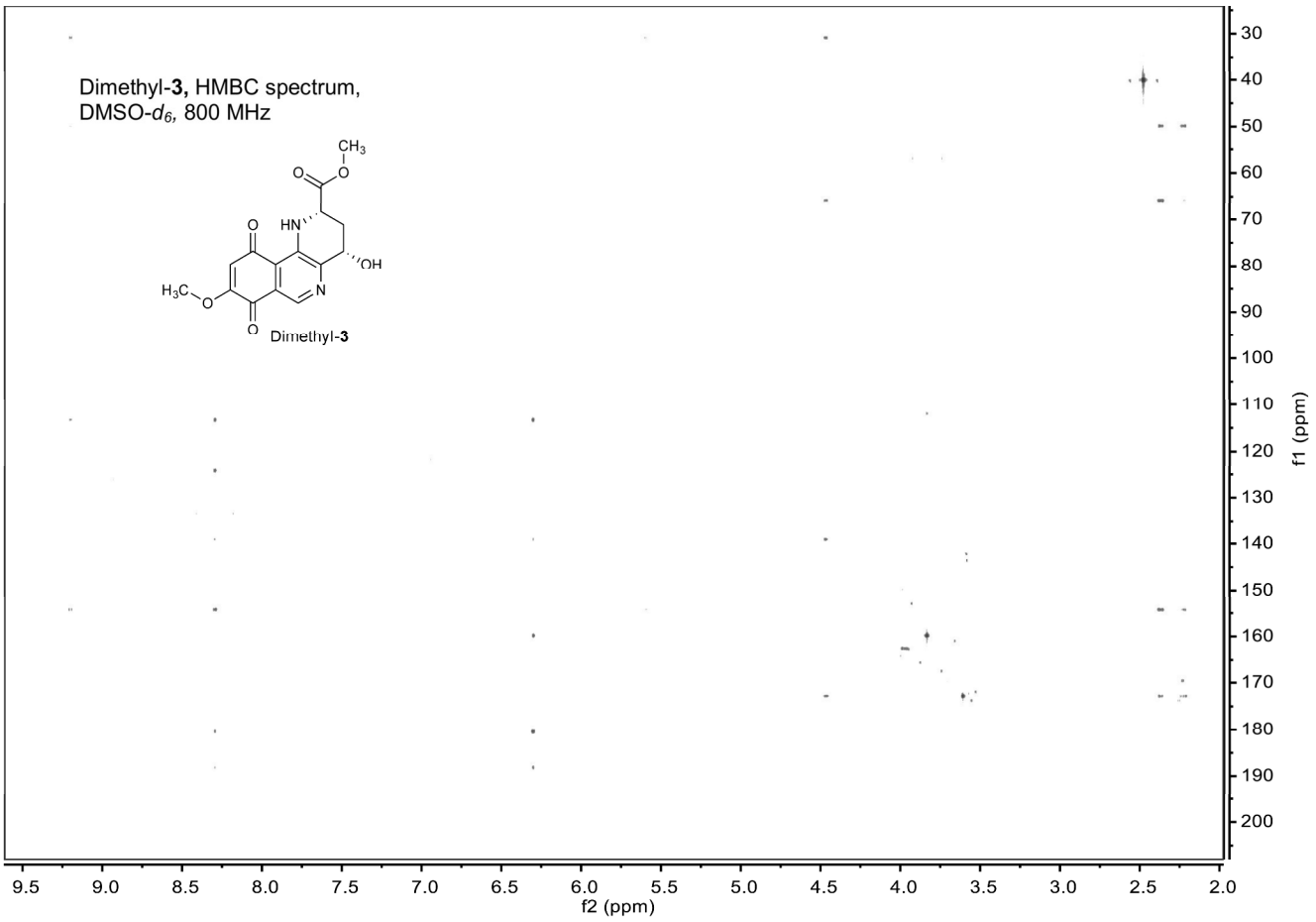

Nature Chemical Biology: doi:10.1038/nchembio.2061

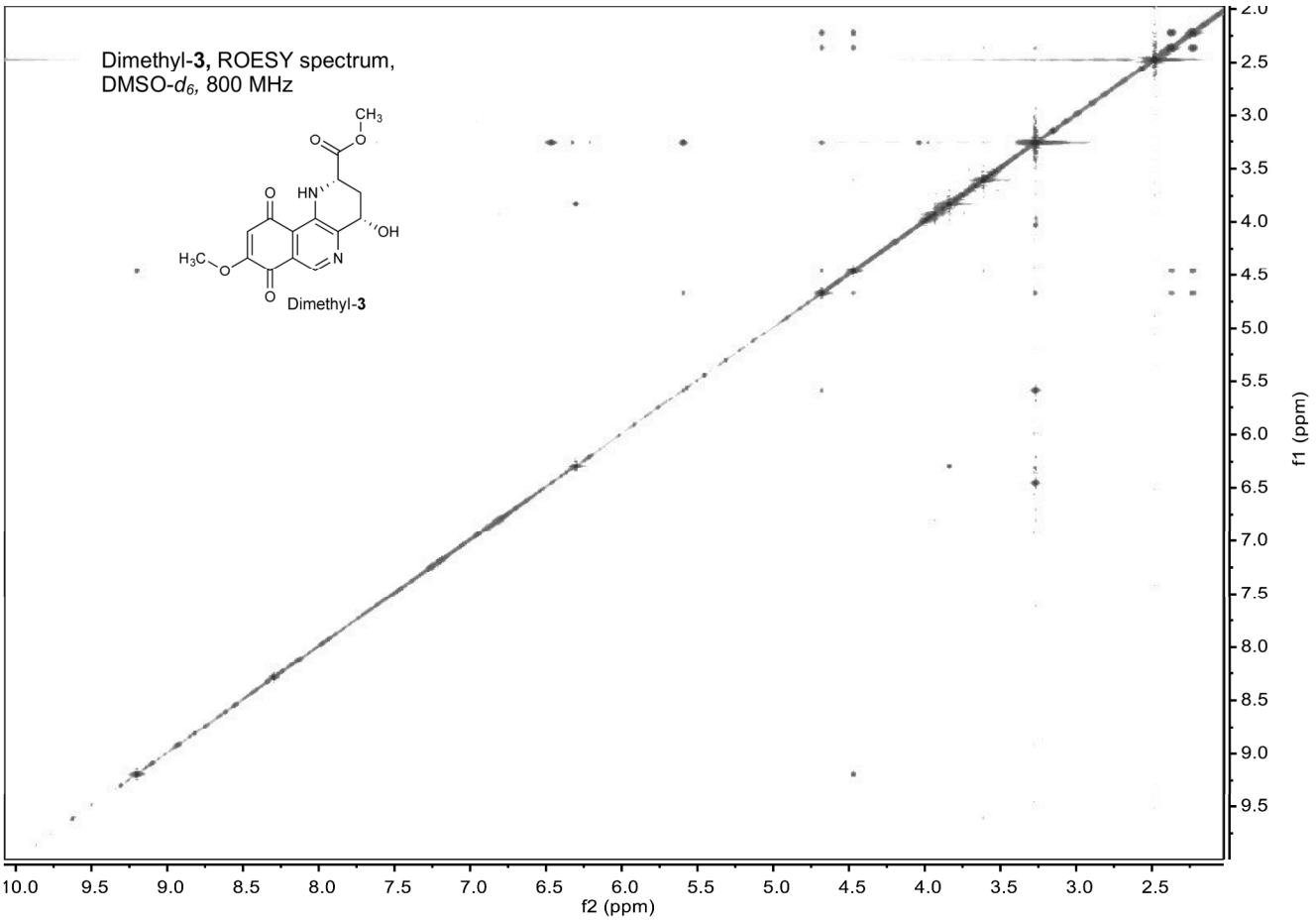

Nature Chemical Biology: doi:10.1038/nchembio.2061

^{1}H (800 MHz) and ^{13}C (200 MHz) NMR spectroscopic data for compound 4 in DMSO-d_6.

Chemical shifts were referenced to δ(C<u>H</u>D$_2$SOCD$_3$) = 2.50 and δ(^{13}<u>C</u>HD$_2$SOCD$_3$) = 39.52. ^{13}C chemical shifts were determined via HMBC and HSQC spectra. ^{1}H, ^{1}H-*J*-coupling constants were determined from the acquired ^{1}H spectrum. HMBC correlations are from the proton(s) stated to the indicated ^{13}C atom.

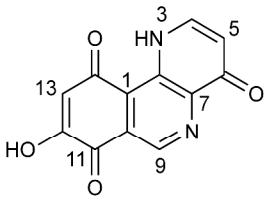

No.	δ_c	Proton	δH (J_{HH}[Hz])	HMBC[a]
1	127.41			
2	134.33			
3		3-NH	13.71 ($J_{3,4}$ = 6.6, $J_{3,5}$ = 1.7)	
4	140.30	4-H	8.06 ($J_{4,3}$ = 6.6, $J_{4,5}$ = 7.3)	2, 5, 6
5	111.88	5-H	6.24 ($J_{5,4}$ = 7.3, $J_{5,3}$ = 1.7)	4, 7
6	175.28			
7	144.61			
8				
9	141.85	9-H	8.91	1, 2w, 7, 10, 11w, 12w
10	125.00			
11	185.04			
12	180.67			
13[b]	108.10	13-H	5.45	1, 2w, 11, 12w, 14w
14[b]	172.04			

[a]w: weak correlation (less than ~10% of the intensity of strongest signals); [b]Position 12 and 14 carbon chemical shifts are interchangeable

Nature Chemical Biology: doi:10.1038/nchembio.2061

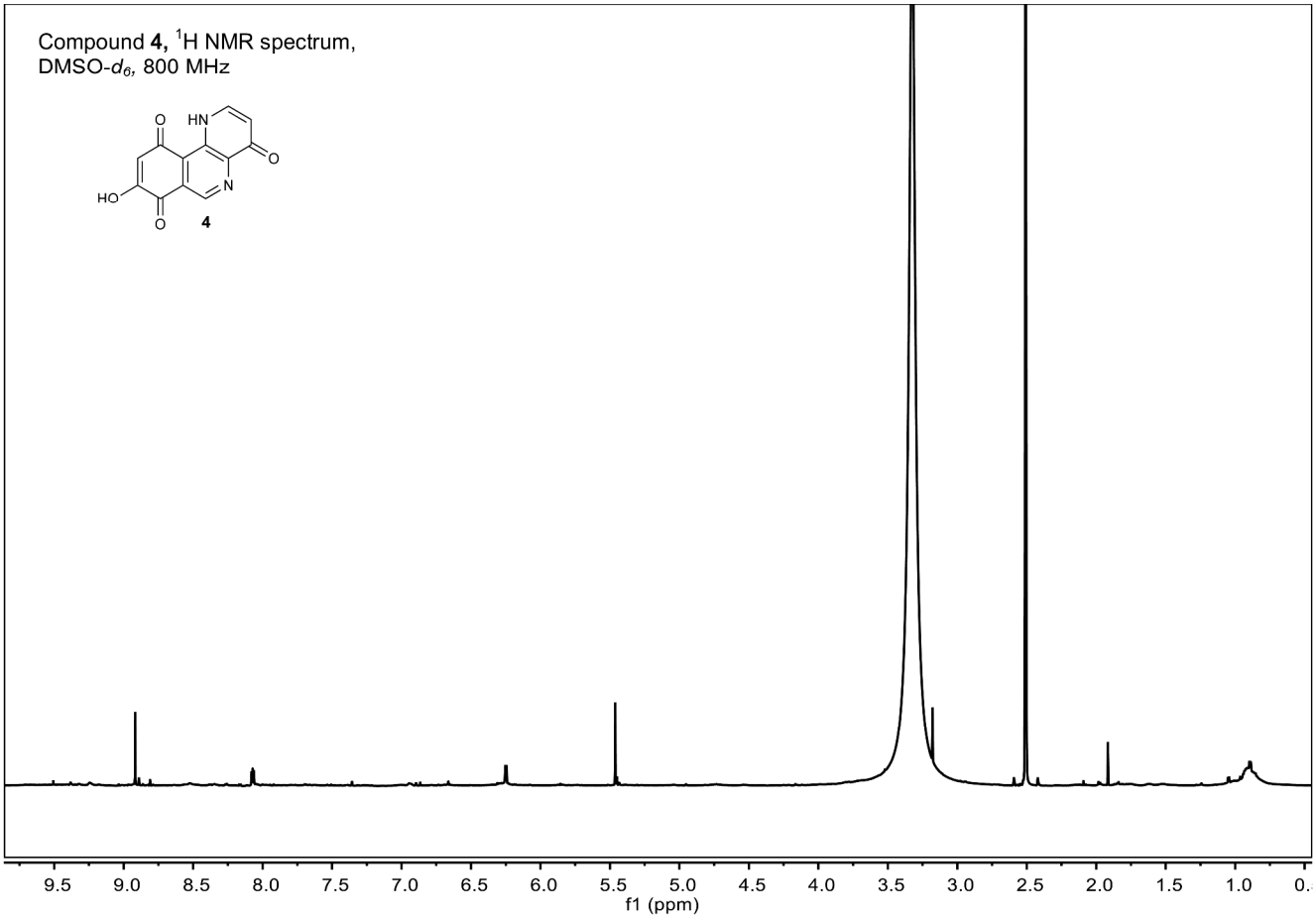

Nature Chemical Biology: doi:10.1038/nchembio.2061

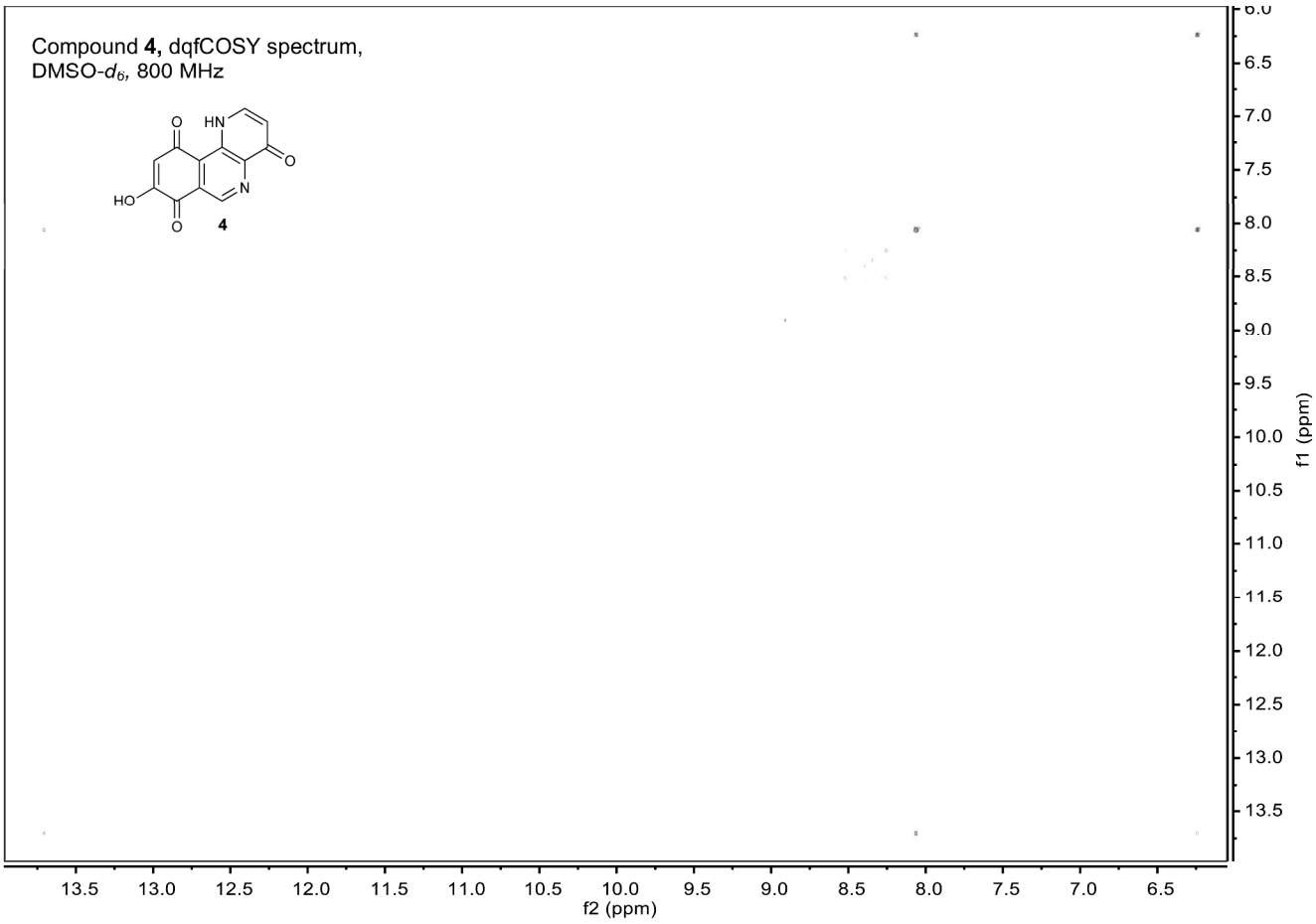

Nature Chemical Biology: doi:10.1038/nchembio.2061

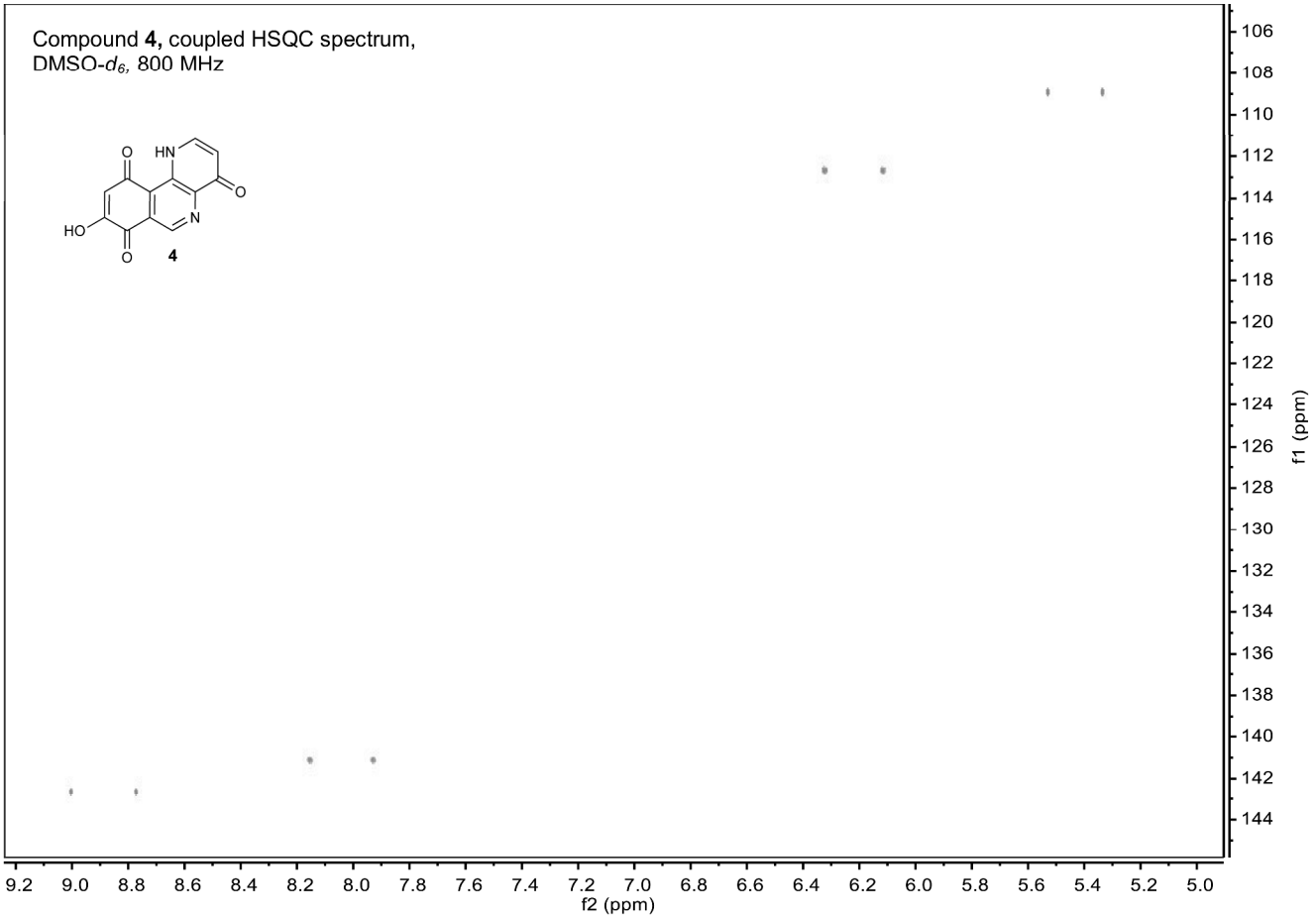

Nature Chemical Biology: doi:10.1038/nchembio.2061

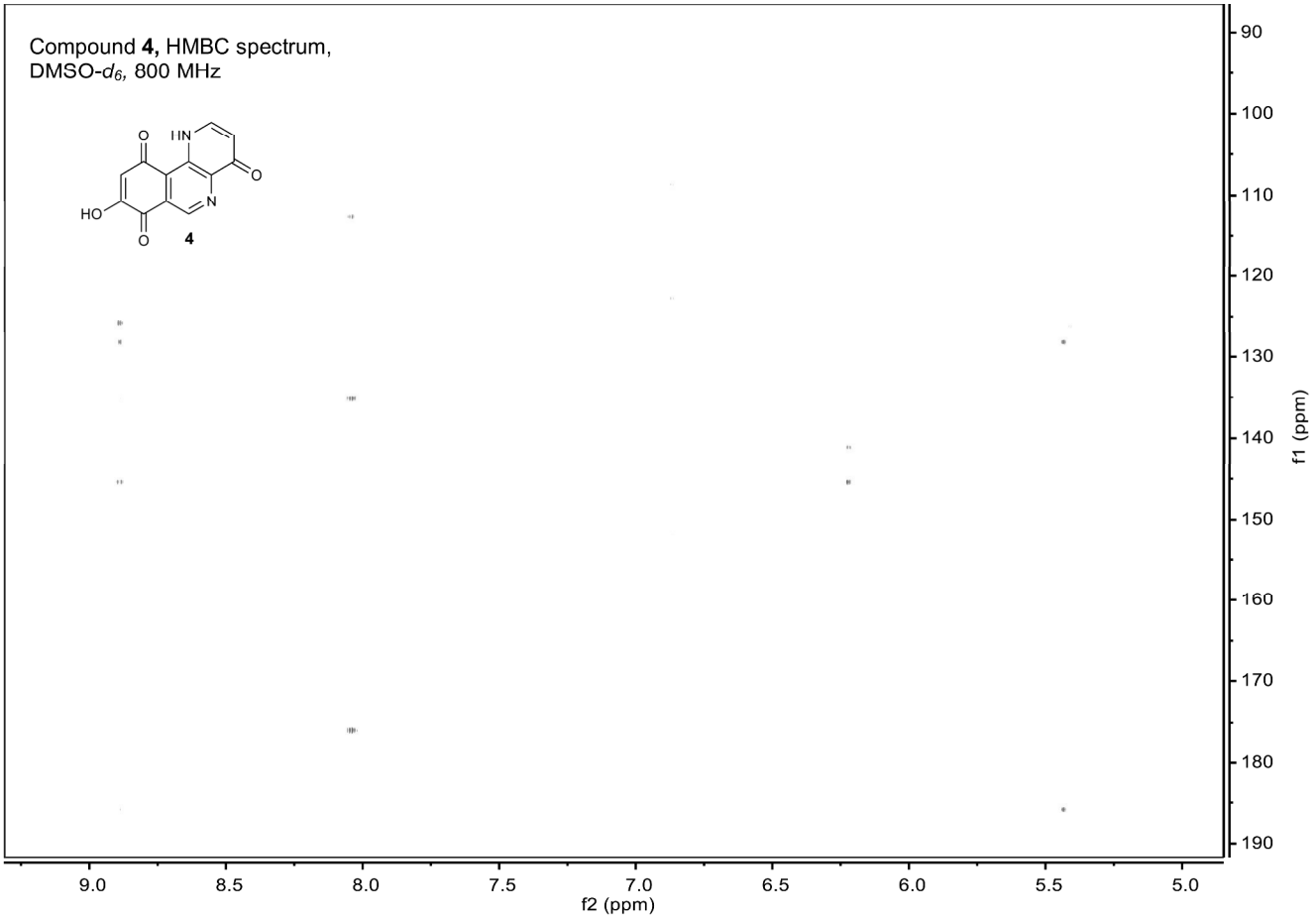

Nature Chemical Biology: doi:10.1038/nchembio.2061

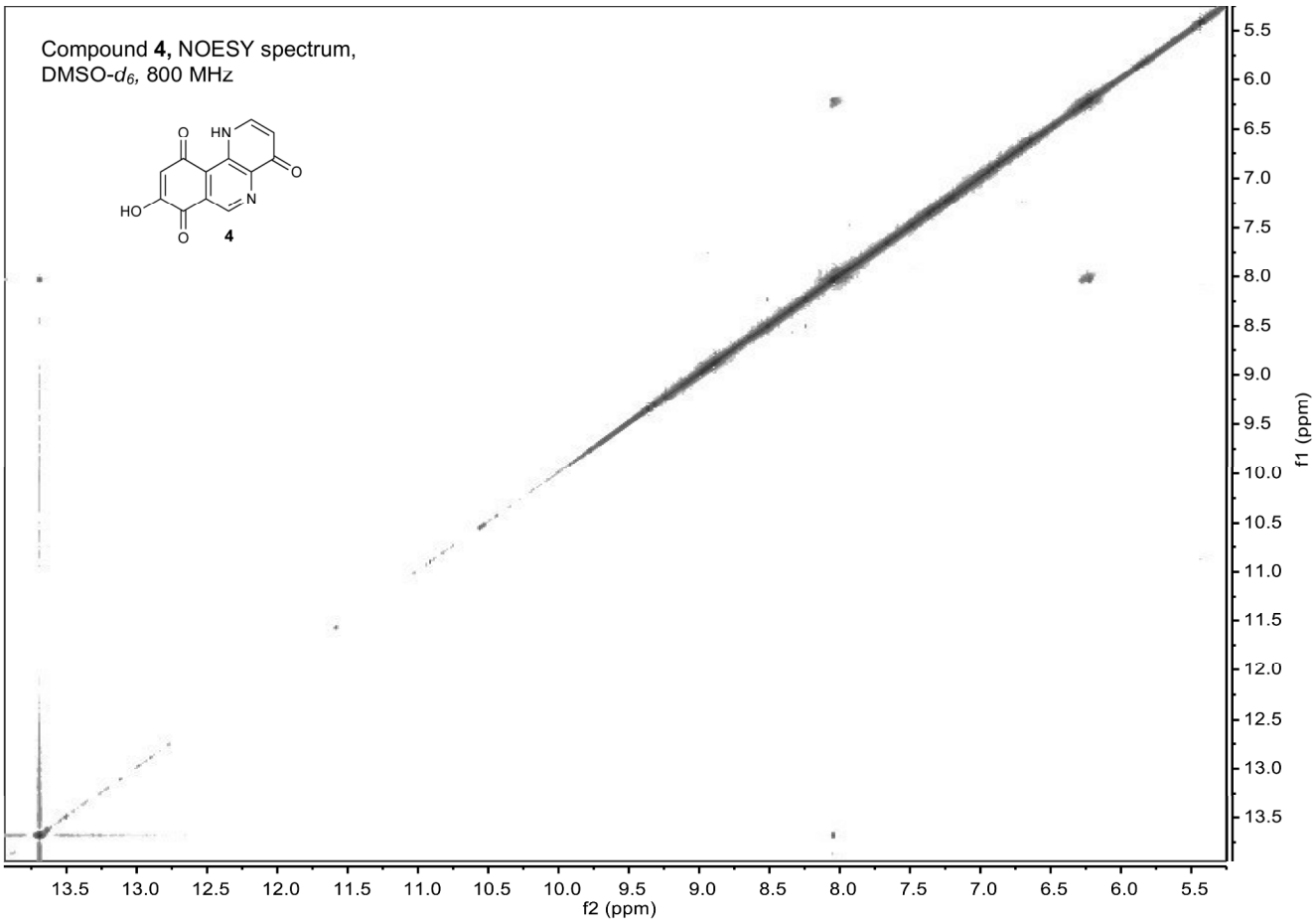

Nature Chemical Biology: doi:10.1038/nchembio.2061

^{1}H (800 MHz) and or ^{13}C (200 MHz) NMR spectroscopic data for compound 5 in DMSO-d_6.

Chemical shifts were referenced to δ(C<u>H</u>D$_2$SOCD$_3$) = 2.50 and δ(^{13}<u>C</u>HD$_2$SOCD$_3$) = 39.52. ^{13}C chemical shifts were determined via HMBC and HSQC spectra. ^{1}H, ^{1}H-*J*-coupling constants were determined from the acquired ^{1}H spectrum. NOESY correlations were observed using a mixing time of 600 ms. HMBC correlations are from the proton(s) stated to the indicated ^{13}C atom.

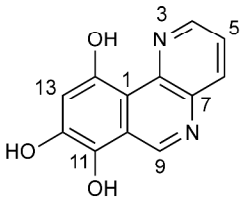

No.	δ_c	Proton	δH (J_{HH}[Hz])	HMBC[a]	NOESY
1	108.19				
2	142.74				
3					
4	146.12	4-H	8.87 ($J_{4,5}$ = 4.7)	2, 5, 6	5, 14-OH
5	121.77	5-H	7.75 ($J_{5,4}$ = 4.7, $J_{5,6}$ = 8.3)	4, 7	4, 6
6	136.97	6-H	8.48 ($J_{6,5}$ = 8.3)	2, 4	5
7	136.52				
8					
9	149.94	9-H	9.52	1, 2w, 7, 10, 11, 14w	
10	118.41				
11	133.63				
12	146.74				
13	106.91	13-H	6.97	1, 2w, 11, 12, 14	
14	150.40				
14		14-OH	13.42	1, 12, 13, 14	4

[a]w: weak correlation (less than ~10% of the intensity of strongest signal)

Nature Chemical Biology: doi:10.1038/nchembio.2061

Compound **5**, ^{1}H NMR spectrum,
DMSO-d_6, 800 MHz

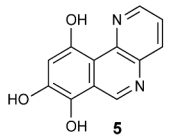

5

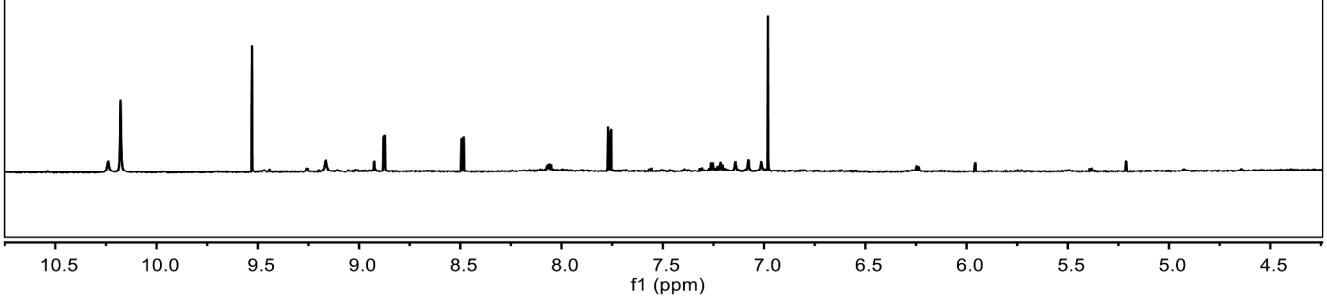

Compound **5,** dqfCOSY spectrum,
DMSO-d_6, 800 MHz

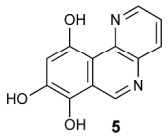

5

Nature Chemical Biology: doi:10.1038/nchembio.2061

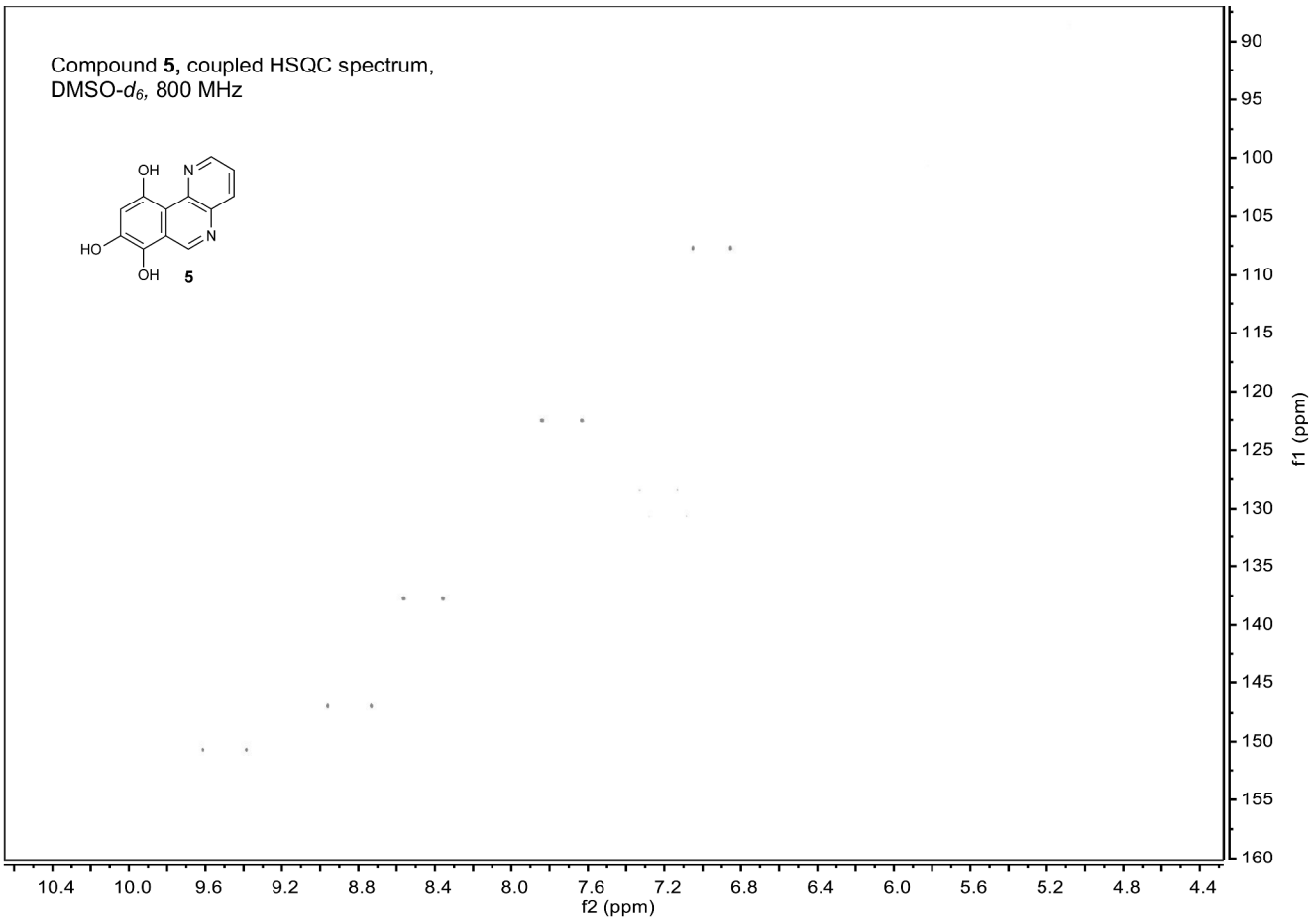

Nature Chemical Biology: doi:10.1038/nchembio.2061

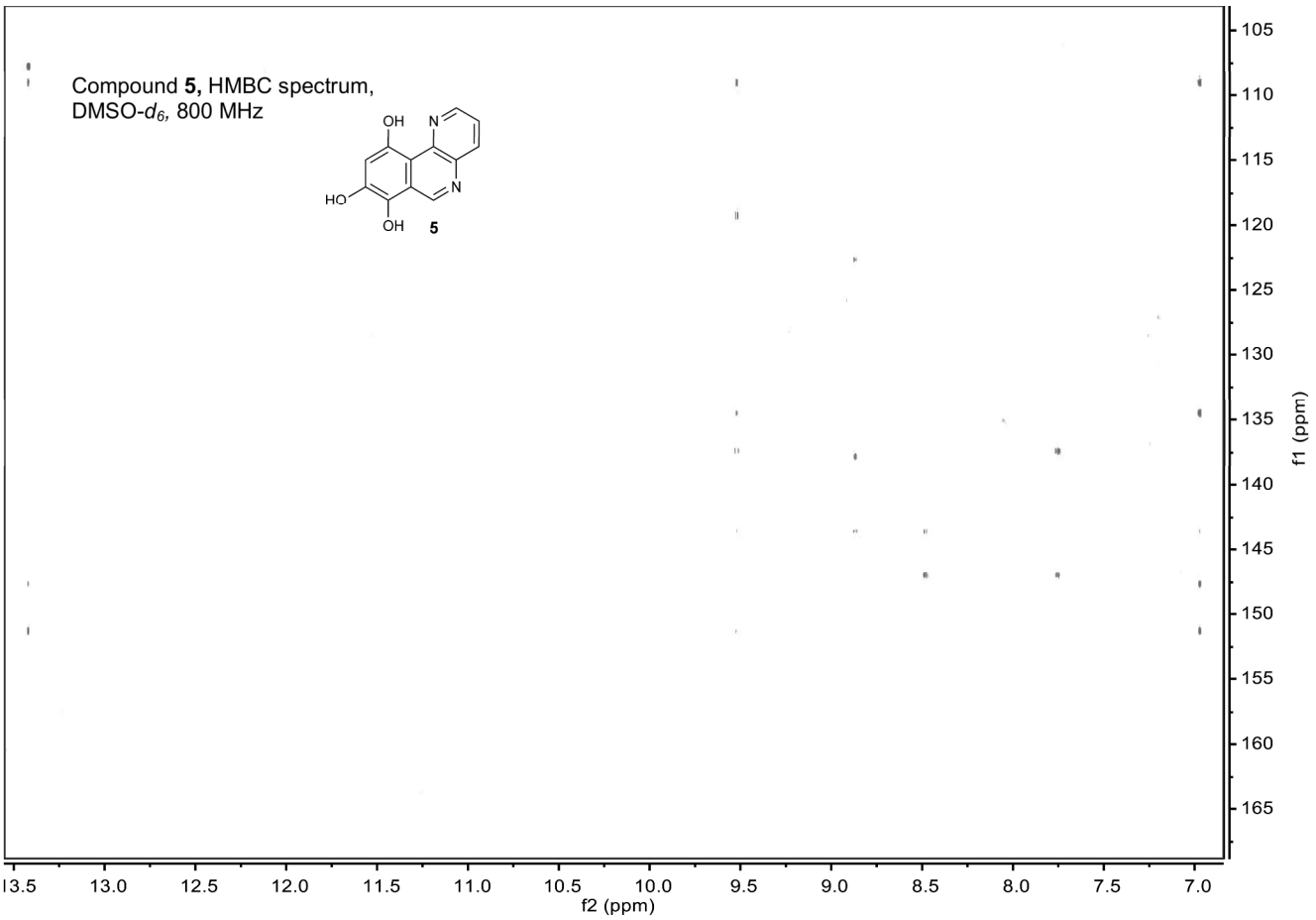

Nature Chemical Biology: doi:10.1038/nchembio.2061

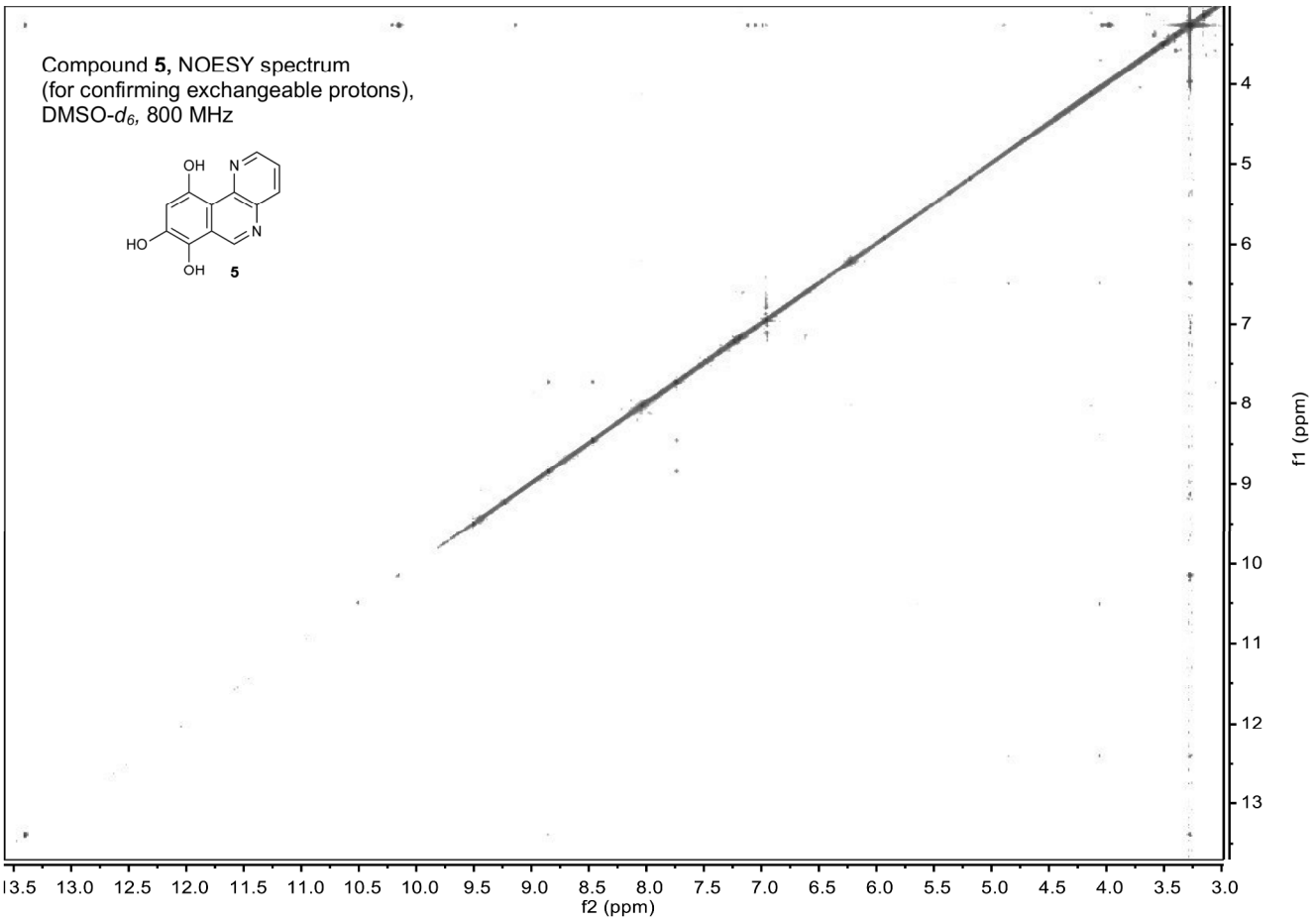

Nature Chemical Biology: doi:10.1038/nchembio.2061

^{1}H (600 MHz) and ^{13}C (151 MHz) NMR spectroscopic data for compound 8 in methanol-d_4.

Chemical shifts were referenced to δ(C<u>H</u>D$_2$OD) = 3.31 and δ(^{13}<u>C</u>HD$_2$OD) = 49.0. ^{13}C chemical shifts were determined via an HMBC spectrum. ^{1}H, ^{1}H-*J*-coupling constants were determined from the acquired ^{1}H spectrum. HMBC correlations are from the proton(s) stated to the indicated ^{13}C atom.

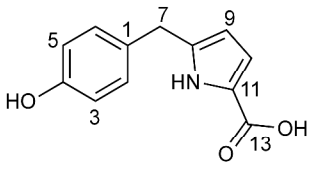

No.	δ_c	Proton	δH (J_{HH}[Hz])	HMBC
1				
2	129.62	2-H	7.03 ($J_{2,3}$ = 8.5)	1, 3, 4, 7
3	130.63	3-H	6.70 ($J_{3,2}$ = 8.5)	1, 4, 5
4	155.91			
5	130.63	5-H	6.70 ($J_{5,6}$ = 8.5)	1, 4, 5
6	129.62	6-H	7.03 ($J_{6,5}$ = 8.5)	1, 3, 4, 7
7	33.04	7-H$_2$	3.83	2, 3, 5, 6, 8, 9
8	138.30			
9	108.30	9-H	5.80 ($J_{9,10}$ = 3.5)	7, 8, 10, 11, 13
10	116.12	10-H	6.62 ($J_{10,9}$ = 3.5)	8, 9, 11, 13
11	122.63			
12		12-NH		
13	164.53			

Nature Chemical Biology: doi:10.1038/nchembio.2061

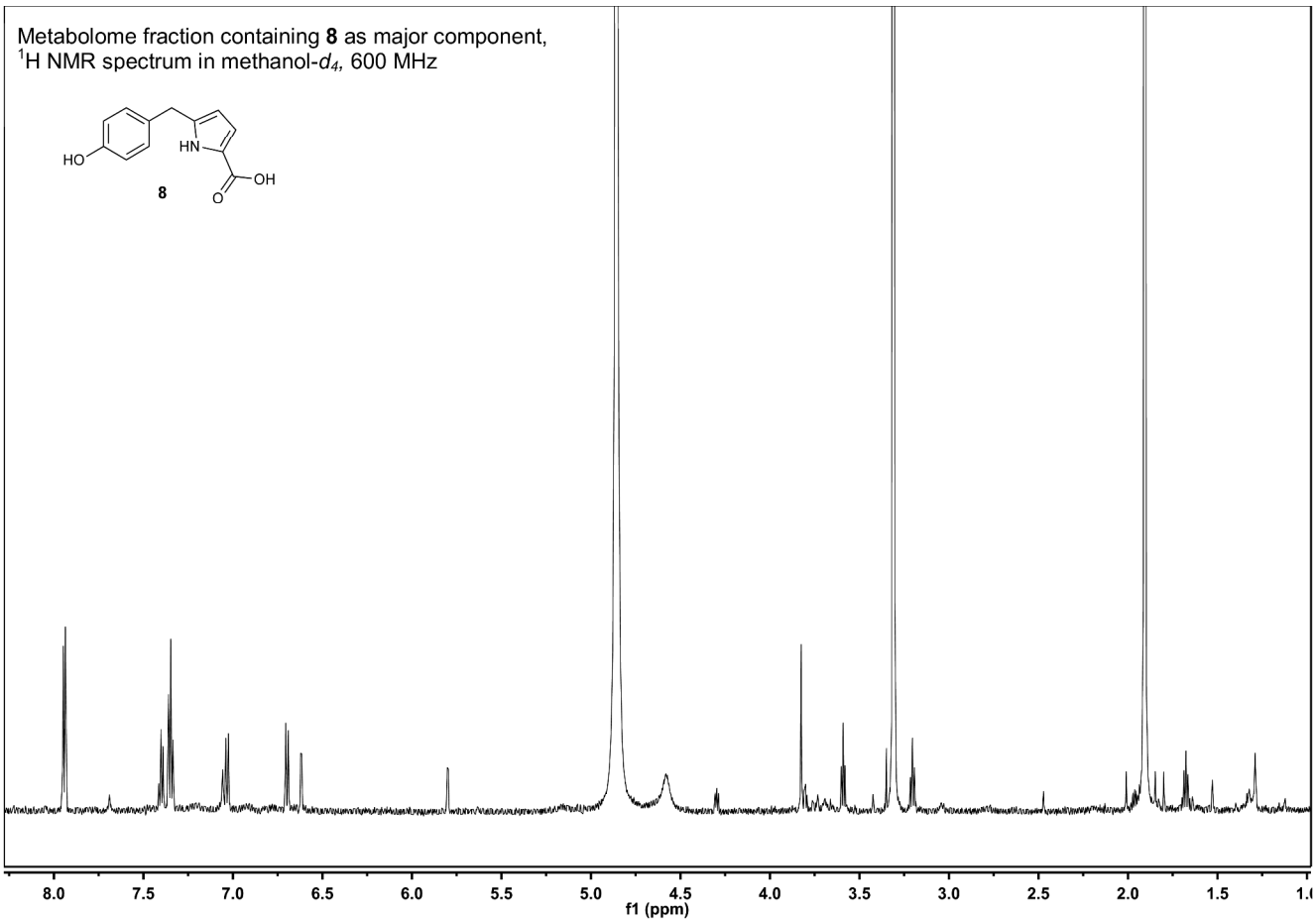

Nature Chemical Biology: doi:10.1038/nchembio.2061

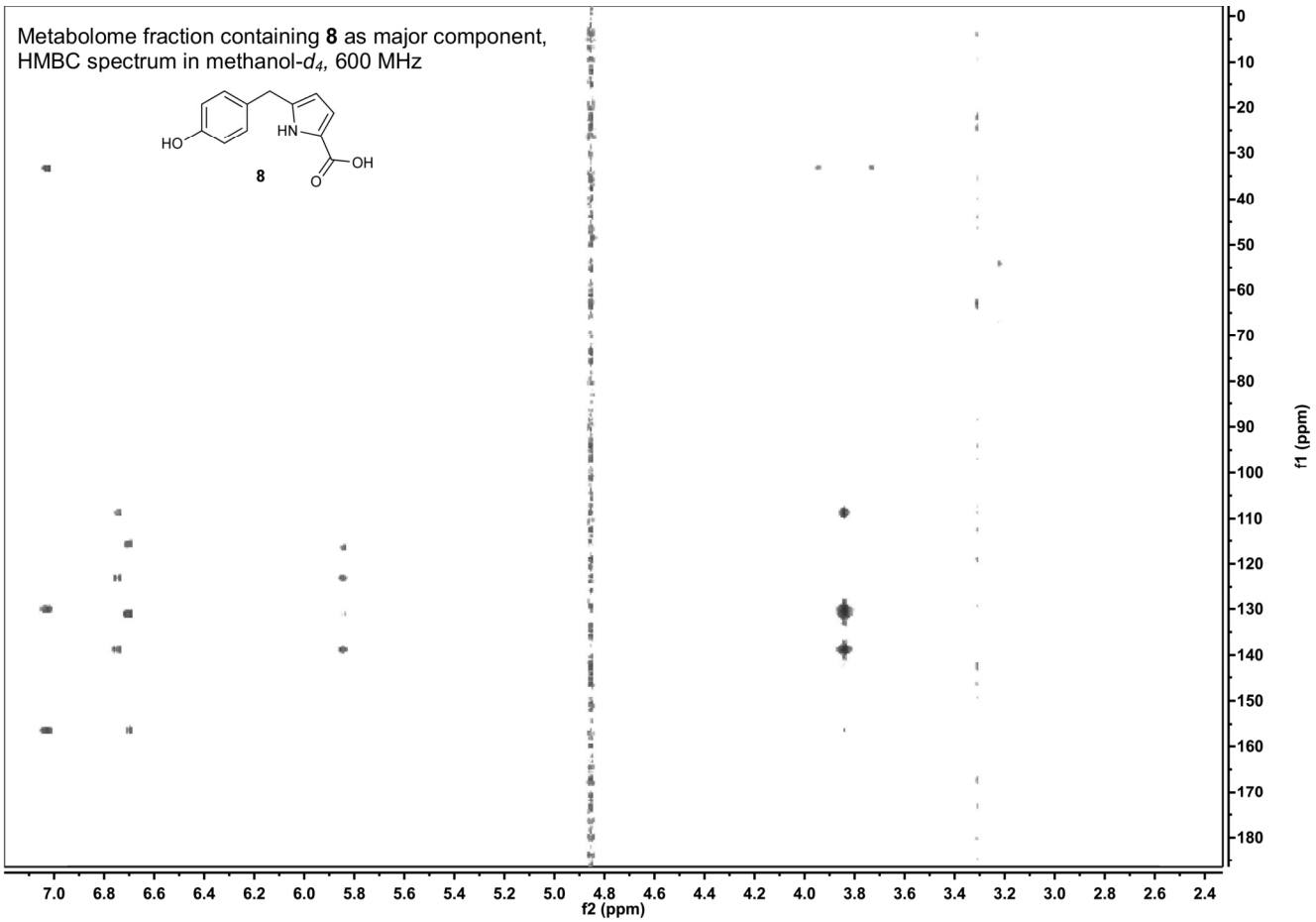

Nature Chemical Biology: doi:10.1038/nchembio.2061

^{1}H (500 MHz) and ^{13}C (125 MHz) NMR spectroscopic data for compound 11 in water-d_2.

Chemical shifts were referenced to δ(HOD) = 2.79 and δ(^{13}CH$_3$OD) = 49.0. ^{13}C chemical shifts were determined via an HMBC and HSQC spectrum. ^{1}H, ^{1}H-*J*-coupling constants were determined from the acquired ^{1}H spectrum. HMBC correlations are from the proton(s) stated to the indicated ^{13}C atom.

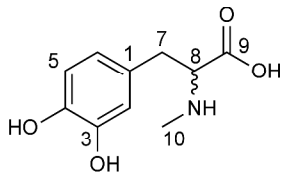

No.	δ_c	Proton	δH (J_{HH}[Hz])	HMBC
1	127.21			
2	117.10	2-H	6.84 ($J_{2,6}$ = 1.8)	4, 6, 7
3	144.36			
4	143.63			
5	116.49	5-H	6.92 ($J_{5,6}$ = 8.0)	1, 3
6	121.86	6-H	6.76 ($J_{6,5}$ = 8.0, $J_{6,2}$ = 1.8)	2, 4, 5, 7
7	35.06	7-H$_2$	3.14 ($J_{7,8}$ = 6.0)	1, 2, 6, 8, 9
8	64.71	8-H	3.82 ($J_{8,7}$ = 6.0)	1, 7, 9, 10
9	173.12			
10	32.16	10-H$_3$	2.71	8

Nature Chemical Biology: doi:10.1038/nchembio.2061

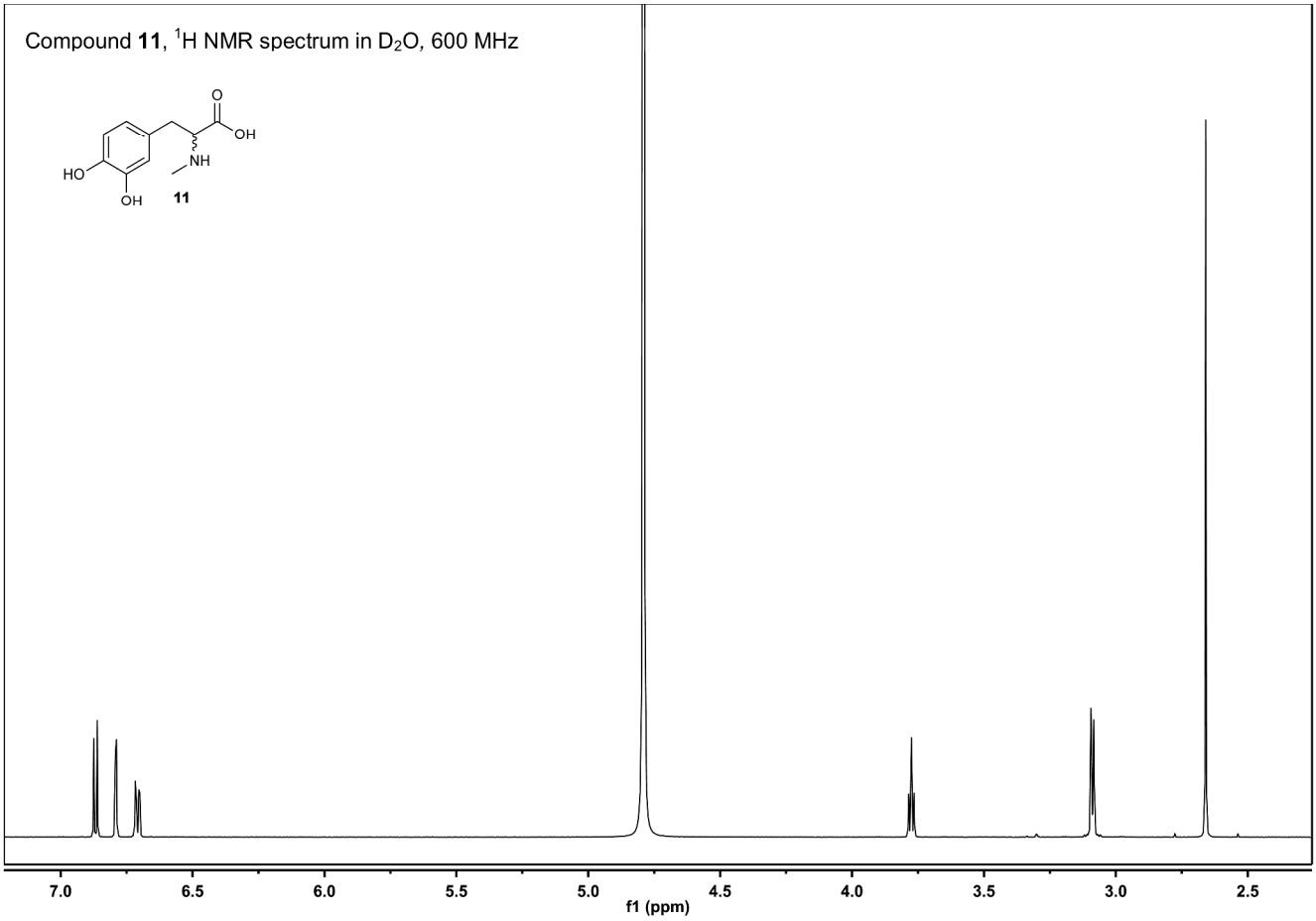

Nature Chemical Biology: doi:10.1038/nchembio.2061

Compound **11**, ^{13}C NMR spectrum in D_2O, 500 MHz

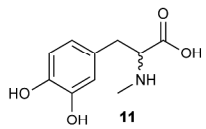

11

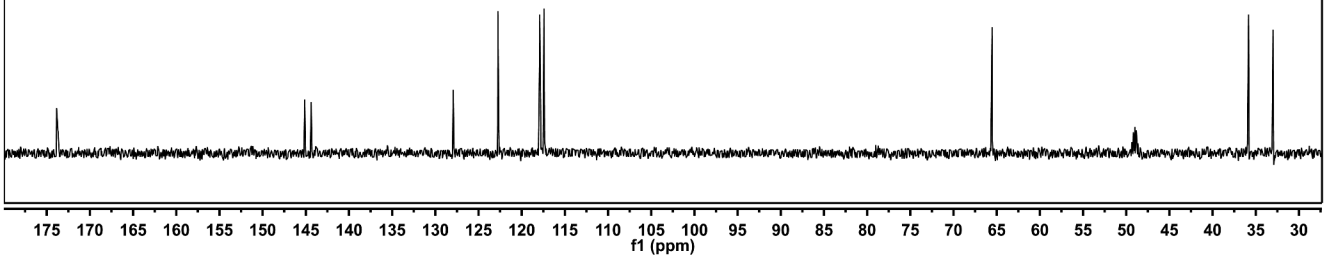

Nature Chemical Biology: doi:10.1038/nchembio.2061

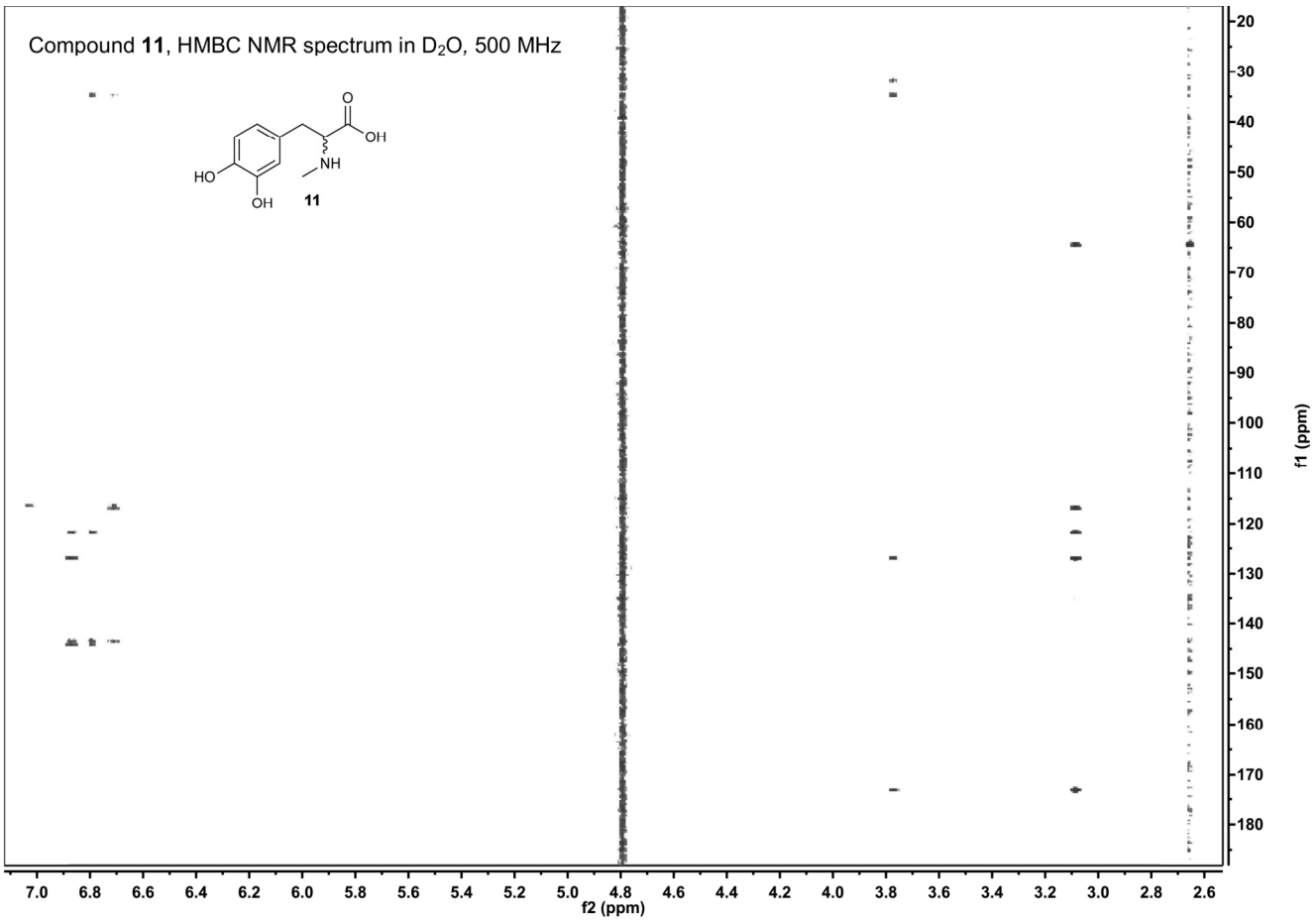

Nature Chemical Biology: doi:10.1038/nchembio.2061

^{1}H (600 MHz) and ^{13}C (151 MHz) NMR spectroscopic data for compound 12 in water-d_2.

Chemical shifts were referenced to δ(HOD) = 2.79 and δ(^{13}CH$_3$OD) = 49.0. ^{13}C chemical shifts were determined via an HMBC and HSQC spectrum. ^{1}H, ^{1}H-*J*-coupling constants were determined from the acquired ^{1}H spectrum. HMBC correlations are from the proton(s) stated to the indicated ^{13}C atom.

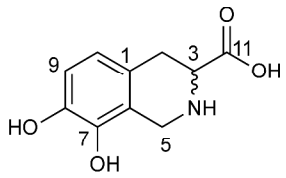

No.	δ_c	Proton	δH (J_{HH}[Hz])	HMBC
1	124.11			
2	28.50	2-Ha	3.08 ($J_{2a,2b}$ = 16.0, $J_{2a,3}$ = 11.5)	1, 3, 6, 10, 11
		2-Hb	3.32 ($J_{2b,2a}$ = 16.0, $J_{2b,3}$ = 5.0)	1, 3, 6, 10, 11
3	56.25	3-H	3.98 ($J_{3,2a}$ = 11.5, $J_{3,2b}$ = 5.0)	1, 2, 5, 11
4		4-NH		
5	40.60	5-Ha	4.25 ($J_{5a,5b}$ = 16.0)	1, 3, 6, 7
		5-Hb	4.54 ($J_{5b,5a}$ = 16.0)	1, 3, 6, 7
6	116.69			
7	140.97			
8	142.61			
9	116.49	9-H	6.93 ($J_{9,10}$ = 8.4)	1, 7
10	121.86	10-H	6.80 ($J_{10,9}$ = 8.4)	2, 6, 8
11	173.12			

Nature Chemical Biology: doi:10.1038/nchembio.2061

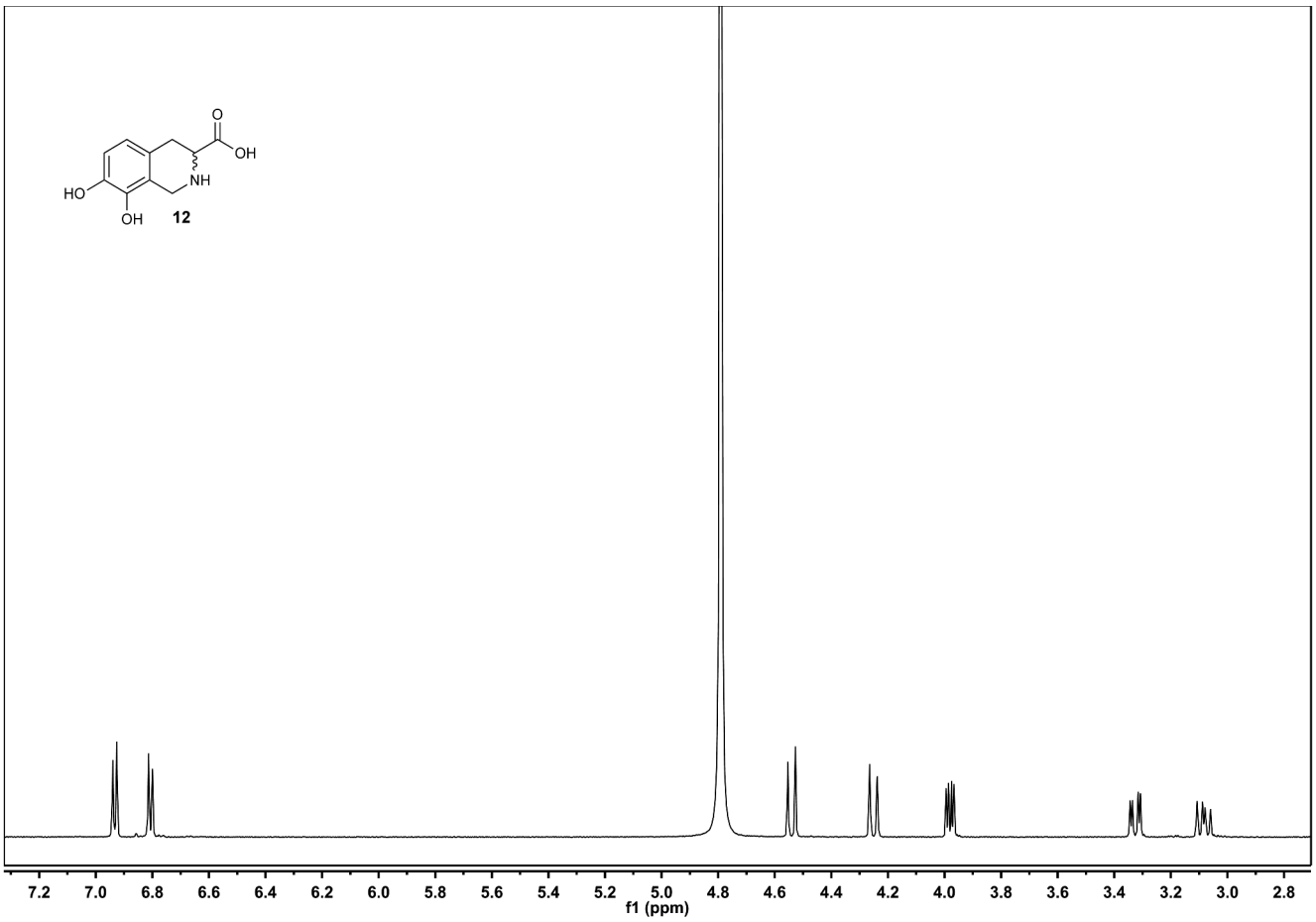

Nature Chemical Biology: doi:10.1038/nchembio.2061

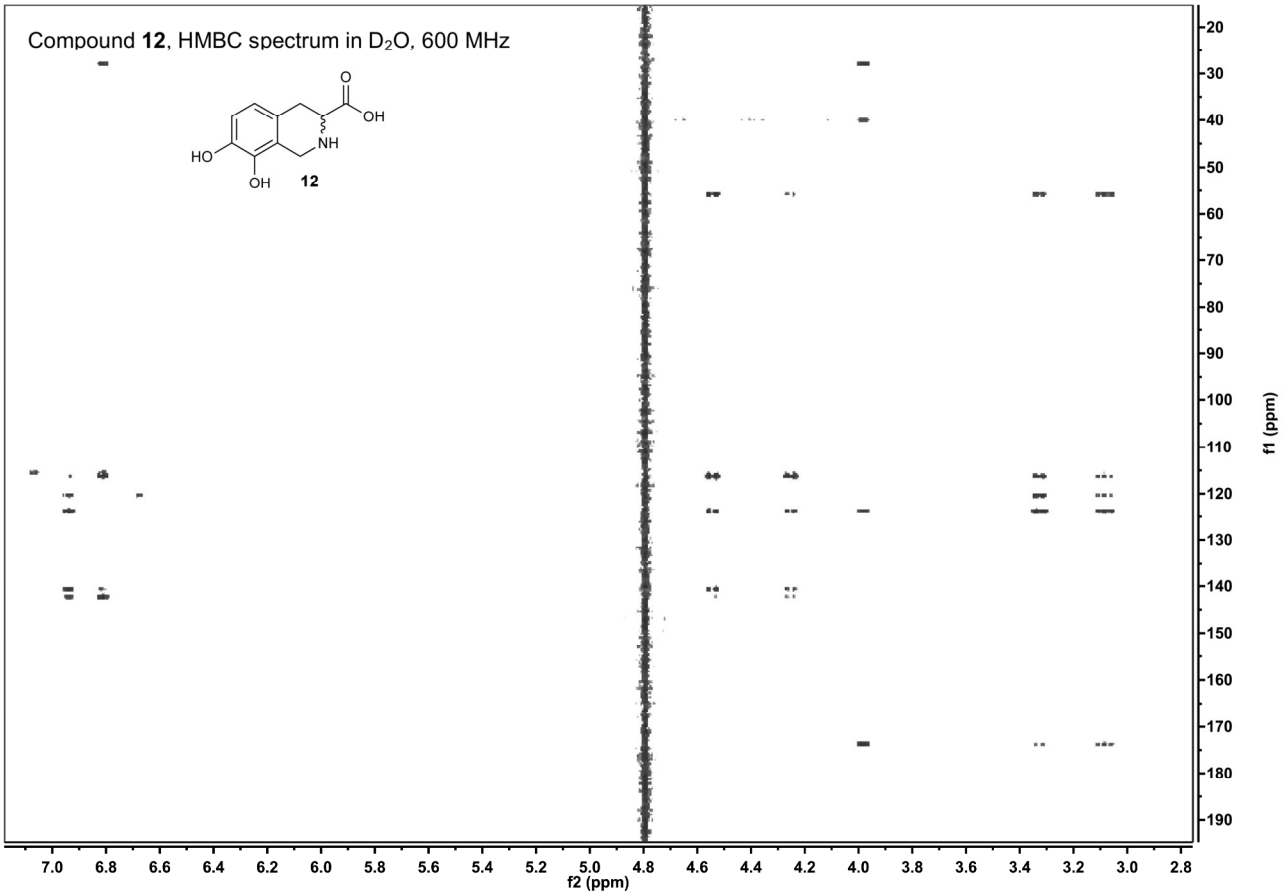

Nature Chemical Biology: doi:10.1038/nchembio.2061

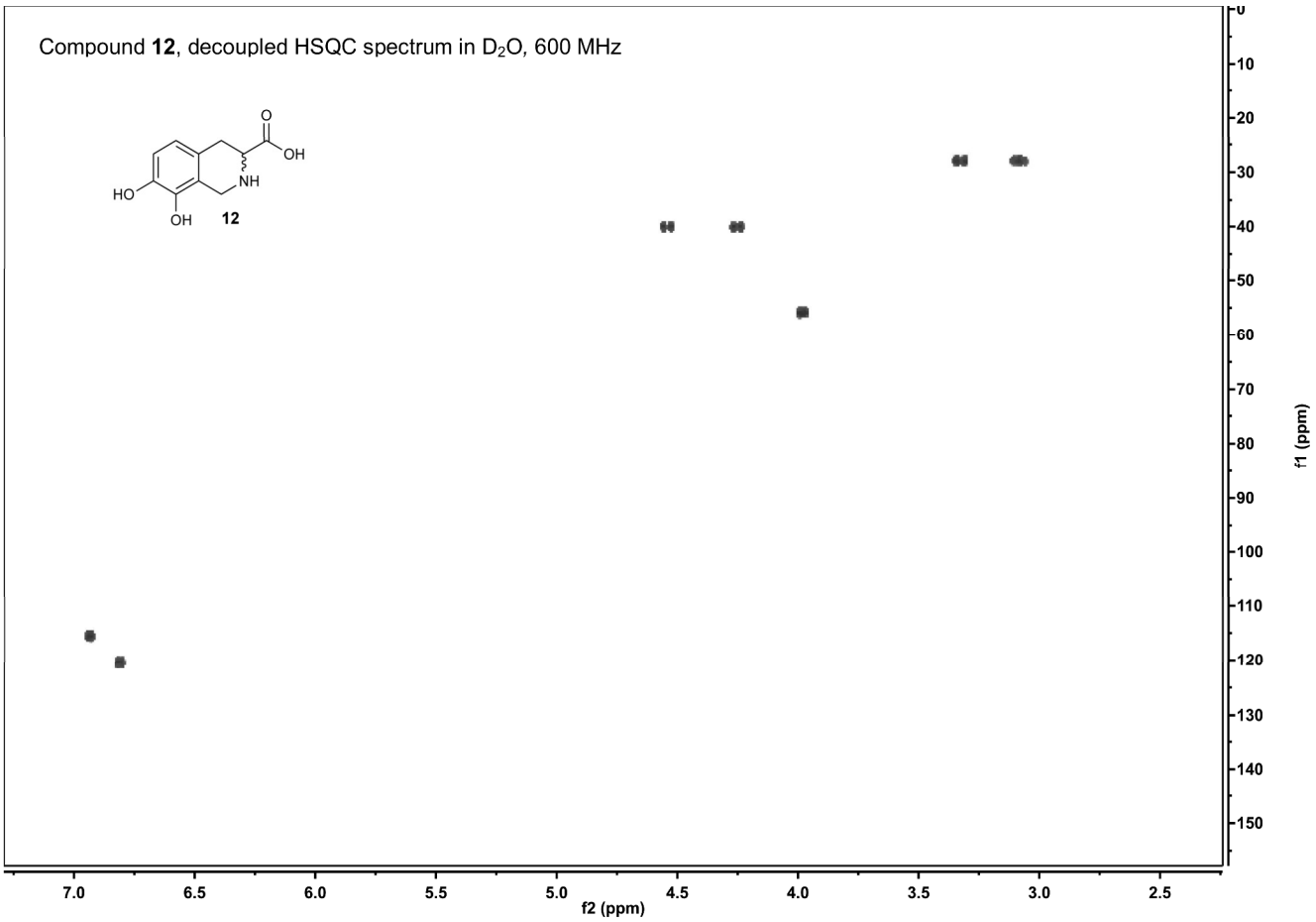

Nature Chemical Biology: doi:10.1038/nchembio.2061

^{1}H (600 MHz) and ^{13}C (151 MHz) NMR spectroscopic data for compound 18 in DMSO-d_6.

Chemical shifts were referenced to δ($C\underline{H}D_2SOCD_3$) = 2.50 and δ($^{13}\underline{C}HD_2SOCD_3$) = 39.52. ^{13}C chemical shifts were determined via HMBC and HSQC spectra. ^{1}H, ^{1}H-*J*-coupling constants were determined from the acquired ^{1}H spectrum. NOESY correlations were observed using a mixing time of 600 ms. HMBC correlations are from the proton(s) stated to the indicated ^{13}C atom.

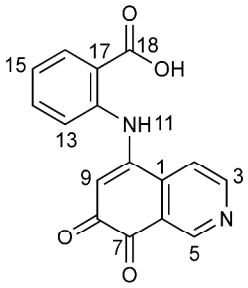

No.	δ_c	Proton	δH (J_{HH}[Hz])	HMBC[a]	NOESY
1	140.40				
2	117.23	2-H	8.05 ($J_{2,3}$ = 5.2)	3, 6, 7, 10	
3	154.59	3-H	9.02 ($J_{3,2}$ = 5.2)	1, 2, 5	
4					
5	148.00	5-H	9.08 ($J_{5,2}$ = 2.3)	1, 3, 6, 7	
6	125.13				
7	181.43				
8	175.31				
9	102.40	9-H	6.45	1, 7, 8, 10w	13
10	149.45				
11		11-NH			
12	142.36				
13	120.03	13-H	7.48 ($J_{13,14}$ = 8.5)	15, 17	9
14	130.23	14-H	7.45 ($J_{14,13}$ = 8.5, $J_{14,15}$ = 7.5)	12, 16	
15	122.68	15-H	7.11 ($J_{15,14}$ = 7.5, $J_{15,16}$ = 7.5)	13, 17	
16	131.10	16-H	8.01 ($J_{16,15}$ = 7.5)	12, 14, 18	
17	126.86				
18	168.47				

[a]w: weak correlation (less than ~10% of the intensity of strongest signal)

Nature Chemical Biology: doi:10.1038/nchembio.2061

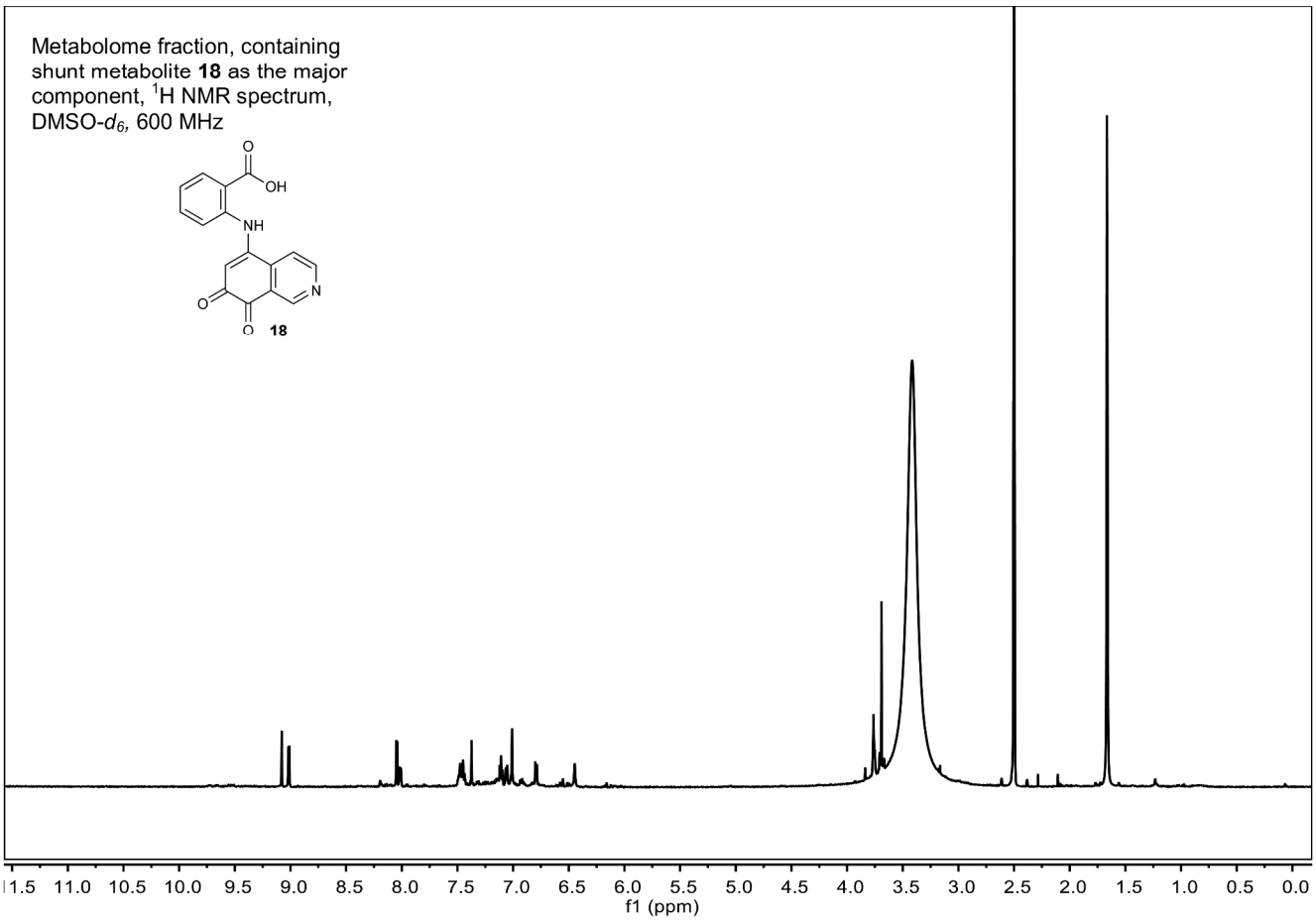

Nature Chemical Biology: doi:10.1038/nchembio.2061

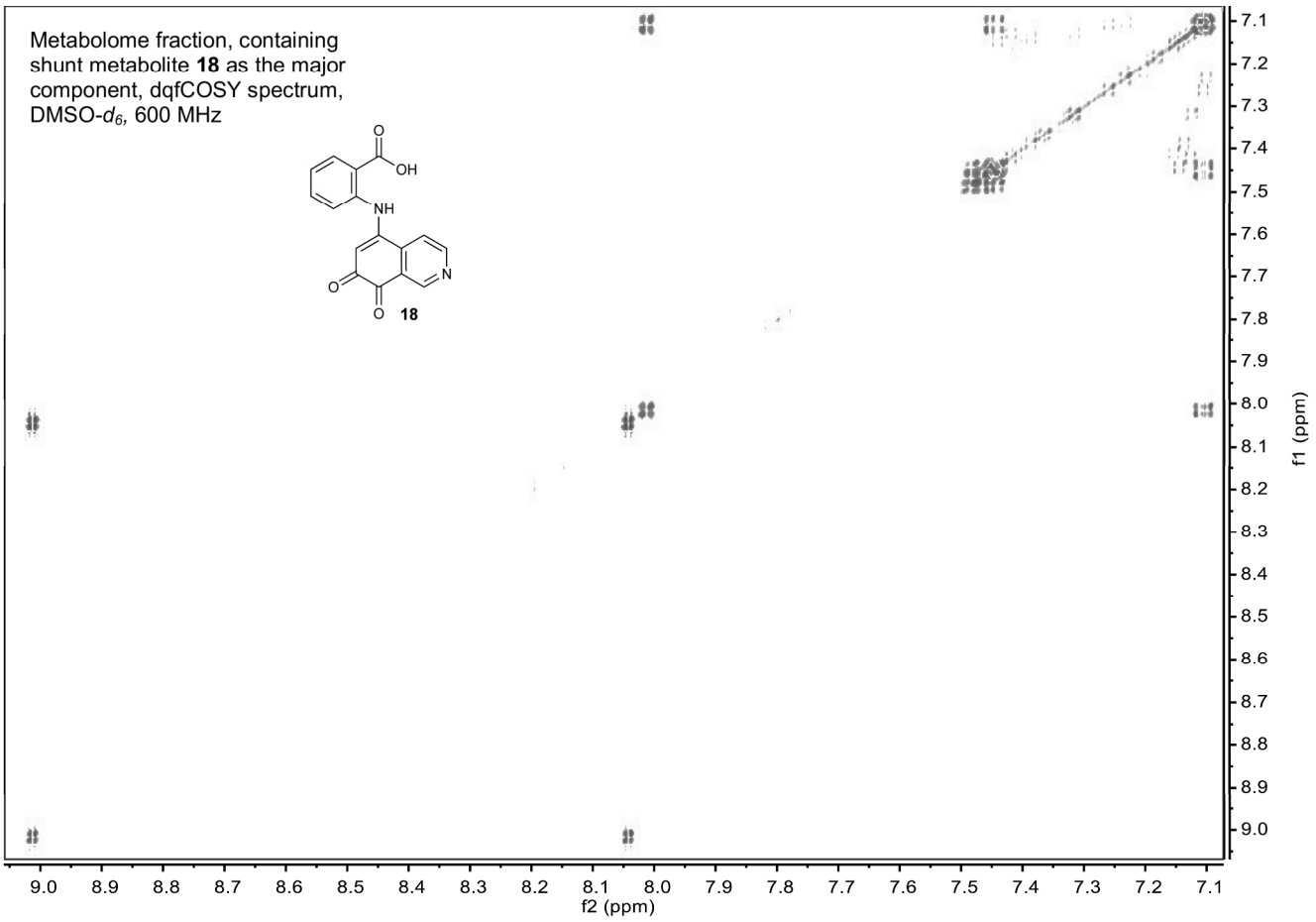

Nature Chemical Biology: doi:10.1038/nchembio.2061

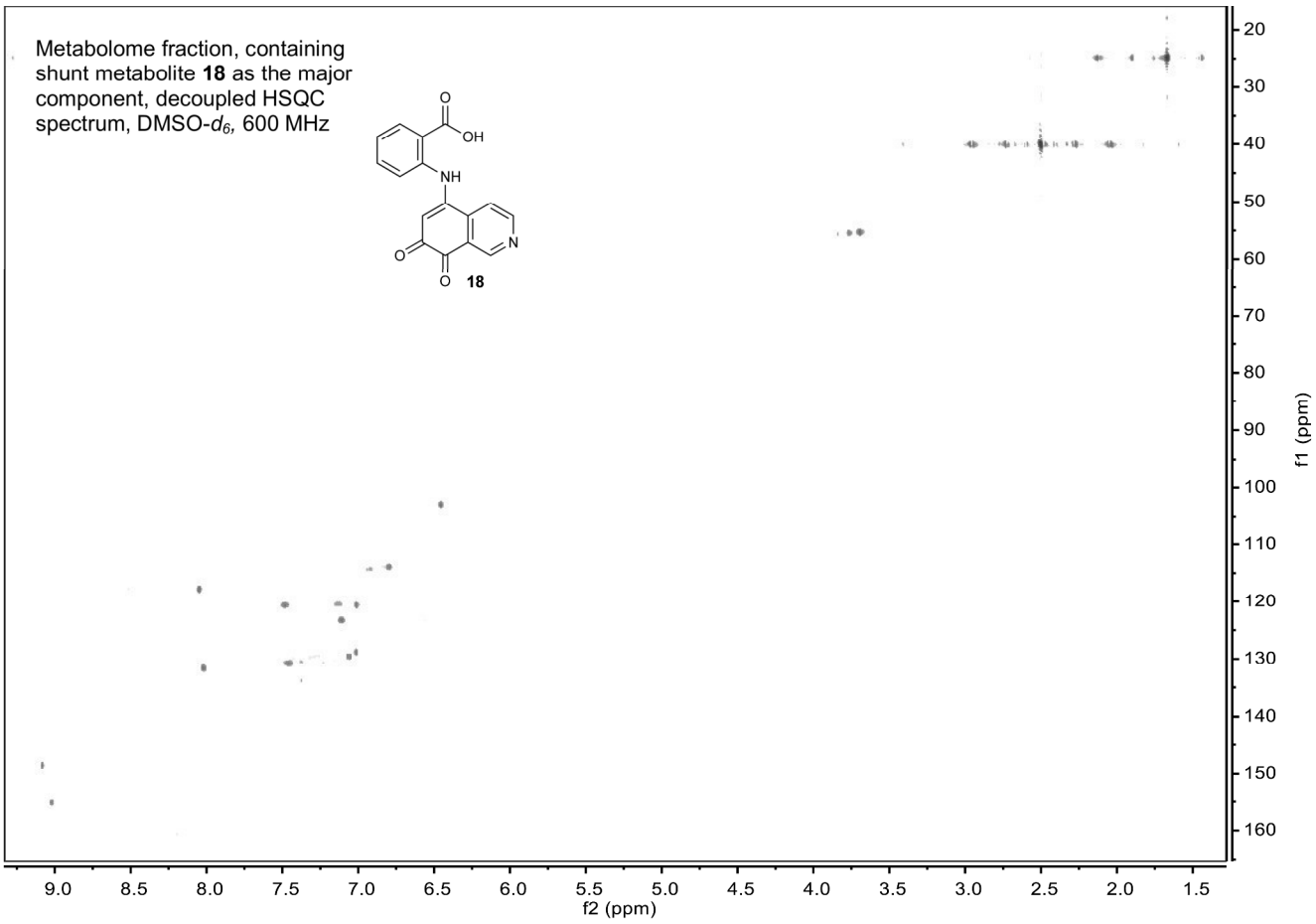

Nature Chemical Biology: doi:10.1038/nchembio.2061

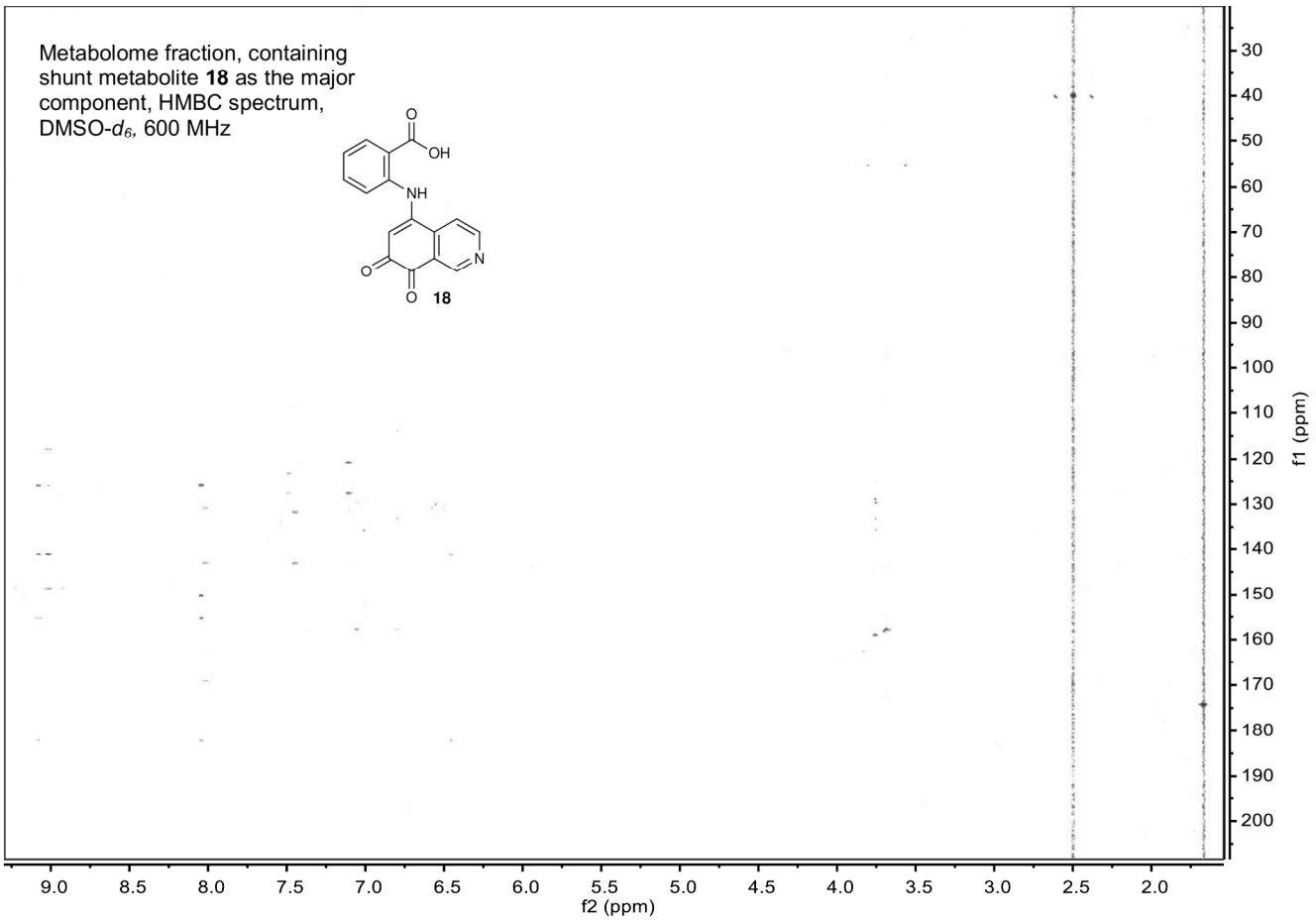

Nature Chemical Biology: doi:10.1038/nchembio.2061

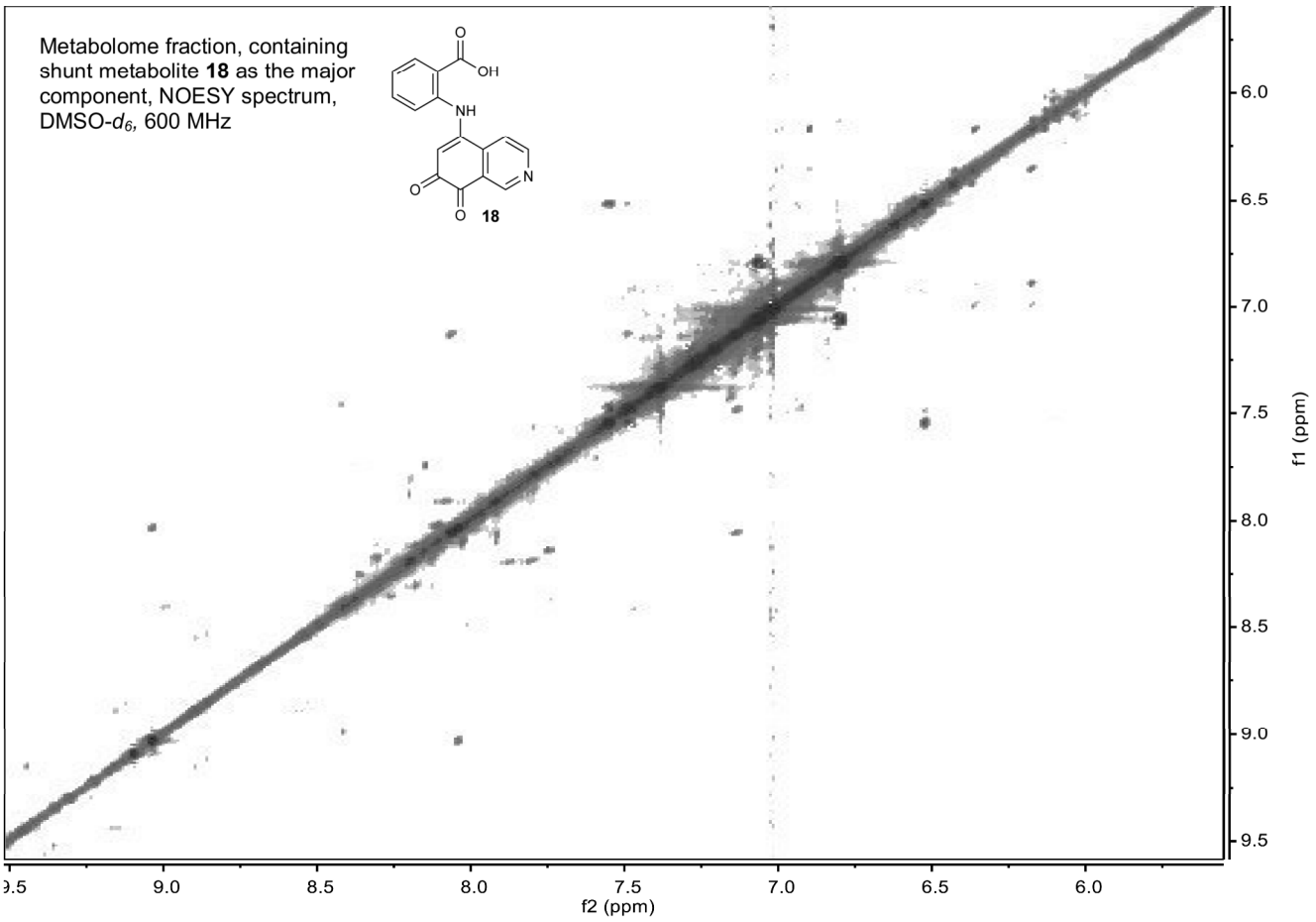

Nature Chemical Biology: doi:10.1038/nchembio.2061

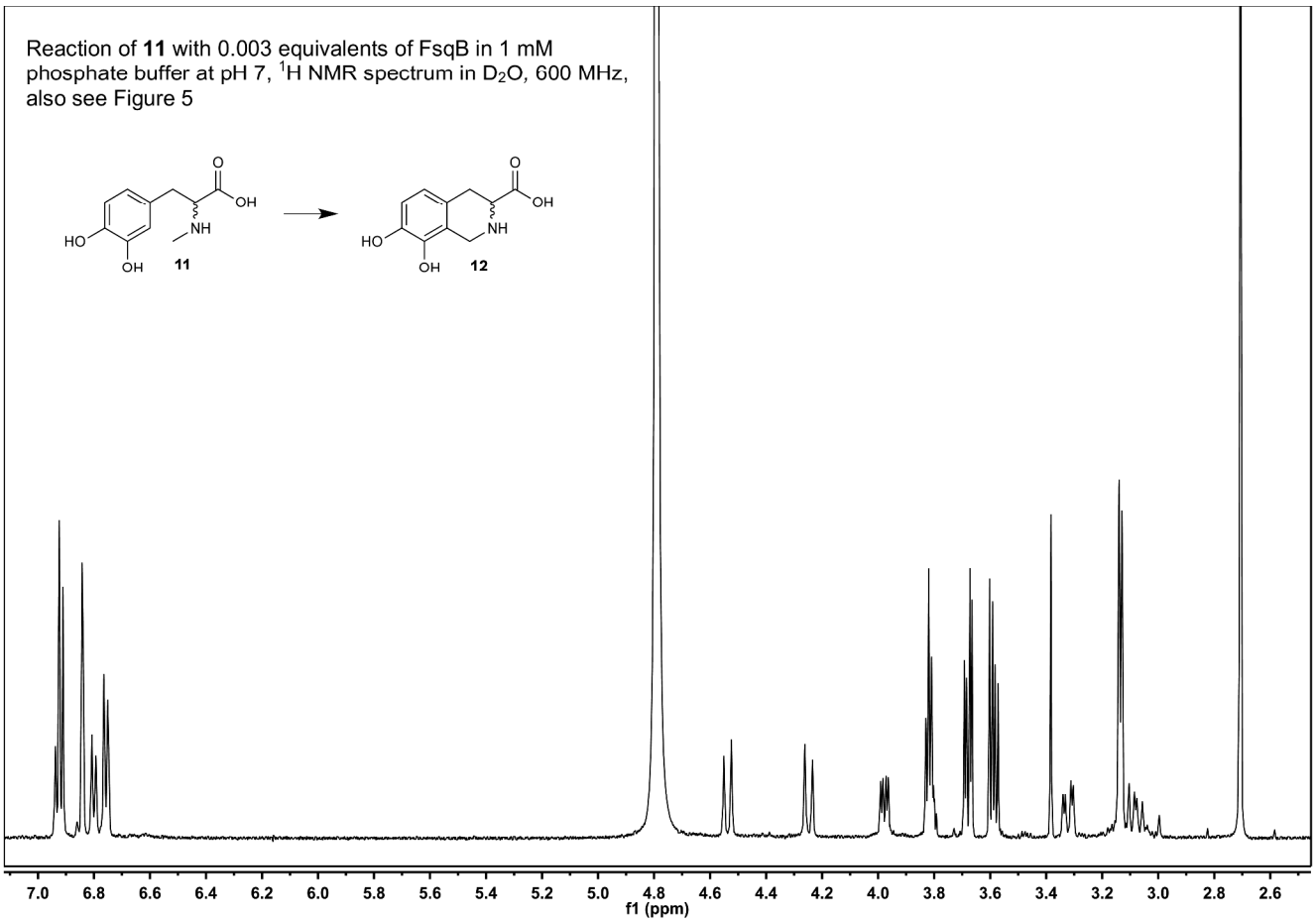

Nature Chemical Biology: doi:10.1038/nchembio.2061

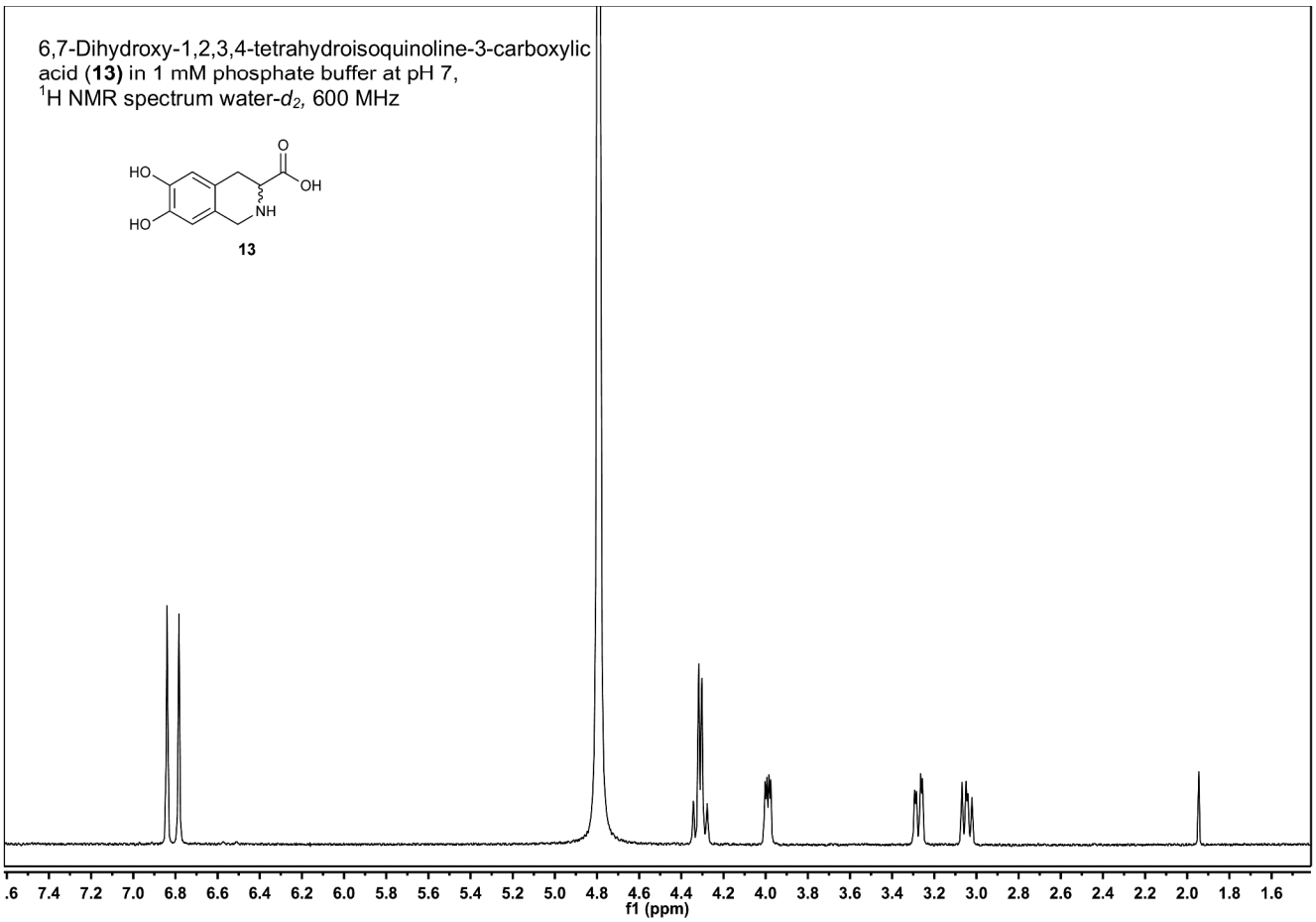

Nature Chemical Biology: doi:10.1038/nchembio.2061

4. Diskussion

Nichtribosomale Peptide (NRP) bilden neben Terpenoiden und Polyketiden eine weitere weit verbreitete Naturstoffklasse. Die Biosynthese erfolgt über multifunktionale, modular aufgebaute Megaenzyme (Nichtribosomale Peptidsynthetasen - NRPSs) in einem mehrstufigen Prozess (Finking and Marahiel, 2004).

Mit der Aufklärung verschiedener Biosynthesewege und dem Verständnis über die Funktionsweise von NRPSs bietet sich die Möglichkeit, die Biosynthese zu verändern und so bessere Wirkmechanismen zu erzielen bzw. neue Naturstoffe zu entdecken. Erst die kombinierte Anwendung von chemischen Analysetechniken (Massenspektrometrie, NMR) und Genomik ermöglichte diese Herangehensweise. Ein überaus großer Erfolg in der Aufschlüsselung der Arbeitsweise einer NRPS wurde mit der Darstellung der Kristallstruktur der A-Domäne PheA der Gramicidin S-Synthetase GrsA erzielt (Conti et al., 1997). Der Komplex aus A-Domäne, gebundenem Adenosinmonophosphat und dem Substrat L-Phenylalanin zeigte für die Substratbindung wichtige Aminosäuren und legte somit den Grundstein zur Definition eines sogenannten spezifischen nichtribosomalen Codes (Stachelhaus et al., 1999; Challis et al., 2000; May et al., 2002). Da so aus den genetischen Daten chemische (Teil-)Strukturen vorausgesagt werden können, soll zukünftig, basierend auf diesem nichtribosomalen Code, die Entdeckung neuer Wirkstoffe vereinfacht werden. Die Fülle an charakterisierten bakteriellen NRPSs macht die Substratvorhersage für bakterielle A-Domänen relativ zuverlässig (Röttig et al., 2011). Für Pilze ist diese Substratspezifitätsbestimmung aufgrund der viel kleineren Datenbasis derzeit jedoch nicht verlässlich.

4.1 Etablierung eines fungalen nichtribosomalen Codes

Die Anzahl an sequenzierten pilzlichen Genomen stieg in den vergangenen Jahren stark an. Damit einher ging die Identifizierung zahlreicher, zum Sekundärmetabolismus gehörender Gencluster, die das große Potenzial der Pilze als Produzenten pharmazeutisch relevanter Naturstoffe verdeutlichten. Für *Aspergillus flavus* wurden z. B. 56 Gencluster für die Biosynthese sekundärer Metabolite identifiziert (Amare and Keller, 2014). Für eine möglichst schnelle Aufklärung der noch unbekannten Naturstoffe sollte im Fall der NRP der

nichtribosmale Code helfen. Charakterisierungen pilzlicher NRPSs haben jedoch eine erhöhte Diversität in den Aminosäuren der Substratbindung gezeigt, was zu einer stetigen Spezifizierung des Codes führte. Der nichtribosomale Code und die sich daraus ergebene Möglichkeit zur Bestimmung der Substanzklasse, die durch die A-Domäne aktiviert wird, wurde erstmals durch Stachelhaus und Kollegen beschrieben. Sie konnten zeigen, dass α-Aminosäuren aktiviert werden, sollte sich in der ersten Position des nichtribosomalen Codes eine Asparaginsäure befinden (Stachelhaus et al., 1999). Die positive Ladung der Aminogruppe der Aminosäure wird durch die negative Ladung der Asp stabilisiert. Die negative Ladung der Carboxylgruppe wird hingegen durch das Lysin in der zehnten Position fixiert. Vergleichende Betrachtungen haben jedoch gezeigt, dass auch innerhalb dieser Substanzklasse unterschieden werden kann. Mit einem Methionin in der zweiten Position und einem Leucin oder Isoleucin in der vierten Position werden z. B. aromatische Aminosäuren und keine aliphatischen Aminosäuren aktiviert (Kalb et al., 2013). Weitere Substanzklassen konnten mit einem spezifischen nichtribosomalen Code in Verbindung gebracht werden (Abbildung 5). Sowohl die erste A-Domäne von SidE als auch von FtpA aus *Aspergillus fumigatus* aktivieren Fumarsäure und anhand des nichtribosomalen Codes wurde der Schluss gezogen, dass ein Serin in der ersten bzw. siebenten Position und ein Arginin in der dritten Position zur Aktivierung von Dicarbonsäuren führt. Modellanalysen *in silico* haben gezeigt, dass die Carboxylgruppen für die Substratbindung erforderlich sind. Die C1-Carboxylgruppe wird dabei durch die charakteristischen Serine stabilisiert (Steinchen et al., 2013; Kalb et al., 2015a). Die α-Ketosäuren wurden als weitere Substanzklasse identifiziert. Am Beispiel der Furanon- bzw. Chinon-Biosynthese durch NRPS-ähnliche Enzyme wie AtrA aus *Tapinella panuoides* (Schneider et al., 2008), EchA aus *Streptomyces spp.* (Zhu et al., 2014), der bakteriellen RalA aus *Burkholderia pseudomallei* (Wackler et al., 2011) oder Vlm2 aus *Streptomyces tsusimaensis* (Cheng, 2006) konnte gezeigt werden, dass ein Valin in der ersten Position zur Aktivierung dieser führt. Erst die biochemische Charakterisierung zahlreicher Chinon- bzw. Furanonsynthetasen führte zur Unterscheidung des nichtribosomalen Codes für aliphatische und aromatische α-Ketosäuren (Wackler et al., 2012). Des Weiteren wurde die Aktivierung von Arylsäuren bei einem Asparagin (May et al., 2002) und von Anthranilsäure bei einem Glycin (Ames and Walsh, 2010) in der ersten Position beschrieben.

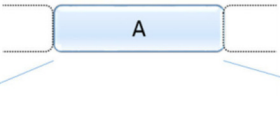

Enzym	Nichtribosomaler Code										Substrat	Referenz
Position	1	2	3	4	5	6	7	8	9	10		
Aminosäure	235	236	239	278	299	301	322	330	331	517		
GliP (A_2)	D	Y	N	T	Y	T	A	I	C	K	L-Serin	(Balibar and Walsh, 2006)
SidE (A_2)	D	V	Y	F	T	G	G	V	L	K	L-Alanin	(Steinchen et al., 2013)
EasA (A_2)	D	A	S	Q	I	G	G	I	Y	K	L-Valin	(Chiang et al., 2008)
CpaA	D	M	A	L	C	G	S	A	C	K	L-Tryptophan	(Seshime et al., 2009)
ApdA	D	M	V	I	C	G	C	A	A	K	L-Tyrosin	(Bergmann et al., 2007)
SidE (A_1)	S	A	R	G	T	V	S	Q	L	K	Fumarsäure	(Steinchen et al., 2013)
FtpA (A_1)	S	A	R	D	V	G	S	Q	L	K	Fumarsäure	(Kalb et al., 2014)
AtrA	V	A	E	F	S	G	G	A	C	K	4-Hydroxyphenylpyruvat	(Wackler et al., 2011)
AnaPS (A_1)	G	A	L	F	F	A	A	G	V	K	Anthranilsäure	(Ames and Walsh, 2010)
DhbE	N	Y	S	A	Q	G	V	V	N	K	2,3-Dihydroxybenzoesäure	(May et al., 2002)

Abbildung 5: Übersicht über den nichtribosomalen 10 Aminosäure Code; Die Nummerierung der Aminosäuren (235-517) und der Positionen (1-10) entspricht der Aminosäuresequenz der A-Domäne PheA der Gramicidin S-Synthetase aus *Bacillus brevis* (Conti et al., 1997), dargestellt sind verschiedene Enzyme, die Nummerierung der A-Domäne in Klammern, außerdem das, durch diese A-Domäne aktivierte, Substrat bestimmt durch die erste Position des nichtribosomalen Codes.

Zusammenfassend zeigen diese Arbeiten, dass die erste Position des nichtribosomalen Codes wichtig für die Vorhersage der Substratklasse ist (Abbildung 5). Jedoch weisen auch die übrigen Positionen häufig eine Regelmäßigkeit auf und tragen so dazu bei, eine Substratspezifität vorherzusagen. Mit der biochemischen Aufklärung der Funktionsweise der Siderophorsynthetase CsNPS2 des Basidiomyceten *Ceriporiopsis subvermispora* wurde eine weitere Spezifizierung bekräftigt (siehe Abschnitt 3.2). Die Aktivierung von N^5-Acetyl-N^5-Hydroxy-L-Ornithin (L-AHO) durch die iterative A-Domäne von CsNPS2 wurde *in vitro* nachgewiesen. Erst die Verwendung von *Aspergillus niger* (tEB09) als Expressionssystem für die heterologe Produktion der Synthetase ermöglichte diesen Nachweis. Die Analyse *in silico* führte zur Definition folgenden nichtribosomalen Codes: DVAGAGFIGK (basierend auf PheA, Abbildung 6), was der Aktivierung einer Aminosäure entsprechen würde. Der Vergleich mit der vierten A-Domäne von NPS2 (DVLDIGGIGK) aus *Cochliobolus heterostrophus* (Lee et al., 2005), welche ebenfalls L-AHO aktiviert oder der dritten A-Domäne von SidN (DVGGGGVIGK)

aus *Neotyphodium lolii* (Lee et al., 2010), die *cis*-Anhydromevalonyl-N^5-Hydroxy-L-Ornithin (*cis*-AMHO) aktiviert, zeigt eine Übereinstimmung in den Positionen 1-2, 6 und 8-10. Sie scheinen demnach ein Indiz für die Aktivierung großer, nichtproteinogener Aminosäuren durch pilzliche A-Domänen zu sein.

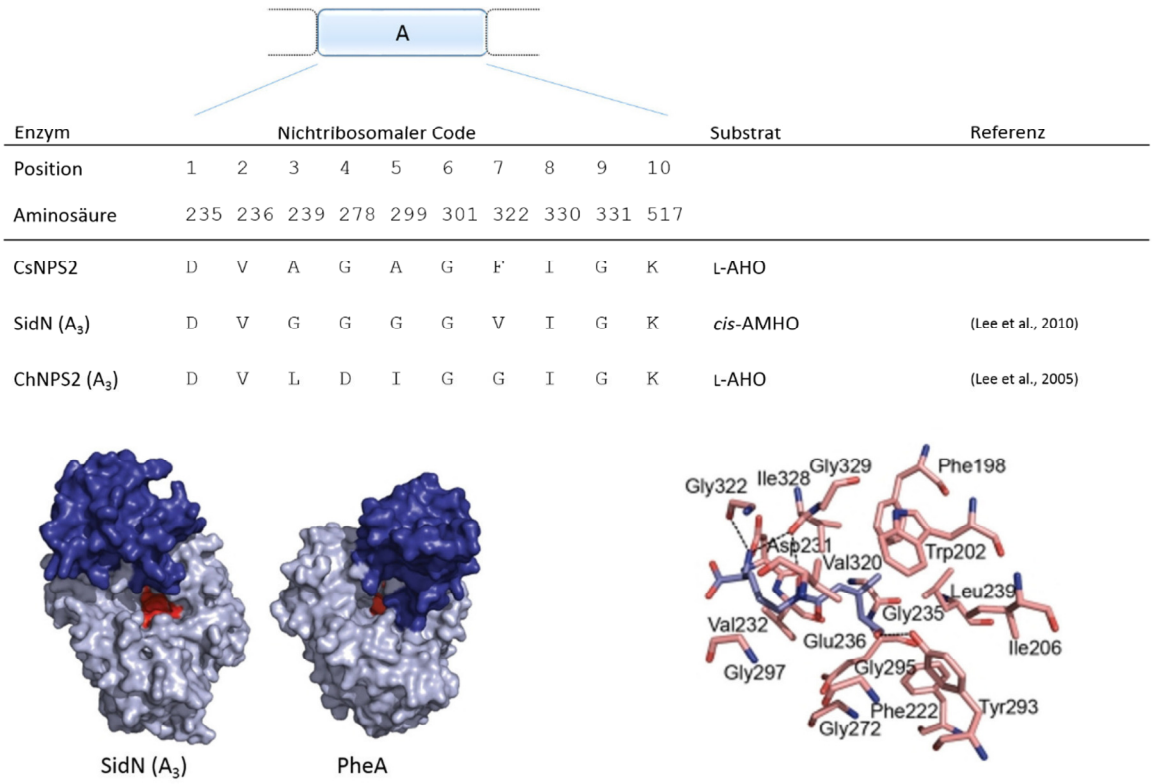

Abbildung 6: Nichtribosomaler Code für A-Domänen von Siderophorsynthetasen; Die Nummerierung der Aminosäuren (235-517) und der Positionen (1-10) entspricht der Aminosäuresequenz der A-Domäne PheA der Gramicidin S-Synthetase aus *Bacillus brevis* (Conti et al., 1997), dargestellt sind verschiedene Enzyme, die Nummerierung der A-Domäne in Klammern, außerdem das, durch diese A-Domäne aktivierte, Substrat bestimmt durch die erste Position des nichtribosomalen Codes bzw. durch biochemische Analysen, außerdem die Größe und Form der Bindetaschen (rot) von SidN (A_3) und PheA, sowie die Aminosäuren, die an der Bindung von *cis*-AMHO (lila) durch SidN (A_3) beteiligt sind (Lee et al., 2010).

Die Struktur der dritten A-Domäne von SidN wurde als erste eukaryotische A-Domäne bereits aufgeklärt. Lee und Kollegen konnten anhand dessen zeigen, dass sich die Bindetasche für große Monomere, wie das *cis*-AMHO, in Größe und Form von denen der prokaryotischen A-Domänen (Conti et al., 1997; May et al., 2002; Tanovic et al., 2008; Lee et al., 2010) unterscheidet (Abbildung 6, rot). Für SidN (A_3) wurde demnach ein erweiterter 18 Aminosäure Code beschrieben. Mithilfe von Modellierungen konnte dargestellt werden, dass die übereinstimmenden Aminosäuren des 10 Aminosäure Codes für die oben erwähnten A-Domänen mit Ausnahme der ersten und letzten Position nicht an der Substratbindung beteiligt sind (Abbildung 6, lila). Es ist möglich, dass diese acht Aminosäuren

erforderlich sind, um das aktive Zentrum der Domäne zu formen. Allerdings widersprechen diese Daten demnach der Hypothese diesen spezifischen nichtribosomalen Codes (DVXXXGXIGK) für große, nichtproteinogene Aminosäuren. Des Weiteren deuten sie darauf hin, dass der 10 Aminosäure Code für eukaryotische A-Domänen wahrscheinlich nicht ausreichend ist. Die Aufklärung weiterer Kristallstrukturen pilzlicher A-Domänen, die große Substrate wie das L-AHO binden, könnten zur Klärung dieses Sachverhaltes beitragen.

Die reduzierte Anwendbarkeit des 10 Aminosäure Codes für pilzliche A-Domänen liegt in dem sehr kleinen Set an biochemisch charakterisierten pilzlichen Enzymen (im Vergleich zu bakteriellen NRPSs) begründet. Wie für CsNPS2 aus *C. subvermispora* konnte auch für die adenylierenden Reduktasen NPS9 und NPS11 aus *Serpula lacrymans* oder NPS10 aus *Heterobasidion annosum* anhand der Proteinsequenz keine Prognose für das entsprechende Substrat getätigt werden (Brandenburger et al., 2016). Bioinformatische Analyseprogramme, wie der NRPSpredictor 2 (Röttig et al., 2011), haben die A-Domänen bzw. wichtigen Positionen wie D235 und K517 (für PheA) nicht erkannt. Andere Programme zur Bestimmung der Spezifität der A-Domäne zeigen für pilzliche NRPSs eine noch geringere Präzision (Ansari et al., 2004; Minowa et al., 2007; Jenke-Kodama and Dittmann, 2009). Erst mit den heterolog produzierten Proteinen konnte *in vitro* gezeigt werden, das durch NPS9 L-Threonin, durch NPS11 Benzoesäure und durch NPS10 Phenylbrenztraubensäure aktiviert wird. Dies verdeutlicht das mit der Untersuchung dieser adenylierenden Reduktasen aus Basidiomyceten erneut A-Domänen charakterisiert wurden, deren Substratbindung von den bakteriellen A-Domänen abweicht. Darüber hinaus wird die Wichtigkeit der biochemischen Charakterisierung weiterer pilzlicher NRPSs unterstrichen. Erst mit steigender Datenmenge ist es möglich, die enorme Diversität der A-Domänen zu verstehen und einen verlässlichen fungalen nichtribosomalen Code zu etablieren. Die im Rahmen dieser Arbeit erzeugten Daten zur Substratspezifität der A-Domänen adenylierender Reduktasen oder NRPSs mit unvollständigen Modulen tragen dazu bei. Ist es möglich, diesen nichtribosomalen Code zu spezifizieren, kann eine Substratvorhersage zu einer schnelleren Aufklärung neuer Naturstoffe beitragen.

4.2 Diversität im Aufbau der NRPSs bedingt die strukturelle Vielfalt der Produkte

Im Durchschnitt bestehen NRP aus 7-9 Monomeren, wobei die Anzahl von 2-23 Monomeren variieren kann (Caboche et al., 2010). Dabei wird durch jedes Modul einer NRPS ein Monomer in die Peptidkette eingebaut. Eine Ausnahme stellen iterativ arbeitende NRPSs dar. Dabei wird zwischen Enzymen unterschieden, bei denen ein bzw. zwei Module oder alle Module für die Synthese eines Produktes wiederholt arbeiten (Corre and Challis, 2009). Das wurde beispielsweise für die NRPS CchH aus *Streptomyces coelicolor* zur Biosynthese des Coelichelin beschrieben (Abbildung 7). N^5-Formyl-N^5-Hydroxy-L-Ornithin wird durch die A-Domäne des ersten Moduls ein zweites Mal in die Oligopeptidkette eingebaut. Darüber hinaus erfolgt auch ein „Modulskipping“. Das bedeutet, nach dem Verbinden der ersten drei Substrate (N^5-Formyl-N^5-Hydroxy-L-Ornithin, L-Threonin und N^5-Hydroxy-L-Ornithin) wird ein weiteres N^5-Formyl-N^5-Hydroxy-L-Ornithin durch die erste, iterative A-Domäne aktiviert und gleich an das am dritten Modul befindliche Trimer gebunden (Lautru et al., 2005). Die Kombination aus iterativ arbeitender A-Domäne und einem Modulskipping wurde ebenfalls für die Ferrichrome-Synthetase Sib1 der Hefe *Schizosaccharomyces pombe* beschrieben (Schwecke et al., 2006). In diesem Fall wird die Aminosäure Glycin durch die erste A-Domäne dreifach aktiviert und das Trimer anschließend mit dem Substrat, welches durch die dritte A-Domäne (ebenfalls iterativ) aktiviert wird, verbunden. Die zweite, verkürzte A-Domäne wird in der Biosynthese übergangen.

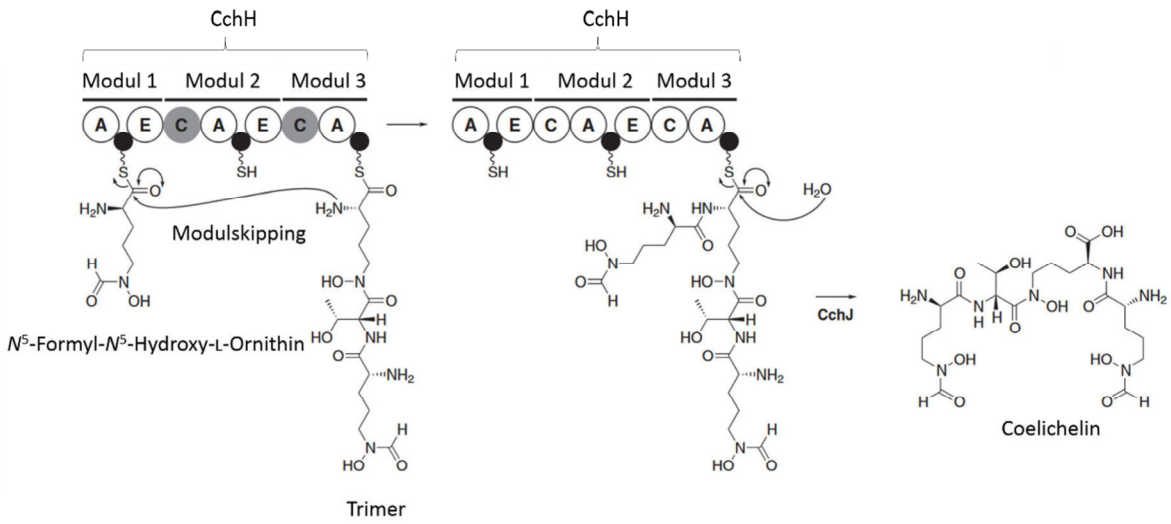

Abbildung 7: Iterative A-Domäne und Modulskipping am Beispiel der Coelichelin Biosynthese (modifiziert (Lautru et al., 2005)); trimodulare NRPS CchH, A_1 arbeitet iterativ, Substrate sind A_1: N^5-Formyl-N^5-Hydroxy-L-Ornithin, A_2: L-Threonin und A_3:N^5-Hydroxy-L-Ornithin, als Trimer an T_3 gebunden, N^5-Formyl-N^5-Hydroxy-L-Ornithin wird ein zweites Mal durch A_1 aktiviert und direkt mit dem Trimer verbunden (Modulskipping), letzter Schritt in der Biosynthese des Coelichelin katalysiert durch Esterase CchJ.

Ein weiteres Beispiel für eine iterativ arbeitende NRPS ist die Siderophorsynthetase CsNPS2 aus *Ceriporiopsis subvermispora* (Abschnitt 3.2). CsNPS2 setzt sich aus einem Initiationsmodul (A-T), zwei unvollständigen Elongationsmodulen (C-T) und einer abschließenden C-Domäne zusammen. Der Nachweis für die Aktivierung von L-AHO durch die A-Domäne mittels ATP-[^{32}P]-Pyrophosphat-Austauschassay, der massenspektrometrische Nachweis des *in vitro* erzeugten linearen Trimers aus L-AHO (Basidioferrin), sowie die Bindung dreiwertiger Eisenionen durch den Trimer bekräftigen die Hypothese, dass die einzige A-Domäne der Siderophorsynthetase iterativ arbeitet. Für ein zyklisches Produkt oder für die Bildung eines Dimers, d. h. das zweimalige Ablaufen der Synthese und einer abschließenden Dimerisierung der Trimere, konnte kein Beweis erbracht werden. Das wiederum führt zu dem Schluss, dass die Substrate durch die A-Domäne aktiviert, auf die T-Domänen geladen und durch die C-Domänen über Peptidbindungen verbunden werden. Die abschließende C-Domäne trägt somit nicht zur Zyklisierung des Produktes bei, wie es für viele weitere Siderophorsynthetasen, wie z. B. die Ferrichrome A-Synthetase Fer3 aus *Ustilago maydis* (Winterberg et al., 2010), nachgewiesen werden konnte (Schwecke et al., 2006).

Diese Ergebnisse unterstreichen die Besonderheiten in der Funktionsweise der NRPSs und die dadurch erzeugte Diversität der Naturstoffklasse der NRP. Erst eine biochemische

Charakterisierung dieser Enzyme legte die genauen Syntheseschritte offen und jede dieser Untersuchungen hilft das Potenzial der NRPSs zu verstehen.

Wie die Charakterisierung von CsNPS2 zeigte, kann auch die Produktfreisetzung einen Einfluss auf die Struktur des entlassenen Naturstoffes haben. Die Freisetzung eines Produktes durch eine endständige C-Domäne wie bei CsNPS2 ist bei pilzlichen NRPSs eine weitere Besonderheit (Bushley and Turgeon, 2010). Als klassische Domäne für die Produktfreisetzung in bakteriellen Systemen gilt die Thioesterasedomäne. Dabei werden zwei Formen unterschieden. Entweder es entsteht ein lineares Produkt durch Hydrolyse oder ein zyklisches Produkt durch Makrozyklisierung (Du and Lou, 2010). Für endständige C-Domänen wurde zunächst angenommen, dass die Freisetzung über eine inter- oder intramolekulare Zyklisierung erfolgt (Keating et al., 2001). Die postulierte Biosynthese des Basidioferrins (Abschnitt 3.2) sowie die aufgeklärte Crocacin-Biosynthese (Müller et al., 2014) deuten darüber hinaus auf die Möglichkeit einer Freisetzung von linearen Produkten durch eine C-Domäne. Das *in vitro* erzeugte Produkt von CsNPS2 konnte *in vivo* nicht nachgewiesen werden. Für einen exakten Beweis der linearen Produktfreisetzung durch eine endständige C-Domäne wie bei der Siderophorsynthetase CsNPS2 ist die Strukturaufklärung der eisenbindenden Substanz notwendig, die durch *C. subvermispora* sekretiert wird. Die Sekretion des Siderophors konnte mit einem Chrome Azurol S Assay nachgewiesen werden. Da im Genom von *C. subvermispora* keine weiteren Gene annotiert wurden, die für eine Siderophorsynthetase kodieren, kann davon ausgegangen werden, dass es sich bei Basidioferrin nicht um einen intrazellulären Siderophor (wie z. B. Ferricrocin aus *A. fumigatus* (Schrettl et al., 2007)) handelt. Eine mögliche Ursache für den fehlenden *in vivo* Nachweis des CsNPS2-Produktes ist eine anschließende Modifikation des NRPs, sodass vermutlich Basidioferrin nicht das Endprodukt des Biosyntheseweges darstellt. So wurde z. B. die Hydroxylierung von Ferricrocin zu Hydroxyferricrocin durch eine Hydroxylase oder die Acetylierung von Fusarinin C zum Triacetylfusarinin C (TAFC) durch die Transacetylase SidG in *Aspergillus fumigatus* beschrieben (Schrettl et al., 2007). Die Gene, die für die Biosynthese des TAFC benötigt werden, sind im Genom geclustert (Haas, 2014). In der unmittelbaren Umgebung des *CsNPS2* Genlokus konnte ein solches Gen allerdings nicht gefunden werden. Eine weitere Möglichkeit der Modifikation ist die Glycosylierung. Als C-glycosylierte Form des Enterobactins konnte z. B. das Salmochelin identifiziert werden (Fischbach et al., 2006). Diese Modifikationen haben somit einen zusätzlichen Einfluss auf die Diversität der NRP und

zeigen, wie komplex die Biosynthese ablaufen kann, die demnach nicht nur auf die NRPSs beschränkt ist.

Neben der klassischen TE-Domäne und der endständigen C-Domäne für die Freisetzung von NRP ist die Reduktasedomäne (R) eine weitere Möglichkeit. In diesem Zusammenhang wurden Enzyme beschrieben, welche in Abhängigkeit von NADPH das Produkt reduzieren oder redoxunabhängig, durch eine Dieckmann-Kondensation, zur Produktfreisetzung beitragen. Die Reduktion kann dabei einfach zu einem Aldehyd (zwei Elektronen) (Kalb et al., 2014) oder zweifach zu einem Alkohol (vier Elektronen) (Read and Walsh, 2007) erfolgen, was sich wiederum positiv auf die Strukturvielfalt der NRP auswirkt. Endständige R-Domänen sind bekannt von Polyketidsynthasen (PKS), NRPS-PKS Hybriden und NRPSs, wie z. B. SfmC für die Biosynthese von Saframycin aus *Streptomyces lavendulae* (Li et al., 2008). Hervorzuheben sind die monomodularen NRPSs mit endständiger R-Domäne. Anhand phylogenetischer Untersuchungen und der Substrate, die durch die A-Domänen aktiviert werden, wurde diese Enzymklasse in vier Gruppen unterteilt (Kalb et al., 2014). Weiterführende biochemische Untersuchungen haben gezeigt, dass diese Enzyme bezogen auf die Substratvielfalt viel komplexer sind, als bisher angenommen (Brandenburger et al., 2016).

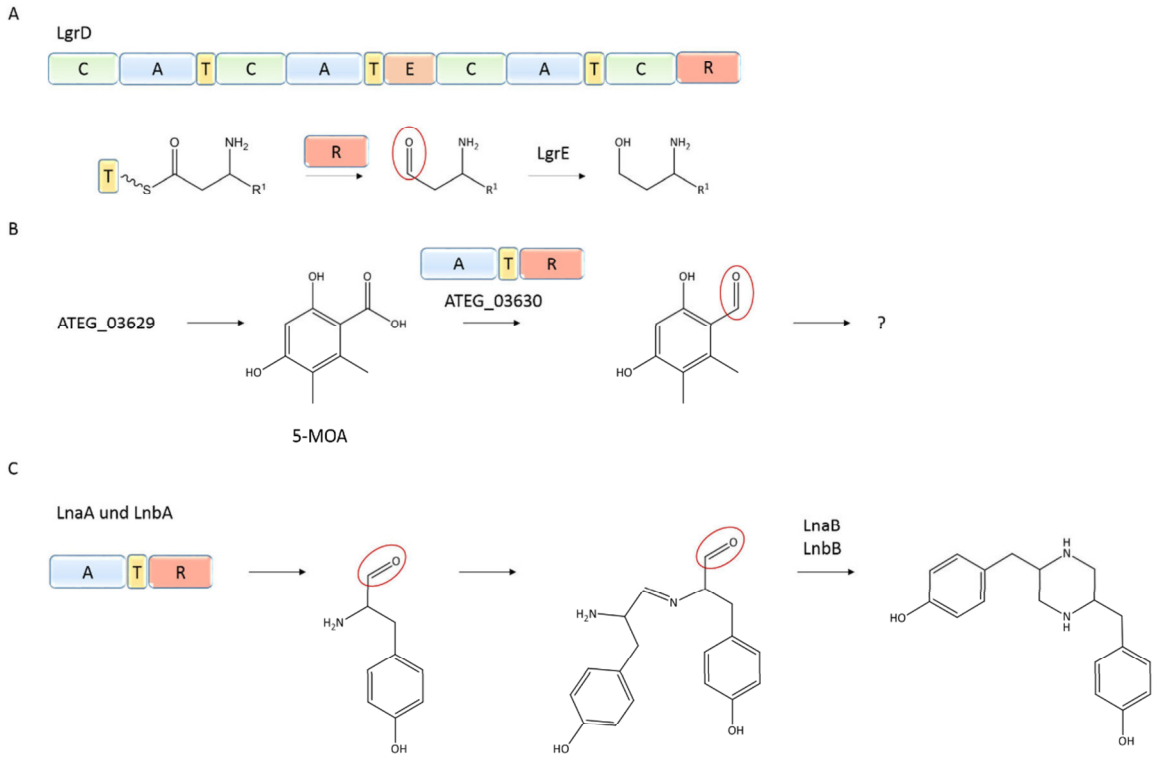

Abbildung 8: Darstellung von Biosynthesewege mit einem Aldehyden als Zwischenprodukt; (A) die letzten Schritte der Gramicidin A Biosynthese in *Bacillus brevis*, Produktfreisetzung durch die Reduktasedomäne von LgrD als Aldehyd, erneute Reduktion durch die Oxidoreduktase LgrE, (B) 5-Methylorsellinsäure (5-MOA) durch ATEG_03629 produziert, wird durch die A-Domäne der monomodularen NRPS ATEG_03630 aktiviert und zum Aldehyd reduziert, das Endprodukt derzeit

unbekannt, (C) LnaA und LnbA aus *Aspergillus flavus* aktivieren und reduzieren L-Tyrosin, es entsteht ein Dimer, nachfolgend wird dieser Dimer durch LnaB und LnbB zu einem Piperazin umgebaut, Aldehydfunktion durch roten Kreis markiert, A: Adenylierungs-, T: Thiolierungs-, C: Kondensations-, R: Reduktase-, E: Epimerisierungsdomäne.

Die oben beschriebenen adenylierenden Reduktasen aus *Serpula lacrymans*, *Heterobasidion annosum* und *Coprinopsis cinerea* bieten die Möglichkeit, neue Sekundärmetabolite zu entdecken, da keine Biosynthesewege in Zusammenhang mit diesen Enzymen bekannt sind. Weiterführende Arbeiten, wie z. B. Fütterungsexperimente mit den markierten Produkten der adenylierenden Reduktasen und eine anschließende Untersuchung der Extrakte mittels NMR sind erforderlich, um zu zeigen, wie diese Produkte weiter prozessiert bzw. in welche Naturstoffe sie eingebaut werden. Für die Biosynthese von Gramicidin A aus *Bacillus brevis* wurde beispielsweise die Verwendung eines solch reduzierten Produktes beschrieben (Schracke et al., 2005). Es konnte gezeigt werden (Abbildung 8), dass für die Biosynthese des Gramicidins das reduzierte Produkt der NRPSs LgrABCD durch die Oxidoreduktase LgrE erneut reduziert wird. Allerdings handelt es sich bei LgrD um eine tetramodulare NRPS (Kessler et al., 2004). Eine weitere Anwendung von adenylierenden Reduktasen in der Naturstoffbiosynthese wurde durch Wang und Mitarbeiter am Modellorganismus *Aspergillus terreus* verdeutlicht. Sie zeigten, dass durch die nichtreduzierende PKS ATEG_03629 5-Methylorsellinsäure gebildet wird und dass dieses Produkt durch die monomodulare NRPS ATEG_03630 aktiviert und reduziert wird. Das Endprodukt dieses Biosyntheseweges ist ebenfalls unbekannt. Es wird postuliert, dass der Aldehyd zur Biosynthese eines Moleküls ähnlich dem Cichorin aus *Aspergillus nidulans* beiträgt (Wang et al., 2014b). Eine weitere Möglichkeit bieten die monomodularen NRPSs LnaA und LnbA aus *Aspergillus flavus*. Diese reduzieren L-Tyrosin und es entsteht ein Dimer. Durch LnaB und LnbB wird dieser zu einem Piperazin umgebaut (Forseth et al., 2013).

Bisher erfolgte die Forschung zu Aminosäure-abgeleiteten Naturstoffen schwerpunktmäßig mit Genclustern, die für große, multimodulare NRPSs kodieren. Jedoch besitzen nicht alle NRP diesen Ursprung. Es konnten zahlreiche Cluster identifiziert werden, die Gene für NRPS-ähnliche Enzyme aufweisen. Ein solches Cluster ist das *fsq*-Cluster in *Aspergillus fumigatus*, das für die Biosynthese der Fumisoquine erforderlich ist (Baccile et al., 2016). FsqF, bestehend aus einer A-Domäne, einer T-Domäne, einer R-Domäne und einer endständigen pyridoxalphosphatabhängigen Aminotransferasedomäne, katalysiert einen sehr frühen Schritt in der Biosynthese. Es wird postuliert, dass dieses Enzym für die Knüpfung einer C-C-Bindung zwischen von L-Serin- und L-Tyrosin-abgeleiteten Monomeren erforderlich ist. Das

wiederum bekräftigt die besondere Stellung der minimalen NRPSs und ihren Beitrag zur Vielfalt der Naturstoffe. Diese besondere Domänenstruktur findet sich auch bei ASN170633 aus *Aspergillus niger* wieder. Anders als bei FsqF, befindet sich allerdings in der C-terminalen Position eine Kinasedomäne. Die Funktion dieses NRPS-ähnlichen Enzyms ist derzeit nicht bekannt. Es wäre denkbar, dass ein gebundenes Substrat durch die Kinasedomäne phosphoryliert und anschließend durch die R-Domäne reduziert wird. Um den Einfluss einer solchen Domäne auf die strukturelle Vielfalt der NRP beurteilen zu können, ist zunächst eine biochemische Charakterisierung erforderlich.

Im Rahmen dieser Arbeit konnten mit den adenylierenden Reduktasen (z. B. NPS9 aus *S. lacrymans*), der Siderophorsynthetase CsNPS2 aus *C. subvermispora* und FsqF aus *A. fumigatus* drei nichtkanonische, strukturell verschiedene NRPSs biochemisch charakterisiert werden. Diese Daten unterstreichen das große Potenzial der Pilze als Produzenten für NRP. Außerdem wird deutlich, dass erst mit einer größer werdenden Zahl an charakterisierten NRPSs die Funktionsweise dieser vollständig aufgeklärt werden kann.

4.3 Neue Möglichkeiten durch besseres Verständnis zur Funktionsweise der NRPSs

Die im Rahmen dieser Arbeit gezeigten Ergebnisse helfen, die strukturelle Vielfalt und Funktionsweise von NRPSs besser zu verstehen. Darüber hinaus verdeutlichen sie die besondere, überaus vielversprechende Stellung der monomodularen NRPSs, der NRPSs mit unvollständigen Modulen sowie die strukturelle Diversität derer Produkte. Weitere Untersuchungen scheinen erforderlich, um mit einer immer größer werdenden Zahl an biochemisch charakterisierten Enzymen, den entsprechenden Biosynthesewegen und dem Wissen aus Genomsequenzierungen neue bioaktive Naturstoffe vorhersagen bzw. entdecken und bereits bekannte Naturstoffe verbessern zu können. Erste Versuche dahingehend werden von immer mehr Forschergruppen unternommen, beispielsweise durch das Einbringen zusätzlicher Modifikationen. So konnte gezeigt werden, dass die Glycosylierung des Ramoplanins einen positiven Effekt auf die Löslichkeit der Substanz hat (Winn et al., 2016). Des Weiteren wurde durch die Synthese des Sulfoniumsalz des Echinomycins im Vergleich zum ursprünglichen Molekül eine stärkere Wirkung auf Tumorzellen erzielt (Park et al., 1998).

Mit dem Austausch von Modulen, eine Möglichkeit, die erst mit der Aufklärung der Funktionsweise und den verschiedenen Formen von NRPSs entstand, wurde ein vielversprechendes Instrument zum Erzeugen neuer NRP geschaffen. Dahingehend wurde viel an der Daptomycin-Biosynthese untersucht. Zunächst wurden einzelne Domänen ausgetauscht, nachfolgend ganze Module. Mit den getesteten Mutanten konnten veränderte, noch antibakteriell wirksame Daptomycin-Moleküle erzeugt werden. Allerdings wiesen alle Varianten im Vergleich zum Daptomycin eine verminderte Aktivität auf. Auch die Produktionsmengen waren nicht adäquat (Winn et al., 2016). Der Austausch von Modulen innerhalb der NRPS kann allerdings einen Einfluss auf die Interaktion der Module untereinander haben. Diese Interaktionen, welche für die T-TE-Didomäne der Enterobactin-Synthetase EntF mittels NMR nachgewiesen werden konnten (Frueh et al., 2008), könnten so die Effizienz der Biosynthese verringern.

Um einen Einfluss von Domäneninteraktionen zu minimieren, besteht die Möglichkeit die Biosynthese von NRP durch den Austausch einzelner Aminosäuren zu verändern. Kries und Kollegen konnten durch den Austausch von Trp239 mit einem Ser in der Substratbindetasche der A-Domäne PheA der Gramicidin S-Synthethase GrsA eine veränderte Substratspezifität beobachten. Sie erreichten so die Aktivierung von *O*-propargyl-L-Tyr (zuvor L-Phe) und etablierten dadurch zusätzlich ein System für eine erleichterte Identifikation bzw. Aufreinigung von Naturstoffen (Kries et al., 2014).

Ähnliches wurde am Beispiel der Fusaricidin Biosynthese durchgeführt. Der Aminosäureaustausch im Bereich der Substratbindetasche der A-Domäne von FusA führte zu einer erhöhten Substratspezifität für Phenylalanin (Han et al., 2012). Auch bei der adenylierenden Reduktase ATEG_03630 aus *Aspergillus terreus* wurde diese Herangehensweise gewählt. Durch den Austausch von His358 durch Alanin konnte neben der Aktivierung von 5-Methylorsellinsäure auch die Aktivierung von Anthranilsäure erreicht werden (Wang and Zhao, 2014).

Die gerichtete Evolution in diesem Zusammenhang, beschrieben durch Evans und Kollegen, bietet eine weitere Möglichkeit. Im Genom von *Pantoea agglomerans* dem Produzenten von Andrimid wurde das Gen *admK* verändert. Transformanten mit einem einfachen oder mehrfachen Aminosäureaustausch in der Substratbindetasche von AdmK führten zur Synthese neuer bioaktiver Andrimid-Derivate (Evans et al., 2011).

Eine weitere Studie wurde an bifunktionalen A-Domänen, d. h. mit inserierten Domänen wie einer Methyltransferase-Domäne, durchgeführt. Diese konnten dahingehend verändert werden, dass die Insertion deletiert und eine funktionelle monofunktionale A-Domäne gebildet wurde (Shrestha and Garneau-Tsodikova, 2016).

All diese Studien wurden durchgeführt, um Naturstoffe mit einem besseren therapeutischen Nutzen gezielt herstellen zu können. Eine weitere Anwendungsmöglichkeit für funktionell aufgeklärte NRP wurde durch Boda und Kollegen beschrieben (Boda et al., 2016). Es konnte gezeigt werden, das Siderophor-ähnliche Strukturen als eine Art „Trojanisches Pferd“ von Bakterienzellen aufgenommen wurden. Diese Strukturen waren so synthetisiert, dass sie in der Lage waren, DNA zu zerstören und so zytotoxisch zu wirken.

5. Zusammenfassung

Für ein besseres Verständnis bezüglich der strukturellen Vielfalt und der Funktionsweise von NRPSs wurde im Rahmen dieser Arbeit die Substratspezifität der Adenylierungsdomänen verschiedener nichtkanonischer NRPSs aus Ascomyceten und Basidiomyceten analysiert. Im Fokus stand die biochemische Charakterisierung von monomodularen NRPSs mit endständiger Reduktasedomäne und NRPSs mit unvollständigen Modulen. Mit der Substratspezifitätsbestimmung für die A-Domänen adenylierender Reduktasen aus *Serpula lacrymans* und *Heterobasidion annosum* wurde erneut die Vielfalt der Substrate unterstrichen, die durch pilzliche A-Domänen aktiviert werden. Für die repräsentativen Vertreter NPS9 und NPS11 aus *S. lacrymans* konnten L-Threonin bzw. Benzoesäure als Substrate identifiziert werden. Die A-Domäne von NPS10 aus *H. annosum* aktiviert Phenylbrenztraubensäure. Diese Ergebnisse zeigen, dass die funktionelle Diversität der adenylierenden Reduktasen größer ist als bisher angenommen. Die iterative A-Domäne der Siderophorsynthetase CsNPS2 mit unvollständigen Modulen aus *Ceriporiopsis subvermispora* aktiviert N^5-Acetyl-N^5-Hydroxy-L-Ornithin (L-AHO). Die Bildung eines chelatierenden Trimers des L-AHO konnte *in vitro* nachgewiesen werden. Obwohl Siderophorsynthetasen mit dieser Domänenstruktur (ATCTCTC) bei den Basidiomyceten als hoch konserviert gelten, ist CsNPS2 der erste charakterisierte Vertreter.

Als eine weitere nichtkanonische NRPS wurde FsqF aus *A. fumigatus* analysiert, die einen sehr frühen Schritt in der Biosynthese der Fumisoquine katalysiert. Es wird postuliert, dass dieses Enzym für die Knüpfung einer C-C-Bindung zwischen von L-Serin- und L-Tyrosin-abgeleiteten Monomeren erforderlich ist.

6. Summary

The structurally diverse nonribosomal peptides build up an important class of natural products. They are synthesized by large, modular, multifunctional nonribosomal peptide synthetases in an assembly line fashion. This study was focused on the characterization of adenylation domains of noncanonical NRPSs of asco- and basidiomycetes. The biochemical characterization of adenylate forming reductases of the basidiomycetes *Serpula lacrymans* and *Heterobasidion annosum* underline the wide range of substrates incorporated by fungal NRPSs and the structurally diversity of these enzyme class. For the representatives NPS9 and NPS11 of *S. lacrymans* we identified L-threonine and benzoic acid as preferred substrates. NPS10 of *H. annosum* activates phenylpyruvic acid. The iterative adenylation domain of the siderophore synthetase CsNPS2 preferred the nonproteinogenic amino acid N^5-acetyl-N^5-hydroxy-L-ornithine (L-AHO). A chelating trimer of L-AHO could be detected *in vitro*. This class VI fungal siderophore synthetase is highly conserved across various basidiomycetes but CsNPS2 is the first biochemically characterized one.

Next, we analyzed the noncanonical NRPS FsqF, which catalyzes the first step during the biosynthesis of fumisoquins. FsqF is required for carbon-carbon bond formation between L-serine and L-tyrosine derived monomers.

7. Referenzen

Amare, M.G., and Keller, N.P. (2014). Molecular mechanisms of *Aspergillus flavus* secondary metabolism and development. Fungal Genet Biol *66*, 11-18.

Ames, B.D., and Walsh, C.T. (2010). Anthranilate-Activating Modules from Fungal Nonribosomal Peptide Assembly Lines. Biochemistry *49*, 3351-3365.

Andersen, M.R., Salazar, M.P., Schaap, P.J., van de Vondervoort, P.J., Culley, D., Thykaer, J., Frisvad, J.C., Nielsen, K.F., Albang, R., Albermann, K., Berka, R.M*., et al.* (2011). Comparative genomics of citric-acid-producing *Aspergillus niger* ATCC 1015 versus enzyme-producing CBS 513.88. Genome Res *21*, 885-897.

Anke, T., Oberwinkler, F., Steglich, W., and Schramm, G. (1977). The strobilurins -new antifungal antibiotics from the basidiomycete *Strobilurus tenacellus*. Jpn J Antibiot *30,* 806-810.

Ansari, M.Z., Yadav, G., Gokhale, R.S., and Mohanty, D. (2004). NRPS-PKS: a knowledge-based resource for analysis of NRPS/PKS megasynthases. Nucleic Acids Res *32*, W405-W413.

Arnaud, M.B., Cerqueira, G.C., Inglis, D.O., Skrzypek, M.S., Binkley, J., Chibucos, M.C., Crabtree, J., Howarth, C., Orvis, J., Shah, P., Wymore, F*., et al.* (2012). The Aspergillus Genome Database (AspGD): recent developments in comprehensive multispecies curation, comparative genomics and community resources. Nucleic Acids Res *40*, D653-D659.

Arnison, P.G., Bibb, M.J., Bierbaum, G., Bowers, A.A., Bugni, T.S., Bulaj, G., Camarero, J.A., Campopiano, D.J., Challis, G.L., Clardy, J., Cotter, P.D*., et al.* (2013). Ribosomally synthesized and post-translationally modified peptide natural products: overview and recommendations for a universal nomenclature. Nat Prod Rep *30*, 108-160.

Baccile, J.A., Spraker, J.E., Le, H.H., Brandenburger, E., Gomez, C., Bok, J.W., Macheleidt, J., Brakhage, A.A., Hoffmeister, D., Keller, N.P., and Schroeder, F.C. (2016). Plant-like biosynthesis of isoquinoline alkaloids in *Aspergillus fumigatus*. Nat Chem Biol *12*, 419-424.

Balibar, C.J., and Walsh, C.T. (2006a). GliP, a multimodular nonribosomal peptide synthetase in *Aspergillus fumigatus*, makes the diketopiperazine scaffold of gliotoxin. Biochemistry *45*, 15029-15038.

Balibar, C.J., and Walsh, C.T. (2006b). GliP, a multimodular nonribosomal peptide synthetase in *Aspergillus fumigatus*, makes the diketopiperazine scaffold of gliotoxin. Biochemistry *45*, 15029-15038.

Bell, M.R., Johnson, J.R., Wildi, B.S., and Woodward, R.B. (1958). The Structure of Gliotoxin. J Am Chem Soc *80*, 1001-1001.

Bloch, F. (1946). Nuclear Induction. Phys Rev *70*, 460-474.

Boda, S.K., Pandit, S., Garai, A., Pal, D., and Basu, B. (2016). Bacterial siderophore mimicking iron complexes as DNA targeting antimicrobials. RSC Adv *6*, 39245-39260.

Bode, H.B., Brachmann, A.O., Jadhav, K.B., Seyfarth, L., Dauth, C., Fuchs, S.W., Kaiser, M., Waterfield, N.R., Sack, H., Heinemann, S.H., and Arndt, H.D. (2015). Structure Elucidation and Activity of Kolossin A, the D-/L-Pentadecapeptide Product of a Giant Nonribosomal Peptide Synthetase. Angew Chem Int Ed Engl *54*, 10352-10355.

Brandenburger, E., Braga, D., Kombrink, A., Lackner, G., Gressler, J., Künzler, M., and Hoffmeister, D. (2016). Multi-genome analysis identifies functional and phylogenetic diversity of basidiomycete adenylate-forming reductases. Fungal Genet Biol, DOI:10.1016/j.fgb.2016.1007.1008.

Bushley, K.E., and Turgeon, B.G. (2010). Phylogenomics reveals subfamilies of fungal nonribosomal peptide synthetases and their evolutionary relationships. BMC Evol Biol *10*, 26.

Caboche, S., Leclere, V., Pupin, M., Kucherov, G., and Jacques, P. (2010). Diversity of monomers in nonribosomal peptides: towards the prediction of origin and biological activity. J Bacteriol *192*, 5143-5150.

Challis, G.L., Ravel, J., and Townsend, C.A. (2000). Predictive, structure-based model of amino acid recognition by nonribosomal peptide synthetase adenylation domains. Chem Biol *7*, 211-224.

Cheng, Y.Q. (2006). Deciphering the biosynthetic codes for the potent anti-SARS-CoV cyclodepsipeptide valinomycin in *Streptomyces tsusimaensis* ATCC 15141. Chembiochem *7*, 471-477.

Conti, E., Stachelhaus, T., Marahiel, M.A., and Brick, P. (1997). Structural basis for the activation of phenylalanine in the non-ribosomal biosynthesis of gramicidin S. EMBO J *16*, 4174-4183.

Corre, C., and Challis, G.L. (2009). New natural product biosynthetic chemistry discovered by genome mining. Nat Prod Rep *26*, 977-986.

Cortes, J., Haydock, S.F., Roberts, G.A., Bevitt, D.J., and Leadlay, P.F. (1990). An unusually large multifunctional polypeptide in the erythromycin-producing polyketide synthase of *Saccharopolyspora erythraea*. Nature *348*, 176-178.

Cramer, R.A., Jr., Gamcsik, M.P., Brooking, R.M., Najvar, L.K., Kirkpatrick, W.R., Patterson, T.F., Balibar, C.J., Graybill, J.R., Perfect, J.R., Abraham, S.N., and Steinbach, W.J. (2006). Disruption of a nonribosomal peptide synthetase in *Aspergillus fumigatus* eliminates gliotoxin production. Eukaryot Cell *5*, 972-980.

Crooke, S.T., and Bradner, W.T. (1976). Mitomycin C: a review. Cancer Treat Rev *3*, 121-139.

Davis, C., Carberry, S., Schrettl, M., Singh, I., Stephens, J.C., Barry, S.M., Kavanagh, K., Challis, G.L., Brougham, D., and Doyle, S. (2011). The role of glutathione S-transferase GliG in gliotoxin biosynthesis in *Aspergillus fumigatus*. Chem Biol *18*, 542-552.

Dimpka, C. (2016). Microbial siderophores: Production, detection and application in agriculture and environment. Endocyt Cell Res *27*, 7-16.

Drew, S.W., and Demain, A.L. (1977). Effect of primary metabolites on secondary metabolism. Annu Rev Microbiol *31*, 343-356.

Dreyfuss, M., Harri, E., Hofmann, H., Kobel, H., Pache, W., and Tscherter, H. (1976). Cyclosporin A and C: New Metabolites from *Trichoderma polysporum* (Link Ex Pers) Rifai. Eur J Appl Microbiol *3*, 125-133.

Du, L., and Lou, L. (2010). PKS and NRPS release mechanisms. Nat Prod Rep *27*, 255-278.

Eastwood, D.C., Floudas, D., Binder, M., Majcherczyk, A., Schneider, P., Aerts, A., Asiegbu, F.O., Baker, S.E., Barry, K., Bendiksby, M., Blumentritt, M.*, et al.* (2011). The plant cell wall-decomposing machinery underlies the functional diversity of forest fungi. Science *333*, 762-765.

Ehmann, D.E., Gehring, A.M., and Walsh, C.T. (1999). Lysine biosynthesis in *Saccharomyces cerevisiae*: mechanism of alpha-aminoadipate reductase (Lys2) involves posttranslational phosphopantetheinylation by Lys5. Biochemistry *38*, 6171-6177.

Evans, B.S., Chen, Y., Metcalf, W.W., Zhao, H., and Kelleher, N.L. (2011). Directed evolution of the nonribosomal peptide synthetase AdmK generates new andrimid derivatives *in vivo*. Chem Biol *18*, 601-607.

Facchini, P.J. (2001). Alkaloid biosynthesis in plants: Biochemistry, cell biology, molecular regulation, and metabolic engineering applications. Annu Rev Plant Physiol *52*, 29-66.

Fenn, J.B., Mann, M., Meng, C.K., Wong, S.F., and Whitehouse, C.M. (1989). Electrospray Ionization for Mass-Spectrometry of Large Biomolecules. Science *246*, 64-71.

Fernandez-Fueyo, E., Ruiz-Duenas, F.J., Ferreira, P., Floudas, D., Hibbett, D.S., Canessa, P., Larrondo, L.F., James, T.Y., Seelenfreund, D., Lobos, S., Polanco, R.*, et al.* (2012). Comparative genomics of *Ceriporiopsis subvermispora* and *Phanerochaete chrysosporium* provide insight into selective ligninolysis. Proc Natl Acad Sci U S A *109*, 5458-5463.

Finking, R., and Marahiel, M.A. (2004). Biosynthesis of nonribosomal peptides. Annu Rev Microbiol *58*, 453-488.

Fischbach, M.A., Lin, H., Liu, D.R., and Walsh, C.T. (2006). How pathogenic bacteria evade mammalian sabotage in the battle for iron. Nat Chem Biol *2*, 132-138.

Fleming, A. (1929). On the antibacterial action of cultures of a *penicillium*, with special reference to their use in the isolation of *B. influenzae*. . Brit J Exp Pathol *10*, 226-236.

Floudas, D., Binder, M., Riley, R., Barry, K., Blanchette, R.A., Henrissat, B., Martínez, A.T., Otillar, R., Spatafora, J.W., Yadav, J.S., Aerts, A., *et al.* (2012). The Paleozoic origin of enzymatic lignin decomposition reconstructed from 31 fungal genomes. Science *336*, 1715-1719.

Forseth, R.R., Amaike, S., Schwenk, D., Affeldt, K.J., Hoffmeister, D., Schroeder, F.C., and Keller, N.P. (2013). Homologous NRPS-like Gene Clusters Mediate Redundant Small-Molecule Biosynthesis in *Aspergillus flavus*. Angewandte Chemie-International Edition *52*, 1590-1594.

Frueh, D.P., Arthanari, H., Koglin, A., Vosburg, D.A., Bennett, A.E., Walsh, C.T., and Wagner, G. (2008). Dynamic thiolation-thioesterase structure of a non-ribosomal peptide synthetase. Nature *454*, 903-906.

Gardiner, D.M., Cozijnsen, A.J., Wilson, L.M., Pedras, M.S., and Howlett, B.J. (2004). The sirodesmin biosynthetic gene cluster of the plant pathogenic fungus *Leptosphaeria maculans*. Mol Microbiol *53*, 1307-1318.

Haas, H. (2003). Molecular genetics of fungal siderophore biosynthesis and uptake: the role of siderophores in iron uptake and storage. Appl Microbiol Biotechnol *62*, 316-330.

Haas, H. (2012). Iron - A Key Nexus in the Virulence of *Aspergillus fumigatus*. Front Microbiol *3*, 10.

Haas, H. (2014). Fungal siderophore metabolism with a focus on *Aspergillus fumigatus*. Nat Prod Rep *31*, 1266-1276.

Han, J.W., Kim, E.Y., Lee, J.M., Kim, Y.S., Bang, E., and Kim, B.S. (2012). Site-directed modification of the adenylation domain of the fusaricidin nonribosomal peptide synthetase for enhanced production of fusaricidin analogs. Biotechnol Lett *34*, 1327-1334.

Haselwandter, K., Passler, V., Reiter, S., Schmid, D.G., Nicholson, G., Hentschel, P., Albert, K., and Winkelmann, G. (2006). Basidiochrome - a novel siderophore of the Orchidaceous Mycorrhizal Fungi *Ceratobasidium* and *Rhizoctonia* spp. Biometals *19*, 335-343.

Hoffmeister, D., and Keller, N.P. (2007). Natural products of filamentous fungi: enzymes, genes, and their regulation. Nat Prod Rep *24*, 393-416.

Jenke-Kodama, H., and Dittmann, E. (2009). Bioinformatic perspectives on NRPS/PKS megasynthases: advances and challenges. Nat Prod Rep *26*, 874-883.

Kalb, D., Heinekamp, T., Lackner, G., Scharf, D.H., Dahse, H.M., Brakhage, A.A., and Hoffmeister, D. (2015a). Genetic engineering activates biosynthesis of aromatic fumaric acid amides in the human pathogen *Aspergillus fumigatus*. Appl Environ Microb *81*, 1594-1600.

Kalb, D., Lackner, G., and Hoffmeister, D. (2013). Fungal peptide synthetases: an update on functions and specificity signatures. Fungal Biol Rev *27*, 43-50.

Kalb, D., Lackner, G., and Hoffmeister, D. (2014). Functional and phylogenetic divergence of fungal adenylate-forming reductases. Appl Environ Microbiol *80*, 6175-6183.
Kalb, D., Lackner, G., Rappe, M., and Hoffmeister, D. (2015b). Activity of α -Aminoadipate Reductase Depends on the N-Terminally Extending Domain. Chembiochem *16*, 1426-1430.

Kauserud, H., Svegarden, I.B., Saetre, G.P., Knudsen, H., Stensrud, O., Schmidt, O., Doi, S., Sugiyama, T., and Högberg, N. (2007). Asian origin and rapid global spread of the destructive dry rot fungus *Serpula lacrymans*. Mol Ecol *16*, 3350-3360.

Kavanagh, F., Hervey, A., and Robbins, W.J. (1951). Antibiotic Substances From Basidiomycetes: VIII. *Pleurotus multilus (Fr.) Sacc.* and *Pleurotus passeckerianus* Pilat. Proc Natl Acad Sci U S A *37*, 570-574.

Keating, T.A., Ehmann, D.E., Kohli, R.M., Marshall, C.G., Trauger, J.W., and Walsh, C.T. (2001). Chain termination steps in nonribosomal peptide synthetase assembly lines: directed acyl-S-enzyme breakdown in antibiotic and siderophore biosynthesis. Chembiochem *2*, 99-107.

Kennedy, J., Auclair, K., Kendrew, S.G., Park, C., Vederas, J.C., and Hutchinson, C.R. (1999). Modulation of polyketide synthase activity by accessory proteins during lovastatin biosynthesis. Science *284*, 1368-1372.

Kessler, N., Schuhmann, H., Morneweg, S., Linne, U., and Marahiel, M.A. (2004). The linear pentadecapeptide gramicidin is assembled by four multimodular nonribosomal peptide synthetases that comprise 16 modules with 56 catalytic domains. J Biol Chem *279*, 7413-7419.

Kries, H., Wachtel, R., Pabst, A., Wanner, B., Niquille, D., and Hilvert, D. (2014). Reprogramming nonribosomal peptide synthetases for "clickable" amino acids. Angew Chem Int Edit *53*, 10105-10108.

Kupfahl, C., Heinekamp, T., Geginat, G., Ruppert, T., Hartl, A., Hof, H., and Brakhage, A.A. (2006). Deletion of the gliP gene of *Aspergillus fumigatus* results in loss of gliotoxin production but has no effect on virulence of the fungus in a low-dose mouse infection model. Mol Microbiol *62*, 292-302.

Lambalot, R.H., Gehring, A.M., Flugel, R.S., Zuber, P., LaCelle, M., Marahiel, M.A., Reid, R., Khosla, C., and Walsh, C.T. (1996). A new enzyme superfamily - The phosphopantetheinyl transferases. Chem Biol *3*, 923-936.

Lautru, S., Deeth, R.J., Bailey, L.M., and Challis, G.L. (2005). Discovery of a new peptide natural product by *Streptomyces coelicolor* genome mining. Nat Chem Biol *1*, 265-269.

Lee, B.N., Kroken, S., Chou, D.Y.T., Robbertse, B., Yoder, O.C., and Turgeon, B.G. (2005). Functional analysis of all nonribosomal peptide synthetases in *Cochliobolus heterostrophus* reveals a factor, NPS6, involved in virulence and resistance to oxidative stress. Eukaryot Cell *4*, 545-555.

Lee, T.V., Johnson, L.J., Johnson, R.D., Koulman, A., Lane, G.A., Lott, J.S., and Arcus, V.L. (2010). Structure of a eukaryotic nonribosomal peptide synthetase adenylation domain that activates a large hydroxamate amino acid in siderophore biosynthesis. J Biol Chem *285*, 2415-2427.

Li, L., Deng, W., Song, J., Ding, W., Zhao, Q.F., Peng, C., Song, W.W., Tang, G.L., and Liu, W. (2008). Characterization of the saframycin A gene cluster from *Streptomyces lavendulae* NRRL 11002 revealing a nonribosomal peptide synthetase system for assembling the unusual tetrapeptidyl skeleton in an iterative manner. J Bacteriol *190*, 251-263.

Limmroth, V., Katsarava, Z., and Diener, H.C. (1999). Acetylsalicylic acid in the treatment of headache. Cephalalgia *19*, 545-551.

Lind, M., Olson, A., and Stenlid, J. (2005). An AFLP-markers based genetic linkage map of *Heterobasidion annosum* locating intersterility genes. Fungal Genet Biol *42*, 519-527.

Marahiel, M.A., Stachelhaus, T., and Mootz, H.D. (1997). Modular peptide synthetases involved in nonribosomal peptide synthesis. Chem Rev *97*, 2651-2673.

May, J.J., Kessler, N., Marahiel, M.A., and Stubbs, M.T. (2002). Crystal structure of DhbE, an archetype for aryl acid activating domains of modular nonribosomal peptide synthetases. Proc Natl Acad Sci USA *99*, 12120-12125.

McGuire, J., Bunch, R.L., Anderson, R.C., Boaz, H.E., Flynn, E.H., Powell, H.M., and Smith, J.W. (1952). Ilotycin, a new antibiotic. Antibiot Chemother (Northfield) *2*, 281-283.

Mebs, D., and Pogoda, W. (2005). Variability of alkaloids in the skin secretion of the European fire salamander (*Salamandra salamadra terrestris*). Toxicon *45*, 603-606.

Minowa, Y., Araki, M., and Kanehisa, M. (2007). Comprehensive analysis of distinctive polyketide and nonribosomal peptide structural motifs encoded in microbial genomes. J Mol Biol *368*, 1500-1517.

Mootz, H.D., and Marahiel, M.R. (1999). Design and application of multimodular peptide synthetases. Curr Opin Chem Biol *10*, 341-348.

Müller, S., Rachid, S., Hoffmann, T., Surup, F., Volz, C., Zaburannyi, N., and Müller, R. (2014). Biosynthesis of crocacin involves an unusual hydrolytic release domain showing similarity to condensation domains. Chem Biol *21*, 855-865.

Nierman, W.C., Pain, A., Anderson, M.J., Wortman, J.R., Kim, H.S., Arroyo, J., Berriman, M., Abe, K., Archer, D.B., Bermejo, C., Bennett, J., *et al.* (2005). Genomic sequence of the pathogenic and allergenic filamentous fungus *Aspergillus fumigatus*. Nature *438*, 1151-1156.

Okamura, J.P., and Sawyer, D.T. (1972). Principles and Practice of Gas-Solid Chromatography with Salt-Modified Adsorbents. Sep Purif Methods *1*, 409-475.

Oldfield, E., and Lin, F.Y. (2012). Terpene biosynthesis: modularity rules. Angew Chem Int Ed Engl *51*, 1124-1137.

Olson, A., Aerts, A., Asiegbu, F., Belbahri, L., Bouzid, O., Broberg, A., Canbäck, B., Coutinho, P.M., Cullen, D., Dalman, K., Deflorio, G.*, et al.* (2012). Insight into trade-off between wood decay and parasitism from the genome of a fungal forest pathogen. New Phytol *194*, 1001-1013.

Park, Y.S., Kim, Y.H., Kim, S.K., and Choi, S.J. (1998). A new antitumor agent: methyl sulfonium perchlorate of echinomycin. Bioorg Med Chem Lett *8*, 731-734.

Read, J.A., and Walsh, C.T. (2007). The lyngbyatoxin biosynthetic assembly line: chain release by four-electron reduction of a dipeptidyl thioester to the corresponding alcohol. J Am Chem Soc *129*, 15762-15763.

Reiber, K., Reeves, E.P., Neville, C.M., Winkler, R., Gebhardt, P., Kavanagh, K., and Doyle, S. (2005). The expression of selected non-ribosomal peptide synthetases in *Aspergillus fumigatus* is controlled by the availability of free iron. FEMS Microbiol Lett *248*, 83-91.

Röttig, M., Medema, M.H., Blin, K., Weber, T., Rausch, C., and Kohlbacher, O. (2011). NRPSpredictor2-a web server for predicting NRPS adenylation domain specificity. Nucleic Acids Res *39*, W362-W367.

Scharf, D.H., Chankhamjon, P., Scherlach, K., Heinekamp, T., Roth, M., Brakhage, A.A., and Hertweck, C. (2012). Epidithiol formation by an unprecedented twin carbon-sulfur lyase in the gliotoxin pathway. Angew Chem Int Ed Engl *51*, 10064-10068.

Scharf, D.H., Habel, A., Heinekamp, T., Brakhage, A.A., and Hertweck, C. (2014). Opposed effects of enzymatic gliotoxin N- and S-methylations. J Am Chem Soc *136*, 11674-11679.

Scharf, D.H., Remme, N., Habel, A., Chankhamjon, P., Scherlach, K., Heinekamp, T., Hortschansky, P., Brakhage, A.A., and Hertweck, C. (2011). A dedicated glutathione S-transferase mediates carbon-sulfur bond formation in gliotoxin biosynthesis. J Am Chem Soc *133*, 12322-12325.

Scharf, D.H., Remme, N., Heinekamp, T., Hortschansky, P., Brakhage, A.A., and Hertweck, C. (2010). Transannular disulfide formation in gliotoxin biosynthesis and its role in self-resistance of the human pathogen *Aspergillus fumigatus*. J Am Chem Soc *132*, 10136-10141.

Schneider, P., Bouhired, S., and Hoffmeister, D. (2008). Characterization of the atromentin biosynthesis genes and enzymes in the homobasidiomycete *Tapinella panuoides*. Fungal Genet Biol *45*, 1487-1496.

Schracke, N., Linne, U., Mahlert, C., and Marahiel, M.A. (2005). Synthesis of linear gramicidin requires the cooperation of two independent reductases. Biochemistry *44*, 8507-8513.

Schrettl, M., Bignell, E., Kragl, C., Sabiha, Y., Loss, O., Eisendle, M., Wallner, A., Arst, H.N., Jr., Haynes, K., and Haas, H. (2007). Distinct roles for intra- and extracellular siderophores during *Aspergillus fumigatus* infection. PLoS Pathog *3*, 1195-1207.

Schwarzer, D., Finking, R., and Marahiel, M.A. (2003). Nonribosomal peptides: from genes to products. Nat Prod Rep *20*, 275-287.

Schwecke, T., Göttling, K., Durek, P., Duenas, I., Käufer, N.F., Zock-Emmenthal, S., Staub, E., Neuhof, T., Dieckmann, R., and von Döhren, H. (2006). Nonribosomal peptide synthesis in *Schizosaccharomyces pombe* and the architectures of ferrichrome-type siderophore synthetases in fungi. Chembiochem *7*, 612-622.

Shah, F., Nicolas, C., Bentzer, J., Ellstrom, M., Smits, M., Rineau, F., Canback, B., Floudas, D., Carleer, R., Lackner, G., Braesel, J.*, et al.* (2016). Ectomycorrhizal fungi decompose soil organic matter using oxidative mechanisms adapted from saprotrophic ancestors. New Phytol *209*, 1705-1719.

Shen, B. (2003). Polyketide biosynthesis beyond the type I, II and III polyketide synthase paradigms. Curr Opin Chem Biol *7*, 285-295.

Shimizu, Y. (1976). Synthesis of Samandarine-Type Alkaloids and Analogs. J Org Chem *41*, 1930-1934.

Shrestha, S.K., and Garneau-Tsodikova, S. (2016). Expanding Substrate Promiscuity by Engineering a Novel Adenylating-Methylating NRPS Bifunctional Enzyme. Chembiochem *17*, 1328-1332.

Stachelhaus, T., Huser, A., and Marahiel, M.A. (1996). Biochemical characterization of peptidyl carrier protein (PCP), the thiolation domain of multifunctional peptide synthetases. Chem Biol *3*, 913-921.

Stachelhaus, T., Mootz, H.D., and Marahiel, M.A. (1999). The specificity-conferring code of adenylation domains in nonribosomal peptide synthetases. Chem Biol *6*, 493-505.

Steinchen, W., Lackner, G., Yasmin, S., Schrettl, M., Dahse, H.M., Haas, H., and Hoffmeister, D. (2013). Bimodular Peptide Synthetase SidE Produces Fumarylalanine in the Human Pathogen *Aspergillus fumigatus*. Appl Environ Microbiol *79*, 6670-6676.

Tanovic, A., Samel, S.A., Essen, L.O., and Marahiel, M.A. (2008). Crystal structure of the termination module of a nonribosomal peptide synthetase. Science *321*, 659-663.

van den Berg, M.A., Albang, R., Albermann, K., Badger, J.H., Daran, J.M., Driessen, A.J.M., Garcia-Estrada, C., Fedorova, N.D., Harris, D.M., Heijne, W.H.M., Joardar, V.*, et al.* (2008). Genome sequencing and analysis of the filamentous fungus *Penicillium chrysogenum*. Nat Biotechnol *26*, 1161-1168.

Wackler, B., Lackner, G., Chooi, Y.H., and Hoffmeister, D. (2012). Characterization of the *Suillus grevillei* quinone synthetase GreA supports a nonribosomal code for aromatic alpha-keto acids. Chembiochem *13*, 1798-1804.

Wackler, B., Schneider, P., Jacobs, J.M., Pauly, J., Allen, C., Nett, M., and Hoffmeister, D. (2011). Ralfuranone biosynthesis in *Ralstonia solanacearum* suggests functional divergence in the quinone synthetase family of enzymes. Chem Biol *18*, 354-360.

Wang, M., Beissner, M., and Zhao, H. (2014a). Aryl-aldehyde formation in fungal polyketides: discovery and characterization of a distinct biosynthetic mechanism. Chem Biol *21*, 257-263.

Wang, M., Beissner, M., and Zhao, H. (2014b). Aryl-aldehyde formation in fungal polyketides: discovery and characterization of a distinct biosynthetic mechanism. Chem Biol *21*, 257-263.

Wang, M., and Zhao, H. (2014). Characterization and Engineering of the Adenylation Domain of a NRPS-Like Protein: A Potential Biocatalyst for Aldehyde Generation. ACS Catal *4*, 1219-1225.

Wang, S., Zhang, S., Zhou, T., Zeng, J., and Zhan, J. (2013). Design and application of an *in vivo* reporter assay for phenylalanine ammonia-lyase. Appl Microbiol Biotechnol *97*, 7877-7885.

Weber, G., Schörgendorfer, K., Schneider-Scherzer, E., and Leitner, E. (1994). The peptide synthetase catalyzing cyclosporine production in *Tolypocladium niveum* is encoded by a giant 45.8-kilobase open reading frame. Curr Genet *26*, 120-125.

Weindling, R., and Emerson, O.H. (1936). The isolation of toxic substance from the culture filtrate of *Trichoderma*. Phytopathology *26*, 1068-1070.

Welzel, K., Eisfeld, K., Antelo, L., Anke, T., and Anke, H. (2005). Characterization of the ferrichrome A biosynthetic gene cluster in the homobasidiomycete *Omphalotus olearius*. FEMS Microbiol Lett *249*, 157-163.

Williams, D.H., Stone, M.J., Hauck, P.R., and Rahman, S.K. (1989). Why are secondary metabolites (natural products) biosynthesized? J Nat Prod *52*, 1189-1208.

Winn, M., Fyans, J.K., Zhuo, Y., and Micklefield, J. (2016). Recent advances in engineering nonribosomal peptide assembly lines. Nat Prod Rep *33*, 317-347.

Winterberg, B., Uhlmann, S., Linne, U., Lessing, F., Marahiel, M.A., Eichhorn, H., Kahmann, R., and Schirawski, J. (2010). Elucidation of the complete ferrichrome A biosynthetic pathway in *Ustilago maydis*. Mol Microbiol *75*, 1260-1271.

Zhu, J., Chen, W., Li, Y.Y., Deng, J.J., Zhu, D.Y., Duan, J., Liu, Y., Shi, G.Y., Xie, C., Wang, H.X., and Shen, Y.M. (2014). Identification and catalytic characterization of a nonribosomal peptide synthetase-like (NRPS-like) enzyme involved in the biosynthesis of echosides from *Streptomyces sp.* LZ35. Gene *546*, 352-358.

8. Anhang

Vektorkarten

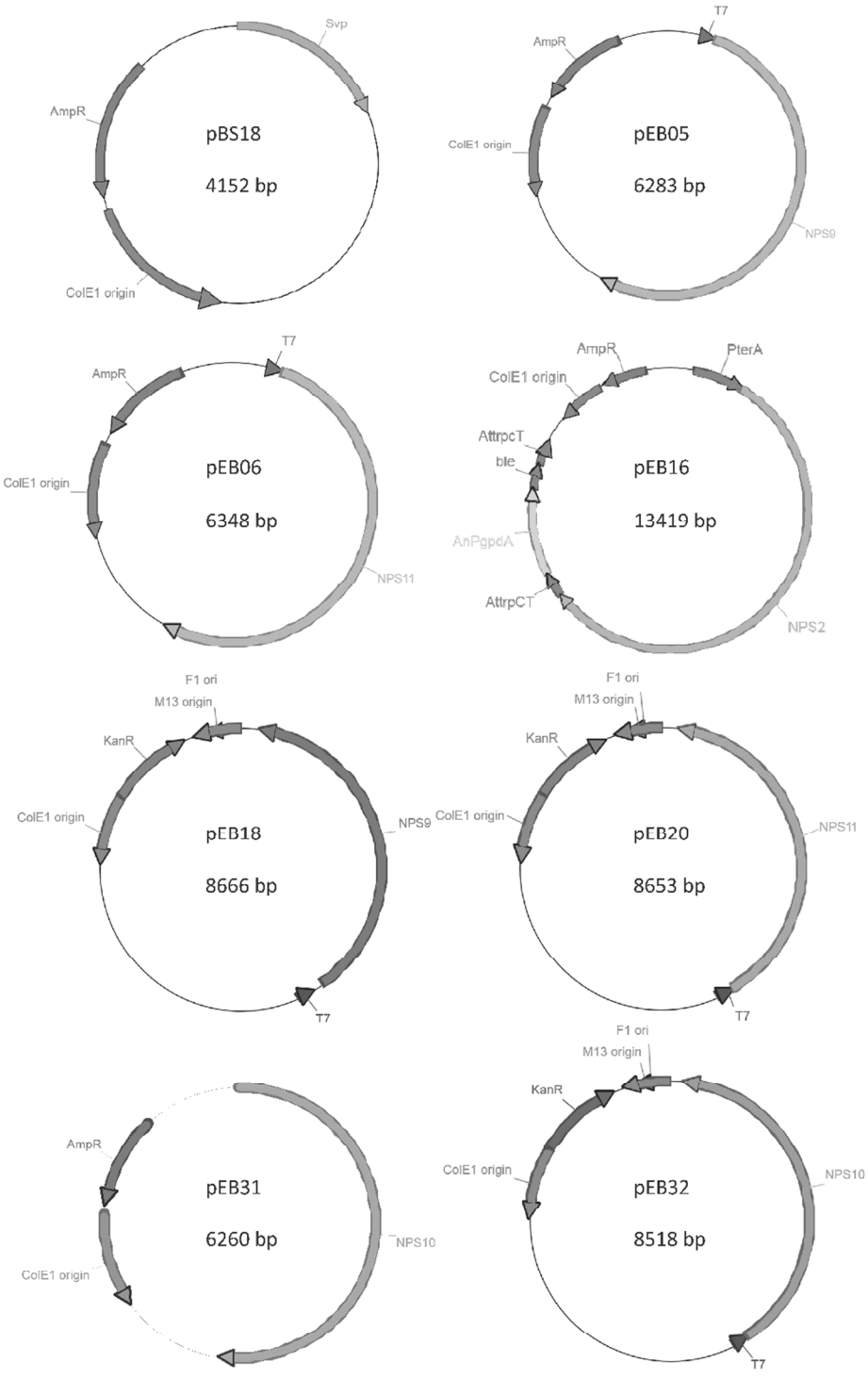

Publikationen, Vorträge und Poster

Publikationen

Brandenburger, E., Braga, D., Kombrink, A., Lackner, G., Gressler, J., Kunzler, M., and Hoffmeister, D. (2016). Multi-genome analysis identifies functional and phylogenetic diversity of basidiomycete adenylate-forming reductases. Fungal Genet Biol., DOI:10.1016/j.fgb.2016.1007.1008

Baccile, J.A., Spraker, J.E., Le, H.H., **Brandenburger, E.**, Gomez, C., Bok, J.W., Macheleidt, J., Brakhage, A.A., Hoffmeister, D., Keller, N.P., Schroeder, F.C. (2016). Plant-like biosynthesis of isoquinoline alkaloids in *Aspergillus fumigatus*. Nat Chem Biol *12*, 419-424.

Brandenburger, E., Gressler, M., Leonhardt, R., Lackner, G., Habel, A., Hertweck, C., Brock, M., Hoffmeister, D. (2016). The basidiomycete peptide synthetase CsNPS2 catalyzes N^5-acetyl-N^5-hydroxy-L-ornithine trimerization for siderophore biosynthesis, Manuskript in Vorbereitung (Applied and Environmental Microbiology)

Vorträge

Peptide-Synthetase NPS2 of the Basidiomycete *Ceriporiopsis subvermispora,* Jahrestagung der Vereinigung für Allgemeine und Angewandte Mikrobiologie (VAAM), 2016, Jena

Poster

Produktion der Peptidsynthetase NPS2 aus *Ceriporiopsis subvermispora* (Basidiomycetes) in *Aspergillus niger*, Evaluierung des Leibniz-Institutes für Naturstoffforschung und Infektionsbiologie, Hans-Knöll-Institut, 2014, Jena

Anteilsverteilung der Co-Autoren an den Publikationen

Brandenburger, E., Braga, D., Kombrink, A., Lackner, G., Gressler, J., Künzler, M., and Hoffmeister, D. (2016). Multi-genome analysis identifies functional and phylogenetic diversity of basidiomycete adenylate-forming reductases. Fungal Genet Biol. DOI:10.1016/j.fgb.2016.1007.1008 (in Druck, akzeptiert 14.07.2016)

Braga, D.	ATP-[^{32}P]-Pyrophosphat-Austausch-Assay für NPS10 aus *H. annosum*, Herstellung von pDB035 und pDB036 heterologe Produktion und ATP-[^{32}P]-Pyrophosphat-Austausch-Assay für 03009 und 06235 aus *Coprinopsis cinerea*, Alignment pilzlicher A-Domänen, Mitarbeit an der Erstellung des Manuskriptes
Kombrink, A.	Herstellung von pGEM_03009 und pGEM_06235
Lackner, G.	Erstellung des phylogenetischen Stammbaums, Mitarbeit an der Erstellung des Manuskriptes
Künzler, M.	Planung der Klonierung von pGEM_03009 und pGEM_06235, Mitarbeit an der Erstellung des Manuskriptes
Hoffmeister, D.	Planung des Projektes, Erstellung des Manuskriptes

Brandenburger, E., Gressler, M., Leonhardt, R., Lackner, G., Habel, A., Hertweck, C., Brock, M., Hoffmeister, D. (2016). The basidiomycete peptide synthetase CsNPS2 catalyzes N^5-acetyl-N^5-hydroxy-L-ornithine trimerization for siderophore biosynthesis., Manuskript in Vorbereitung (Applied and Environmental Microbiology)

Gressler, M.	Hilfe bei der Planung und Durchführung der Herstellung der *A. niger* Transformanten
Leonhardt, R.	Klonierung *CsNPS2*, Herstellung pRL1/3/5, Heterologe Produktion der A-T-Didomäne, ATP-[^{32}P]-Pyrophosphat-Austausch-Assays

Lackner, G.	Erstellung des Phylogenetischen Stammbaums, Mitarbeit bei der Planung und Durchführung der Untersuchungen bezüglich der A-T-Didomäne
Habel, A.	Synthese der Substrate L-AHO und L-AMHO
Hertweck, C.	Planung der Synthese der Substrate, Mitarbeit an der Erstellung des Manuskriptes
Brock, M.	Hilfe bei der Planung und Durchführung der Herstellung der *A. niger* Transformanten, Mitarbeit an der Erstellung des Manuskriptes
Hoffmeister, D.	Planung des Projektes, Erstellung des Manuskriptes

Baccile, J.A., Spraker, J.E., Le, H.H., **Brandenburger, E.**, Gomez, C., Bok, J.W., Macheleidt, J., Brakhage, A.A., Hoffmeister, D., Keller, N.P., Schroeder, F.C. (2016). Plant-like biosynthesis of isoquinoline alkaloids in *Aspergillus fumigatus*. Nat Chem Biol *12*, 419-424.

Baccile, J.A.	Charakterisierung und Identifizierung der Metabolite und des Biosyntheseweges, Experimente mit stabilen Isotopen, Erstellung des Manuskriptes
Spraker, J.E.	Erzeugung der *A. fumigatus* Mutanten, Erstellung des Manuskriptes
Le, H.H.	Biochemische Assays
Gomez, C.	Experimente mit stabilen Isotopen
Bok, J.W.	Erzeugung der *A. fumigatus* Mutanten
Macheleidt, J. Brakhage, A.A.	Zuarbeit zur Identifizierung der Metabolite
Hoffmeister, D.	Planung der biochemischen Assays, Erstellung des Manuskriptes

Keller, N.P.	Erstellung des Manuskriptes
Schroeder, F.C.	Charakterisierung und Identifizierung der Metabolite und des Biosyntheseweges, Erstellung des Manuskriptes

Abkürzungsverzeichnis

A.	*Aspergillus*
ADA	adenylation activating domain
Akz.	akzeptiert
AMP	Adenosinmonophosphat
Asp	Asparaginsäure
ATP	Adenosintriphosphat
C-	Carboxy
C	Condensations-
C.	*Ceriporiopsis*
C.	*Coprinopsis*
Cy	Zyklisierungs-
D	Asparaginsäure
DNA	Desoxyribonukleinsäure
E	Epimerisierungs-
E.	*Escherichia*
ETP	Epipolythiodioxopiperazin
FNR	Ferredoxin-$NADP^+$-Reduktase
H.	*Heterobasidion*
K	Kinase-
K	Lysin
L-AHO	N^5-Acetyl-N^5-Hydroxy-L-Ornithin
L-AMHO	N^5-Anhydromevalonyl-N^5-Hydroxy-L-Ornithin
MDa	Megadalton
MT	Methylierungs-
NADP	Nicotinamidadenin-dinukleotidphosphat
NMR	Nuclear Magnetic Resonance
NRP	Nichtribosomale Peptide
NRPS	Nichtribosomale Peptidsynthetase
P	Pyridoxalphosphat abhängige Aminotransferase
Phe	Phenylalanin
PKS	Polyketidsynthase
R	Reduktase-
RiPPs	ribosomally-synthesized and posttranslationally-modified peptides
S.	*Serpula*
SDR	Kurzketten Dehydrogenase/Reduktase
Ser	Serin
T	Thiolierungs-
TE	Thioesterase-
Trp	Tryptophan
Tyr	Tyrosin

Abbildungsverzeichnis

Abbildung 1: Strukturen ausgewählter Sekundärmetabolite 8
Abbildung 2: Darstellung der Funktionsweise einer NRPS 13
Abbildung 3: Beispielhafte Darstellung NRPS und NRPS-ähnlicher Enzyme 14
Abbildung 4: Phylogenie der A-Domänen pilzlicher adenylierender Reduktasen 15
Abbildung 5: Übersicht über den nichtribosomalen 10 Aminosäure Code 163
Abbildung 6: Nichtribosomaler Code für A-Domänen von Siderophorsynthetasen 164
Abbildung 7: Iterative A-Domäne und Modulskipping am Beispiel der Coelichelin Biosynthese 167
Abbildung 8: Darstellung von Biosynthesewege mit einem Aldehyden als Zwischenprodukt 169

Eigenständigkeitserklärung

Ich versichere hiermit, dass ich die vorliegende Dissertation zum Thema

Untersuchung der Substratspezifitäten von Adenylierungsdomänen aus Ascomyceten und Basidiomyceten

selbstständig und ohne Benutzung anderer als der angegebenen Quellen und Hilfsmittel angefertigt habe. Die geltende Promotionsordnung der Biologisch-Pharmazeutischen Fakultät der Friedrich-Schiller-Universität Jena ist mir bekannt. Personen, die mich bei der Auswahl und Auswertung des Materials sowie der Herstellung des Manuskriptes unterstützt haben, sind in der Danksagung der Dissertation oder den entsprechenden Manuskripten genannt. Die Hilfe eines Promotionsberaters wurde nicht in Anspruch genommen. Die Dissertation ist in gleicher oder ähnlicher Form von mir noch nicht als Arbeit für eine staatliche oder andere wissenschaftliche Prüfung eingereicht worden.

Jena, den

_____

Eileen Brandenburger

Lebenslauf

3/2014 – 2/2017	**Promotionsstudium** Friedrich-Schiller-Universität Jena
10/2012 – 10/2013	**Anfertigung der Masterarbeit** Universitätsklinikum Jena
10/2011- 10/2013	**Studium Master Molecular Life Sciences** Friedrich-Schiller Universität Jena
10/2010 – 9/2011	**Technische Assistenz** Universitätsklinikum Jena; Institut für Biochemie II unter der Leitung von Prof. Dr. Otmar Huber
3/2010 – 6/2010	**Anfertigung der Bachelorarbeit** Universitätsklinikum Jena
10/2007 – 8/2010	**Studium Bachelor Biotechnologie** Ernst-Abbe-Fachhochschule Jena

Danksagung

„Dankbarkeit ist das Gedächtnis des Herzens.“

Jean-Baptiste Massillon

Mein Dank gilt zuallererst Prof. Dr. Dirk Hoffmeister für die Möglichkeit in seiner Arbeitsgruppe meine Promotionsarbeit anfertigen zu dürfen. Die exzellente Betreuung, die hilfreichen Diskussionen, die gezielten Nachfragen und nicht zuletzt die motivierenden Worte haben maßgeblich zu den produktiven und erfolgreichen letzten drei Jahren beigetragen. Erst mit dieser Unterstützung war es mir möglich mich persönlich und ganz besonders wissenschaftlich weiter zu entwickeln.

Des Weiteren möchte ich mich bei allen bedanken, die mich in der Anfertigung meiner Publikationen unterstützt haben. Ich möchte Dr. habil. Matthias Brock und Dr. Markus Greßler für die Anleitung und Betreuung in der Anfertigung der *Aspergillus niger* Transformanten, Andrea Perner aus der Arbeitsgruppe Biomolekulare Chemie des Hans-Knöll-Instituts Jena für die Assistenz bei der hochauflösenden Massenspektrometrie und Dr. Gerald Lackner für die phylogenetischen Untersuchungen meinen Dank aussprechen.

Darüber hinaus möchte ich mich bei allen aktuellen und ehemaligen Mitgliedern der Arbeitsgruppe Pharmazeutische Mikrobiologie bedanken. Ich habe mich sehr über die herzliche Aufnahme in die Gruppe gefreut und ohne die hilfreichen Gespräche, die Unterstützung bei analytischen Fragestellungen oder den guten Zuspruch in der ein oder anderen Kaffeepause wäre ich nicht da, wo ich jetzt bin.

Abschließend möchte ich mich bei meinen Freunden, bei Bastian Kindermann, bei meinen Schwestern Anja Kaluza und Lisa Brandenburger und auf jeden Fall bei meinen Eltern bedanken. Eure Unterstützung, euer Rückhalt, eure Hilfestellungen und nicht zuletzt das Korrekturlesen haben dazu beigetragen, dass ich diese Promotionsarbeit anfertigen konnte. Ich bin glücklich, euch stets an meiner Seite zu wissen.